ABSTRACT

Title of Dissertation: ALKYNYL AMINOISOQUINOLINES, NOVEL FLT3 KINASE INHIBITORS WITH POTENT ACTIVITY AGAINST ACUTE MYELOID LEUKEMIA

Xiaochu Ma, Doctor of Philosophy, 2018

Dissertation Directed By: Professor Herman O. Sintim
Department of Chemistry and Biochemistry

Acute myeloid leukemia (AML) is a type of blood cancer. If not properly treated, this subclass of leukemia can progress quickly, and be fatal after a few months. Aberrantly expressed FMS (Feline McDonough Sarcoma)-like tyrosine kinase (FLT3) is observed in approximately 30% of AML patients, so it is a promising molecular target for AML. Midostaurin (commercial name, Rydapt) was the first approved FDA drug for AML that targets FLT3. However, Midostaurin, is not a single agent drug and is only effective when used in combination with other cytotoxic drugs. Therefore, there is a need for FLT3 inhibitors that are effective as a single agent.

In Chapter 2, the synthesis of a series of amidine-acetylene-isoquinoline-3-amines is described. Amidine-acetylene-isoquinoline-3-amine compounds have

the potential to serve new FLT3 inhibitors with inhibition IC_{50} values in the nanomolar region against wild type FLT3, FLT3-ITD (internal tandem duplications) and FLT3-D835Y (a tyrosine kinase domain mutant, commonly found in AML patients).

Amidine drugs are generally not orally bioavailable, the synthesis of amide-acetylene-isoquinoline-3-amines, our second generation FLT3 inhibitors are described in Chapters 3 and 4. The amide-acetylene-isoquinolines inhibit FLT3-driven AML cell lines with single digit nanomolar IC_{50} values and are either comparable to or better than most FLT3 inhibitors reported to date.

ALKYNYL AMINOISOQUINOLINES, NOVEL FLT3 KINASE INHIBITORS WITH POTENT ACTIVITY AGAINST ACUTE MYELOID LEUKEMIA

By

Xiaochu Ma

Dissertation submitted to the Faculty of the Graduate School of the
University of Maryland, College Park, in partial fulfillment
of the requirements for the degree of
Doctor of Philosophy
2018

Advisory Committee:
Professor Herman O. Sintim, Chair
Professor Jeffery Davis
Professor Philp DeShong
Professor John Moult
Professor Osvaldo Gutierrez

Dedication

To my father, mother, my beloved wife and my son for their endless love, support and encouragement.

Acknowledgements

I would like to thank my dissertation advisor Dr. Herman O. Sintim, who has given me precious advice and ideas in the past three years. I would like to also thank my dissertation committee members Professor Jeffery Davis, Professor Phil DeShong, Professor John Moult and Assistant Professor Osvaldo Gutierrez for their valuable advice and suggestions.

I would like to thank Dr. Min Guo, former member of the Sintim group, for teaching me AI2 synthesis and autodock trainings; Dr. Jie for determining the biological activities of amidine series compounds in Chapter 2; Ms. Delmis E. Hernandez for proof-reading of this dissertation; Mr. Clement Opoku-temeng for autodock tranings. Special thanks goes to Elizabeth Larocque, a member of the Sintim group, who helped me determine the biological activities of my compounds synthesized in Chapter 3 and 4 and proof-read my dissertation with great patience. I also thank all members of the Sintim group for the past three years.

Last but not least, I thank China Scholarship Council (No. 201406140119) and Purdue University for the generous financial support. Some of the work described in this thesis was conducted at Purdue University, where I was a visiting scientist from January 2016 till October 2017.

Table of Contents

List of Tables

List of Figures

List of Schemes

List of Abbreviations

AML	Acute Myeloid Leukemia
ALL	Acute Lymphoblastic Leukemia
CLL	Chronic Lymphocytic Leukemia
CML	Chronic Myelogenous Leukemia
T-PLL	T-cell Prolymphocytic Leukemia
HCL	Hairy Cell Leukemia
APL	Acute Promyelocytic Leukemia
FAB	French-American-British classification
ATP	Adenosine Triphosphate
FLT3	Fms-like Tyrosine Kinase 3
GRB2	Growth Factor Receptor-bound Protein2
GAB1	GRB2 Associated Protein 1
SOS	Son of Sevenless Homolog 1
STAT5	Signal Transducer and Activator of Transcription 5
JAK	Janus Kinase
EZH2	Histone-lysine N-methyl Methyltransferase Enhancer of Zester Homolog 2
PRC2	Polycomb Repressive Complex 2
Bcl-2	B-cell lymphoma 2
BAD	Bcl-2-associated death promoter
MAPKK	Mitogen-activated Protein Kinase Kinase
MAP3K	Mitogen-activated Protein Kinase Kinase Kinase
FDA	Food and Drug Administration
RTK	Receptor Tyrosine Kinase
RSK	Ribosomal Protein S6 Kinase
PI3K	Phosphatidylinositol-4, 5-bisphosphate 3-kinase
Akt	Protein kinase B
PH domain	Pleckstrin Homology Domain
mTORC2	Mechanistic Target of Rapamycin Complex 2
mTOR	Mechanistic Target of Tapamycin

MDM2	Mouse Double Minute 2 Homolog
ATRA	All-trans Retinoic Acid
NCCN	National Comprehensive Cancer Network
EGFR	Epidermal Growth Factor Receptor
VEGFR	Vascular Endothelial Growth Factor
FGFR	Fibroblast Growth Factor Receptor
TKI	Tyrosine-kinase Inhibitor
PDGFR	Platelet-derived Growth Factor Receptor
AURK	Aurora A kinase
HCK	Hematopoietic Cell Kinase
fes	Feline Sarcoma Oncogene

Chapter 1. Introduction to blood cancer, leukemia.

1.1 Cancer statistics in 2017.

The first mention of cancer in written documents can be traced back to 1600 BC when the Egyptians described breast cancer[1, 2]. Cancer is a deadly disease, causing 8.8 million deaths annually[3]. From an estimation released by American Cancer Society (ACS), males have a 42% risk of developing cancer during their lifetime, and 23% of them will eventually die from cancer. Females have a 37% risk of developing cancer during their lifetime, and 19% of them will die from cancer[4]. Compared to other diseases, the probability of an individual dying because of cancer is very high. For example, an estimated 1.5 million new cancer cases will arise in the U.S. alone and 600,000 people will die in 2017 from cancer[5]. The National Cancer Institute estimates that approximately 40% of all men and women will be diagnosed with cancer[4]. **Figure 1-1** shows the estimated number of people per state that will suffer from cancer in 2017. **Table 1-1** illustrates the diagnosed number of deaths associated with different cancers for both males and females. For males, digestive and genital are the most prevalent while for female breast cancer is the most likely cancer to occur. **Table 1-2** further shows the number of cases and deaths of both male and female for four different subclasses of leukemia. AML (acute myeloid leukemia) is a subclass of leukemia which has a 50% death rate. The five-year survival rate for AML is approximately 27%.

To treat cancer, various initiatives have been implemented to accelerate anti-cancer drug discovery. In 1971, former U.S. President Richard Nixon declared war on cancer and signed the National Cancer Act of 1971[6] with the hope of curing cancer before the 21st century. In 2016, former U.S. President Barack Obama signed Cancer Moonshot 2020 (which is currently known as Cancer Breakthroughs 2020) with 6.3 billion U.S. dollars for cancer-related science research[7]. Despite all the money and efforts put forward, we are still far from completely curing cancer. Great insights into the fundamental biology that drives tumorigenesis have been uncovered in the last several decades[8].

Figure 1-1. Estimated numbers of new cancer cases in the US in 2017[9].

	Estimated new cancer		Estimated deaths	
	Male	Female	Male	Female
All sites	836,150	852,630	318,420	282,500
Oral cavity & pharynx	35,720	13,950	7,000	2,700
Digestive system	175,650	134,790	92,350	65,350
Respiratory system	133,050	110,120	88,100	72,320
Bones & joints	1,820	1,440	890	660

Soft tissue	6,890	5,500	2,670	2,320
Skin	57,140	38,220	9,250	4,340
Breast	2,470	252,710	460	40,610
Genital system	172,330	107,470	27,500	31,600
Urinary system	103,480	43,170	22,260	9,930
Eye & orbit	1,800	1,330	180	150
Brain & other nervous system	13,450	10,350	9,620	7,080
Endocrine system	15,610	43,640	1,440	1,570
Lymphoma	44,730	35,770	12,080	9,130
Myeloma	17,490	12,790	6,660	5,930
Leukemia	36,290	25,840	14,300	10,200
Other	18,230	15,540	23,660	18,610

Table 1-1. Estimation of new cancer and death cases in different cancer types[9].

	Estimated new cancer		Estimated deaths	
	Male	Female	Male	Female
Acute lymphocytic leukemia	3,350	2,620	800	640
Chronic lymphocytic leukemia	12,310	7,800	2,880	1,780
Acute myeloid leukemia	11,960	9,420	6,110	4,480
Chronic myeloid leukemia	5,230	3,720	610	470
Other leukemia	3,440	2,280	3,900	2,830

Table 1-2. Estimation of new cancer and death in different subclass of leukemia[9].

1.2 History of leukemia and human hematopoiesis system.

In ancient Egyptian texts dated back to 3000 BC, people observed “thick blood” which is possibly the earliest record of leukemia[10]. The early discovery and diagnosis of leukemia is associated with five physicians in the 19th century all of whom worked in Paris during that time (**Figure 1-2**)[11]. Their patients all had the symptoms of fever, difficulty in breathing, and severe abdominal pain. In 1811, Peter Cullen first described a case where his patient had unexplainably milky blood. During that time, blood-letting was thought of as a standard method to treat any diseases. Hence, those physicians observed the unusual color of their patient’s

blood and treated them by blood-letting. In 1825, French surgeon Alfred Velpeau noted pus in the blood vessels from one of his patients[12]. In 1844, French bacteriologist Alfred Donne found a differentiation arrest of white blood cells[13]. During 1845 to 1847, German physician Rudolf Virchow detected a reversed ratio of white to red blood cells and introduced the term leukemia[14]. In 1879, F. Mosler was the first to describe the technique of bone marrow examination to diagnose leukemia. In 1889, German physician Whihelm Ebstein introduced the term acute leukemia which defines as a rapid progression and fetal version of leukemia and the remaining was called chronic leukemia[15]. In 1900, Swiss hematologist Otto Naegeli further divided leukemia into myelogenous and lymphocytic subclasses.

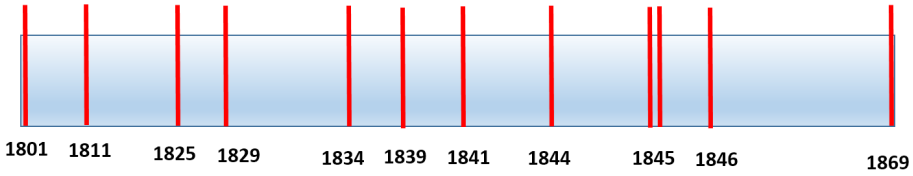

1801 Bichat first defined the term leukocytosis
1811 Cullen reported the first case that patient has milky blood
1825 Velpeau reported the second case with more accurate description of associated symptoms
1829 Collineau reported the third case that patient has milky blood
1834 Duplay reported the fourth case
1839 Barth reported and published the fifth case
1841 Craigie published the fifth case
1844 Donne examed patient's blood under microscope
1845 Bennett termed Leucocythemia
1846 Fuller reported the tenth case and using leukemia for the first time
1859 Neumann connected leukemia to the bone marrow

Figure 1-2. Timeline of early understanding of leukemia[11].

Interestingly, the early description of leukemia was entirely consistent; the physicians described the patients' blood as milky, pus-filled. Normally, humans' serum is an amber transparent fluid, however, in those patients, all of their serum looks milky white. As a consequence, they came to the conclusion that this altered

composition of blood was characteristic of leukemia. This is still characteristic of leukemia today. Leukemia is defined as the excess accumulation of white blood cells and thus more abnormal cells are in serum (**Figure 1-3**).

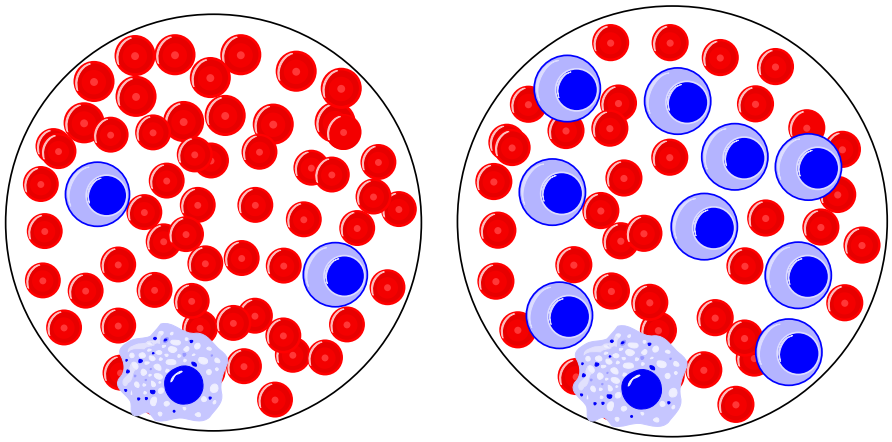

Figure 1-3. Compare of normal blood and leukemia patient's blood under microscope.

A better understanding of how different blood cells are made in our body is needed to understand the classification of different types of leukemia. All the blood cells come from multipotential hematopoietic stem cells[16], the so-called hemocytoblast, which are self-renewing cells and can also proliferate indefinitely. Those blasts derived from mesoderm in the very early embryo and located in the red bone marrow (See **Figure 1-4**). Eventually, they divide into two types of cells, myeloid progenitor and lymphoid progenitor. These two cell types, in turn, divide into more specific blood cells. Myeloid progenitor can become four main types of cells, erythroblast, megakaryoblast, monoblast, and myeloblast. Erythroblast will divide into erythrocyte (red blood cell) and megakaryoblast. Megakaryoblast will become megakaryocyte and finally, will become platelets. The myeloblast path can

divide into basophilic, neutrophilic and neutrophil myelocyte and finally basophil, neutrophil, and eosinophil.

The lymphoid progenitor will lead to B lymphocyte, T lymphocyte, and natural killer cells, all of which are important parts of the human immune system to defend against outside invaders[17].

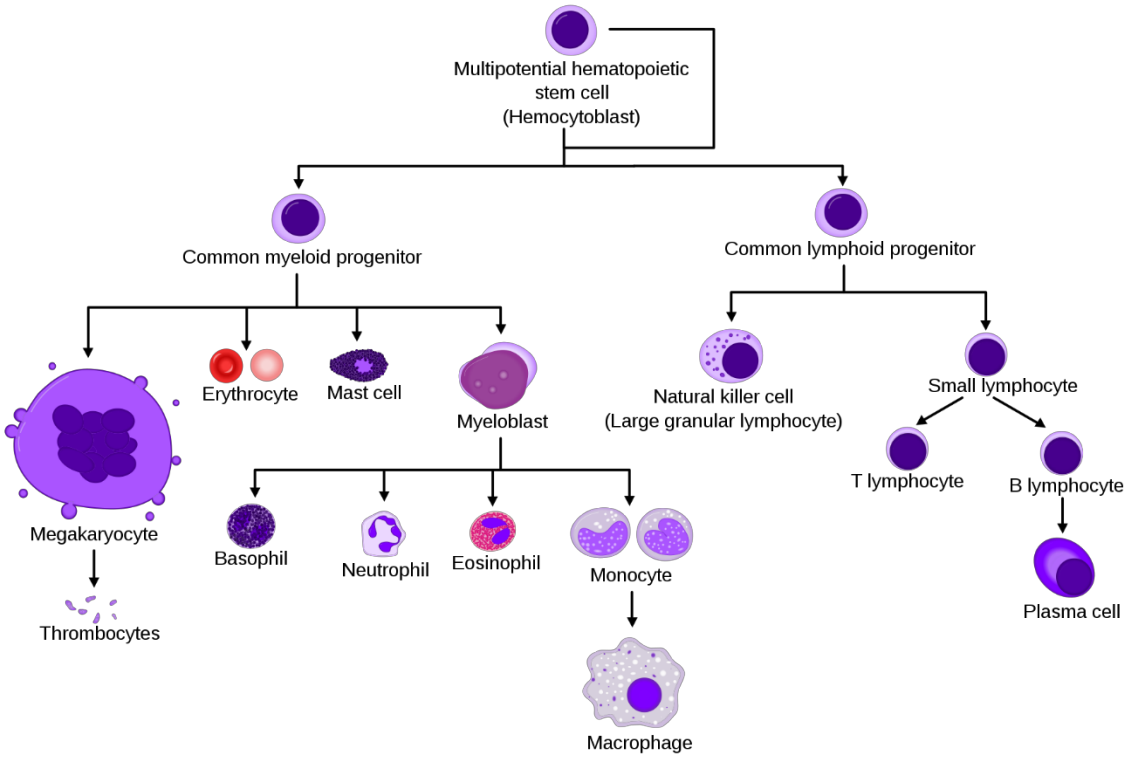

Figure 1-4. The development of different blood cells from hematopoietic cell to different mature blood cells (https://en.wikipedia.org/wiki/Haematopoiesis).

1.3 Leukemia causes, classifications, and diagnosis.

Although still in debate, three factors have been put forth as causes of leukemia; exposure to ionizing radiation, benzene or cytotoxic chemotherapy [18].

1) Exposure to ionizing radiation[19]:

Researchers have shown that Japanese people who survived the atomic bombs have an increased risk of developing AML. Moreover, workers in the nuclear industry also have a higher risk of developing AML. Crew members who fly commercial airplanes extensively, especially in high latitudes, are exposed to a substantial amount of ionizing radiation leading to a higher propensity to develop AML than the general population. A report found an increased number of AML patients in Danish airplane crews who flew more than 5000 hours [20].

2) Exposure to benzene[21]:

Benzene is a known carcinogen, specifically causing leukemia. Cigarette smoke (also a common source for benzene) increases benzene exposure and can lead to leukemia. Studies show a 1.2 to 2.3 times increase of developing AML for smokers compared to non-smokers [22].

3) Exposure to cytotoxic chemotherapy[18]:

Up to 10-15% solid tumor patients who are treated with cytotoxic agents develop AML within 5 to 10 years after treatment. This results from damage to their DNA, especially chromosomes 5 and 7 during the cytotoxic agent treatment [23]. If patients are treated with doxorubicin and etoposide, both of which can interact with DNA topoisomerase II, they typically develop AML within 1-5 years due to cytogenetic abnormalities in chromosome 11 and translocations of chromosome 15 and 17[24].

Leukemia is divided into four types: Acute Lymphoblastic Leukemia (ALL)[25], Chronic Lymphocytic Leukemia (CLL)[26], Acute Myelogenous

Leukemia (AML)[27] and Chronic Myelogenous Leukemia (CML)[28]. Apart from those four main categories, there are other leukemia subtypes that are very rare. For example, T-cell prolymphocytic leukemia (T-PLL)[29], large granular lymphocytic leukemia[30], adult T-cell leukemia[31], Hairy cell leukemia (HCL)[32] and Clonal eosinophilia[33] are all rare subtypes of leukemia. **Table 1-3** shows the classification of leukemia into two types, lymphocytic leukemia and myelogenous leukemia which originates from the cell type that causes leukemia. For each type of leukemia, we can further divide it into two subtypes, and the acute or chronic form depends on the progression or severity of the disease.

Cell Type	Acute	Chronic
Lymphocytic/Lymphoblastic Leukemia	Acute Lymphoblastic Leukemia (ALL)	Chronic Lymphocytic Leukemia (CLL)
Myelogenous/Myeloid/Non-Lymphocytic Leukemia	Acute Myelogenous Leukemia (AML)	Chronic Myelogenous Leukemia (CML)

Table 1-3. The development of different blood cells from hematopoietic cell to different mature blood cells.

Acute leukemia can become very severe within weeks of the disease diagnosis. There is a rapid increase of immature blood cells in the bone marrow, this makes the bone marrow unable to produce any regular functionalized blood cells. Patients typically need immediate medical treatment since the malignant cells will eventually invade the whole body. Chronic leukemia develops slower compared to the acute form. It can take years for the disease to progress. In some cases, patients display some symptoms, but can usually live a normal life. Although those malignant cells are abnormal cells, they are slightly more mature

than blast cells, so they can still function in some ways. Another reason is that in chronic leukemia, the bone marrow can still produce healthy blood cells even though there is an excessive accumulation of leukemia cells.

Leukemia is a heterogeneous disease, and hence physicians must diagnose the disease correctly in order to treat patients with the best therapy available. Currently, there are two classifications for leukemia that is widely used, the World Health Organization (WHO) classification and French-American-British classification (FAB). WHO classification relies on more in-depth genetic information of the disease and FAB classification is more focused on the morphology of the leukemia cells. Although first proposed in 1976, the FAB classification is still the most widely used classification system in the clinic.

French-American-British (FAB) classification[34]:

Type	Name	Percentage
M0	Acute myeloblastic leukemia, minimally differentiated	5%
M1	Acute myeloblastic leukemia, without maturation	15%
M2	Acute myeloblastic leukemia, with granulocytic maturation	25%
M3	Acute promyelocytic leukemia	10%
M4	Acute myelomoncytic leukemia	20%
M4eo	Myelomonocytic together with bone marrow eosinophilia	5%
M5	Acute monoblastic leukemia (M5a) / acute monocytic leukemia (M5b)	10%
M6	Erythroleukemia (M6a) / pure erythroid leukemia (M6B)	5%
M7	Acute megakaryoblastic leukemia	5%

M8	Acute basophilic leukemia	rare

Table 1-4. French-American-British (FAB) classification on leukemia and the estimated percentage of cases.

In order to determine the subtypes of leukemia, the peripheral blood and bone marrow tissues are collected from patients, and a peripheral blood differential count and a 500-cell bone marrow differential count are done[35, 36]. For certain subtypes of AML to distinguish myeloid leukemia from lymphoid leukemia, immunohistochemistry is sometimes used[37]. It is feasible to distinguish myeloid cells or lymphoid cells based on markers on the cell membrane. (See **Table 1-5**).

	Precursor Cells Markers			Myeloid Cells Markers				Monocyte Markers	
	TdT	HLA-DR	CD34	CD13	CD33	CD117	CD15	CD11b	CD14
M0	+/-	+	+	(+)	+/-	(+)	(-)	(-)	(-)
M1	+/-	+	(+)	(+)	+	(+)	(-)	+/-	(-)
M2	-	+	(-)	+	+	+	+	+/-	(-)
M3	-	-	-	+	+	+/-	+/-	(-)	(-)
M4	(-)	+	+/-	(+)	+	+/-	+	+	(+)
M5	(-)	+	+/-	+/-	+	+/-	+	+	(+)
M6	-	+/-	+/-	+/-	+/-	+	(-)	+/-	(-)
M7	-	(+)	(+)	(-)	+/-	(+)	(-)	-	-

Table 1-5. Different antigen that can be used to distinguish different AML subclass. + means positive for certain CD marker, +/- means may be positive or negative for certain CD marker, (+) and (-) mean mainly positive or mainly negative for certain CD marker[36].

As we can see from the above table, it is sometimes ambiguous to use CD marker to diagnose certain subtypes of AML. In these cases, the morphology of bone marrow cells will help. The criteria for M0 AML diagnosis includes more than 30% of the blast and nonerythroid cells in the bone marrow are nucleated. Less

than 3% of blast cells are positive for either Sudan Black B or myeloperoxidase. The morphology of M0 AML is very similar to M1 myeloblasts or L2 lymphoblasts. Thus the diagnosis of M0 AML is always with the help of immunocytochemistry or flow cytometric immunophenotyping with an anti-MPO monoclonal antibody. The detection of CD13, CD14, CD15, CD33, CD64, CD65 and CD117 will provide substantial evidence for M0 AML. M0 AML is typically associated with seniors and thus results in a poor prognosis. These patients typically have mutations in the RUNX1 gene, FLT3, and KARS.

1.4 FLT3 and its relation to AML.

Fischer and Krebs published their famous work on protein phosphorylation and its regulatory function in cellular pathways in 1966[38]. Today, over 518 kinases capable of donating a phosphate group to a target protein have been identified[39].

A kinase is an enzyme capable of transferring a phosphate group from adenosine triphosphate (ATP) to a substrate, specifically to hydroxyl-containing substrates, like tyrosine and threonine. Depending on the substrates the kinase can phosphorylate, they can be further divided into three broad categories: protein kinases, lipid kinases, and carbohydrate kinases. Protein kinases can phosphorylate serine, threonine, tyrosine, and histidine. Once the substrates have been phosphorylated, they can trigger other signal transductions or act as an activated protein.

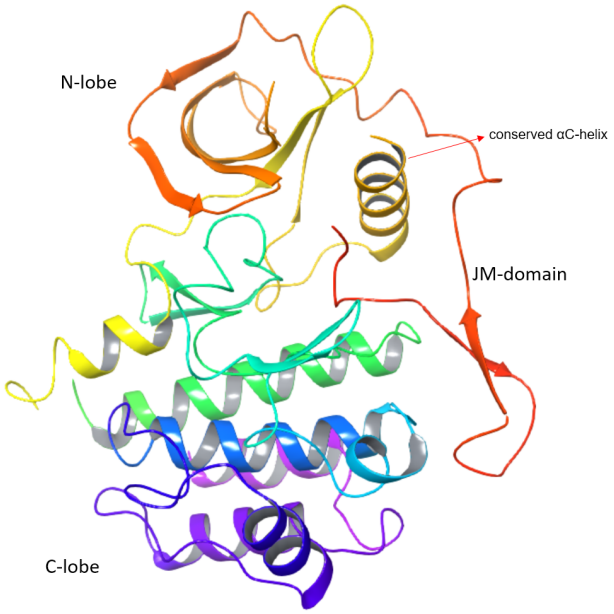

Figure 1-5. A cartoon structure of FLT3.

All receptor kinases share the same 3D-shape[40] and have a similar amino acid sequence; as a consequence, they have a highly similar internal architecture. From a structural point of view, protein kinases have a characteristic bi-lobal fold, consists of two main lobes, the N-terminal lobe (N-lobe) and the C-terminal lobe (C-lobe)[41]. The N-lobe contains five β strands (denoted as β1, β2, β3, β4, and β5) and a universally conserved αC-helix. The αC-helix has a Glycine-rich loop that can coordinate with the phosphate groups on an ATP molecule. On the other hand, the C-lobe is mainly helical and binds substrates. An ATP molecule is always bound to the deep cleft created by the two lobes. The activation loop connects both the N-lobe and C-lobe which plays a crucial role in the state of the kinase; whether it is in its on state or off state. The activation loop starts with a highly conserved amino acid sequence at the N terminus of the activation loop, the DFG-motif (Asp-Phe-Gly) which plays an import role in the regulation of kinase activity[42].

All the activated kinases show a highly conserved conformation, while inactivated kinases can pose different conformations. The difference in kinase conformation can be attributed to a different de-activation pathway. Protein kinases can adapt to the DFG-out conformation to partially de-activate its activity[43]. The pathway to activate protein kinases begins by binding of an exterior ligand, leading to homo-dimerization and followed by phosphorylation of the kinase activation loop which ultimately changes the conformation of protein kinase. However, there also protein phosphatases that can reverse phosphorylation and thus modulate biological activities[44]. The phosphorylation mechanism makes kinases a good

target to control biological activity. This can be done by altering the on or off state of the kinase which is critical for cell growth, differentiation, and death.

FLT3[45], also known as Fms-like tyrosine kinase 3[46], fetal liver kinase 2, or CD135[47] can be activated by an exterior FLT3 ligand which triggers a series of important signal transductions. This is vital for both the development and proliferation of hematopoietic stem cells and progenitor cells[48]. FLT3 is translated by the FLT3 gene which is located on chromosome 13q12.2[39].

As seen in other kinases, FLT3 has a highly conserved 3D shape and amino acid sequence. It has all the features of a receptor tyrosine kinase. FLT3 has three main domains: an extracellular domain (Five Immunoglobulin-like domains consisting of 541 amino acids), a transmembrane domain (21 amino acids), an intracellular domain which has a juxta-membrane domain and two kinase domains split by an inter-kinase insert [49](See **Figure 1-6**).

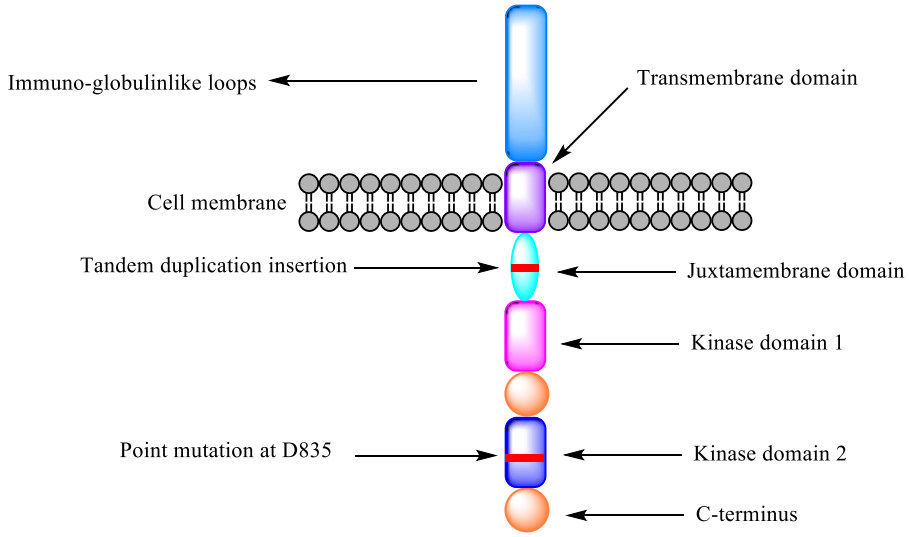

Figure 1-6. Detailed structure for FLT3, also showing positions that are often mutated (duplication in the juxtamembrane domain and mutation in the kinase domain).

The extracellular domain has an open horseshoe shape with five immunoglobulin-like domains (each consists of eight beta strands), denoted as D1 to D5. The natural FLT3 ligand binds to D3 Ig-like domain exclusively. Researchers purified glycosylated FLT3 (D1-D5), FLT3 (D1-D4) and FLT3 (D1-D3) with recombinant human FLT3 ligand in *E. coli*. The K_d for FLT3 (D1-D5) is 8.7nM; K_d for FLT3 (D1-D4) is 40nM; K_d for FLT3 (D1-D3) is 74.6nM.

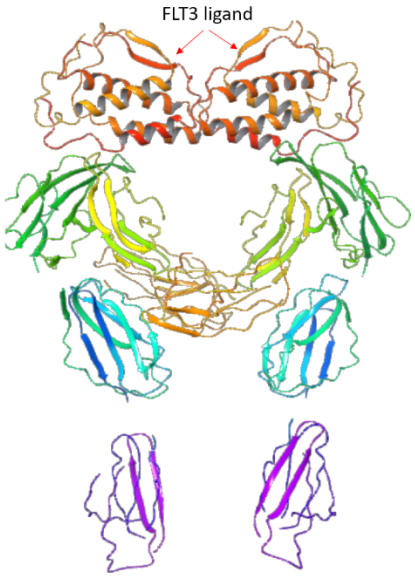

Figure 1-7. FLT3 ligand binds to D3 in extracellular domain of FLT3.

The linker that connects the juxta-membrane domain, and transmembrane domain is highly disordered. Researchers further divided the kinase domains of FLT3 into the N-lobe, C-lobe, and JM-domain[50].

The majority of the N-lobe is a five-stranded beta-sheet and a C-helix subdomain. In the N-lobe, a highly conserved GxGxxG sequence can be found[51]. This Glycine-rich loop which is important for ATP and magnesium binding. The C-helix has strong interactions with the JM-domain moiety which is important for FLT3 auto-inhibition. The C-lobe mainly consists of helices. Excluding the

outermost helices, all other helices are shielded from the solvent, and they serve as the protein/peptide binding domain.

The JM-domain and the activation loop connect the N-lobe and C-lobe. The activation loop is the most critical motif in FLT3 because it can allow ATP binding to the cleft created by N-lobe and C-lobe and it can also turn FLT3 on/off by altering the geometry of the lobes. The activation loop always starts with three highly conserved amino acid sequences Asp829-Phe830-Gly831, also called the DFG motif. When Asp829 points towards the ATP binding pocket, it is called the DFG-in conformation, while when Phe830 points to the ATP binding pocket, it is called the DFG-out conformation. Typically, the DFG-out conformation represents the auto-inhibited form of the kinase due to its catalytically incompetent state, but it will also create another allosteric pocket besides the general ATP binding pocket which makes it possible for selective kinase inhibitor to bind.

There is only one un-phosphorylated tyrosine residue in the activation loop, Tyr842, which is located almost in the middle of the activation loop. The hydroxyl group in Tyr842 points towards the ATP binding pocket and forms an important salt bridge with Asp811 and Arg834 in the side chain. The Juxta-membrane domain can be further divided into three subdomains according to their separate functions.

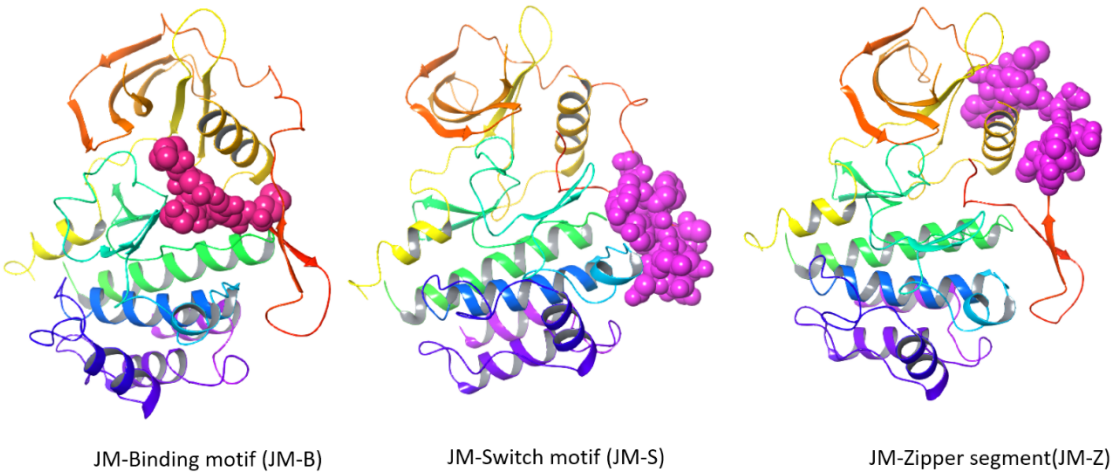

Figure 1-8. CPK representations of JM-B (Tyr572-Met578), JM-S (Val579-Val592), and JM-Z (Asp593-Trp603).

The juxta-membrane binding domain (JM-B domain) starts from Tyr572 and ends at Met578; it is a finger-like segment insert into space created by Glycine-rich loop, the activation loop, C-helix in the N-lobe (**Figure 1-8**). It appears as though JM-B domain has interactions with virtually all the important segments in the FLT3 kinase domain. The function of JM-B domain is to stabilize the inactive conformer of FLT3 by inserting into the space mentioned above as a wedge. As long as JM-B is in its correct orientation, one of two things occur. Either ATP cannot bind to the cleft created by N-lobe or C-lobe or the N-lobe and C-lobe are not in a catalytically-relevant distance which makes FLT3 inactive. Researchers have shown that the activation loop cannot fold to the fully open form, or even partially open when the JM-B domain is in its correct place.

The juxta-membrane switch motif (JM-S motif) is adjacent to the JM-B. JM-S has 14 residues; it forms a two-stranded beta-twist motif. The role for JM-S is to provide a rigid and correct orientation of the FLT3 kinase domain.

The juxta-membrane zipper motif (JM-Z) has only 11 residues and folds up above the N-lobe, especially the C-helix in N-lobe (**Figure 1-8**). The most frequent mutations in FLT3 has ITD (internal tandem duplications); this phenomenon happens in JM-Z domain as well. Once ITD occurs, it will disrupt the folding of JM-Z. This disrupts folding of JM-S and JM-B. This disruption does not allow interactions to occur between JM-B and important motifs in the N-lobe. Another effect this can cause is JM-B moves and eventually leads the constitutive activation of FLT3.

When endogenous FLT3 ligand (FL) binds to the D3 Ig-like domain in the extracellular domain of FLT3, FLT3 dimerizes in the juxta-positioning cytoplasmic domains. After transphosphorylation of tyrosine residues (Tyr589 and Tyr591) on the juxta-membrane domain, FLT3 becomes fully activated since the fully charged tyrosine residue cannot fold up in the original JM-S domain. Therefore, JM-B also cannot insert into the correct space that would make FLT3 active. However, in non-mutated FLT3, this process can be reversed by the tyrosine phosphatases via dephosphorylation of those tyrosine residues. This shuts down the activity of FLT3 kinase because the JM-S can fold into its original position and leads to the insertion of JM-B which in turn leads to the closure of the activation loop or decrease the space for ATP to bind.

In newly diagnosed AML patients, about 23% have FLT3-ITD mutation[52]. As discussed above, FLT3-ITD occurs in the JM-Z domain and leads to constitutively activated FLT3 signaling. The sequence length of FLT3-ITD varies from patient to patient, but replicates of three nucleotides are always present. This

does not interface the reading frame of FLT3. One experiment shows the longer the sequence of ITD (more than 40 nucleotides) the poorer the prognosis (13%-26% five-year survival rate in patients who have a nucleoside sequence shorter than 40 base pairs in ITD mutations).[53] Other experiments show that patients harboring shorter ITD sequences have worse the prognosis[54].

1.4.1 FLT3 signal transduction.

Once the FLT3 ligand binds to FLT3, homodimerization of FLT3 takes place, and auto-phosphorylation occurs in the activation loop which in turn fully activates the catalytic activity of FLT3. As a receptor tyrosine kinase, the phosphorylated form of FLT3 can be recognized by adapter proteins that have a Src Homology 2 (SH2) domain, such as growth factor receptor-bound protein2 (GRB2), GRB2 associated protein 1 (GAB1), son of sevenless homolog 1 (SOS), etc[48].

After activation of the adapter proteins, further downstream kinase cascades can be initiated. MAPK/ERK and PI3K/Akt/mTOR pathways are the main intracellular pathways that are activated by wild-type FLT3. Both of these two pathways lead to complex kinase cascades, further activation of downstream kinase activity, and regulation of transcription factors crucial for cell survival, or inhibition of apoptosis (**Figure 1-9**).

Mutated FLT3 pathway:

Large expression of wild type FLT3 can activate MAPK/ERK and PI3K/Akt/mTOR pathway. The mutated form of FLT3 has been shown to constitutively phosphorylate and activate Akt, which leads to constitutive activation of signal pathways. Cross talks between these pathways can further enlarge the

signal. As a consequence, mutated FLT3 will amplify signals, leading to abnormal cell growth and inhibit apoptosis, eventually lead to cancer[55].

Recent research shows that FLT3-ITD can directly activate the signal transducer and activator of transcription 5 (STAT5)[56] without the help of Janus kinase (JAK), presumably by their SH2 domain[57]. The activation of STAT5 will further lead to either homodimerization with another STAT5 or heterodimerization with other STATX via their SH2 domain. STAT5 can form complex with histone-lysine N-methyl methyltransferase enhancer of zester homolog 2 (EZH2). EZH2 acts as a transcriptional repression factor that is involved in histone methylation and a component of the Polycomb Repressive Complex 2 (PRC2) that plays a role in cell differentiation. STAT5 can also inhibit apoptosis by increasing the activity of B-cell lymphoma 2 (Bcl-2) via Bcl-2-associated death promoter (BAD) inactivation.

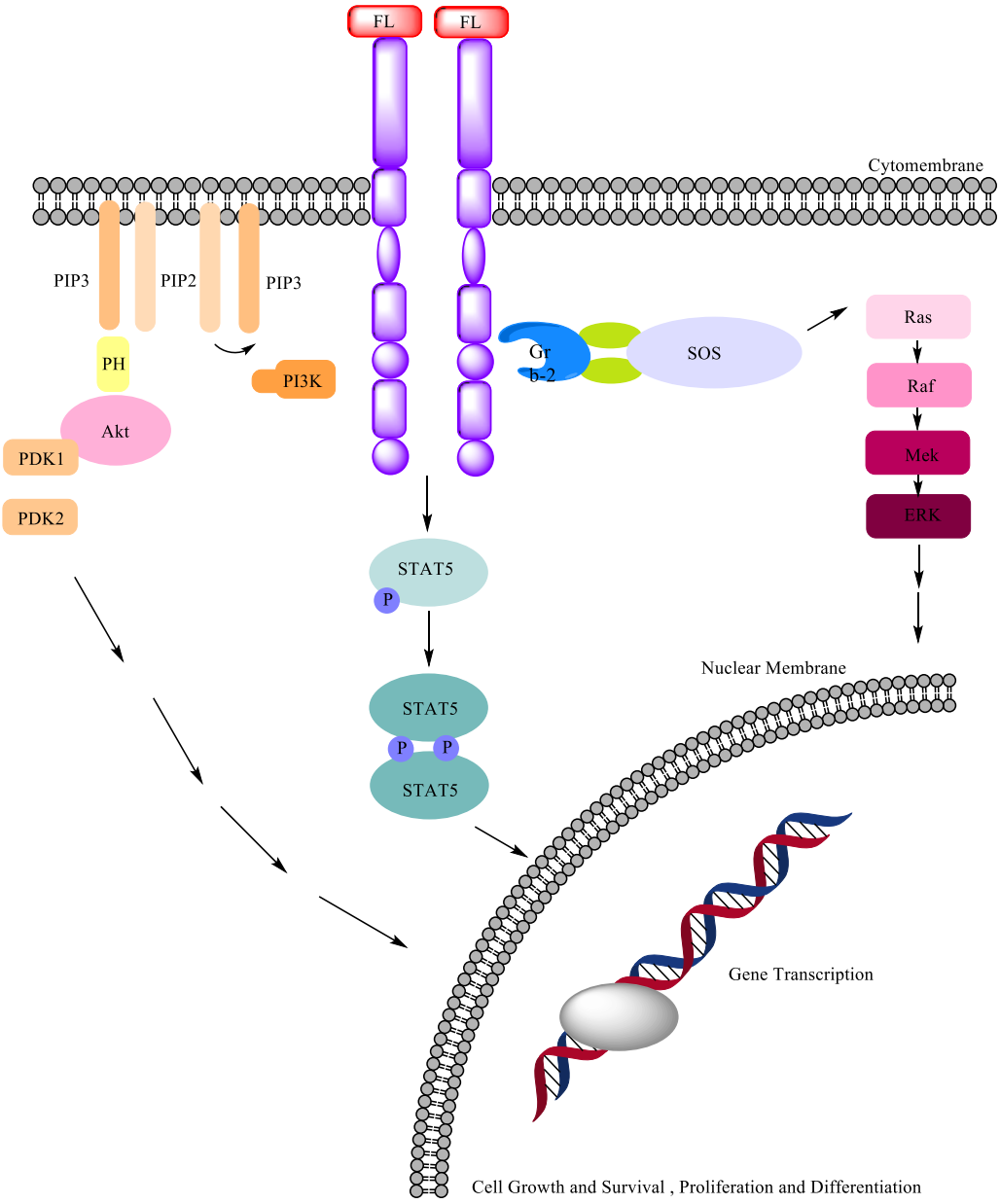

Figure 1-9. FLT3 signal transduction.

1.4.2 **MAPK/ERK pathway**[58].

MAPK/ERK (Ras-Raf-MEK-ERK) pathway, one of the best-studied signal transduction cascades plays important roles in cell differentiation. MAPKs act as a

signal relay or transmitter in MAPK/ERK pathway, they send the signal to downstream proteins or enlarge signals through multiple pathways.

MAPKs need to be activated before they can act as activated kinases in the signal transduction. The kinases that phosphorylate MAPKs are called mitogen-activated protein kinase kinase (MAP2K, also known as MEK, MAPKK). MAP2Ks show little kinase activity when they are not activated. Hence, MAP2Ks need to be phosphorylated by their upstream kinase, mitogen-activated protein kinase kinase kinase (MAP3K, also known as MEKK). MAP3Ks are serine/threonine-specific kinase, and the most famous MAP3Ks include RAF family.

There are three members in RAF MAP3k subfamily, a-Raf, b-Raf, and c-Raf. Little is known regarding a-Raf except scientists are aware they act as MAP3Ks. Unlike a-Raf, people have found strong correlations of cancers to mutated b-Raf[59]. Several b-Raf inhibitors have been approved by Food and Drug Administration (FDA) already. Sorafenib[60] is an inhibitor to both b-Raf and c-Raf to treat liver and kidney cancer while Vemurafenib[61] is for late-stage melanoma. Dabrafenib[62] is also a b-Raf inhibitor and currently in phase one and two clinical trials. More chemical entities are being investigated as b-Raf inhibitors. C-Raf is a member of MAP3Ks, and it is a proto-oncogene serine/threonine-specific protein kinase encoded by the human RAF1 gene[63]. Although c-Raf is the first member identified in Raf MAP3K subfamilies, more focus is on b-Raf due to high correlations to human cancers.

In the MAPK pathway, Raf acts as the downstream of Ras (GTPases). The most common oncogenes in human cancer are HRas, KRas, and NRas. KRas

mutations have been found in many human cancers, especially in leukemia, colorectal cancer, lung cancer and pancreatic cancer. Because of the high mutated rates in certain types of cancers, FDA also approved several KRAS tests to help physicians identify patients with the cancers mentioned above.

The MAPK pathway is initiated when an exterior ligand binds to receptor tyrosine kinase (RTK), this leads to homodimerization and activation of RTK. Once RTK is activated, it has at least one phosphoryl group on the residue. Growth factor receptor-bound protein 2(Grb2) will bind to the activated RTK via the SH2 domain. The SH2 domain is highly specific for the recognition of tyrosine phosphorylated sequences. Grb2 also binds to SOS (Son of Sevenless), a guanine nucleotide exchange factor via its two SH3 domains which in turn binds to proline-rich sequences specifically to form a Grb2-SOS complex, thus activating SOS. The activated SOS can then activate Ras, a GTPase, by exchanging its GDP for GTP. Subsequent activation of Raf (MAP3K) by Ras starts the MAPK pathway. Activated Raf will activate MEK (MAP2K) which in turn activates MAPK. Once MAPK is activated, further downstream pathways are activated such as, ribosomal protein S6 kinase (RSK), c-Myc, CREB or regulation of c-Fos gene begin. Although the exact function of ribosomal protein S6 is still being investigated, some studies showed this protein is involved in the regulation of cell proliferation.[64]

C-Myc is a regulator gene that codes for a short-life time transcription factor. The half-life Myc is 20 to 30 minutes[65], however, once c-Myc is mutated, many genes will become unregulated and result in uncontrolled cell proliferation[66].

Activated c-Fos will form a complex with c-jun (MAPK), this heterodimer Jun-Fos can binds to DNA and acts as a transcription factor.

1.4.3 PI3K/AKT/mTOR pathway[67].

Phosphatidylinositol-4, 5-bisphosphate 3-kinase (PI3K) is a lipid kinase and is critical for cell growth, proliferation, and differentiation[68]. PI3Ks can phosphorylate the inositol ring at three position. There are four main subclasses for PI3K divided mainly by their structures and substrate specificity. Once PI3Ks are activated, they will phosphorylate phosphatidylinositol, and the subsequent phospholipids will be recognized by Protein kinase B (Akt) via its Pleckstrin homology domain (PH domain)[69]. The PH domain is highly specific for phosphoinositide binding. Akt is a serine/threonine-specific protein kinase[70] that is often overexpressed in many cancers[71]. For example, both ovarian[72], pancreatic[73] and breast cancer[74] have Akt2 overexpressed. The main function of Akt is to inhibit the apoptotic process. Once Akt binds to phosphatidylinositol (3, 4, 5)-trisphosphate, it can be phosphorylated by the mechanistic target of rapamycin complex 2 (mTORC2).

Mechanistic target of rapamycin (mTOR, also named the mammalian target of rapamycin) is a PI3K-related kinase. The isolation of a natural product named rapamycin in the 1970s was found to arrest many cells in the G1 phase of the cell cycle. Currently, this natural product is being used as an immunosuppressant after organ transplantation[75]. Similar natural compounds were found in the 1980s, displaying similar features as rapamycin. This led to the discovery of mTOR as the mechanistic target of rapamycin in 1993. mTOR can form two completely different

complexes, mTORC1 and mTORC2 with distinct functions. mTORC1 mainly controls protein synthesis while mTORC2 can phosphorylate Akt thus affecting cell survival. However, both mTORC1 and mTORC2 can be inhibited by rapamycin like molecules. Once Atk is activated, it can translocate to the cytosol and nucleus and activate its substrate. Akt can inhibit transcription factors that are necessary for cell death and increase the transcription of anti-apoptotic genes. Akt inhibits Forkhead family transcription factors, FoxO1, FoxO3 and FoxO4 in the nucleus. FoxO4 is of particular interest because of its interactions with mouse double minute 2 homolog (MDM2), a negative regulator of tumor suppresser gene p53. Akt can degrade the Fox family protein via proteasome pathways thus suppressing p53-mediated apoptosis[76].

Akt can also phosphorylate MAK3K and start Ras-Raf-ERK pathway described in the above section. Akt can also activate BCL-2 or Caspase-9, both of which will eventually stop cells from dying.

1.5 Chemotherapy to treat AML.

As described in the previous section, during the 19th century, when people first observed abnormal blood disease, patients were treated with highly toxic mercury salts. Mercury salts had been long pursued as a generic drug to treat disease all over the world. After the treatment of mercury salts, patients seemed to recover from this “milky blood” disease. However, most patients died later from a severe relapse[11].

In the late 20th century, effective drugs were discovered to treat many diseases, including leukemia.

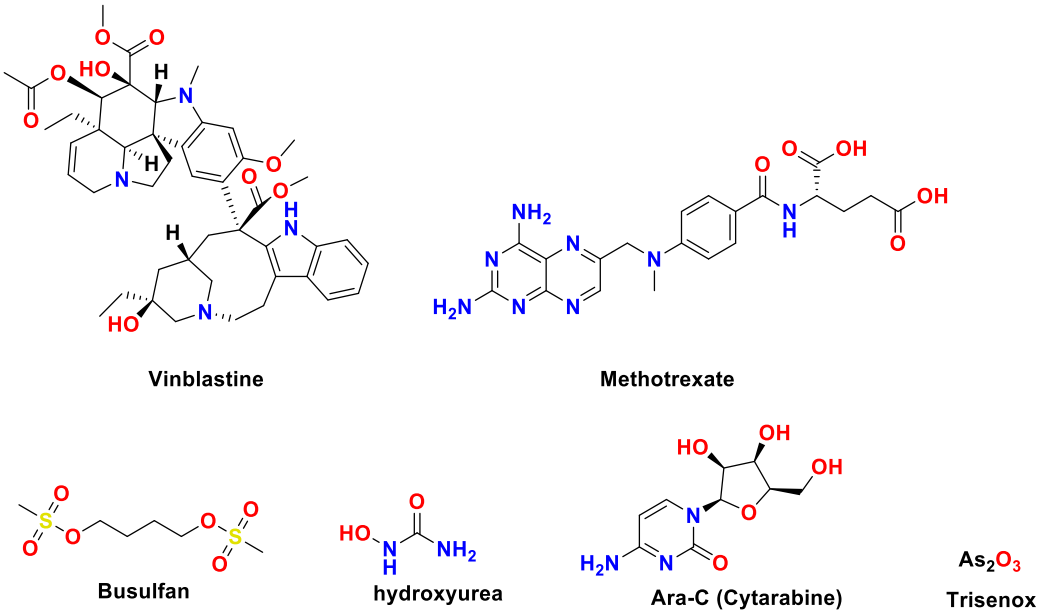

Figure 1-10. Chemical structures for classic anti-cancer reagents

Busulfan developed by GlaxoSmithKline in 1959 is an alkylating antineoplastic agent under the class of alkyl sulfonates[77]. The history of Busulfan dates back to mustard gas, which was used as a chemical weapon during World War I[78]. In 1943, scientists found the white blood cell count in survivors exposed to mustard gas was decreased dramatically. This lead to a study conducted at Yale University in 1942 by Goodman, Gilman, and others[79]. Although the results were highly variable, this lead to the discovery of Busulfan as an anti-leukemia agent. However, due to its high toxicity, hydroxyurea was developed by BMS and University of Chicago in 1969 as a ribonucleotide reductase inhibitor[80].

Despite the well-known toxicity related to arsenic trioxide[81], it has been used to treat acute promyelocytic leukemia (APL) when APL shows no response to the first-in-line agent, all-trans retinoic acid[82, 83]. Currently, except M3 AML, all other patients of AML subclasses are administrated a “7+3” therapy as first-line induction therapy. This consists of seven days of standard-dose cytarabine and

three days of daunorubicin (idarubicin, mitoxantrone can be used to substituted daunorubicin if needed)[84].

On the other hand, M3 AML patients will typically be treated with Tretinoin (all-trans retinoic acid, ATRA) and/or arsenic trioxide. The mechanism of ATRA is not completely clear at the current moment. It either forces the cancerous cells to differentiate into normal cells or stops them from proliferating[85].

Drug	Dose	Mode	Days
Cytarabine	100-200 mg/m^2	IV over 24 hours	Days 1-7
Daunorubicin	*60-90 mg/m^2*	*IV bolus*	*Days 1-3*
Idarubicin	*12 mg/m^2*	*IV bolus*	*Days 1-3*
Mitoxantrone	*7 mg/m^2*	*IV infusion*	*Days 1, 3, 5*

Table 1-6. Dosage of selected anti-cancer agents recommended by National Comprehensive Cancer Network (NCCN).

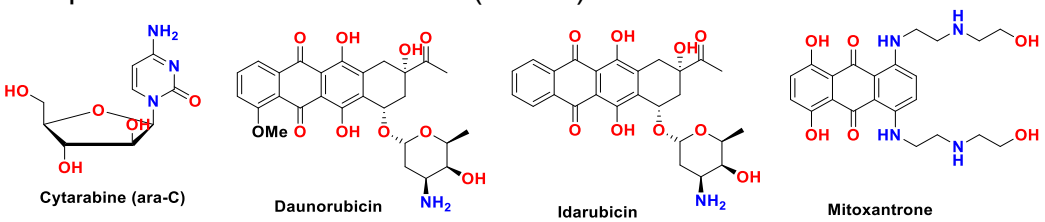

Figure 1-11. More chemical structures for classic anti-cancer reagents.

Ara-C combines a cytosine base with an arabinose sugar instead of deoxyribose in human DNA. Hence, the structure of ara-C mimics cytosine deoxyribose and can be incorporated into human DNA. The epimeric 2'-hydroxyl group on ara-C makes it conformationally different from normal cytosine. As a result, it will eventually kill cells because it cannot be used as a building block in cell development. Ara-C also inhibits both DNA and RNA polymerases and nucleotide reductase enzymes needed for DNA synthesis[86].

Mechanism of Anthracycline Antibiotics[87]:

Both daunorubicin, idarubicin, and mitoxantrone belong to the anthracycline antibiotics family. Daunorubicin was first isolated in 1963 from Streptomyces, the largest genus of Actinobacteria[88]. Daunorubicin stabilizes the topoisomerase II complex[89], and the DNA chain breaks during replication, thus prevents DNA double helix from recombining and shut down the replication. Idarubicin is an analog of daunorubicin. They have a similar mechanism of action and idarubicin poses better lipophilicity and permeability due to lack of the methoxy group, suitable for IV bolus.

1.6 Targeted-Drug for leukemia.

The drugs described previously destroy both healthy cells and cancer cells indiscriminately. These drugs are effective because cancer cells divide quicker than normal cells, so the effect of the drugs on cancer cells is more than on normal cells. This is usually referred as the carpet bombing method in cancer chemotherapy.

This carpet bomb will destroy any cells present in the body, causing patients severe side effects such as, hair loss and weakness because the active dividing hair follicle cells or body immune cells are destroyed by those drugs. Due to the disadvantage of these traditional anti-cancer agents, there is a search for a more precise way to kill cancer cells, usually referred to as targeted therapy. Targeted therapy will specifically attack cancer cells and the toxicity to health cells is reduced. This will enhance the living quality of those cancer patients. This is referred to as precision bombing method in cancer chemotherapy.

1.6.1 FDA approved kinase inhibitor.

Kinases are important for regulating cell growth, cell division, differentiation and death. If a small molecule that can stop the kinase from being turned on can be found, then the downstream signal transduction could be interrupted. Utilizing small molecules to block the abnormal signal transduction that is crucial to cancer development is a promising therapy. These inhibitors can compete with ATP, resulting in the failure of kinase autophosphorylation.

After the approval of Imatinib in 2001[90], there has been an increase in the number of approved kinase inhibitors every year.[91]. Kinases, specifically receptor tyrosine kinases, play such a vital role in signal transduction and initiate signaling pathway related to cell proliferation. In the late 1980s, inhibitors against epidermal growth factor receptor (EGFR) were found via screening of a broad array of compounds. The main finding was that certain quinolone containing molecules were good candidates for EGFR inhibition[92].

At the start of 2011, a huge explosion in kinase inhibitor approval by the FDA began. Six kinase inhibitor drugs were approved in 2011[91]. There are now 34 kinase inhibitors that have been approved by FDA as of July 2017 (**Figure 1-12**).

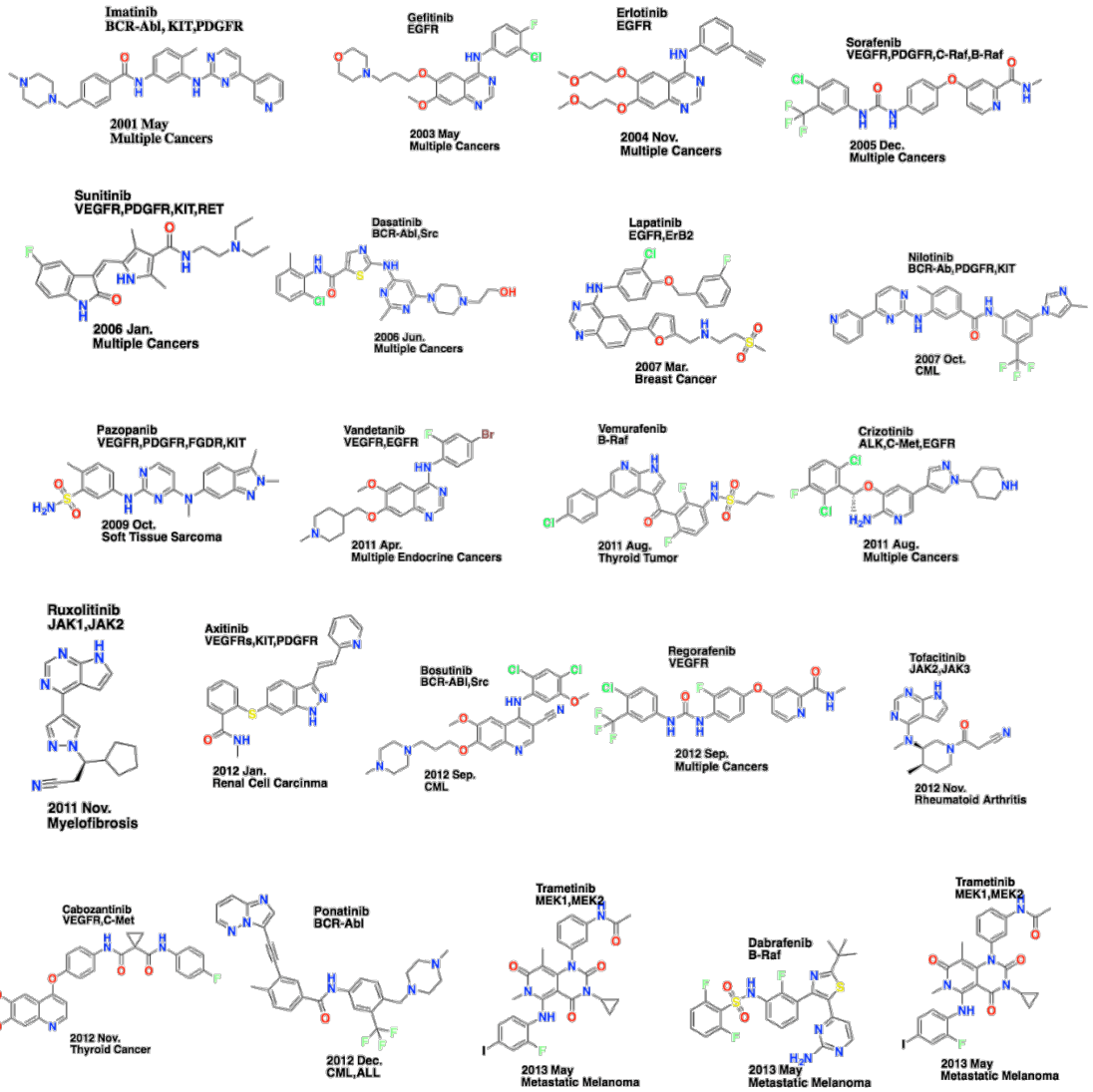
Imatinib
BCR-Abl, KIT,PDGFR
2001 May
Multiple Cancers
Gefitinib
EGFR
2003 May
Multiple Cancers
Erlotinib
EGFR
2004 Nov.
Multiple Cancers
Sorafenib
VEGFR,PDGFR,C-Raf,B-Raf
2005 Dec.
Multiple Cancers
Sunitinib
VEGFR,PDGFR,KIT,RET
2006 Jan.
Multiple Cancers
Dasatinib
BCR-Abl,Src
2006 Jun.
Multiple Cancers
Lapatinib
EGFR,ErB2
2007 Mar.
Breast Cancer
Nilotinib
BCR-Ab,PDGFR,KIT
2007 Oct.
CML
Pazopanib
VEGFR,PDGFR,FGDR,KIT
2009 Oct.
Soft Tissue Sarcoma
Vandetanib
VEGFR,EGFR
2011 Apr.
Multiple Endocrine Cancers
Vemurafenib
B-Raf
2011 Aug.
Thyroid Tumor
Crizotinib
ALK,C-Met,EGFR
2011 Aug.
Multiple Cancers
Ruxolitinib
JAK1,JAK2
2011 Nov.
Myelofibrosis
Axitinib
VEGFRs,KIT,PDGFR
2012 Jan.
Renal Cell Carcinma
Bosutinib
BCR-ABl,Src
2012 Sep.
CML
Regorafenib
VEGFR
2012 Sep.
Multiple Cancers
Tofacitinib
JAK2,JAK3
2012 Nov.
Rheumatoid Arthritis
Cabozantinib
VEGFR,C-Met
2012 Nov.
Thyroid Cancer
Ponatinib
BCR-Abl
2012 Dec.
CML,ALL
Trametinib
MEK1,MEK2
2013 May
Metastatic Melanoma
Dabrafenib
B-Raf
2013 May
Metastatic Melanoma
Trametinib
MEK1,MEK2
2013 May
Metastatic Melanoma

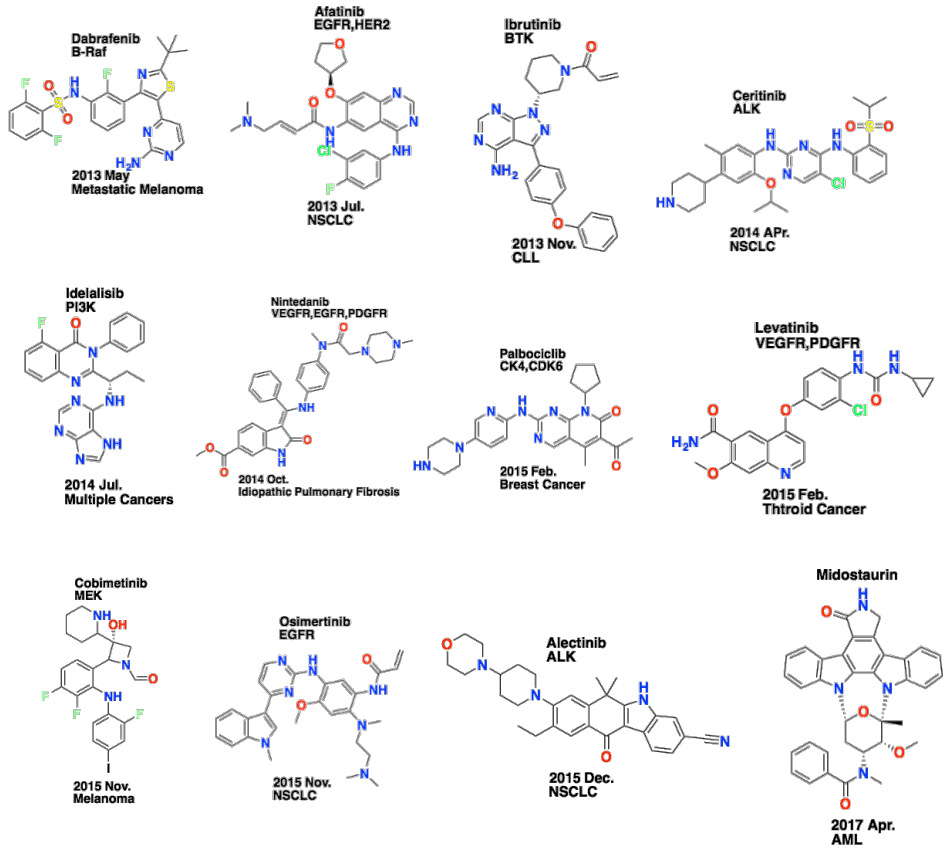

Figure 1-12. All receptor tyrosine kinase inhibitors approved by U.S. FDA till July 2017.

1.6.2 Gleevec (Imatinib) and Iclusig (Ponatinib).

Imatinib was the first orally available kinase inhibitor approved[93]. Imatinib combats CML and ALL. The approval of Imatinib initated a new era for targeted therapy[90].The discovery of the Philadelphia chromosome in 1959[94], subsequent elucidation of the mechanism of this abnormal translocation chromosome in 1973 and it's relation to certain subtypes of leukemia in the late 1980s paved the way for Imatinib. In early 1990, the search for the inhibitor of Bcr-Abl kinase began since it was found that Bcr-Abl fusion gene was the only cause

for CML. However, it took another 30 years for a drug to be discovered for this type of chromosome abnormality.

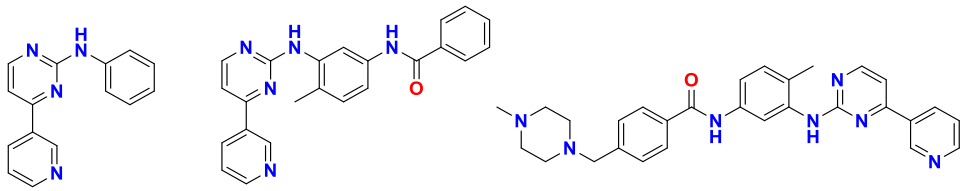

Figure 1-13. The development of Imatinib.

Phenylamino-pyrimidine was identified (HTS hit) as a potent inhibitor of BCR-ABL1. Further SAR optimization of this hit compound led to a more potent compound, CGP 53716 which contains a flag methyl group and an amide instead of aromatic aniline. The methyl group provides profound activity (3-fold increase) compared to the parent compound without a methyl group. Furthermore, the change from aromatic aniline to amide also increased the potency, selectivity and reduced the toxicity of this compound. However, CGP 53716 only displayed an IC_{50} of 1.5 μM against v-Abl. Addition of a piperazine ring onto the lead molecule increased the potency to 38 nM against v-Abl. About 20% of CML patients will eventually develop resistance against Imatinib within three years. However, Dasatinib and Sunitinib, second-line drugs used after resistance for Imatinib has occurred. Imatinib is of great importance, before this drug people diagnosed with CML were basically given a death sentence. Imatinib was the first drug to cure a cancer thought to be incurable.

Iclusig (Ponatinib)[95]:

About 30% of CML patients eventually develop resistance against Imatinib therapy[96]. Ponatinib, previously known as AP24534, is the second generation

kinase inhibitor for CML. More resources are being put onto the research to develop new kinase inhibitors for secondary mutations in Bcr-Abl at T315, especially the T315I mutation[97]. Ponatinib was designed by using a computational assisted drug discovery platform with the aim to inhibit Bcr-Abl and the secondary mutation T315I in Bcr-Abl which is resistant to first generation CML drug Imatinib[98]. Ponatinib was first approved by the FDA in December 14th, 2012 for Ph+ ALL and resistant CML under the accelerated approval program[99]. Ponatinib got full approval in 2016. However, this drug has a black box warning due to some severe adverse effects[100].

1.6.3 Midostaurin (Rydapt)[101].

Midostaurin is a derivative from the natural product staurosporine which was isolated from the bacterium *Streptomyces staurosporeus* in 1977. From a chemical structure point of view, those compounds belong to the indolocarbazole family which is the subclass of bis-indoles family. Staurosporine can inhibit almost all human kinases and a simple acylation leads to Midostaurin making it selective, albeit it still inhibits many kinases. Initially, Midostaurin was identified as a highly effective protein kinase C inhibitor[102], however, research later found data to disprove this. Later, it was found to be a good FLT3 inhibitor[103]. Midostaurin accelerated approval was granted by the FDA in May 2017 under the brand name Rydapt for newly dragonized AML with FLT3 mutations[104]. The recommended dose of Rydapt with AML is 50 mg orally twice daily at approximately 12 hours intervals on days eight to twenty-one of each cycle of induction with cytarabine and daunorubicin[105]. Since Rydapt is a multikinase inhibitor, side effects for Rydapt

include nausea, radiation mucositis, stomatitis, laryngeal pain vomiting, hemorrhoids, febrile neutropenia, petechiae, headache, back/bone/laryngeal pain, arthralgia, epistaxis, device-related infection, nasopharyngitis, sinusitis, hyperglycemia, hyperhidrosis, blood creatinine increased, renal failure, acute kidney injury and insomnia.

1.6.4 FLT3 kinase inhibitors.

There is an urgent need to find novel anti-AML therapeutic agents, however, due to the heterogeneity of AML, a monotherapy regimen is always associated with resistance after the initial treatment. Phase I/II clinical studies of FLT3 inhibitors as monotherapy in AML patients often showed partial and transient clinical response, followed by drug resistance developed after the initial treatment.

The signal transduction initiated by FLT3 can be interrupted by small molecule inhibitors. These inhibitors are either ATP competitive or non-ATP competitive inhibitors according to their binding mechanism. Non-ATP competitive inhibitors can be further divided into type I and II inhibitors. Type I inhibitors, the “DFG-in” inhibitors, compete with ATP in the ATP binding site while Type II inhibitors, the “DFG-out” inhibitors, compete partially in the ATP binding site and also extend to an adjacent hydrophobic pocket. This hydrophobic pocket can only be accessed in the inactive FLT3 form. Most FLT3 inhibitors developed so far fall into Type II inhibitors. However, Type II inhibitors are more prone to have tyrosine kinase domain secondary mutations which will decrease activities of these inhibitors.

Mechanism of FLT3 resistance by using single FLT3 agent:

The FLT3 kinase inhibitors can be divided into two main generations. The first generation FLT3 inhibitors are normally non-specific. These FLT3 inhibitors may also inhibit other important kinases as well. The inhibition of important kinases, such as c-Kit, VEGFR, FGFR may cause severe side effects. AML patients administrated with these FLT3 inhibitors may have vomiting, bone pain, headache and acute kidney damage due to the inhibition of these important kinases. Later, second generation FLT3 inhibitors were developed with the aim to specifically target FLT3 to lower side effects. However, drug resistance typically emerged within several months.

A highly selective FLT3 kinase inhibitor, such as Quizartinib, typically showed good tolerability than pan-FLT3 kinase inhibitor. Despite that, responses to Quizartinib are typically transient due to the acquired resistance in AML patients. The proposed mechanisms of resistance include the acquisition of point mutations in the ATP binding site in the tyrosine kinase domain of FLT3, increased expression of native FLT3 ligands and the activation of downstream signal transduction, including PI3K/AKT/mTOR and STAT5 pathways.

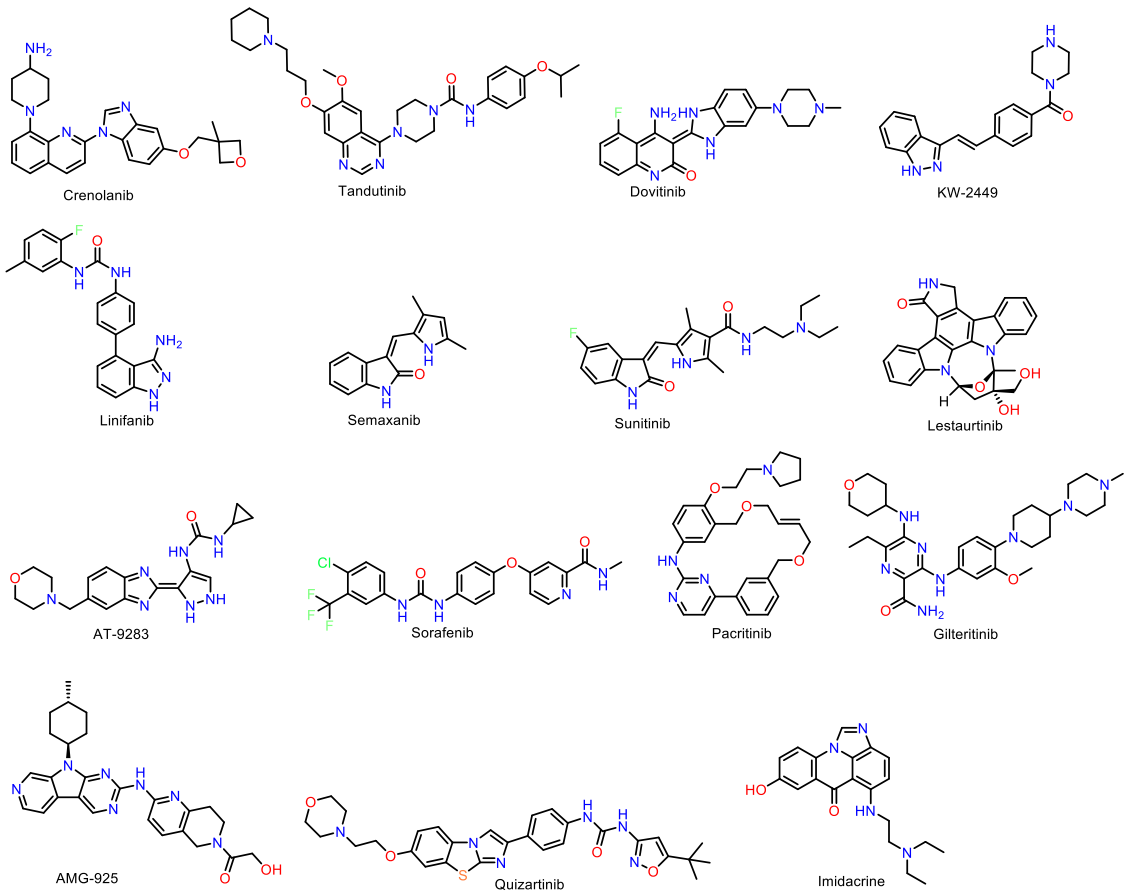

Figure 1-14. Structures of selected FLT3 kinase inhibitors.

Currently, there are more than 20 small molecule FLT3 inhibitors that are being investigated at different phases in clinical trials (See Figure **1-14**). Sunitinib is a multitargeted TKI that is used for treating renal cell carcinoma and imatinib-resistant gastrointestinal tumors. Because Sunitinib also can inhibit PDGFR and c-Kit, it showed significant toxicities as a single agent to treat AML in a phase I study. In phase I/II trials, it also showed prolonged hepatotoxicity, hand-foot syndrome, and incomplete hematological recovery rate.

Lestaurtinib[106], a semi-synthetic analog of staurosporine, inhibits FLT3, JAK2, and Trk. In phase II clinical trial, Lestaurtinib was used as monotherapy in

previously untreated old AML patients with either wild-type or mutated FLT3 for eight weeks. However, only partial remission was achieved and no overall survival rate difference was observed compared with the control arm.

Quizartinib[107], a second-generation FLT3 inhibitor, is active against AML with either PDGFR or c-KIT mutations. In phase II studies, Quizartinib was used as a single agent for patients with relapsed and refractory AML. Despite the promising response rates at around 60%, grade 3 QTc prolongation was observed. Currently, researchers are focusing on to study Quizartinib in combination with standard of care induction or consolidation chemotherapy and as maintenance therapy in newly diagnosed patients with FLT3-ITD mutated AML.

Sorafenib[108], a multitargeted kinase inhibitor approved for the treatment of hepatocellular carcinoma and renal cell carcinoma, also inhibits FLT3. When Sorafenib is used combined with idarubicin, the overall CR rates are around 75% to 92% in patients with mutated FLT3. In another Phase II study, Sorafenib showed high CR rates when used as a single agent and over 50% of the patients had complete eradication of FLT3-mutated clones. However, 55% of patients relapsed after 9 months treatment.

Gilteritinib[109], a second generation FLT3 kinase inhibitor, selectively inhibit both FLT3 and AXL. Higher drug doses of Gilteritinib showed a favorable safety profile and promising results in a phase I/II trial in FLT3-mutated relapsed AML. Currently, Gilteritinib is being investigated under different phase III trials in comparison to other salvage regimens and shows consistent FLT3 inhibition in relapsed or refractory AML. The maximum-tolerated dose of Gilteritinib was 300

mg daily. Gilteritinib also received FDA fast-track designation for AML in October 2017.

Crenolanib[110], a pan-selective FLT3 kinase inhibitor, may bypass the resistance caused by TKD mutations. It also received FDA fast-track designation in relapsed or refractory FLT3-positive AML in December 2017. Crenolanib is well tolerant at maximal doses in combination with the standard "7+3" induction. Currently, it is being investigated in a multicenter, randomized, double-blinded phase III trial. The preliminary results are better than the Rydapt trial results that eventually led to the approval of Rydapt.

Compound	FLT3 IC_{50} (nM)	Trial Phase	Other Targets
Crenolanib	3	II	PDGFR, c-Kit
Tandutinib	220	II	PDGFR, c-Kit
Dovitinib	1	III	VEGFR, PDGFR, c-Kit
KW-2449	6.6	II (discontinued)	Aurora, Abl, FGFR1
Linifanib	5	III	VEGFR,ERK,STAT5,PDGFR
Semaxanib	100	II	VEGFR, HGFR
Sunitinib	2.7	Launched	VEGFR, Kit, Ret, PDGFR
Lestautinib	3	II/III	JAK2, Trk
AT-9283	10	I	Aurora, Bcr-Abl, JAK
Sorafenib	32.6	Launched	VEGFR, PDGFR, Kit, Ret
Pacritinib	22	II	JAK2, CDK2
AMG-925	<1	I	CDK
Quizartinib	0.2	III	Ret, Kit
Imidacrine	8	II (discontinued)	VEGF

Table 1-7. FLT3 kinase inhibitors that are currently being investigated in different clinical trials.

Table **1-7** shows FLT3 kinase inhibitors that are currently being investigated in clinical trials. Quizartinib shows the best IC_{50} of 0.2 nM against FLT3. It also inhibit Ret and Kit. Targeting other kinase important to AML together with FLT3 is

a promising approach. Rydapt was approved by FDA in 2017 combined with cytarabine and daunorubicin to treat AML. Particularly, Rydapt is not indicated as a single agent induction therapy for the treatment of AML patients as mentioned in the official prescribing information. Besides Rydapt, all the other FLT3 kinase inhibitors showed in **Figure 1-14** are either pan-kinase inhibitors or FLT3 kinase inhibitors specifically for FLT3 and other important kinase, such as c-Kit, VEGFR, FGFR, etc. It is already known that the inhibition of other important kinases will cause severe side effects. However, highly selective FLT3 kinase inhibitors, such as Quizartinib, also showed higher rates of resistance when administrated alone due the acquired TKD mutations. The acquired TKD mutations will decrease the affinity for those FLT3-specific kinase inhibitors. Hence, it is highly desired to develop FLT3 kinase inhibitors that are both active for FLT3 and FLT3-releated kinases that are important for FLT3. In recent years, people have begun to pursue such strategies to develop dual FLT3 inhibitors.

Currently, only a handful of dual FLT3 kinase inhibitors have been developed. Koyama *et. al* developed dual HCK and FLT3 inhibitors and evaluated the synthesized pyrrolo[2,3-d]pyrimidines in viability studies with MV4-11 cell lines[111]. Hematopoietic cell kinase (HCK) is a non-receptor tyrosine kinase in the Src family and is highly expressed in AML stem cells. The best compound shows 5 nM IC_{50} against FLT3-ITD, 13 nM IC_{50} against HCK and 18 nM IC_{50} against MV4-11.

Hsieh *et. al*[112] developed dual AURK and FLT3 kinase inhibitors. AURK belongs to the serine and threonine kinase family and is important to mitosis. AURK serves as a biomarker for AML patients.

Smithgall *et. al*[113] developed dual Fes and FLT3 kinase inhibitors. Feline sarcoma oncogene is the downstream kinase in the FLT3 signal transduction. Fes has interaction with BCAR1 and is involved acute promyelocytic leukemia as well as in normal hematopoiesis

Advantages of dual FLT3 kinase inhibitor:

Pan-FLT3 kinase inhibitors normally have more side effects compared to the second generation, more specific FLT3 inhibitors. However, for these specific FLT3 inhibitors, resistance typically emerged after the initial treatment. Based on these reasons, dual FLT3 kinase inhibitors that can inhibit both FLT3 and one other kinase closely related to FLT3 is highly desired.

Researchers already showed the Src family kinase Lyn is expressed in multiple myeloid leukemia cell lines[114]. Src family has eight non-receptor tyrosine kinases, such as Hck and Fyn, and they have also been implicated in leukemic cell signal transduction. In leukemic blasts isolated from AML patients, the activity of Lyn kinase is high. The overexpression of Lyn is also linked to Imatinib resistance in CML patients. Recently, Duyster further confirmed Src is a signaling mediator in FLT3-ITD positive AML[115]. They found STAT5 pathway can be blocked after the knockdown of SRC and proved FLT3-ITD activates STAT5 via SRC. Recently, Ronnstrand also observed the overexpression of LCK, one member in SRC family, leads to the constitutively activation of FLT3-ITD[116].

They also provided strong evidence that LCK can cooperate with STAT5. Thus, Src is a promising target for anti-AML drug discovery.

Secondary mutations of FLT3 kinase:

	Rydapt	Ponatinib	Lestaurtinib	Linifanib	Quizartinib	Sunitinib	Sorafenib	Crenolanib	KW2449
FLT3-ITD	9.3	<1.0	8.6	2.4	1.2	5.4	18.5	57.0	41.0
D835Y	10.0	92.0	9.8	>100	>100	>100	>2000	58.0	>200
D835A	5.0	148.2	5.0	>200	>200	>200	>200.0	78.1	62.0
D835G	7.9	<1.0	6.0	8.6	9.0	48.1	34.5	110	56.0
D835N	8.4	<1.0	7.6	10.3	7.2	46.4	31.6	80.0	58.3
D835L+K	1.0	>1000	2.1	>200	>200	>200	>200	>1000	>200

Table 1-8. Proliferation IC_{50} (nM) of FLT3 against different FLT3 mutants.

Table 1-8 shows IC_{50} of selected FLT3 kinase inhibitors that are currently being investigated in clinical trials against different FLT3 secondary mutations. Quizartinib shows the best inhibition for FLT-ITD but it fails to inhibit D835Y/A/L+K. Sunitinib, Sorafenib, and Crenolanib also fail to inhibit specific secondary mutations in FLT3. The response of TKI therapy to AML only last for 3 to 6 months due to the emergence of resistance[117]. The major mutation in the receptor tyrosine kinase FLT3 is in the ATP binding region of the kinase domain, leading to the alteration of the conformational state and thus weakening the binding affinity to specific FLT3 inhibitors. The FLT3 activation loop residue mutations are D835V/Y/F/H, D839G, and Y842C/H while the FLT3 gatekeeper residue mutation is F691L/I[118]. D835V/F/H and gatekeeper F691L mutations confer acquired clinical resistance to Quizartinib while D835V/Y/F and gatekeeper F691L mutations are detected at the time of resistance of Sorafenib. These secondary mutations in the kinase domain region hampered the ability of small molecule FLT3 inhibitors to adequately bind and inhibit the kinase activity in two major ways.

These mutations will create a steric clash with the kinase inhibitor, leading to decreased binding affinity or remove the favorable hydrophobic contacts, leading to the destabilization of the conformation of the hinge segment. Researchers have shown that the D835 secondary mutations are the most common mutations for the emergence of FLT3 TKI therapy resistance found in clinical[119]. D835 mutations will induce an active “DFG-in” kinase conformation which is unfavorable for type II kinase inhibitors[120], such as Sorafenib, Quizartinib, and Ponatinib to bind. D835/Y/V/F are bulky hydrophobic amino acid residues. They are predicted to be sterically incompatible with the short a-helix, shifting the equilibrium to the active DFG-in conformation and thus preventing type II TKI’s binding. Researchers also showed patients only have these secondary mutations after several months’ therapy of Quizartinib, indicating the resistance is due to novel mutations occurring during the therapy rather than selective expansion of a preexisting clone under the pressure of FLT3 inhibitor therapy[121].

The goal of this work is to discover and provide novel chemical entities that are active against FLT3 especially FLT3 secondary mutations, a driver kinase for acute myeloid leukemia. Dual FLT3 kinase inhibitor strategy was pursued to develop such kinase inhibitors. After validation of enzymatic activity, further cell-based assay was used to determine the actual cellular activity.

Chapter 2. Identification of new amidine-acetylene-isoquinoline conjugates as FLT3 inhibitors that potently inhibit AML cell lines

2.1 Background.

The Sintim group had previously discovered that azo containing 3-aminoisoquinolines were FLT3 inhibitors [122, 123]. However, it is known that azo groups are not ideal to incorporate into drugs because they can be readily reduced into toxic aromatic amines. A few members of the Sintim group had therefore tried to replace the azo group with other mimics, such as an alkyne group. However only a few alkyne amino isoquinoline amidines had been synthesized (see **2-3** in **Figure 2-1**) and good coupling protocols that gave good yields of alkyne amidines had not been identified.

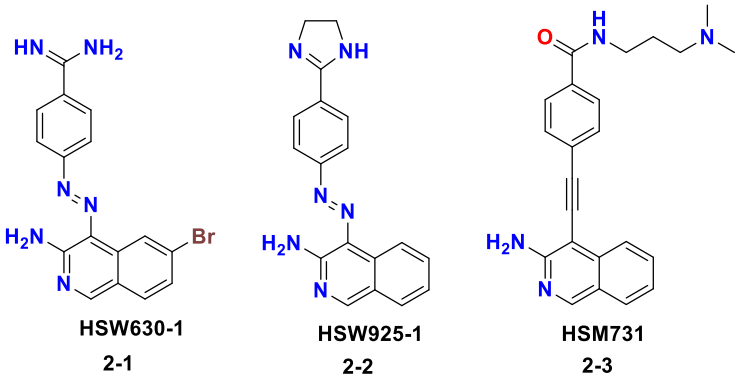

Figure 2-1. Azo molecules identified by previous lab members. **2-3**, an example to replace the azo group with a stable alkyne liner.

2.2 Chemical synthesis of amidine-acetylene-isoquinoline conjugates.

Retrosynthetically, it was decided a library of 4-amidine containing acetylenes would be synthesized via imine formation of 4-ethynylbenzaldehyde with different substituted 1, 2-diamine substrates followed by iodine mediated oxidative ring closure. Subsequent Sonogashira cross-coupling of the 4-amidine containing acetylenes prepared above with 6-chloro-4-iodo-isoquinoline-3-amine (obtained directly from iodine induced electrophilic iodination of 6-chloroisoquinoline) (**Scheme 2-1**) gave the anticipated analog. The starting material is commercially available and can also be constructed from simple and cheap substituted benzyl amine and 2, 2-diacetyl acetonitrile (**Figure 2-2**).

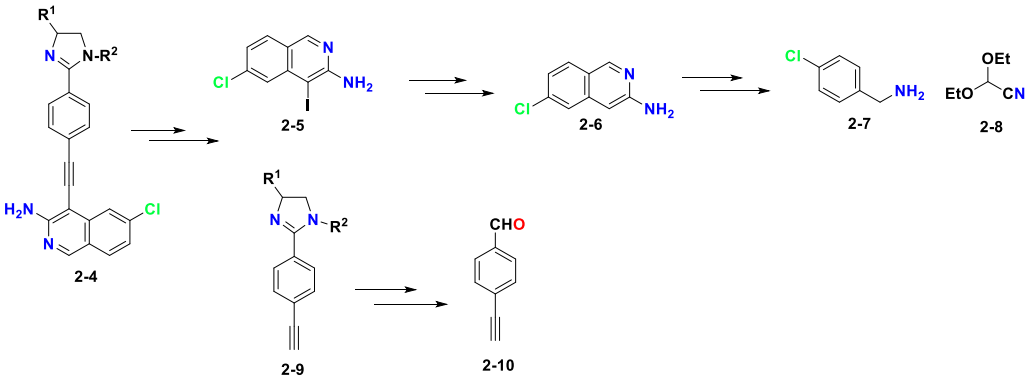

Figure 2-2. Retrosynthesis of amidine-acetylene-isoquinoline conjugates from simple commercially available starting materials.

2.2.1 Iodinated isoquinoline-3-amine synthesis.

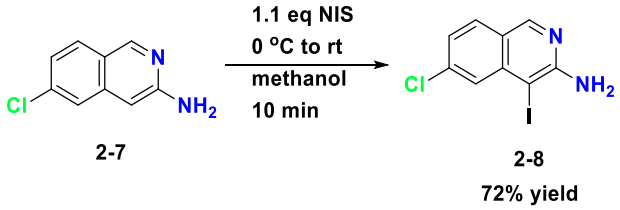

Scheme 2-1. Iodination of 6-chloroisoquinoline-3-amine with NIS.

6-chloro-4-iodoisoquinolin-3-amine is synthesized from 6-chloroisoquinoline-3-amine with an excess of NIS (N-iodosuccinimide) in methanol at 0 °C and subsequently warming of the reaction mixture to room temperature. The iodination of isoquinoline-3-amine is fast, and the reaction is complete within 10 minutes according to TLC (in 100% DCM). Prolonging the reaction time or quenching the reaction with water greatly affected the reaction yield. The reaction was evaporated to dryness under reduced pressure, then desired compound was purified by flash column with a good yield (average 72% yield based on three runs). The iodinated compound is stable for at least six months when shielded it from light.

2.2.2 Amidine head group formation.

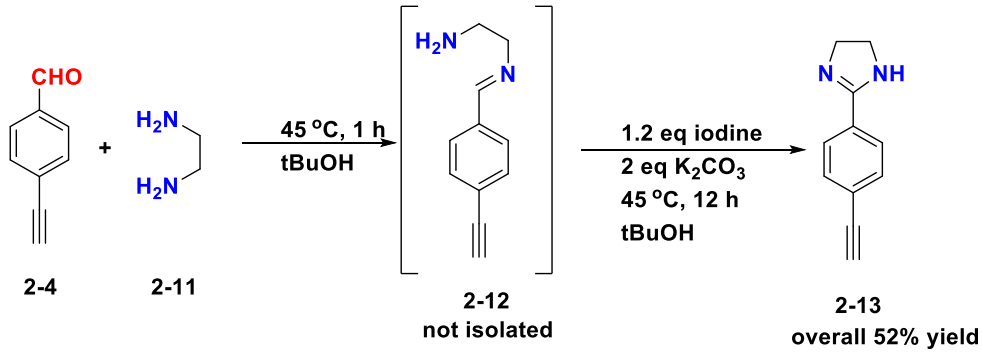

Scheme 2-2. Amidine head group synthesis using imine formation, nucleophilic ring closure onto the imine and subsequent iodine-induced oxidation.

The requisite acetylene containing aromatic amidine head group, 2-(4-ethynylphenyl)-4, 5-dihydro-1*H*-imidazole **2-13** is synthesized via a two-step one-pot synthesis from 4-ethynylbenzaldehyde **2-4**. Stirring equal equivalents of 4-ethynylbenzaldehyde **2-4** with ethane-1, 2-diamine **2-11** in *tert*-butyl alcohol at 45 ^{o}C for 1 hour gave the imine intermediate **2-12**. Subsequent addition iodine solid (1.2 eq.) followed by potassium carbonate (2 eq.) led to the oxidative cyclization of the imine intermediate. TLC showed the reaction was complete within 10 hours. To quench the reaction, water was added to the reaction mixture and extracted with ethyl acetate three times, finally, ethyl acetate was removed under reduced pressure and flash column purification gave the desired amidine head group **2-13** with (**Scheme 2-2**) 52% yield as beige solid.

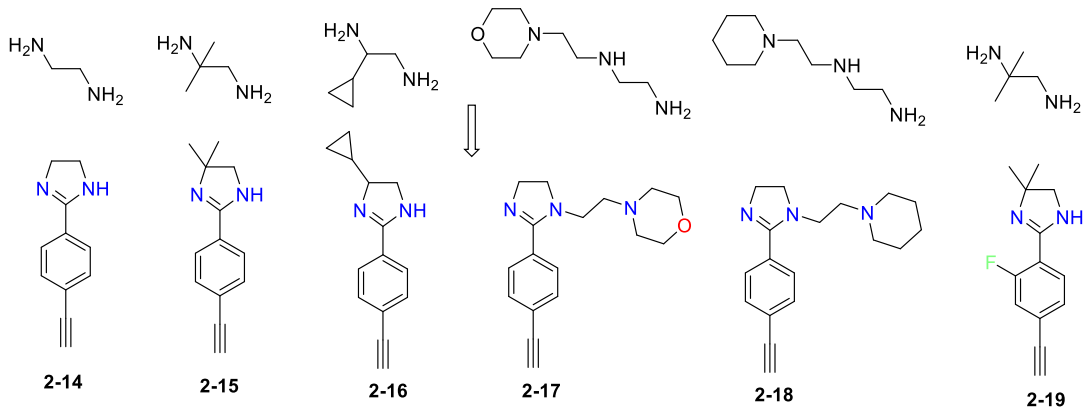

Scheme 2-3. Different amidine head groups prepared using the same imine formation, iodine-induced oxidative ring closure method.

Using the abovementioned protocol, six novel amidine head groups with different substitutes had been synthesized (**Scheme 2-3**). **2-15** and **2-16** were synthesized with the aim to study if our inhibitor can tolerant small alkyl groups on the amidine ring while **2-17** and **2-18** were synthesized to explore if the free -NH

is important for biological activity. **2-19** was synthesized to study if fluorine substitute on the phenyl ring will increase the biological activity.

2.2.3 Sonogashira Cross-coupling.

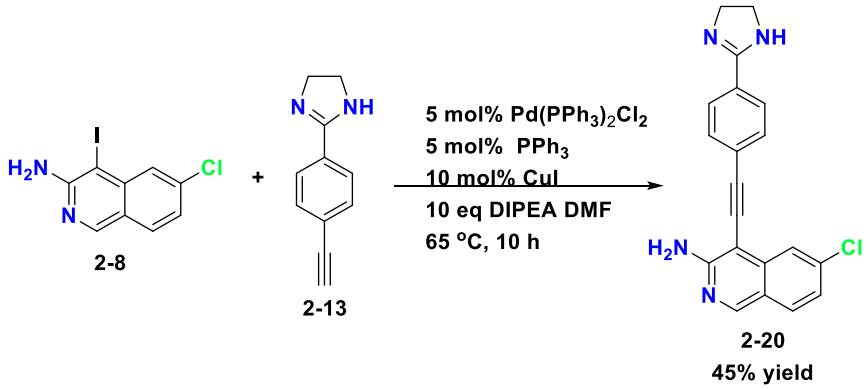

Scheme 2-4. Standard Sonogashira cross-coupling in amidine-acetylene-isoquinoline conjugates synthesis.

The key Sonogashira cross-coupling was achieved using the following conditions: 1 eq. of iodo starting material, 1.5 eq. of aromatic acetylene, 5 mol% of bis(triphenylphosphine)palladium(II) dichloride, 5 mol% of triphenylphosine, 10 mol% copper(I) iodide, 10 eq. of N,N-diisopropylethylamine in DMF at 65 ^{o}C for 10 hours (**Scheme 2-4**). The aromatic acetylene starting material can be dissolved in small amounts of anhydrous DMF (typically less than 1 mL) and introduced to the system slowly *via* syringe in 10 minutes. The desired molecule was purified on Combi-flash system using silica gel columns with 0% to 20% methanol in dichloromethane. After purification and characterization, a small portion of the target molecule was prepared as a 100 mM stock solution in DMSO and stored at -20 ^{o}C for biological assay. All the remaining solid was kept at -20 ^{o}C in a closed cap vial.

2.3 Biological results and discussion on amidine-acetylene-isoquinoline conjugates.

Table 2-1 shows some predictable drug-like properties from www.molinspiration.com, a website used to calculate molecular properties and predict bioactivity. This information was used to guide the design of the compound library. According to Lipinski's Rule of Five, an orally active drug should have less than one violation of the following criteria: less than five in the numbers of hydrogen bond donors (nOHNH), less than ten in the numbers of hydrogen bond acceptors (nON), less than 500 in molecular weight (MW), less than five in partition coefficient between n-octanol and water (logP). As seen in **Table 2-1,** all the compounds designed fall within the determined criteria.

entry		MW	LogP	TPSA	nON	nOHNH	nrotb	volume
1	**2-17**	346.82	2.7	63.31	4	3	1	300.68
2	**2-18**	386.89	3.61	63.31	4	3	0	340.30
3	**2-19**	374.88	3.56	63.31	4	3	1	333.50
4	**2-20**	458.01	3.94	57.76	5	2	4	420.62
5	**2-21**	296.76	1.37	63.31	4	3	1	256.69
6	**2-22**	297.36	2.33	37.28	3	1	1	275.86
7	**2-23**	346.82	2.75	63.31	4	3	1	300.68
8	**2-24**	298.35	1.85	50.17	4	1	1	271.70
9	**2-25**	312.38	2.10	63.31	4	3	1	287.14
10	**2-26**	301.35	1.11	79.10	5	4	1	272.13
11	**2-27**	313.36	1.76	76.20	5	3	1	282.99
12	**2-28**	312.38	1.93	63.31	4	3	1	287.14
13	**2-29**	312.38	2.29	63.31	4	3	1	287.14
14	**2-30**	312.38	1.99	63.31	4	3	1	287.14

15	**2-31**	348.84	3.70	63.31	4	3	3	305.95
18	**2-32**	293.73	4.05	38.91	2	2	0	247.19
19	**2-33**	303.75	3.64	62.71	3	2	0	259.12
20	**2-34**	303.75	3.62	62.71	3	2	0	259.12
21	**2-35**	336.78	2.33	95.02	5	5	2	284.97
22	**2-36**	336.78	2.30	95.02	5	5	2	284.97
23	**2-37**	321.77	2.70	82.01	4	4	1	272.53
24	**2-38**	338.80	3.28	95.02	5	5	4	290.25
25	**2-39**	388.86	4.49	95.02	5	5	4	334.24
26	**2-40**	345.79	2.69	69.63	5	2	1	290.72
27	**2-41**	346.35	2.23	133.95	8	5	4	293.96
28	**2-42**	345.36	2.57	121.05	7	5	4	298.11
29	**2-43**	361.43	2.96	107.91	6	5	4	307.26
30	**2-44**	346.35	2.23	133.95	8	5	4	293.96

Table 2-1. Drug-like properties for all amidine/hydroxyamdidine-acetylene-isoquinoline/quinoline conjugates, includes MW, LogP, TPSA (molecular polar surface area), nON, nOHNH, ntrob (number of rotatable bond), volume (molecular volume).

Compound **2-21** to **2-24,** synthesized from the corresponding head groups (**Scheme 2-3**) with iodo compound **2-5** using Sonogashira Coupling, were mainly focus on studying different substitutes on amidine ring (**Figure 2-3**).

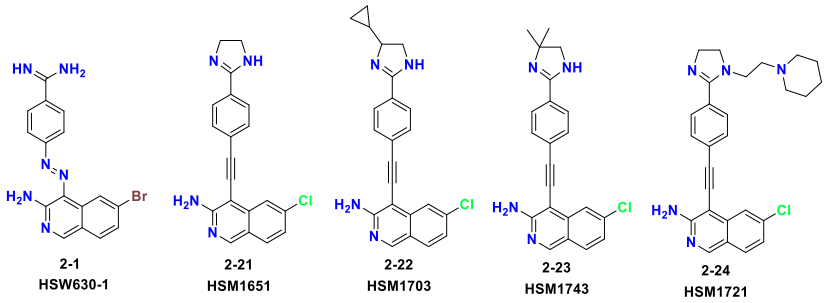

Figure 2-3. Amidine-acetylene-isoquinoline conjugates mainly used to explore if substitutes can be added to head group without affecting biological activities too much.

To our delight, **2-21** inhibited 60% FLT3 kinase at 500 nM (data provided by Reaction Biology Company). Although the inhibition for FLT3 was lower compared to the azo compound **2-1** (**Figure 2-1**), which had an inhibition of 92%, we were still excited because it showcased that the azo-to-alkyne strategy is a viable one to make FLT3 inhibitors. Further cell inhibition data showed that **2-21** was better against different leukemia cell lines compared to azo lead **2-1** (See **Table 2-2** below, data provided by Dr. Jie Zhou). **2-21** was three times better than HSW630-1 against MV4-11, and almost as good as HSW630-1 on MOLM14 and THP-1. **2-21** showed good dose response as can see from **Figure 2-5 (A)**. Even at 10 nM, it can inhibit 37% MV4-11 cells and almost 88% at 1 uM (**Figure 2-6**). Western blot analysis of MV4-11 revealed that **2-21** can inhibit FLT3 phosphorylation (**Figure 2-5 B**) as well as inhibit phosphorylation of the downstream signal pathway STAT5 (**Figure 2-5 C**). From these promising data, we planned to explore SAR on our new hit molecule **2-21** further.

Anti-proliferative effects in leukemia cancer cell lines (μM)				
	MV4-11	MOLM14	THP-1	K-562
HSW630-1	0.15 ± 0.01	0.15 ± 0.01	1.20 ± 0.20	3.00 ± 0.96
2-21	0.05 ± 0.01	0.11 ± 0.02	1.85 ± 0.92	1.39 ± 0.07

Table 2-2. Anti-proliferative effects of HSW630-1 and **2-21** towards MV4-11, MOLM14, THP-1, K-562 cell lines (Experiment done by Dr. Jie in Sintim's lab).

As seen from **Figure 2-5**, all subsequent modifications to the amidine ring of **2-21**, yielded in slightly worse overall activity. These results imply that the un-substituted amidine ring is ideal for optimal FLT3 binding.

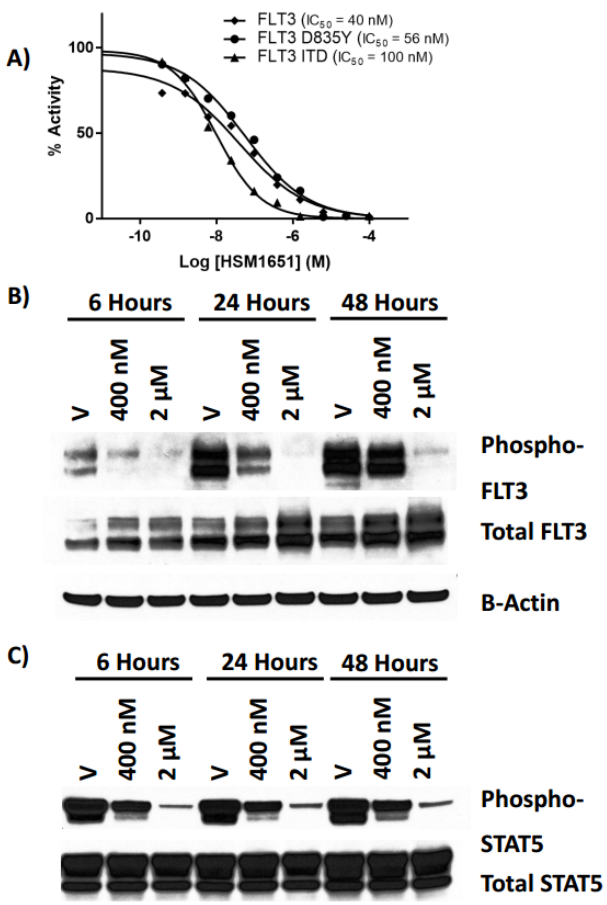

Figure 2-4. (A) Dose−response curves of **2-21** against FLT3 and important FLT3 mutants. (B, C) Western blot analyses of p-FLT3/ total FLT3 (B) and p-STAT5/STAT5 (C) protein expression in MV4−11 after treatment with 2-17 and DMSO vehicle (V) control. Scanned images were analyzed using ImageJ software. (Experiment done by Rena G. Lapidus at University of Maryland Greenebaum Cancer Center)

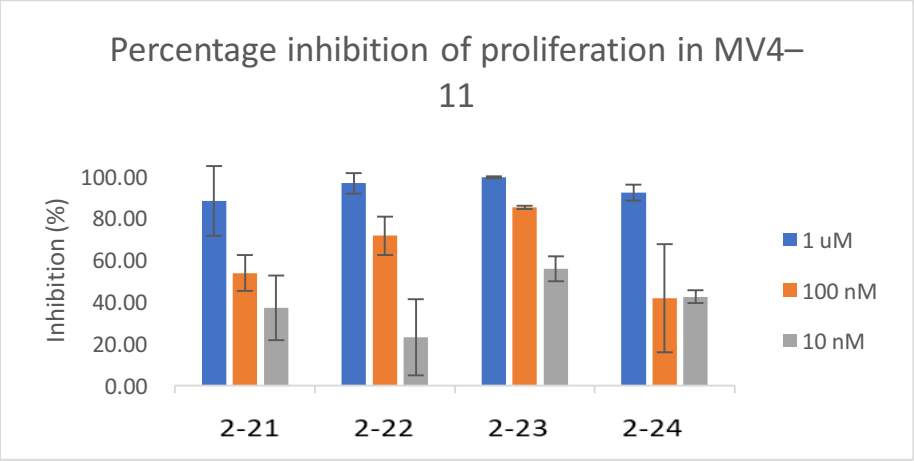

Figure 2-5. Percentage inhibition of proliferation of amidine-acetylene-isoquinoline conjugates in AML cancer cell line MV4-11 at three different concentrations (Data provided by Ms. Elizabeth Larocque in Sintim's lab).

Compounds **2-25** to **2-33** were synthesized to determine the importance of the 6-chloro-3-aminoisoquinoline (**Figure 2-6**).

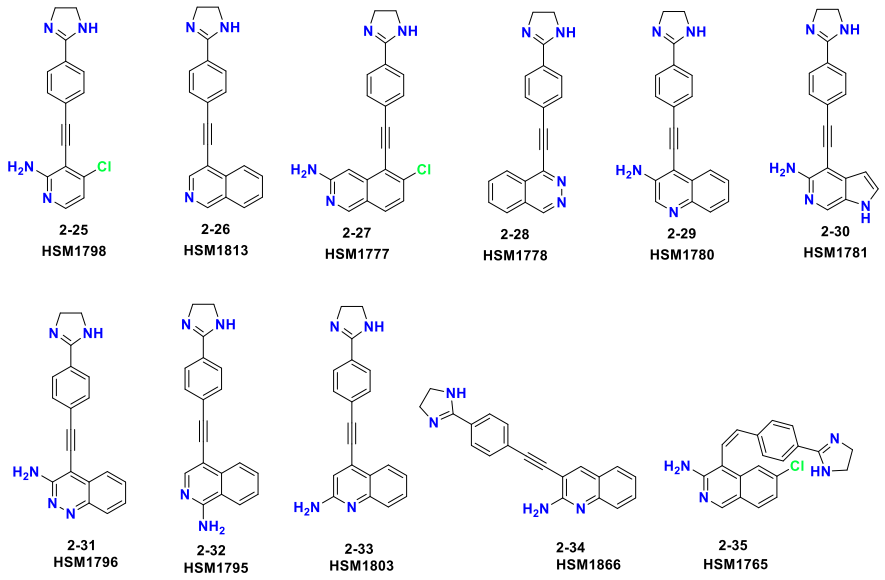

Figure 2-6. More amidine-acetylene/alkene-heterocyclic amine conjugate for SAR study.

entry		% FLT3 inhibition	MV4-11 (uM)	MOLM14(uM)
1	**2-21**	60	0.05 ± 0.01	0.11 ± 0.02
2	**2-22**	43	0.30 ± 0.20	0.10 ± 0.02

3	**2-23**	56	0.07 ± 0.02	0.30 ± 0.01
4	**2-24**	51	0.08 ± 0.02	0.30 ± 0.08
5	**2-25**	17	>5	>5
6	**2-26**	36	>5	>5
7	**2-27**	24	0.48 ± 1.27	ND
8	**2-28**	14	1.50 ± 1.23	ND
9	**2-29**	2	3.82 ± 2.49	ND
10	**2-30**	1	>5	>5
11	**2-31**	6	>5	>5
12	**2-32**	51	0.10 ± 1.20	ND
13	**2-33**	23	0.08 ± 0.01	ND
15	**2-35**	ND	0.11 ± 1.2	ND

Table 2-3. Percentage inhibition of FLT3 and IC50 towards MV4-11 and MOLM14 (ND: not determined. Data provided by Reaction Biology Company).

At the current stage, we questioned if all the fragments in our hit molecule are needed for biological activity. Hence, a library of control compounds were designed and synthesized. To study if the bicyclic ring is necessary, **2-25** was synthesized as a monocyclic ring analog of **2-21**. Compound **2-25** which only has a monocyclic amino pyridine ring instead of the isoquinoline-3-amine ring shows only 36% inhibition towards FLT3 at 500nM. Further cellular data also gave negative results (the IC_{50} of **2-25** are great than five micro molar towards MV4-11 and MOLM14) which suggested fused aromatic ring is a must at least in this amidine series (See **Table 2-3**, entry 5 vs entry 1).

To study if the exterior 3-amino group is a must, **2-26** was synthesized and similar results were obtained when the free amino group was deleted as seen from the **Table 2-3** which suggested the amino group also contributed critically to the

biological activities (**Table 2-3** entry 6 vs entry 1). 5-position isomer **2-27** showed dramatically lower enzymatic activity compared to parent compound **2-21** (**Table 2-3** entry 7 vs entry 1). To study if only the isoquinoline-3-amine motif works in this series of compounds, scaffold hopping methods were used to further explore other new motifs that are all privilege scaffolds in drug discovery. **2-28** presents the phthalazine ring (**Table 2-3**, entry 8); **2-29** presents quinoline-3-amine, a regioisomer from isoquinoline-3-amine (**Table 2-3**, entry 9); **2-30** (**Table 2-3**, entry 13) and **2-31** (**Table 2-3**, entry 14) are other regioisomers which have 1-amino-isoquinoline and 2-aminoquinoline rings respectively.

Some literature reported the instability of isoquinoline at position one, **2-32** was synthesized with a nitrogen atom instead of carbon to block that position for the stability of our compound. Carbon carbon double bond linker analog **2-35** and six membered ring fused with a five membered ring analog **2-30** were synthesized to study if they can provide some benefits regarding ADMET properties.

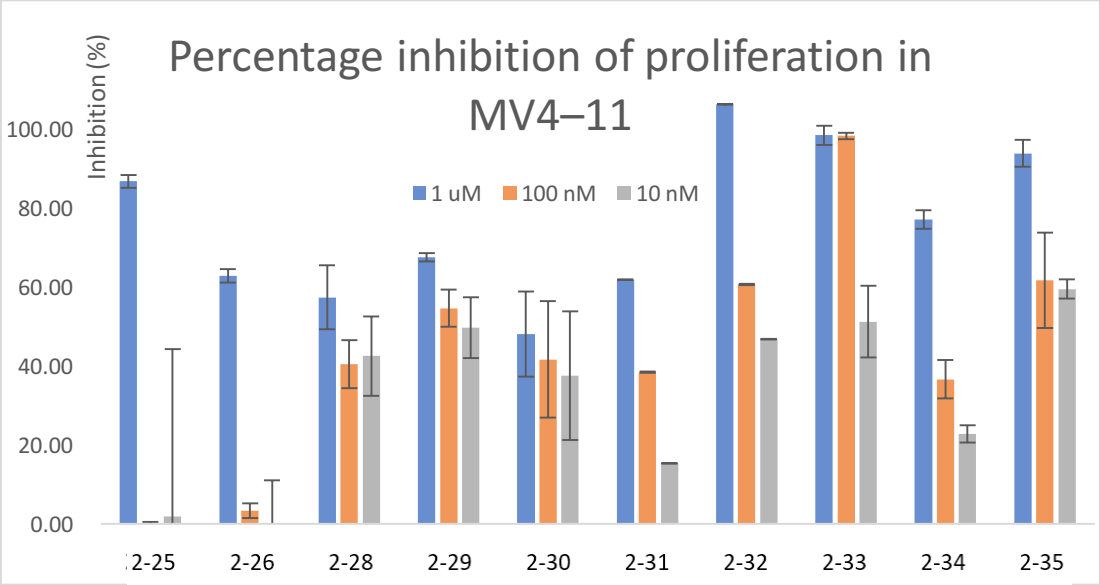

Figure 2-7. Percentage inhibition of proliferation of Class B compounds in AML cancer cell line MV4-11 at three different concentrations (Data provided by Ms. Elizabeth Larocque in Sintim's lab).

As seen in **Figure 2-7**, all other modifications led to un-fruitful results. Compounds **2-25** and **2-26** completely lost their activities below 100 nM while other compounds are not showing any superior activities compared to **2-21**. 1-aminoisoquinoline was identified as a good candidate for our compound library despite slightly lower on enzymatic data but still promising for future development (50% FLT3 inhibition at 500 nM).

The 2-aminoisoquinoline scaffold, as seen in **2-34**, although was a poor FLT3 inhibitor (23% FLT3 inhibition at 500 nM), showed 52% inhibition against BTK. This promoted the design and synthesize of compound **2-36** and **2-37**. After established the fused aromatic ring, free amino group, 4-substituted isoquinoline-3-amine ring were vital to the biological activities observed, we decided to modify our molecules further.

Compound **2-36** and **2-37** show another interesting activity and ongoing study shows they are BTK inhibitor (**Figure 2-8**).

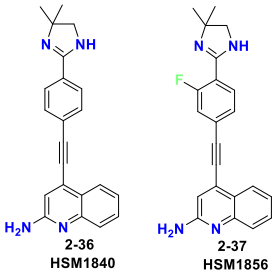

Figure 2-8. Structures for two 1-aminoquinoline amidine conjugates.

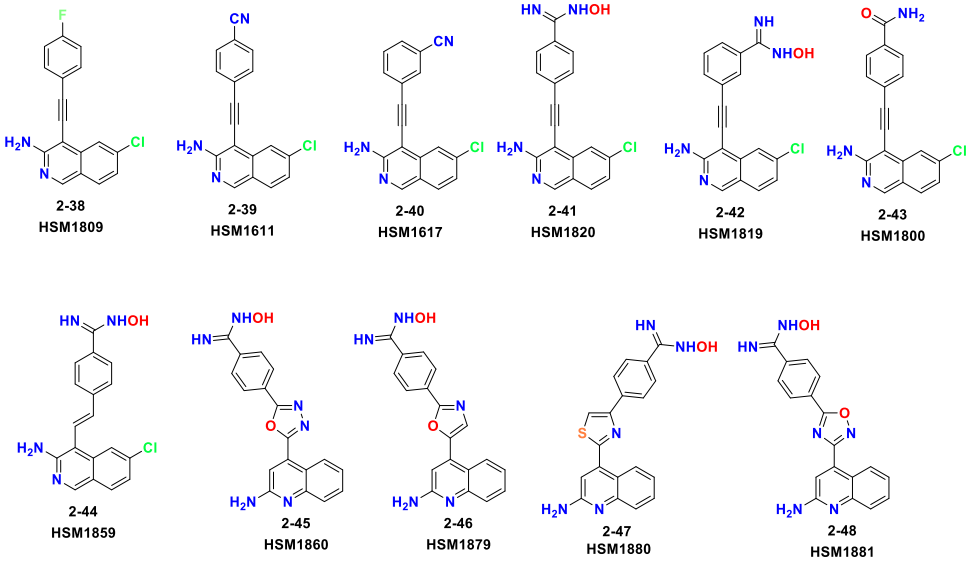

Figure 2-9. Class D of isoquinoline/quinoline-amine based inhibitors.

To improve water solubility of the compound library, novel hydroxyamidine containing compounds were synthesized (**2-41**, **2-42**) from the corresponding cyano containing compound *via* Sonogashria cross-coupling. After purification on silica gel column, the intermediate cyano compounds were further transformed into the hydroxyamidine by stirring excess hydroxylamine solution in ethanol at reflux for 4 hours. (**Scheme 2-5**).

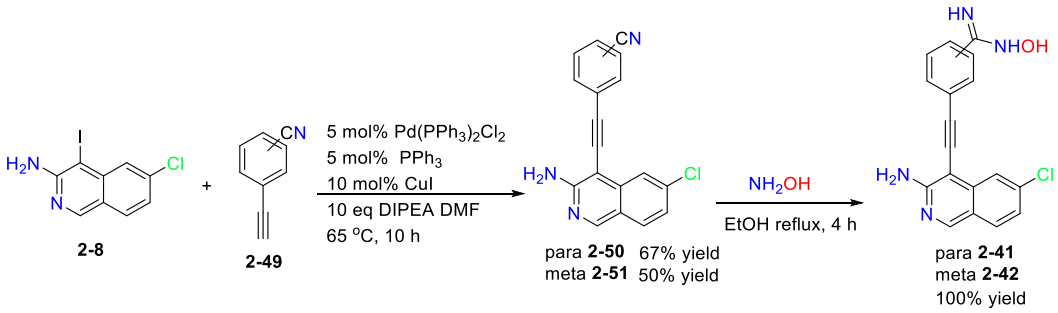

Scheme 2-5. Synthesis of para/meta hydroxyamidine-acetylene-isoquinoline conjugates using Sonogashira coupling and hydroxyamidine formation.

The free amide analog **2-43** was synthesized by coupling of 4-ethynylbenzamide to 4-iodo-6-chloro-isoquinoline-3-amine with acceptable yield (**Scheme 2-6**). The 4-ethynylbenzamide can be synthesized by a modified protocol from 4-ethynylbenzoic acid by treating with ammonium chloride, silicon dioxide, p-toluene sulfonyl chloride and trimethylamine.

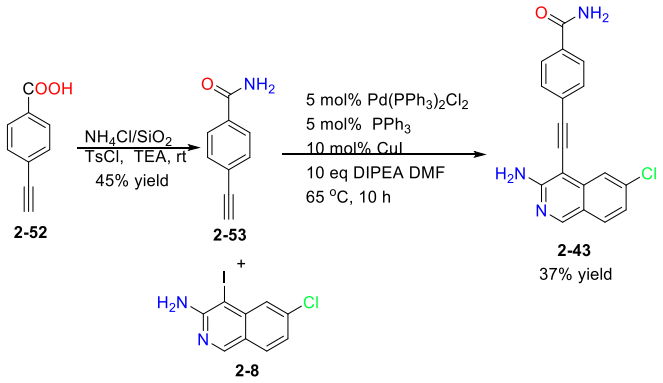

Scheme 2-6. Synthesis of 4-benzamide substituted acetylene-isoquinoline conjugate via benzamide formation and Sonogashira coupling.

Alkene analog **2-44** was synthesized using the following two steps synthesis. Heck coupling of 4-vinylbenzonitrile and 4-iodo-6-chloro-isoquinoline-3-amine in the presence of 10 mol% palladium acetate and N, N-diisopropylethylamine in DMF at elevated temperature gave the alkene linkage intermediate. After refluxing the intermediate in ethanol with hydroxylamine, **2-44** can be formed in quantitative yield (**Scheme 2-7**).

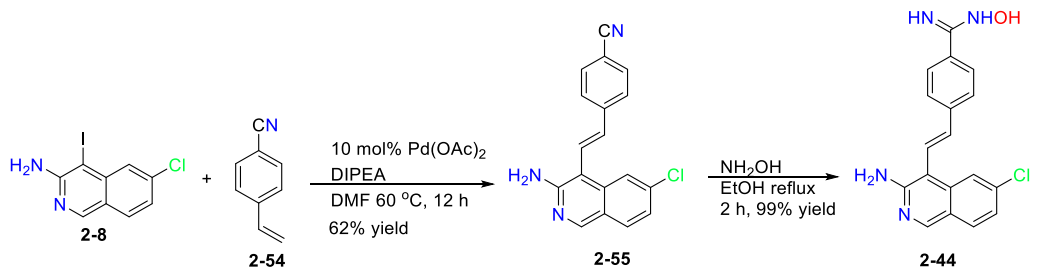

Scheme 2-7. Synthesis hydroxyamidine-alkene-isoquinoline conjugate via Heck reaction and hydroxyamidine formation.

1,3,4-oxadiazole, oxazole, 1,2,4-oxadiazole, thiazole linkers were synthesized to determine the importance of the linker between isoquinoline and head group. All these analogs were synthesized from commercially available starting materials 2-aminoquinoline-4-carboxylic acid or 2-aminoquinoline-4-carbonitrile.

As shown in **Scheme 2-8**, 2-aminoqinoline-4-carboxylic acid in methanol was treated with one drop of concentrated sulfuric acid at reflux. The methyl ester was then converted into acyl hydrazine with anhydrous hydrazine. After treating with phosphoryl chloride in the presence of 4-cyano benzoic acid, the desired 1,3,4-oxadiazole ring was complete, after hydroxyamidine formation, **2-45** was made.

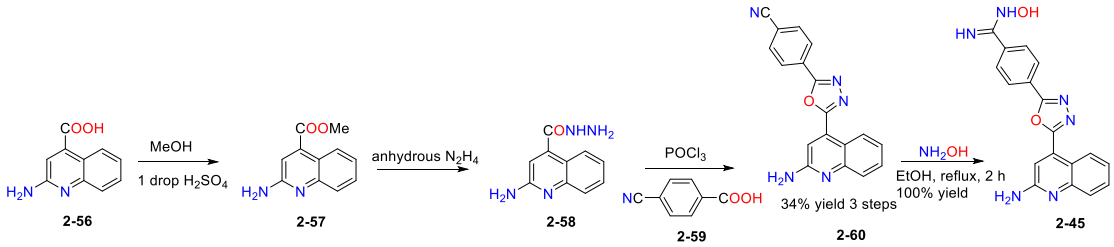

Scheme 2-8. Synthesis of hydroxyamidine-1,3,4-oxadiazol-quinoline conjugate via esterification/ hydrazinolysis /ring formation/hydroxyamidine formation sequences.

The oxazole analog **2-46** was synthesized by refluxing equal equivalents of 2-aminoqinoline-4-carboxylic acid with 4-(2-bromoacetyl)benzonitrile in the presence of 2 eq. potassium carbonate in anhydrous DMF and then urea was added and solvent was changed to acetic acid. The mixture was heated to 140 ^{o}C for 6 hours to afford intermediate **2-62.** Further hydroxyamidine formation by refluxing the cyano intermediate **2-62** in absolutely ethanol with excess hydroxylamine gave the final product **2-46** (**Scheme 2-9**).

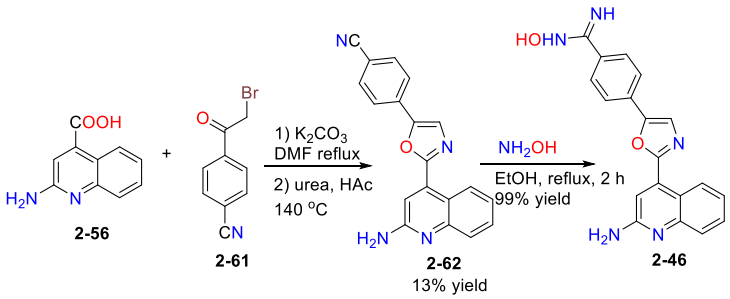

Scheme 2-9. Synthesis of hydroxyamidine-oxazole-quinoline conjugate via urea induced oxazole formation/hydroxyamidine formation.

The 1,2,4-oxadiazol ring was synthesized from 2-aminoquinoline-4-carbonitrile. Converted the cyano starting material to hydroxyamidine, followed by treatment with 4-cyanobenzoyl chloride at reflux in acetonitrile/pyridine. This afforded the 1,2,4-oxadiazol ring **2-65** and after further modification, **2-48** is the desired end product (**Scheme 2-10**).

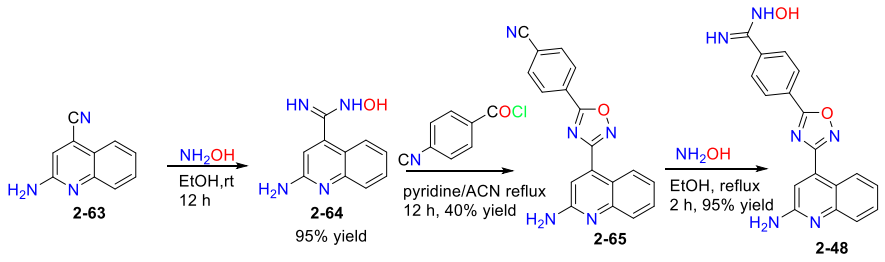

Scheme 2-10. Synthesis of hydroxyamidine/1,2,4-oxadiazol-quinoline conjugate via hydroxyamidine formation/1,2,4-oxadiazol ring formation/hydroxyamidine formation.

Treating 2-aminoquinoline-4-carbonitrile with sodium hydrosulfide and magnesium chloride at room temperature in DMF gave the thioamide **2-66**. Potassium carbonate was added to induce the cyclization of **2-66** with 4-(2-bromoacetyl)benzonitrile. Hydroxyamidine formation on **2-67** gave final thiazole product **2-47**. (**Scheme 2-11**).

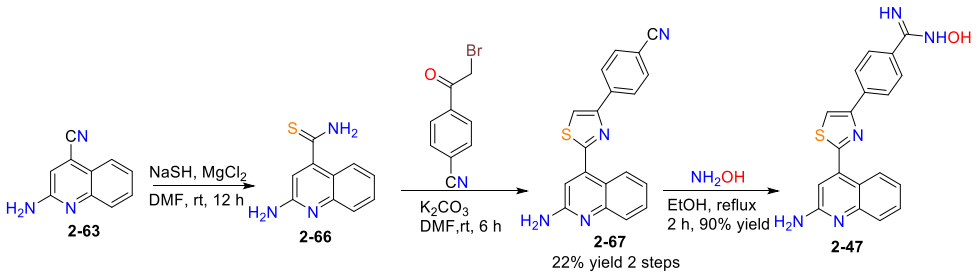

Scheme 2-11. Synthesis of hydroxylamidine-thiazole-quinoline conjugate via NaSH participated thioamide formation/ base induced thiazole ring formation/hydroxylamidine formation sequences.

With these novel compounds in hand, we tested the effects of the compounds of MV4-11 cell line at three different concentrations (1 uM, 100 nM, 10 nM, see **Figure 2-10**). With the exception of two hydorxylamidine-acetylene-isoquinoline analogs, **2-41** and **2-42**, the analogs showed complete loss of activity against the proliferation of MV4-11. For the two active compounds an enzymatic-based assay by Reaction Biology Company was performed (**Table 2-5**). The compounds only showed moderate inhibition against FLT3. **2-41** has an IC_{50} of 217 ±6 nM for FLT3 wild type and 240 ±3 nM for FLT3-ITD. **2-42** has an IC_{50} of 359 ± 5 nM for FLT3, 350 ± 2 nM for FLT3-ITD (**Figure 2-11**), both of which showed promising evidence for further development of the hydroxyamidine prodrug.

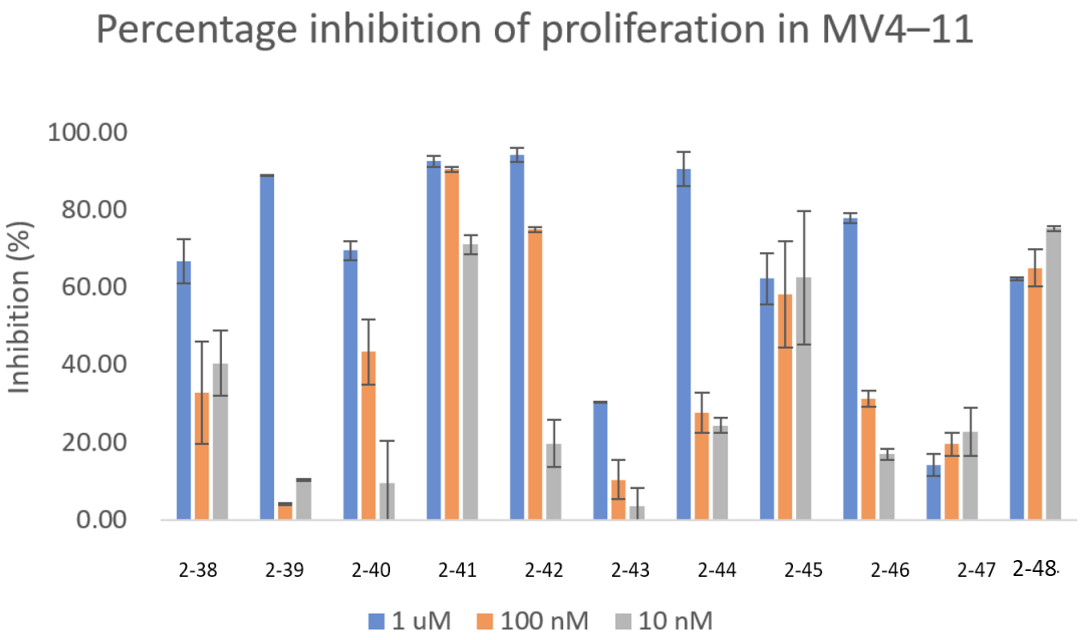

Figure 2-10. Percentage inhibition of proliferation of Class D compounds in AML cancer cell line MV4-11 at three different concentrations (Data provided by Ms. Elizabeth Larocque in Sintim's lab).

entry	% FLT3 inhibition	MV4-11 (uM)
2-38	25	2.74 ± 1.33
2-39	36	0.94 ± 1.09
2-40	34	0.79 ± 1.20
2-41	48	0.07 ± 0.01
2-42	56	0.03 ± 0.01
2-43	62	0.96 ± 1.90
2-44	41	0.37 ± 1.17

Table 2-4. Percentage inhibition of FLT3 and IC50 towards MV4-11 of selected compounds (FTL3 inhibiton data provided by Reaction Biologoy Company, and cellular data proved by Ms. Elizabeth Larocque in Sintim's lab).

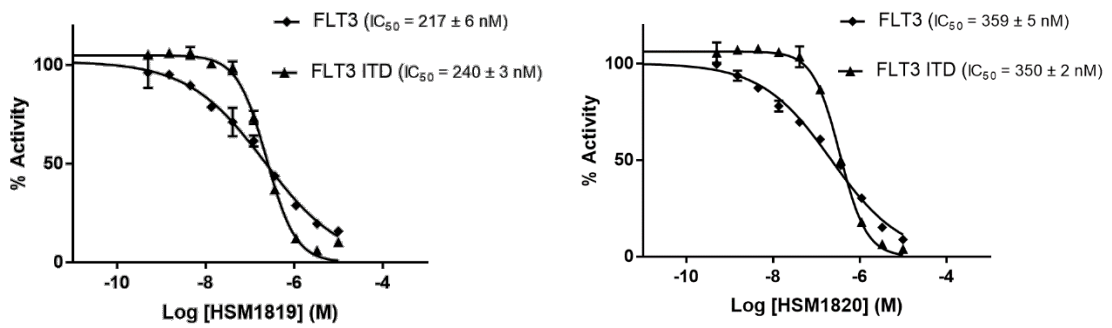

Figure 2-11. IC_{50} curve of **2-41** (HSM1820) and **2-42** (HSM1819) towards FLT3 and FLT3 ITD (Data provided by Reaction Biology Company).

2.4 Conclusion.

The structure-activity-relationship (SAR) studies of the amidine/hydroxyamidine-acetylene-isoquinoline relationship appears that by altering the isoquinoline ring dramatically changes both kinase inhibition and antiproliferative activity. The antiproliferative activity of **2-21** is 100 times higher than **2-26** and the difference is **2-21** has an amino group at 3-position on isoquinoline ring while **2-26** has a proton at that position. Furthermore compounds **2-25**, **2-30**, and **2-31** differ from **2-21** at the isoquinoline ring while keeping the amidine head group the same. These analogs are ineffective anti-proliferative agents. As a consequence, the amidine group appears to be essential for antiproliferative activity. Furthermore, the cyano analog **2-52** is ineffective against MV4-11 and MOLM14 whereas the hydroxyamidine analog **2-41**, which is derived from **2-52**, is very potent against AML suggests potential prodrugs for our amidine conjugates is a possibility for further development.

Chapter 3: Amide-acetylene-isoquinoline/quinoline conjugates potently inhibit proliferation of acute myeloid leukemia cell lines.

3.1 Background.

After a library of amidine containing 6-chloroisoquinoline-3-amine analogs was synthesized, we turned our attention to other more drug-like head groups. We were more focused on drug-likeness to develop an anti-AML drug. Although several amidine drugs have been approved by US Food and Drug Administration[124] (**Figure 3-1**), they are typically not orally bioavailable and have to be used intravenously[125]. Therefore amidine drugs are not an ideal way to develop anti-AML drugs because old people have a high chance to suffer from AML and they are less tolerant of amidine drugs[126]. Amides, are less basic than amidines, orally bioavailable, and are the most widely used functional group in modern drugs (**Figure 3-2**).

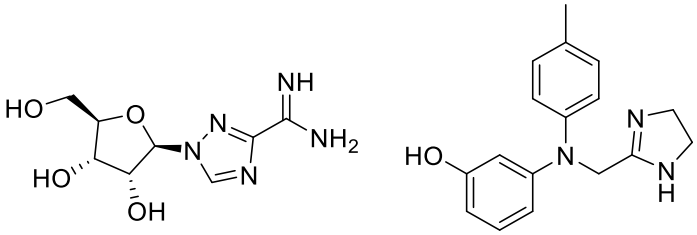

Figure 3-1. Selected FDA approved amidine based drugs.

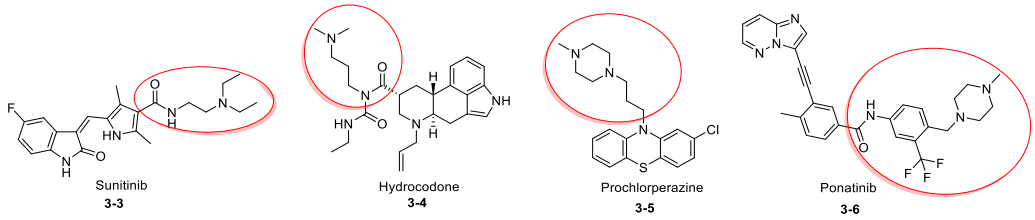

Figure 3-2. Privileged amide side chains used in approved drugs.

Researchers can claim to have discovered some molecules that have an extremely high affinity towards certain targets, but activities are not the only criteria in drug discovery. There must be a balance between activity and other bio-related aspects. There is no doubt that Lipinski's Rules are still widely used as rule of the thumb in drug discovery to quickly and roughly determine if a certain compound will likely to be orally active in humans[127]. This rule describes absorption, distribution, metabolism, and excretion (ADME) but it cannot predict the activities of a certain compound[128]. The original rules are as follows:

No more than 5 hydrogen bond donors
No more than 10 hydrogen bond acceptors
Molecular weight less than 500 Daltons
Octanol-water partition coefficient log P is less than 5

Table 3-1. Lipinski's rule of five for orally active drugs design.

Octanol-water partition coefficient log P is in the range of -0.4 to +5.6
Molecular weight no less than 180 Daltons and no more than 500 Daltons
Total number of atoms range from 20 to 70
Polar surface area less than 140 $Å^2$
Ratable bonds less than 10

Table 3-2. More rules for orally active drugs design.

Table **3-2** shows modifications to the original Lipinski's Rules. However, in drug discovery process, more aspects must be taken into consideration. There are

five main categories of interest for drug discovery, structural properties, physicochemical properties, biochemical properties, safety, and pharmacokinetics.

For instance, structural properties include lipophilicity[129], topological polar surface area[130], hydrogen bond acceptors and donors[131], and molecular weight. Physicochemical properties include solubility[132], permeability[133], and chemical stability[134]. Biochemical properties include metabolic stability[135], transporters[136], blood-brain barrier[137], and plasma stability[138]. Safety includes drug-drug interaction[139], reactive metabolites[140], secondary pharmacology[141], hERG (human ether-à-go-go-related gene) blocking[142], mutagenicity[143], cytotoxicity, and teratogenicity[144]. PK include clearance, volume of distribution, area under the curve, half-life, and bioavailability[145]. In a word, drug discovery is to find a balance between activities among all these properties. Researchers have to fine tune their hit or lead molecules to become a drug.

The amidine inhibitor described in Chapter 2 can be treated as a lead compound, after further SAR and analogs synthesis, the project moved to the third phase in early drug discovery (**Figure 3-3**).

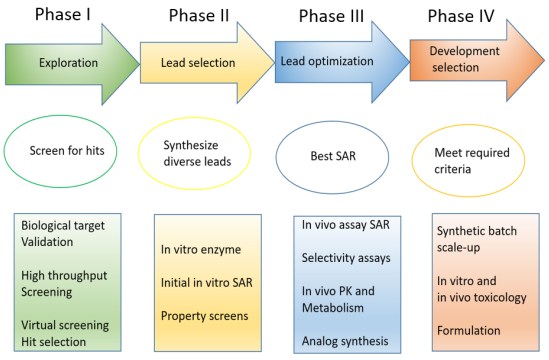

Figure 3-3. Typical flowchart for early stage drug discovery.

3.2 Chemical synthesis of amide-acetylene-isoquinoline conjugates and discussion on biological activities.

In order to move away from the possible problematic amidine head group, we selected some rather simple but still privileged amide side chains in approved drugs [146] (See **Figure 3-2**). Dr. Saeed made an amide analog of 3-aminoisoquinolines (M731) but he did not further explore this class of compounds. Amide side chains were introduced into our molecules by using the most robust chemical reaction[147], amide coupling[148] in one step. The desired product can be synthesized by stirring equal equivalents of aromatic carboxylic acid and amine side chain in anhydrous dichloromethane with slightly excess HATU and trimethylamine at room temperature for 6 hours in moderate yield. After quenching the reaction with water and back extracting with dichloromethane three times, crude amide product can be obtained. Further purification on silica column gave the intermediate for the following palladium catalyzed Sonogashira cross-coupling (**Scheme 3-1**).

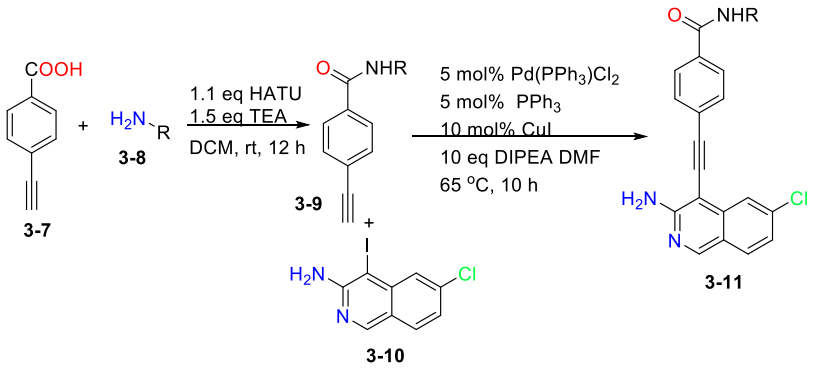

Scheme 3-1. General protocol for amide-acetylene-isoquinoline conjugate synthesis via HATU participated amide coupling/Sonogashira coupling sequences.

Using this protocol, the design and preparation of a series of amide-acetylene-isoquinoline conjugates was achieved (**Figure 3-4)**. **Table 3-1** shows predictable drug-like properties of all these amide-acetylene-isoquinoline conjugates. Of all the analogs we design, we still use Lipinski's Rules as a filter to remove any molecules that may violate at least two rules.

With compounds in hand, cell proliferation assay were performed to determine the inhibition ratios at three representative concentrations (1 uM, 100 nM, 10 nM). Our criteria to define a compound as a promising molecule is over 70% inhibition at 10 nM and both over 95% inhibition at 100 nM and 1 uM. Only compounds that fall in this criteria will be further evaluated to determine IC_{50} against different AML cell lines.

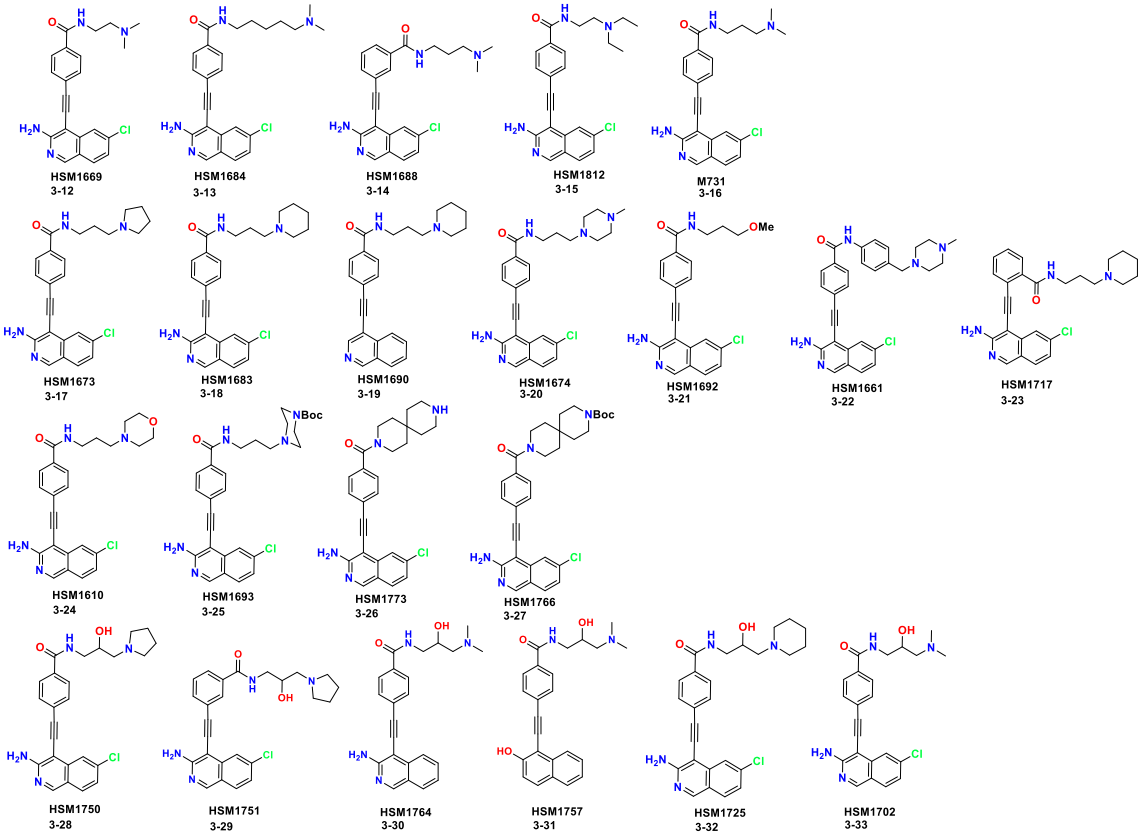

Figure 3-4. Amide-acetylene-isoquinoline conjugates synthesized using standard Sonogashira coupling.

entry		MW	LogP	TPSA	nON	nOHNH	nrotb	volume	Violations
1	**3-12**	392.89	3.11	71.25	5	3	4	353.15	0
2	**3-13**	434.97	4.16	71.25	5	3	7	403.56	0
3	**3-14**	406.92	3.35	71.25	5	3	5	369.95	0
4	**3-15**	420.94	3.86	71.25	5	3	6	386.75	0
5	**3-17**	432.95	3.78	71.25	5	3	5	393.20	0
6	**3-18**	446.98	4.29	71.25	5	3	5	410.00	0
7	**3-19**	397.52	3.86	45.23	4	1	5	385.17	0
8	**3-20**	462.00	3.27	74.49	6	3	5	422.54	0
9	**3-21**	393.87	3.33	77.25	5	3	5	349.59	0
10	**3-22**	510.04	4.47	74.49	6	3	4	460.35	1
11	**3-23**	446.98	4.24	71.25	5	3	5	410.00	0
12	**3-24**	448.95	3.23	80.48	6	3	5	402.18	0
13	**3-25**	548.09	4.30	100.79	8	3	7	500.13	1
14	**3-26**	458.99	3.16	71.25	5	3	1	415.66	0
15	**3-27**	559.11	4.79	88.77	7	2	1	510.20	1
16	**3-28**	448.95	2.87	91.48	6	4	5	401.24	0
17	**3-29**	448.95	2.84	91.48	6	4	5	401.24	0
18	**3-30**	388.47	1.81	91.48	6	4	5	364.46	0
19	**3-31**	388.47	3.04	72.79	5	3	5	365.35	0
20	**3-32**	462.98	3.37	91.48	6	4	5	418.04	0
21	**3-33**	422.92	2.46	91.48	6	4	5	378.00	0

Table 3-3. Drug-like properties for all amide-acetylene-isoquinoline conjugates, includes MW (molecular weight), LogP(octanol-water partition coefficient), TPSA (molecular polar surface area), nON (number of hydrogen bond acceptor),nOHNH (number of hydrogen bond do nor), ntrob (number of rotable bond), volume(molecular volume).

entry	% FLT3 inhibition	% c-kit inhibition
3-12	78	89

3-13	60	81
3-14	54	67
3-15	60	88
3-17	69	86
3-18	65	86
3-19	3	6
3-20	48	82
3-21	15	36
3-22	42	85
3-23	44	61
3-24	57	83
3-25	32	63
3-26	39	ND
3-27	ND	ND
3-28	ND	ND
3-29	ND	ND
3-30	ND	ND
3-31	ND	ND
3-32	63	83
3-33	64	83

Table 3-4. Percentage enzymatic inhibition of FLT3 and c-kit by amide-acetylene-isoquinoline conjugates at 500 nM (Data provided by Reaction Biology Company).

Compound **3-12**, with N^1, N^1-dimethylethane-1, 2-diamine as head group, it showed 78% FLT3 kinase inhibition as well as 89% c-kit inhibition (**Table 3-4**). The good kinase activity data promoted us to do more SAR work. As a consequence, a library of 22 compounds were made to explore SAR on our hit molecule.

First, the length of the amide head group chain was optimized for enzymatic activity. Two (**3-12**), three (**3-16**, synthesized by Dr. Saeed) and five carbon linkers (**3-13**) were synthesized, with three carbons being the optimized length. Next,

pyrrolidine (**3-17**), piperidine (**3-18**), N-methylpiperazine (**3-20**), methoxy (**3-21**), morpholine (**3-24**), piperazine (**3-25**), 3,9-diazaspiro[5.5]undecane (**3-26**), 4-((4-methylpiperazin-1-yl)methyl)aniline (**3-22**) analogs were synthesized using the standard two steps amide coupling/Sonogashira cross-coupling synthesis described previously.

As we can see from **Table 3-4**, compounds **3-17** and **3-18** show identical FLT3 and c-kit inhibition activity which means these two terminal groups are well tolerant. However, by changing the terminal group to methoxy group (**3-21**) or removing the free amine group on isoquinoline ring (**3-19**) completely killed the activities. (**Table 3-4**). All other modifications on side chains led to compounds that fall within an inhibition range of 40% to 70% of FLT3. According to the docking results showed below (**Figure 3-6**), the amide head group points to the outside of the binding pocket, presumably acts to improve solubility. **3-18** (N-methylpiperzine side chain), **3-22 (**4-((4-methylpiperazin-1-yl)methyl)aniline side chain), and **3-24** (morpholine side chain) showed slightly worse FLT3 inhibition data compared to **3-12** while **3-25** (piperazine side chain) and **3-26** (3,9-diazaspiro[5.5]undecane side chain)were less active compared to **3-20** (N-methylpiperazine side chain) and **3-24** (morpholine side chain).

According to the data above, we suggested a basic nitrogen several atoms away from the amide bond may have a critical impact on the enzymatic activities. This could be observed due to the possibility that nitrogen may have some electrostatic interactions within FLT3 kinase. To further endorse this hypothesis, we synthesized **3-21** with a methoxy group at the terminal instead of a basic

nitrogen. The enzymatic activities dropped to only 15% inhibition towards FLT3 when a methoxy group is presence versus a basic nitrogen which supported the hypothesis. Docking the active compounds in this series to FLT3 using AutoDock Vina[149] showed that the hydroxyl group on the side chain has an interaction with VAL675 which may explain the high affinity of **3-33** to FLT3 [150]. Compound **3-19**, with deletion of exterior amine group, shows dramatically low enzymatic activities (3% for FLT3 inhibition, 6% for c-kit inhibition) and complete loss of MV4-11 cell inhibition activity as can be seen from **Figure 3-5**.

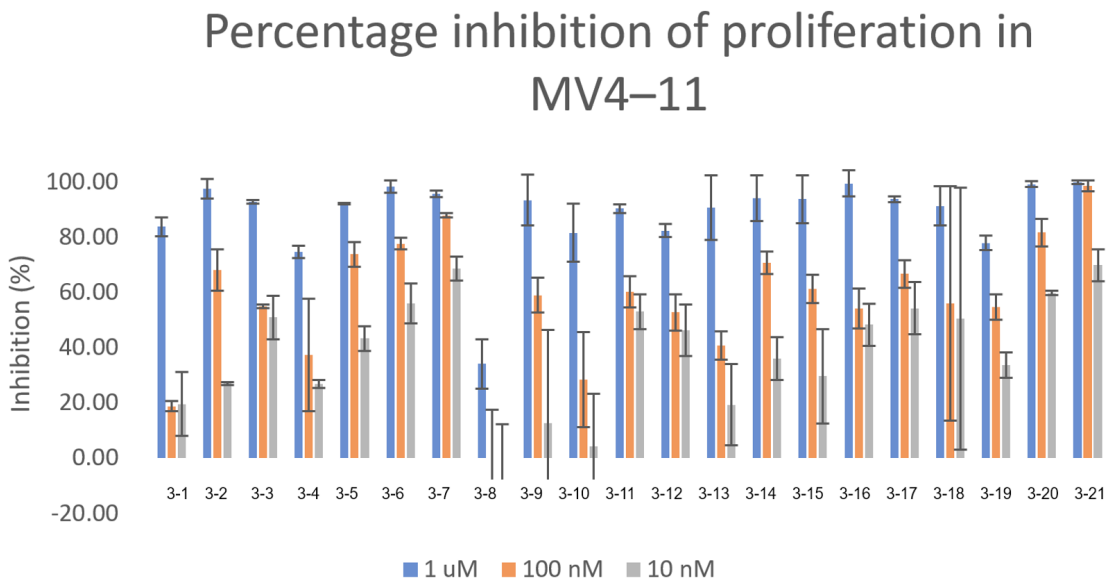

Figure 3-5. Percentage inhibition of proliferation of amide-acetylene-isoquinoline conjugates in AML cancer cell line MV4-11 at three different concentrations (Data provided by Ms. Elizabeth Larocque in Sintim's lab).

Compound **3-18** (68% inhibition at 10 nM) and **3-33** (70% inhibition at 10 nM) showed good activities in cell proliferation assay (**Figure 3-5**). **3-33** (with a 1-amino-3-(dimethylamino) propan-2-ol side chain) showed 99% inhibition at 100 nM and 100% inhibition at 1 uM. To find some clues on the excellent activities observed on **3-33**, docking was used to shed light on this. **3-33** overlapped well compared to Quizartinib and this may explain the biological activity observed

(**Figure 3-6**). Moreover, docking results also showed the possibility to modify on the isoquinoline ring because the six chloro on isoquinoline-3-amine pointed outside the binding pocket (**Figure 3-7**).

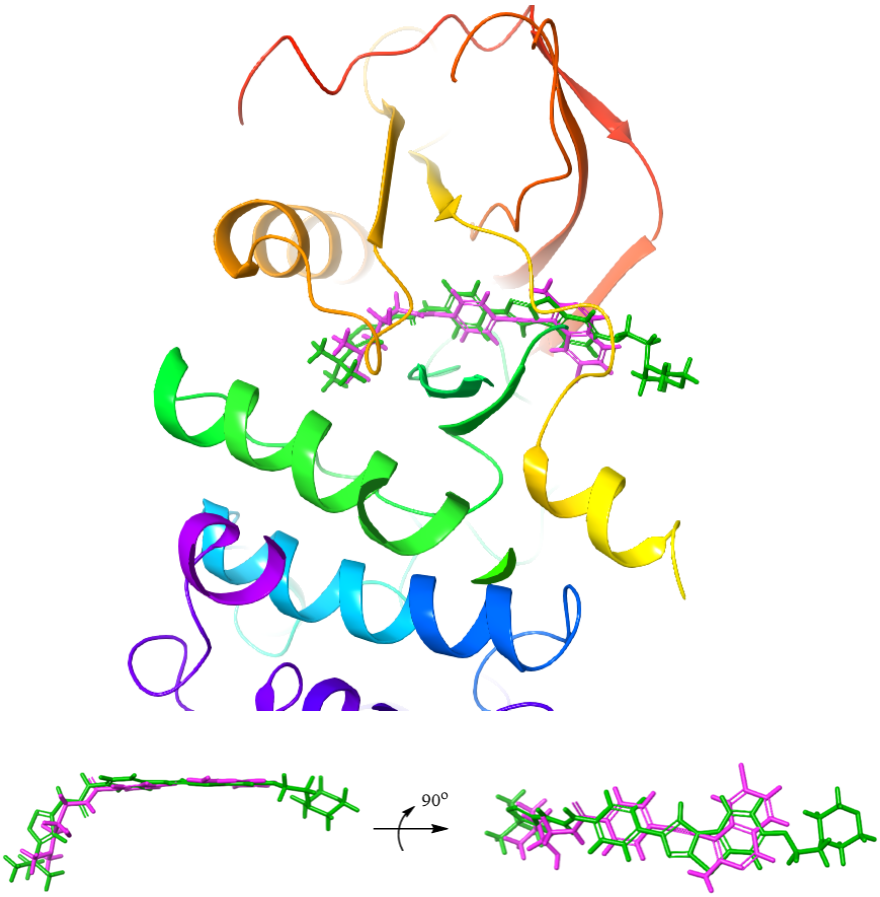

Figure 3-6. Docked **3-33** bound to the inactive form of wild-type FLT3 (PDB number: 4xuf). Docking was done on AutoDock Vina. The docked quizartinib matched the ligand in the crystal structure in 4xuf. Quizartinib showed as green, **3-33** showed as purple.

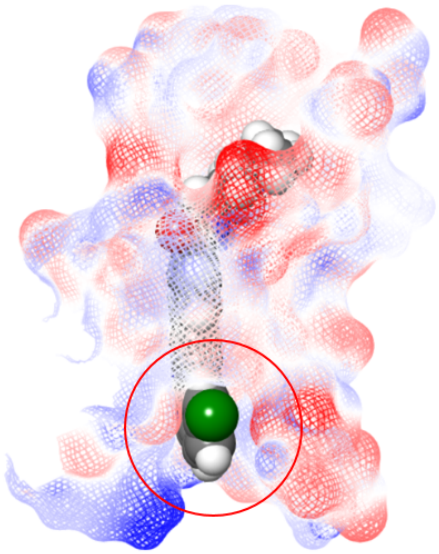

Figure 3-7. Docking results on **3-33** showed 6 position (green atom is 6-chloro) can be further modified because it pointed to the outside of the binding pocket in FLT3.

When an additional hydroxyl group was added to the C3 of the linker (**3-33**), the compounds showed promising results. Although the enzymatic data was similar to that of other synthesized compounds, the proliferation data (see **Figure 3-5**) yielded promising results, and further IC_{50} results supported this (**Figure 3-8**).

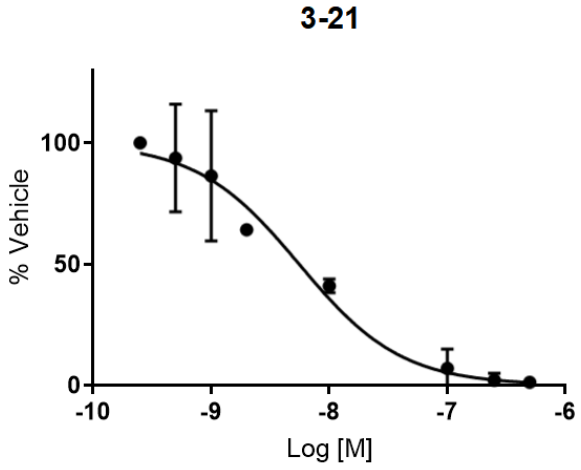

Figure 3-8. 3-33 is active towards FLT3-ITD driven AML cancer cell line MV4-11 with IC_{50} of 71 nM (Data provided by Ms. Elizabeth Larocque in Sintim's lab).

To evaluate **3-33** for future development, we carried out a full kinase panel screen on compound **3-33,** and the data is shown in Figure **3-9**. Out of all the 368 kinases screened against **3-33**, 21 kinases were inhibited by over 50% by **3-33** which translates to about 6% of all the kinases screened. According to the kinase inhibition data, c-kit, CDK series kinases, DLK, DYRK1, FLT3, IRAK4, MLCK2, MYLK4, TRKA, and TRKC are the top kinases that are inhibited by our compound. Further kinase selectivity report from DiscoverX Company further supports the fact that our molecule is more selective to FLT3/FLT3-autoinhibited and KIT/KIT-autoinhibited compared to other kinases (See **Table 3-5**).

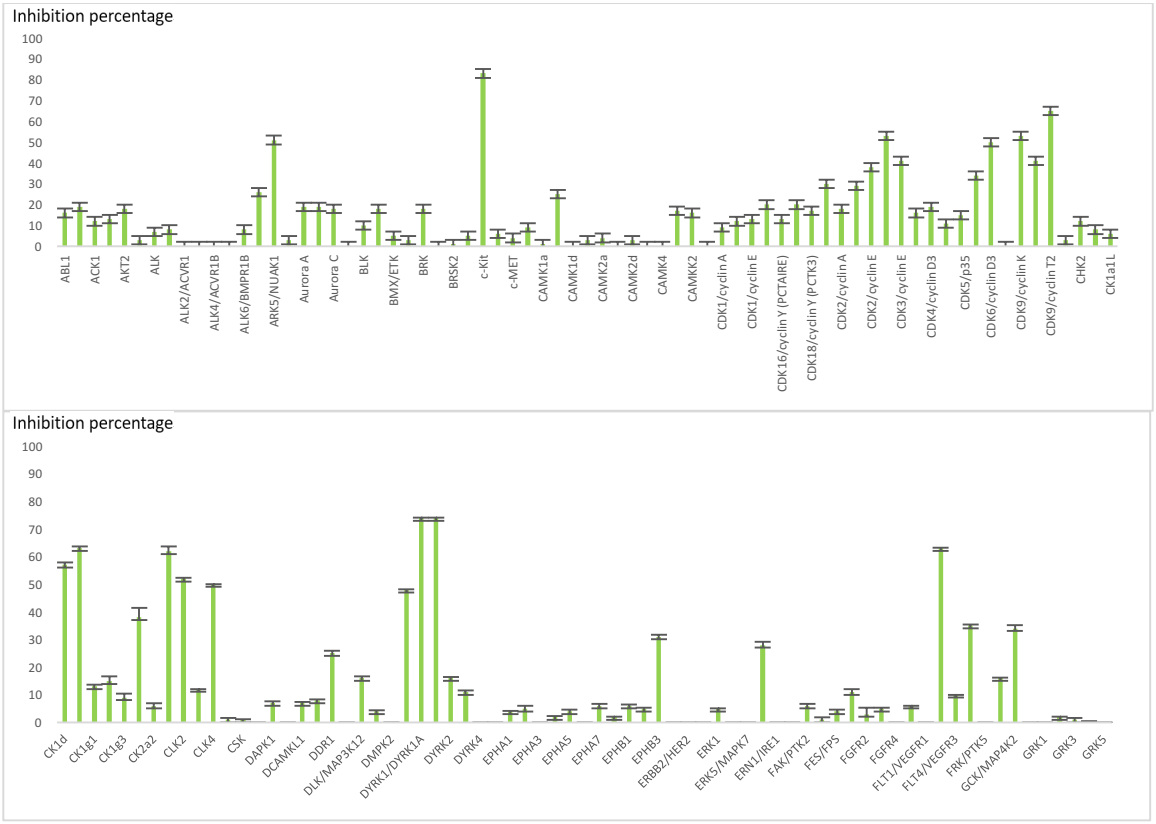

Figure 3-9. Full kinase panel of **3-33** showing high rate kinase inhibition towards kinases that are important for developing different cancers (Data provided by Reaction Biology Company).

Target	3-21 Kd (nM)
CDK6	1700
CDK9	>10000
CLK2	>10000
DYRK1A	>10000

FLT3	200
FLT3-autoinhibited	550
HIPK1	>10000
IRAK4	>10000
KIT	140
KIT-autoinhibited	890
MYLK2	2300

Table 3-5. KINOMEscan profiling service provided by DiscoverX Company for kinase selectivity assay of **3-33**.

3.3 Conclusions.

Through SAR study, another head group different than the amidine that keeps the same level of activities against AML cell line MV4-11 was found. The activities of our inhibitors can be easily tuned by changing the amide head groups. Docking results also showed that the 6-position on isoquinoline can be altered bacause it is located outside of the binding pocket. This gave rise to the opportunity to develop our molecules further to balance activities and drug-likeness properties.

Chapter 4: Developing more potent molecules that potently inhibit proliferation of acute myeloid leukemia cell lines with nano molar IC_{50}.

4.1 Introduction.

After identified N-(3-(dimethylamino)-2-hydroxypropyl)-4-ethynylbenzamide as a promising side chain in our FLT3 inhibitor library, other group members also identified the 4-methyl-N-(4-((4-methylpiperazin-1-yl)methyl)-3-(trifluoromethyl)phenyl)benzamide head group as a promising head group at the same time. HSN286 (**Figure 4-1**), synthesized by Dr. Naganna in the Sintim group inhibited MV4-11 with an IC_{50} of less than 1 nM [151]. This prompted us to make other analogs that are similar to HSN286 but with a different amide group, see **Figure 4-2**.

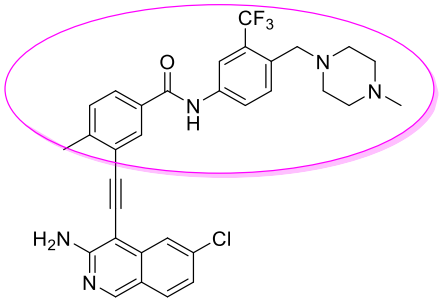

HSN286

Figure 4-1. Structures of HSN286.

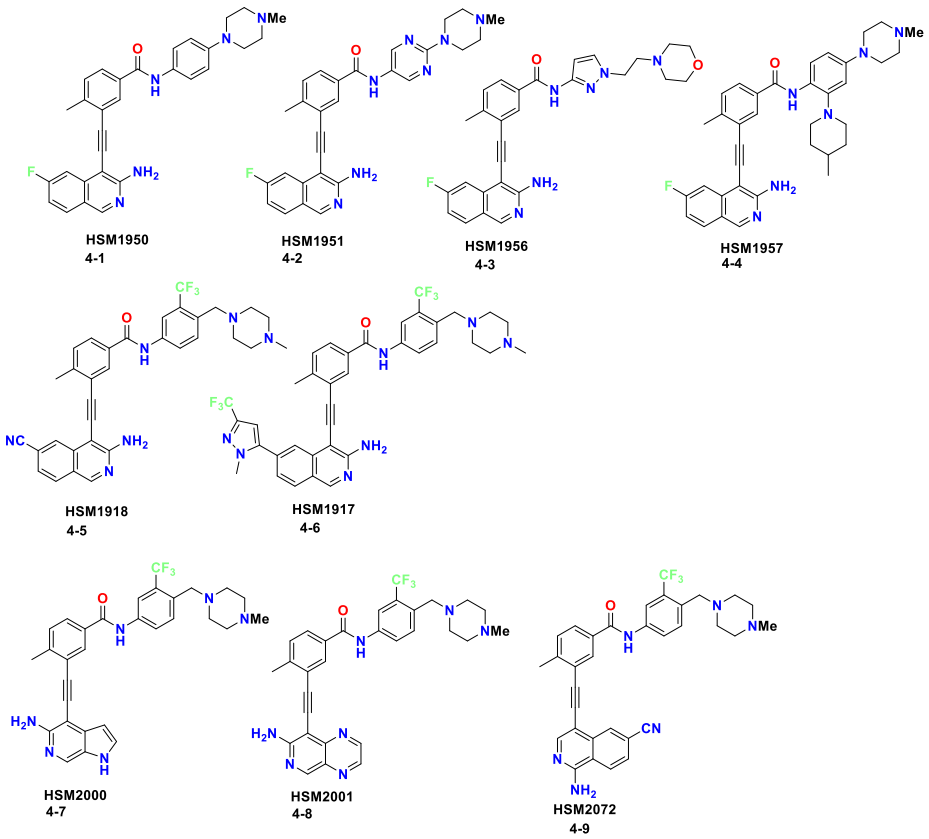

Figure 4-2. More amide-acetylene-heterocycle conjugates synthesized with the emphasis on efficacy

entry		MW	LogP	TPSA	nON	nOHNH	nrotb
1	**4-1**	493.59	3.66	74.49	6	3	3
2	**4-2**	495.56	2.74	100.27	8	3	3
3	**4-3**	498.56	2.11	98.31	8	3	5
4	**4-4**	590.75	4.84	77.73	7	3	4
5	**4-5**	582.63	4.75	98.28	7	3	5
6	**4-6**	705.71	6.25	92.31	8	3	7
7	**4-7**	546.60	4.03	90.28	7	4	5
8	**4-8**	559.60	3.61	100.27	8	3	5
9	**4-9**	582.63	4.58	98.28	7	3	5

Table 4-1. Drug-like properties for all amide-acetylene-isoquinoline conjugates, includes MW, LogP, TPSA, nON, nOHNH, and ntrob.

4.2 Results and discussions.

We synthesized and tested four new analogs to see if all the motifs of HSN286 are necessary. We removed the benzyl position in HSN286 and synthesized **4-1** as well as analog **4-2** with nitrogen in the phenyl ring. The phenyl ring in the head group was further changed to a pyrazole ring analog **4-3** (**Figure 4-3**). The 3-ethynyl-4-methylbenzoic acid can be synthesized from commercially available 3-iodo-4-methylbenzoate using a one-pot-four-step synthesis. First, converted the iodo **4-11** into trimethylsilyl protected acetylene **4-12** under Sonogashira cross-coupling conditions. Silyl group was deprotected by TBAF to give methyl ester **4-13**. After using lithium hydroxide to hydrolyze the methyl ester and acidified the reaction with dilute hydrochloric acid, the required 3-ethynyl-4-methylbenzoic acid **4-15** can be synthesized in gram scale with 42% overall yield. **4-15** was coupled with 6-fluoro-4-iodoisoquinolin-3-amine under standard Sonogashira cross-coupling conditions to give the end product **4-18** (**Scheme 4-1**).

At the current stage, we choose 6-fluoroisoquinoline-3-amine instead of 6-chloroisoquinoline-3-amine mainly for the following three reasons: 1) 6-fluoro analogs gave us lower logP compared to 6-chloro analogs 2) fluoro compound reduced the molecular weight compared to chloro compound 3) preliminary animal studies showed fluoro compound had lower toxicity compared to chloro compound.

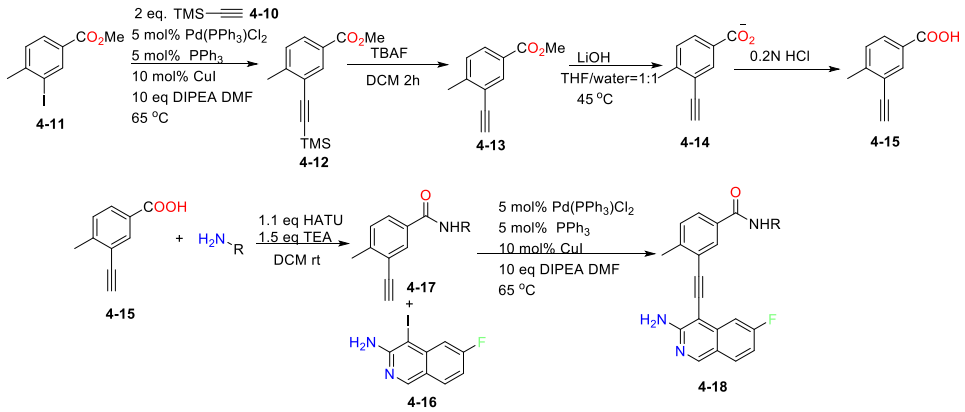

Scheme 4-1. Synthesis of 3-ethynyl-4-methylbenzoic acid from commercial available methyl 3-iodo-4-methylbenzoate via Sonogashira cross-coupling/TBAF induced TMS deprotection/LiOH participated hydrolysis of methyl ester/acidification sequences. Synthesis 3-((3-amino-6-fluoroisoquinolin-4-yl) ethynyl)-N, 4-dimethylbenzamide analogs.

Docking results shown in Chapter 3 and experimental data obtained from previous azo series, position six on isoquinoline-3-amine scaffold might be modified without affecting biological activity. 6-bromo-isoquinoline-3-amine was used as a common starting material and converted to different novel isoquinoline-3-amines to enhance the efficacy further improve drug properties of our inhibitor.

A cyano group was added to the 6-position of the isoquinoline-3-amine ring to increase the solubility of our molecule as seen from predictable logP of **4-5** (**Table 4-3**, entry 5 compared to 5.67 logP for HSN286). The synthesis started from cyanation of 6-bromoisoquinoline-3-amine by combined use of zinc cyanide and metal zinc under palladium catalyst in DMF at elevated temperature. After iodination with NIS in methanol at room temperature, Sonogashira cross-coupling was carried out with 3-ethynyl-4-methyl-N-(4-((4-methylpiperazin-1-yl)methyl)-3-(trifluoromethyl)phenyl)benzamide (**Scheme 4-2**).

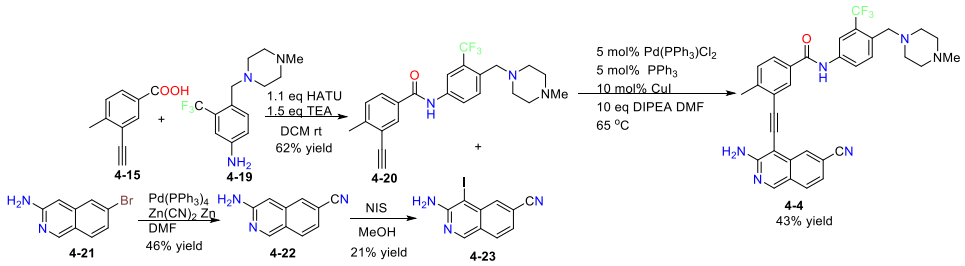

Scheme 4-2. Cyanation of 6-bromo-isoquinoline-3-amine by zinc cyanide under palladium catalyst followed by NIS participated iodination and Sonogashira coupling with 3-ethynyl-4-methyl-N-(4-((4-methylpiperazin-1-yl) methyl)-3-(trifluoromethyl) phenyl) benzamine.

1-methyl-3-(trifluoromethyl)-1H-pyrazol-5-yl was substituted six position via Suzuki coupling of 6-bromoisoquinoline-3-amine with 1-methyl-5-(4,4,5,5-tetramethyl-1,3,2-dioxaborolan-2-yl)-3-(trifluoromethyl)-1H-pyrazole. After iodination and Sonogashira with the head group, **4-6** can be synthesized in acceptable yield.

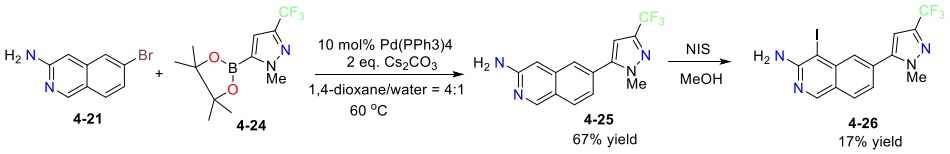

Scheme 4-3. Suzuki coupling of 1-methyl-5-(4,4,5,5-tetramethyl-1,3,2-dioxaborolan-2-yl)-3-(trifluoromethyl)-1H-pyrazole with 6-bromoisoquinoline-3-amine followed by iodnation.

To further explore the importance of the isoquinoline-3-amine, novel pyrido[3,4-b]pyrazin-7-amine was synthesized. This was done by stirring pyridine-2,4,5-triamine with oxalaldehyde solution in ethanol. After standard iodination and Sonogashira cross-coupling with head group **4-21**, **4-8** can be synthesized (**Scheme 4-4**).

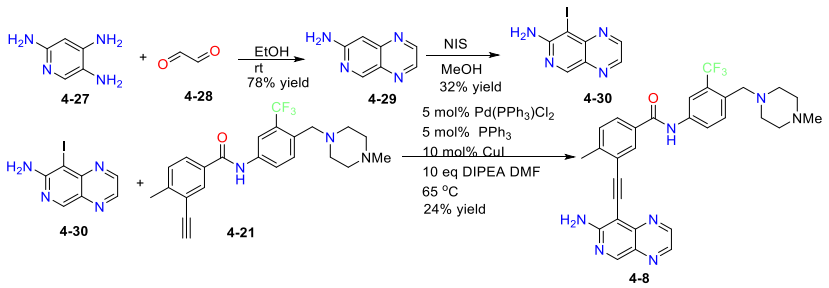

Scheme 4-4. Pyrido[3,4-b]pyrazin-7-amine synthesis followed by iodination and Sonogashira coupling.

A 6-5 fused ring system was also tested to determine if it can replace the 6-6 ring system. Typically, a fused 6-5 system will have lower toxicity compared to 6-6 ring system. 4-bromo-1H-pyrrolo[2,3-c]pyridin-5-amine, can be directly couple with the head group, and **4-7** can be synthesized. In Chapter 2, it was determined that 1-aminoisoquinoline scaffold is a promising bottom for further development, thus the analog **4-9** was synthesized using a similar cyanation/iodination/Sonogashira cross-coupling sequences.

4-5 and **4-6**, with modifications on the six position on isoquinoline ring showed good FLT3 inhibition. Other ring systems, such as 1H-pyrrolo[2,3-c]pyridin-5-amine (**4-7**) and pyrido[3,4-b]pyrazin-7-amine(**4-8**) also showed good FLT3 inhibition.(**Table 4-2**). Ongoing work by Sintim group are evaluating the effects of these compounds on AML cell proliferation. Preliminary data indicates that these compounds inhibit AML at low single digit nanomolar concentrations and results will be published elsewhere in due course.

entry	% FLT3 inhibition	% c-kit inhibition	% ABL1 inhibition	% c-Src inhibition
4-1	29	4	9	3
4-2	22	ND	14	1

4-3	33	ND	0	13
4-4	8	ND	0	0
4-5	97	81	99	99
4-6	98	4	96	100
4-7	82	45	96	97
4-8	94	93	99	100

Table 4-2. Percentage inhibition of FLT3, c-kit, ABL1, and c-Src by amide-acetylene-heterocycle conjugates at 500 nM (Data provided by Reaction Biology Company).

The active compounds **4-5** and **4-6** also show good to excellent inhibition to other important kinases like PDGFRa (gastrointestinal cancer[152], leukemia[153]), VEGFR2 (non-small cell lung cancer[154], breast cancer[155]), EGFR (non-small cell lung cancer[156]), RAF1 (breast cancer[157]) and DDR2(ovarian cancer[158], lung cancer[154]) as we can see from **Table 4-3**.

entry	PDGFRa	VEGFR2	EGFR	RAF1	DDR2
4-5	94	96	61	93	87
4-6	81	85	86	81	79

Table 4-3. More percentage inhibition of PDGFa, VEGFR2, EGFR, RAF1, DDR2 by selected lead molecules at 500 nM (Data provided by Reaction Biology Company).

Docking results showed compound **4-5** has some polar interaction with the inactive form of wild-type FLT3. To our surprise, the cyano group in the isoquinoline ring has a strong interaction with LYS614 which may be contributed to the high activity observed (**Figure 4-3**).

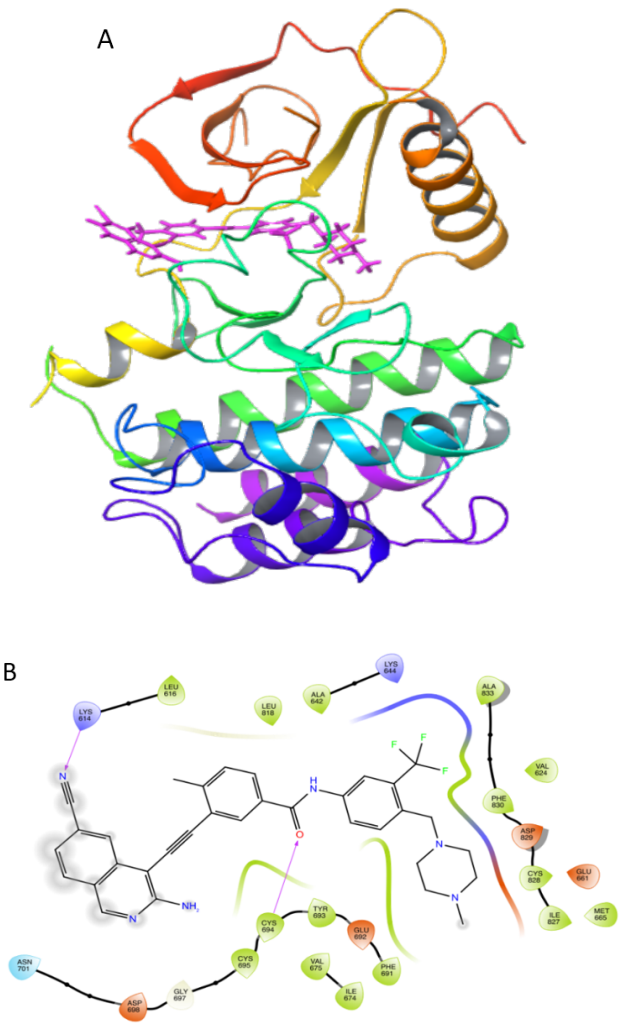

Figure 4-3. A: Docked **4-5** bound to the inactive form of wild-type FLT3 (PDB number: 4xuf). Docking was done on AutoDock Vina. B: Ligand interaction diagram of **4-5** with wild-type FLT3.

4.3 Conclusions.

A new series of compounds bearing substitutes at the six position on isoquinoline ring. 3-((3-amino-6-cyanoisoquinolin-4-yl)ethynyl)-4-methyl-N-(4-((4-methylpiperazin-1-yl)methyl)-3-(trifluoromethyl)phenyl)benzamide **4-5**, 3-((5-amino-1H-pyrrolo[2,3-c]pyridin-4-yl)ethynyl)-4-methyl-N-(4-((4-methylpiperazin-1-yl)methyl)-3-(trifluoromethyl)phenyl)benzamide **4-7**, and 3-((7-aminopyrido[3,4-

b]pyrazin-8-yl)ethynyl)-4-methyl-N-(4-((4-methylpiperazin-1-yl)methyl)-3-(trifluoromethyl)phenyl)benzamide **4-8,** showed over 80% FLT3 enzymatic inhibition at 500 nM. Docking results further suggested the 6-cyano group may have interactions with side chain residues on FLT3. This allowed us further modified this group to make more potent analogs.

Chapter 5: Conclusion and future work.

Acute myeloid leukemia is the cancer of blood. If not properly treated, this subclass of leukemia can progress quickly, and be fatal in less than few months. Aberrantly expressed FLT3 is the main driving force in approximately 30% AML patients which makes it an ideal target for curing AML. In Chapter 2, a library of amidine-acetylene-isoquinoline conjugates based on our group's previous azo compound library was synthesized. These molecules represent the first stable amidine inhibitors that are effective against FLT3. The concept that hydroxylamine acted as a prodrug for amidine was also validated. Through SAR studies on amidine **2-21**, novel 1-aminoisoquinoline was identified as a comparable scaffold for FLT3 inhibitors design other than isoquinoline-3-amine. In Chapter 3, further SAR studies on amide **3-33** (more drug-like than amidine) proved that by fine tuning amide head group, biological activities changed dramatically and led to several effective FLT3 inhibitors *in vitro*. In Chapter 4, several potent FLT3 inhibitors with nanomolar IC_{50}'s were synthesized. The inhibitors can tolerant the modifications at the six position on isoquinoline-3-amine as can see from **4-5** and **4-6.** Docking results further supported this due to the six position on isoquinoline-3-amine pointing outside of the binding pocket of FLT3. One can safely assume that modifications on six position on isoquinloine-3-amine would provide more analogs with same or even higher inhibition activities against MV4-11. Furthermore, two new scaffolds, 1H-pyrrolo[2,3-c]pyridin-5-amine in **4-7** and pyrido[3,4-b]pyrazin-7-amine in **4-8** with promising activities have been identified. These

findings will accelerate future work on those novel scaffolds for the development of general kinase inhibitors. Future work in Sintim lab will focus more on the ADMET properties of this series of compounds as well as pre-clinical study on active compounds.

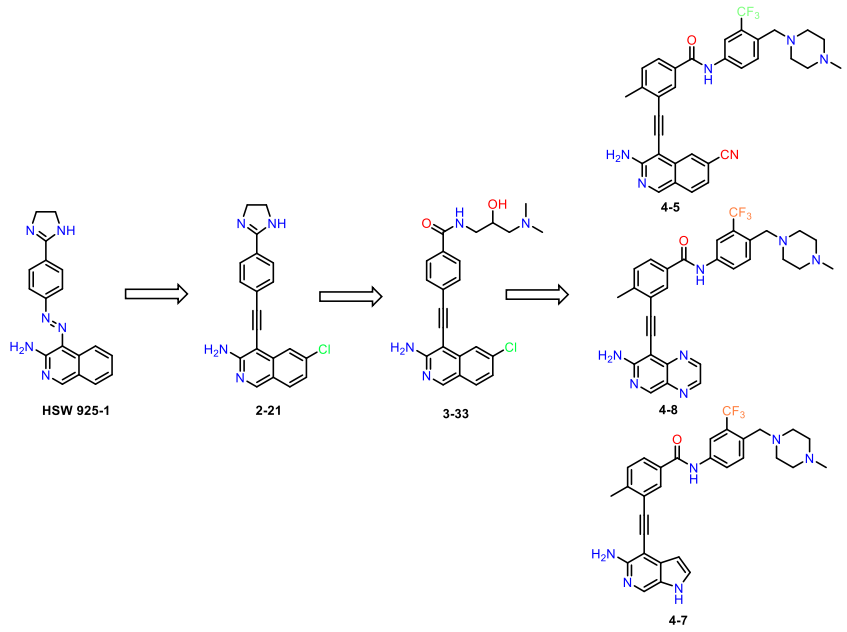

Figure 5-1. Evolve from azo compound to first stable amidine conjugate **2-21**, to first highly active amide conjugates **3-33**, and finally, through reasonable design, a series of highly active novel FLT3 inhibitors have been identified.

Chapter 6: Experimental Sections.

6.1 *In vitro* kinase assays.

The Reaction Biology Corporation (www.reactionbiology.com, Malvern, PA) HotSpot assay platform was used to measure kinase/inhibitor interactions as previously described. Kinase and substrate were mixed in a buffer containing 20 mM HEPES pH 7.5, 10 mM $MgCl_2$, 1 mM EGTA, 0.02% Brij35, 0.02 mg/mL BSA, 0.1 mM Na_3VO_4, 2 mM DTT and 1% DMSO. Single-dose of compounds (500 nM) were then added to each reaction mixture. After 20-minute incubation, ATP (Sigma) and [γ-^{33}P] ATP (Perkin Elmer) were added at a final total concentration of 100 μM for addition 2 hours at room temperature, followed by spotting onto P81 ion exchange cellulose chromatography paper (Whatman, Inc.). Filter paper was washed in 0.75% phosphoric acid to remove unincorporated ATP. Percent remaining kinase activity of a vehicle (DMSO) containing kinase reaction was calculated for each kinase/inhibitor pair using Prism 5 (GraphPad).

6.2 Docking method for FLT3.

AutoDock Vina was used to identify docking poses of our compounds in the binding site of FLT3 kinases. The structure of FLT3 was obtained from the protein databank (PDB# 4XUF).

6.3 Chemical Synthesis.

NMR and MS data: NMR spectra were measured on Bruker AV-III-500-HD (^{1}H at 500 MHz, ^{13}C at 125 MHz). Data for ^{1}H-NMR spectra are reported as follows:

chemical shift (ppm, relative to residual solvent peaks; s = singlet, t = triplets, m = multiplet), coupling constant (Hz), and integration. Data for ^{13}C-NMR are reported in terms of chemical shift (ppm) relative to residual solvent peak. Mass spectra (MS) were recorded by JEOL AccuTOF-CS (ESI positive, needle voltage 1800~2400 eV).

6.3.1 General procedures for preparation of isoquinoline-3-amine amidine FLT3 kinase inhibitors.

6.3.1.1 Synthesis of 6-chloro-4-iodoisoquinolin-3-amine 2-1.

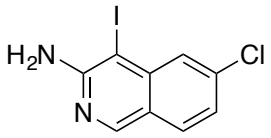

2-1

A modification of the synthesis of **2-1** was used. 6-chloroisoquinolin-3-amine (1 g) was dissolved in methanol (20 mL) at room temperature. The solution was cooled to 0 ^{o}C using an ice bath and stirred vigorously to make a homogeneous suspension solution. N-iodosuccinimide (1.39 g, 1.1equiv.) was slowly introduced to the solution within 10 minutes. After complete addition of N-iodosuccinimde, the solution was stirred until complete consumption of 6-chloroisoquinolin-3-amine indicated by TLC using dichloromethane as eluent. Solvent was evaporated under reduced pressure and directly subjected to silica column chromatography (100% dichloromethane) to afford pure **2-1** as a brown solid in 72% yield. **^{1}H-NMR** (500 MHz, DMSO-d6) δ 8.80 (s, 1H), 7.89 (d, *J* = 8.6 Hz, 1H), 7.61 (d, *J* = 2.0 Hz, 1H), 7.26 (dd, *J* = 8.6, 2.0 Hz, 1H), 6.40 (s, 2H); **^{13}C-**

NMR (126 MHz, DMSO) δ 157.40, 152.78, 140.70, 137.85, 131.58, 126.78, 123.48, 122.12; **HR-MS** (**ESI**): *m/z* calcd for $C_9H_7ClIN_2$ ([M+H]+) 304.9337, found 304.9339.

6.3.1.2 Synthesis of cyclic amidine containing head group.

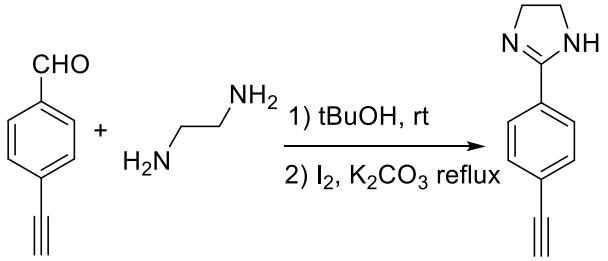

To a 50 mL round bottom flask, 1equiv. of 4-ethynylbenzaldehyde was dissolved in *tert*-Butyl alcohol and 1 equiv. of the corresponding diamine was added all at once. The reaction mixture was stirred for 1 hour at room temperature. 1.1 equiv. of iodine and 3 equiv. of potassium carbonate were added in sequence and the mixture was refluxed for 12 hours. After TLC showed the reaction was complete, equal volume of distilled water was added, and the reaction mixture was extracted with DCM three times (50 mL *3), washed with brine and dried with anhydrous sodium sulfate. After solvents removed under reduced pressure, pure product was obtained by Combi-flash purification using 35% MeOH in DCM in 30 minutes. **^{1}H-NMR** (500 MHz, DMSO-d6) δ 7.79 (d, *J* = 8.4 Hz, 2H), 7.50 (d, *J* = 8.4 Hz, 2H), 7.27 (s, 1H), 4.31 (s, 1H), 3.35 (s, 2H); **^{13}C-NMR** (126 MHz, DMSO) δ 160.50, 132.23, 131.97, 127.74, 123.82, 83.57, 82.87; **HR-MS** (**ESI**): *m/z* calcd for $C_{11}H_{11}N_2$ ([M+H]+) 171.0922, found 171.0910.

6.3.1.3 Sonogashira reaction on amidine acetylene head group.

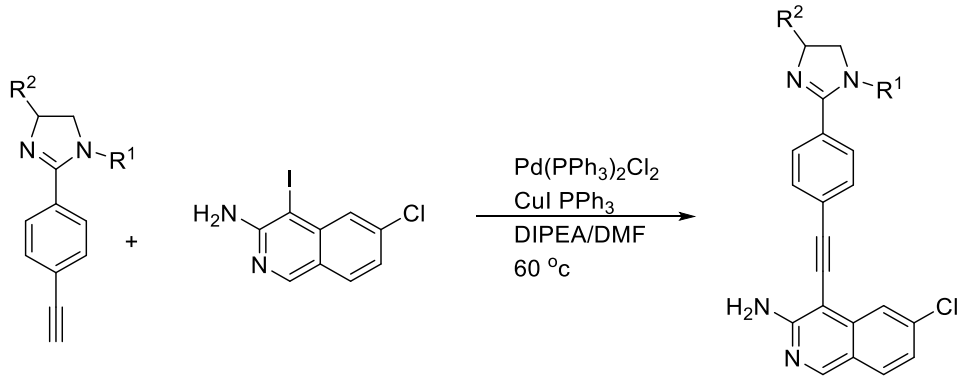

In a 50 mL round bottom flask, 50 mg of 6-chloro-4-iodoisoquinolin-3-amine, 10 mol% bis(triphenylphosphine)palladium(II) dichloride, 10 mol% triphenylphosphine were added, and the system was purged with nitrogen three times before 5 mL anhydrous DMF was added. The reaction mixture was stirred at 60 ^{o}C for another 5 minutes before the corresponding amidine acetylene head group was introduced to the system via syringe in 1 mL anhydrous DMF within 2 minutes. 2 mL DIPEA was added and the reaction mixture was sealed and stirred overnight. After TLC showed the reaction was complete, equal volume of distilled water was added, extraction with DCM three times (50 mL *3), washed with brine and dried with anhydrous sodium sulfate. Solvents was removed under reduced pressure to give crude product. Pure product was obtained by further purification on Combi-flash using 100% DCM to 35% MeOH.

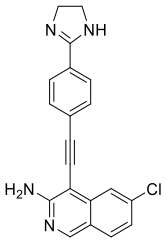

2-21

6-chloro-4-((4-(4,5-dihydro-1H-imidazol-2-yl)phenyl)ethynyl)isoquinolin-3-amine 2-21.

This compound was synthesized using the general protocol described in **6.3.1.3** in 45% yield. **^{1}H-NMR** (500 MHz, DMSO) δ 8.92 (s, 1H), 7.96 (d, *J* = 8.6 Hz, 1H), 7.93-7.81 (m, 5H), 7.28 (dd, *J* = 8.6, 1.8 Hz, 1H), 6.85 (s, 2H), 3.68 (s, 4H); **^{13}C-NMR** (125 MHz, DMSO) δ 163.73, 158.70, 153.30, 138.73, 137.42, 131.64, 131.56, 129.45, 127.78, 125.60, 123.52, 121.33, 120.61, 99.69, 88.45, 85.91, 49.51; **HR-MS**(ESI) m/*z* calcd for $C_{20}H_{16}ClN_4$ ($[M+H]^+$) 347.1063, found 347.1057; **TLC**: R_f = 0.40 (MeOH:DCM = 1:10).

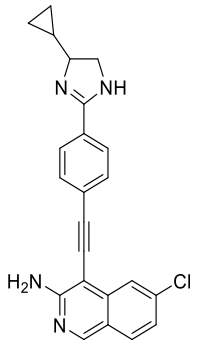

2-22

6-chloro-4-((4-(4-cyclopropyl-4,5-dihydro-1H-imidazol-2-yl)phenyl)ethynyl)isoquinolin-3-amine 2-22.

This compound was synthesized using the general protocol described in **6.3.1.3** in 25% yield. **^{1}H-NMR** (500 MHz, MeOD) δ 8.83 (s, 1H), 7.88 (ddd, *J* = 62.4, 45.2, 5.0 Hz, 6H), 7.29 (dd, *J* = 8.7, 1.9 Hz, 1H), 4.05-3.90 (m, 1H), 3.67 (dd, *J* = 11.9, 8.0 Hz, 1H), 3.53 (dd, *J* = 18.2, 7.9 Hz, 1H), 1.10-0.98 (m, 1H), 0.66-0.29 (m, 4H). **HR-MS (ESI**) m/*z* calcd for $C_{23}H_{20}ClN_4$ ($[M+H]^+$) 387.1376, found 387.1375; **TLC**: R_f = 0.41 (MeOH:DCM = 1:10).

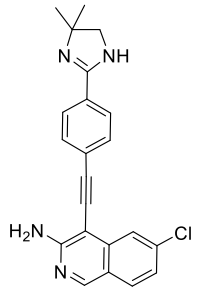

2-23

6-chloro-4-((4-(4,4-dimethyl-4,5-dihydro-1H-imidazol-2-yl)phenyl)ethynyl)isoquinolin-3-amine 2-23.

This compound was synthesized using the general protocol described in **6.3.1.3** in 52% yield. **^{1}H-NMR** (500 MHz, MeOD) δ 8.75 (s, 1H), 7.88 (d, *J* = 1.2 Hz, 1H), 7.81 (d, *J* = 7.4 Hz, 3H), 7.70 (d, *J* = 8.2 Hz, 2H), 7.22 (dd, *J* = 8.7, 1.9 Hz, 1H), 3.53 (s, 2H), 1.35 (s, 6H); **^{13}C-NMR** (126 MHz, MeOD) δ 162.62, 157.51, 151.80, 138.75, 138.02, 131.01, 130.32, 129.49, 127.18, 125.73, 123.67, 121.34, 120.78, 99.38, 90.34, 84.27, 62.77, 61.61, 27.34; **HR-MS(ESI)** m/*z* calcd for $C_{22}H_{20}ClN_4$ ($[M+H]^+$) 375.1376, found 375.1368; **TLC**: R_f = 0.41 (MeOH:DCM = 1:10).

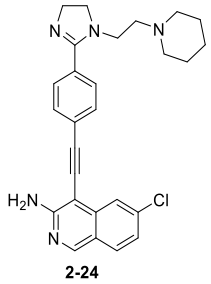

2-24

6-chloro-4-((4-(1-(2-(piperidin-1-yl)ethyl)-4,5-dihydro-1H-imidazol-2-yl)phenyl)ethynyl)isoquinolin-3-amine 2-24.

This compound was synthesized using the general protocol described in **6.3.1.3** in 15% yield. **^{1}H-NMR** (500 MHz, DMSO) δ 8.93 (s, 1H), 7.99-7.78 (m, 6H), 7.29 (dd, *J* = 8.6, 2.0 Hz, 1H), 6.86 (s, 2H), 3.53-3.46 (m, 2H), 3.42 (dd, *J* = 7.9, 3.1 Hz, 2H), 3.25-3.16 (m, 2H), 2.38 (dd, *J* = 24.1, 22.3 Hz, 6H), 1.55-1.47 (m, 4H),

1.39 (s, 2H); **^{13}C-NMR** (126 MHz, DMSO) δ 206.36, 166.05, 158.59, 157.55, 153.58, 138.92, 137.12, 133.90, 131.37, 128.40, 126.15, 123.15, 121.23, 120.71, 99.32, 88.09, 86.12, 72.35, 67.21, 60.93, 54.76, 45.46, 32.08, 26.11, 23.84; **HR-MS(ESI)** m/*z* calcd for $C_{27}H_{29}ClN_5$ ($[M+H]^+$) 458.2111, found 458.2084; **TLC**: R_f = 0.45 (MeOH:DCM = 1:10).

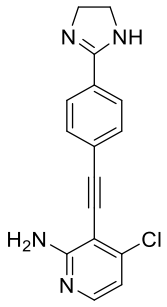

2-25

4-chloro-3-((4-(4,5-dihydro-1H-imidazol-2-yl)phenyl)ethynyl)pyridin-2-amine 2-25.

This compound was synthesized using the general protocol described in **6.3.1.3** in 68% yield. **^{1}H-NMR** (500 MHz, DMSO) δ 8.20 (s, 1H), 7.86 (dd, *J* = 10.8, 8.5 Hz, 3H), 7.54 (d, *J* = 8.2 Hz, 2H), 6.78 (s, 2H), 6.62 (s, 1H), 3.62 (s, 4H); **^{13}C-NMR** (126 MHz, DMSO) δ 163.44, 160.61, 153.33, 144.18, 132.80, 131.21, 127.83, 124.65, 107.44, 106.47, 93.28, 86.83; **HR-MS(ESI)** m/*z* calcd for $C_{16}H_{14}ClN_4$ ($[M+H]^+$) 297.0907, found 297.0900; **TLC**: R_f = 0.35 (MeOH:DCM = 1:20).

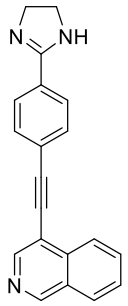

2-26

4-((4-(4,5-dihydro-1H-imidazol-2-yl)phenyl)ethynyl)isoquinoline 2-26.

This compound was synthesized using the general protocol described in **6.3.1.3** in 55% yield. **^{1}H-NMR** (500 MHz, DMSO) δ 9.37 (s, 1H), 8.79 (s, 1H), 8.35 (d, *J* = 8.2 Hz, 1H), 8.24 (d, *J* = 8.0 Hz, 1H), 7.96 (dd, *J* = 19.4, 7.8 Hz, 3H), 7.81 (dd, *J* = 13.7, 7.7 Hz, 3H), 3.65 (s, 4H); **^{13}C-NMR** (126 MHz, DMSO) δ 163.43, 153.15, 146.66, 134.95, 132.48, 131.96, 131.31, 128.96, 128.85, 127.93, 127.85, 124.84, 124.02, 115.01, 96.65, 86.36, 50.06; **HR-MS(ESI)** m/*z* calcd for $C_{20}H_{16}N_3$ ($[M+H]^+$) 298.1344, found 298.1341; **TLC**: R_f = 0.60 (hexane:EtOAc = 1:5).

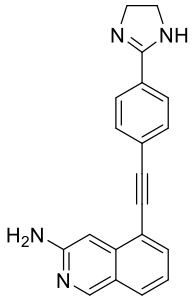

2-27

5-((4-(4,5-dihydro-1H-imidazol-2-yl)phenyl)ethynyl)isoquinolin-3-amine 2-27.

This compound was synthesized using the general protocol described in **6.3.1.3** in 47% yield. **^{1}H-NMR** (500 MHz, MeOD) δ 8.87 (s, 1H), 7.93 – 7.86 (m, 3H), 7.77 (t, *J* = 9.2 Hz, 3H), 7.24 (d, *J* = 3.5 Hz, 2H), 3.80 (s, 4H); **^{13}C-NMR** (126 MHz, MeOD) δ 165.16, 157.18, 152.16, 139.14, 134.73, 131.46, 129.54, 129.25, 127.49, 125.77, 122.74, 121.67, 116.77, 96.66, 93.74, 88.66, 49.11; **HR-MS(ESI)**

m/*z* calcd for $C_{20}H_{17}N_4$ ([M+H]$^+$) 313.1453 found 313.1445; **TLC**: R_f = 0.40 (MeOH:DCM = 1:10).

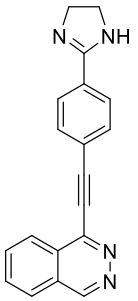

2-28

1-((4-(4,5-dihydro-1H-imidazol-2-yl)phenyl)ethynyl)phthalazine 2-28.

This compound was synthesized using the general protocol described in **6.3.1.3** in 56% yield. **^{1}H-NMR** (500 MHz, MeOD) δ 9.59 (s, 1H), 8.50 (d, J = 8.0 Hz, 1H), 8.22 (d, J = 7.8 Hz, 1H), 8.14 (dt, J = 15.0, 7.1 Hz, 2H), 7.89 (dd, J = 19.2, 8.1 Hz, 4H), 3.83 (s, 4H); **^{13}C-NMR** (126 MHz, MeOD) δ 150.38, 134.15, 133.79, 132.27, 132.17, 130.42, 127.50, 127.30, 127.02, 126.16, 125.17, 123.86, 109.92, 96.45, 84.37, 48.45; **HR-MS(ESI)** m/*z* calcd for $C_{19}H_{15}N_4$ ([M+H]$^+$) 299.1297 found 299.1294; **TLC**: R_f = 0.35 (MeOH:DCM = 1:50).

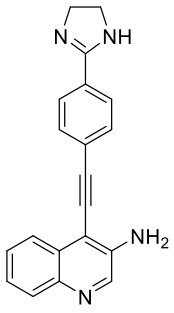

2-29

4-((4-(4,5-dihydro-1H-imidazol-2-yl)phenyl)ethynyl)quinolin-3-amine 2-29.

This compound was synthesized using the general protocol described in **6.3.1.3** in 45% yield. **^{1}H-NMR** (500 MHz, MeOD) δ 8.51 (s, 1H), 8.08 (d, J = 8.3 Hz, 1H),

7.83 (d, J = 8.1 Hz, 3H), 7.75 (d, J = 8.2 Hz, 2H), 7.54 (dd, J = 8.0, 7.1 Hz, 1H), 7.48 – 7.38 (m, 1H), 3.78 (s, 5H); **^{13}C-NMR** (126 MHz, MeOD) δ 165.38, 143.35, 141.88, 140.33, 131.32, 129.63, 128.26, 127.96, 127.63, 127.21, 125.43, 125.00, 123.60, 104.41, 104.31, 101.77, 83.69, 48.96, 48.12; **HR-MS(ESI)** m/*z* calcd for $C_{20}H_{17}N_4$ ($[M+H]^+$) 313.1453 found 313.1457; **TLC**: R_f = 0.25 (MeOH:DCM = 1:30).

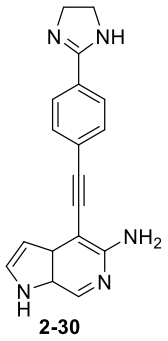

2-30

4-((4-(4,5-dihydro-1H-imidazol-2-yl)phenyl)ethynyl)-3a,7a-dihydro-1H-pyrrolo[2,3-c]pyridin-5-amine 2-30.

This compound was synthesized using the general protocol described in **6.3.1.3** in 22% yield. **^{1}H-NMR** (500 MHz, MeOD) δ 8.24 (s, 1H), 7.90 (d, J = 8.5 Hz, 2H), 7.79 (d, J = 8.5 Hz, 2H), 7.51 (d, J = 2.9 Hz, 1H), 6.53 – 6.42 (m, 1H), 4.01 (s, 4H); **^{13}C-NMR** (126 MHz, MeOD) δ 208.83, 205.32, 194.12, 165.52, 153.08, 149.61, 143.40, 136.88, 133.96, 132.14, 131.63, 131.27, 128.33, 128.20, 127.85, 123.18, 99.54, 96.35, 87.85, 41.16; **HR-MS(ESI)** m/*z* calcd for $C_{18}H_{18}N_5$ ($[M+H]^+$) 304.1562 found 304.1560; **TLC**: R_f = 0.45 (MeOH:DCM = 1:10).

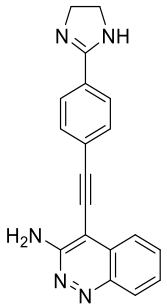

2-31

4-((4-(4,5-dihydro-1H-imidazol-2-yl)phenyl)ethynyl)cinnolin-3-amine 2-31.

This compound was synthesized using the general protocol described in **6.3.1.3** in 32% yield. **^{1}H-NMR** (500 MHz, DMSO) δ 8.19 (d, *J* = 8.5 Hz, 1H), 8.03 (d, *J* = 2.1 Hz, 1H), 7.91 (d, *J* = 11.9 Hz, 3H), 7.75 – 7.68 (m, 1H), 7.56 – 7.48 (m, 1H), 7.11 (d, *J* = 17.1 Hz, 3H), 3.62 (s, 4H); **^{13}C-NMR** (126 MHz, DMSO) δ 163.46, 157.83, 145.17, 132.88, 132.59, 132.25, 131.49, 130.35, 127.69, 127.32, 126.36, 125.17, 124.06, 123.77, 103.13, 94.50, 83.62, 41.23; **HR-MS(ESI)** m/*z* calcd for $C_{19}H_{16}N_5$ ($[M+H]^+$) 314.1406, found 314.1396; **TLC**: R_f = 0.35 (MeOH:DCM = 1:10).

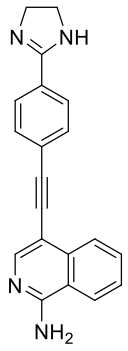

2-32

4-((4-(4,5-dihydro-1H-imidazol-2-yl)phenyl)ethynyl)isoquinolin-1-amine 2-32.

This compound was synthesized using the general protocol described in **6.3.1.3** in 58% yield. **^{1}H-NMR** (500 MHz, DMSO) δ 8.27 (d, *J* = 8.3 Hz, 1H), 8.17 – 8.06 (m, 2H), 7.85 (d, *J* = 7.9 Hz, 2H), 7.77 (t, *J* = 7.5 Hz, 1H), 7.63 (d, *J* = 7.9 Hz,

2H), 7.57 (d, *J* = 7.5 Hz, 1H), 7.37 (s, 2H), 6.97 (s, 1H), 3.34 (s, 4H); **^{13}C-NMR** (126 MHz, DMSO) δ 163.54, 158.16, 147.64, 136.44, 131.55, 131.16, 130.38, 127.82, 126.78, 125.34, 124.94, 116.75, 103.03, 93.42, 88.87, 55.48, 44.89; **HR-MS(ESI**) m/*z* calcd for $C_{20}H_{17}N_4$ ($[M+H]^+$) 313.1453, found 313.1455; **TLC**: R_f = 0.25 (MeOH:DCM = 1:10).

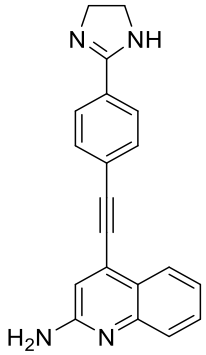

2-33

4-((4-(4,5-dihydro-1H-imidazol-2-yl)phenyl)ethynyl)quinolin-2-amine 2-33. This compound was synthesized using the general protocol described in **6.3.1.3** in 67% yield. **^{1}H-NMR** (500 MHz, DMSO) δ 8.03 (dd, *J* = 8.1, 0.8 Hz, 1H), 7.91 (d, *J* = 8.4 Hz, 2H), 7.76 (d, *J* = 8.4 Hz, 2H), 7.57 – 7.44 (m, 2H), 7.26 (ddd, *J* = 8.1, 6.7, 1.4 Hz, 1H), 7.00 (s, 1H), 6.59 (s, 2H), 3.62 (s, 4H); **^{13}C-NMR** (126 MHz, DMSO) δ 163.40, 158.16, 148.49, 132.19, 131.72, 130.37, 129.10, 127.95, 126.24, 125.64, 123.57, 122.52, 122.00, 115.50, 96.07, 86.97; **HR-MS(ESI)** m/*z* calcd for $C_{20}H_{17}N_4$ ($[M+H]^+$) 313.1453, found 313.1487; **TLC**: R_f = 0.30 (MeOH:DCM = 1:10).

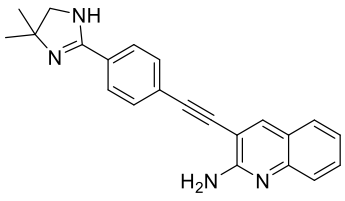

2-34

3-((4-(4,4-dimethyl-4,5-dihydro-1H-imidazol-2-yl)phenyl)ethynyl)quinolin-2-amine 2-34.

This compound was synthesized using the general protocol described in **6.3.1.3** in 71% yield. **^{1}H-NMR** (500 MHz, DMSO) δ 8.24 (s, 1H), 7.85 (d, *J* = 8.4 Hz, 2H), 7.74 (d, *J* = 8.5 Hz, 2H), 7.67 (dd, *J* = 8.3, 0.9 Hz, 1H), 7.55 – 7.43 (m, 2H), 7.19 (ddd, *J* = 8.0, 6.7, 1.3 Hz, 1H), 6.69 (s, 2H), 3.36 (s, 2H), 1.21 (s, 6H); **^{13}C-NMR** (126 MHz, DMSO) δ 160.58, 157.18, 147.84, 140.91, 131.91, 131.34, 130.86, 128.05, 127.64, 125.57, 124.22, 122.68, 122.44, 105.95, 94.97, 87.12, 29.08; **TLC**: R_f = 0.40 (MeOH:DCM = 1:10).

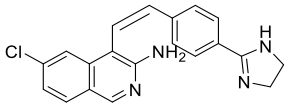

2-35

(*Z*)-6-chloro-4-(3-(4,5-dihydro-1H-imidazol-2-yl)styryl)isoquinolin-3-amine 2-35.

100 mg **2-17** with 20 mg Lindlar catalyst, 500 mg ammonium formate were stirred in 5 mL anhydrous methanol at room temperature overnight. After TLC showed reaction was completed, the reaction mixture was filtered and solvent was removed under reduced pressure. The obtained crude product was directly subjected to flash column purification to afford pure **2-31** in quantitative yield. **^{1}H-NMR** (500 MHz, MeOD) δ 8.73 (s, 1H), 7.89 (d, *J* = 0.6 Hz, 1H), 7.83 (d, *J* = 8.5 Hz, 3H), 7.73 (d, *J* = 8.3 Hz, 2H), 7.38 (d, *J* = 16.6 Hz, 1H), 7.21 (dd, *J* = 8.7, 1.8 Hz, 1H), 7.07 (d, *J* = 16.6 Hz, 1H), 3.79 (s, 4H); **^{13}C-NMR** (126 MHz, MeOD) δ 165.82, 153.37, 150.47, 140.08, 137.19, 137.04, 134.52, 130.28, 128.14, 127.49, 126.28, 123.12, 123.01, 121.71, 120.83, 105.96, 53.40, 48.47; **HR-**

MS(ESI) m/*z* calcd for $C_{20}H_{18}ClN_4$ ($[M+H]^+$) 349.1220, found 349.1208; **TLC**: R_f = 0.35 (MeOH:DCM = 1:15).

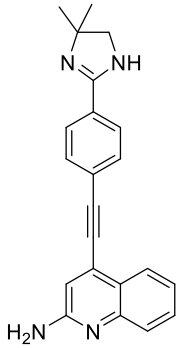

2-36

4-((4-(4,4-dimethyl-4,5-dihydro-1H-imidazol-2-yl)phenyl)ethynyl)quinolin-2-amine 2-36.

This compound was synthesized using the general protocol described in **6.3.1.3** in 52% yield. **^{1}H-NMR** (500 MHz, DMSO) δ 8.04 (d, J = 8.0 Hz, 1H), 7.90 (d, J = 8.2 Hz, 2H), 7.84 (d, J = 8.2 Hz, 2H), 7.75 (d, J = 8.2 Hz, 2H), 7.64 (d, J = 8.2 Hz, 2H), 7.52 (dt, J = 15.6, 7.8 Hz, 2H), 7.26 (t, J = 7.2 Hz, 1H), 7.00 (s, 1H), 6.59 (s, 2H), 3.37 (d, J = 8.7 Hz, 4H), 1.22 (s, 6H); **^{13}C-NMR** (126 MHz, DMSO) δ 160.54, 160.41, 158.16, 148.49, 132.77, 132.31, 132.15, 131.86, 130.35, 129.11, 127.95, 127.92, 126.23, 125.64, 123.51, 122.51, 122.32, 122.00, 115.50, 96.10, 86.98, 82.62, 75.25, 49.06, 29.04, 29.01; **HR-MS(ESI)** m/*z* calcd for $C_{22}H_{21}N_4$ ($[M+H]^+$) 341.1766, found 341.1769; **TLC**: R_f = 0.20 (MeOH:DCM = 1:10).

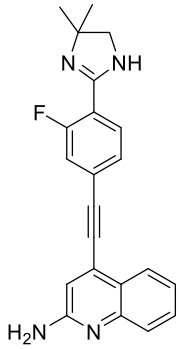

2-37

4-((4-(4,4-dimethyl-4,5-dihydro-1H-imidazol-2-yl)-3-fluorophenyl)ethynyl)quinolin-2-amine 2-37.

This compound was synthesized using the general protocol described in **6.3.1.3** in 68% yield. **^{1}H-NMR** (500 MHz, DMSO) δ 8.08 (d, *J* = 8.0 Hz, 1H), 7.89 (d, *J* = 7.8 Hz, 1H), 7.75 (s, 1H), 7.58 – 7.47 (m, 2H), 7.29 (dd, *J* = 10.9, 4.0 Hz, 1H), 7.05 (s, 1H), 6.66 (s, 2H), 3.61 (s, 2H), 1.38 (s, 6H); **^{13}C-NMR** (126 MHz, DMSO) δ 160.58, 157.18, 147.84, 140.91, 131.91, 131.34, 130.86, 128.05, 127.64, 125.57, 124.22, 122.68, 122.44, 105.95, 94.97, 87.12, 29.08; **HR-MS(ESI)** m/*z* calcd for $C_{22}H_{20}FN_4$ ($[M+H]^+$) 359.1672, found 359.1670; **TLC**: R_f = 0.35 (MeOH:DCM = 1:10).

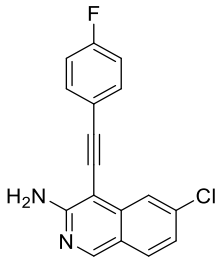

2-38

6-chloro-4-((4-fluorophenyl)ethynyl)isoquinolin-3-amine 2-38.

This compound was synthesized using the general protocol described in **6.3.1.3** in 87% yield.

^{1}H-NMR (500 MHz, DMSO) δ 8.88 (s, 1H), 7.92 (d, *J* = 8.6 Hz, 1H), 7.85 – 7.78 (m, 3H), 7.33 – 7.20 (m, 3H), 6.77 (s, 2H); **^{13}C-NMR** (126 MHz, DMSO) δ 163.33, 161.37, 158.53, 152.93, 138.73, 137.30, 134.19, 134.13, 131.52, 123.45, 121.36, 120.61, 119.88, 116.32, 116.15, 98.95, 88.70, 83.54; **HR-MS(ESI)** m/*z* calcd for $C_{17}H_{11}ClFN_2$ ($[M+H]^+$) 297.0509, found 297.0590; **TLC**: R_f = 0.60 (hexane:EtOAc = 1:10).

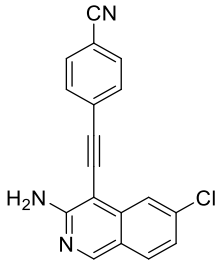

2-39

4-((3-amino-6-chloroisoquinolin-4-yl)ethynyl)benzonitrile 2-39.

This compound was synthesized using the general protocol described in **6.3.1.3** in 74% yield. **^{1}H-NMR** (500 MHz, DMSO) δ 8.91 (s, 1H), 7.91 (ddd, *J* = 12.4, 9.9, 5.0 Hz, 6H), 7.26 (d, *J* = 8.6 Hz, 1H), 6.95 (s, 2H); **^{13}C-NMR** (126 MHz, DMSO) δ 159.04, 153.96, 138.83, 137.63, 132.78, 132.41, 131.61, 128.36, 123.61, 121.33, 120.58, 119.18, 110.60, 98.86, 88.51, 87.73; **HR-MS(ESI)** m/*z* calcd for $C_{18}H_{11}ClN_3$ ($[M+H]^+$) 304.0642, found 304.1411; **TLC**: R_f = 0.35 (MeOH:DCM = 1:20).

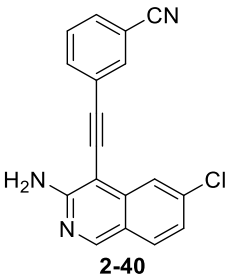

2-40

3-((3-amino-6-chloroisoquinolin-4-yl)ethynyl)benzonitrile 2-40.

This compound was synthesized using the general protocol described in **6.3.1.3** in 65% yield. **^{1}H-NMR** (500 MHz, DMSO) δ 8.92 (s, 1H), 8.37 (s, 1H), 8.10 (d, *J* = 7.9 Hz, 1H), 7.93 (dd, *J* = 11.6, 5.0 Hz, 2H), 7.83 (s, 1H), 7.64 (s, 1H), 7.27 (d, *J* = 1.8 Hz, 1H), 6.93 (s, 2H); **^{13}C-NMR** (126 MHz, DMSO) δ 158.96, 153.59, 138.76, 137.53, 136.14, 135.16, 131.91, 131.50, 130.21, 124.84, 123.54, 121.40, 120.55, 118.71, 112.27, 97.91, 87.91, 86.19; **HR-MS(ESI)** m/*z* calcd for $C_{18}H_{11}ClN_3$ ($[M+H]^+$) 304.0642, found 304.0640; **TLC**: R_f = 0.35 (MeOH:DCM = 1:20).

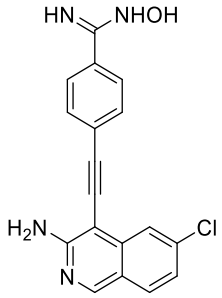

2-41

4-((3-amino-6-chloroisoquinolin-4-yl)ethynyl)-N-hydroxybenzimidamide 2-41.

^{1}H-NMR (500 MHz, DMSO) δ 9.79 (s, 1H), 8.91 (s, 1H), 7.96 (d, *J* = 8.6 Hz, 1H), 7.88 (d, *J* = 1.5 Hz, 1H), 7.76 (dd, *J* = 8.6, 2.0 Hz, 4H), 7.28 (dd, *J* = 8.6, 2.0 Hz, 1H), 6.80 (s, 2H), 5.90 (s, 2H); **^{13}C-NMR** (126 MHz, DMSO) δ 158.54, 153.01, 150.70, 138.69, 137.32, 133.41, 131.53, 125.80, 123.66, 123.47, 121.35, 120.62, 99.94, 88.75, 84.85; **HR-MS(ESI)** m/*z* calcd for $C_{18}H_{14}ClN_4O$ ($[M+H]^+$) 337.0856, found 337.0865; **TLC**: R_f = 0.15 (MeOH:DCM = 1:10).

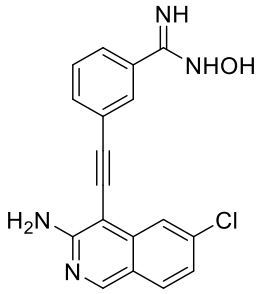

2-42

3-((3-amino-6-chloroisoquinolin-4-yl)ethynyl)-N-hydroxybenzimidamide 2-42.

^{1}H-NMR (500 MHz, DMSO) δ 9.75 (s, 1H), 8.92 (s, 1H), 8.04 (s, 1H), 7.96 (d, *J* = 8.6 Hz, 1H), 7.88 (s, 1H), 7.78 (d, *J* = 7.5 Hz, 1H), 7.72 (d, *J* = 7.8 Hz, 1H), 7.46 (t, *J* = 7.7 Hz, 1H), 7.28 (d, *J* = 8.5 Hz, 1H), 6.80 (s, 2H), 5.93 (s, 2H); **^{13}C-NMR** (126 MHz, DMSO) δ 158.57, 153.00, 150.66, 138.73, 137.33, 134.15, 132.13, 131.55, 128.89, 128.65, 125.84, 123.48, 123.22, 121.31, 120.63, 99.88, 88.73, 83.91; **HR-MS(ESI)** m/*z* calcd for $C_{18}H_{14}ClN_4O$ ($[M+H]^+$) 337.0856, found 337.0873; **TLC**: R_f = 0.20 (MeOH:DCM = 1:10).

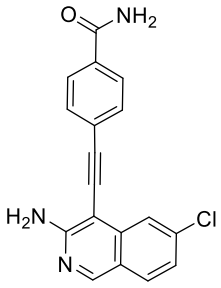

2-43

4-((3-amino-6-chloroisoquinolin-4-yl)ethynyl)benzamide 2-43.

Yield = 37%. **^{1}H-NMR** (500 MHz, DMSO) δ 8.93 (d, *J* = 2.8 Hz, 1H), 8.00 (s, 1H), 7.98 (d, *J* = 4.4 *Hz*, 1H), 7.95 (d, *J* = 2.3 *Hz*, 1H), 7.91 – 7.87 (m, 2H), 7.29 (dd, *J* = 8.6, 1.9 *Hz*, 1H), 6.90 (s, 1H); **^{13}C-NMR** (126 MHz, DMSO) δ 167.39, 158.62, 153.59, 139.05, 137.69, 131.78, 129.82, 128.33, 127.41, 126.06, 123.93, 121.33,

120.78, 99.60, 88.36, 86.56; **HR-MS(ESI)** m/z calcd for $C_{18}H_{12}ClN_3O$ ($[M+H]^+$) 322.0747 found 322.0747; **TLC**: R_f = 0.60 (MeOH:DCM = 1:20).

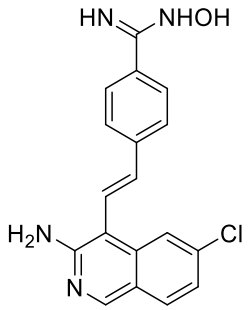

2-44

(E)-4-(2-(3-amino-6-chloroisoquinolin-4-yl)vinyl)-N-hydroxybenzimidamide 2-44.

Yield = 61%. **^{1}H-NMR** (500 MHz, DMSO) δ 9.66 (d, *J* = 6.2 Hz, 1H), 8.88 – 8.75 (m, 1H), 7.89 (dt, *J* = 17.8, 5.5 Hz, 2H), 7.77 – 7.63 (m, 4H), 7.33 (t, *J* = 17.4 Hz, 1H), 7.28 – 7.09 (m, 1H), 7.06 – 6.94 (m, 1H), 6.24 (s, 2H), 5.83 (s, 2H); **^{13}C-NMR** (126 MHz, DMSO) δ 154.75, 151.48, 151.00, 138.28, 136.75, 136.24, 134.02, 132.80, 131.32, 126.82, 125.88, 122.80, 122.59, 121.50, 121.20, 104.46; **HR-MS(ESI)** m/z calcd for $C_{18}H_{16}ClN_4O$ ($[M+H]^+$) 339.1013 found 339.1010; **TLC**: R_f = 0.55 (MeOH:DCM = 1:20).

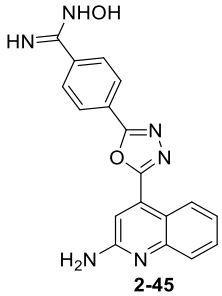

2-45

4-(5-(2-aminoquinolin-4-yl)-1,3,4-oxadiazol-2-yl)-N-hydroxybenzimidamide 2-45.

1 mmol 2-aminoquinoline-4-carboxylic acid was dissolved in 5 mL methanol and one drop of concentrated sulfuric acid was added to the reaction mixture and the mixture was refluxed for 12 hours. Saturated sodium carbonate solution was added to neutralize the reaction mixture. After removed solvent under reduced pressure, the methyl ester was re-dissolved in absolutely ethanol and 194 uL of 98% hydrazine was added at room temperature. The reaction mixture was stirred for another 2 hours and solvent removed under reduced pressure. 1.1 equiv. of 4-cyanobenzoic acid and 1.2 mL phosphoryl chloride were added to the acyl hydrazine and the reaction mixture was refluxed for 20 hours. The reaction was quenched with ice carefully at 0 ^{o}C, and extracted three times with ethyl acetate. Purification on silica gel column (90% DCM in methanol) provided 132 mg cyano intermediate. The cyano intermediate was further dissolved in 1 mL hydroxylamine solution and was refluxed for 6 hours. Purification on silica gel column (10% methanol in DCM) provided final product in 34% overall yeild.

^{1}H-NMR (500 MHz, DMSO) δ 9.92 (d, *J* = 9.2 Hz, 1H), 8.80 (dd, *J* = 17.4, 8.5 Hz, 1H), 8.23 – 8.05 (m, 2H), 8.00 – 7.92 (m, 2H), 7.63 – 7.55 (m, 2H), 7.39 – 7.26 (m, 1H), 6.86 – 6.73 (m, 2H), 6.10 – 5.90 (m, 2H); **^{13}C-NMR** (126 MHz, DMSO) δ 164.26, 163.24, 158.07, 150.41, 149.43, 137.22, 130.31, 128.79, 127.17, 126.73, 126.57, 126.02, 123.66, 123.12, 118.17, 113.60; **HR-MS(ESI)** m/z calcd for $C_{18}H_{15}N_6O_2$ ($[M+H]^+$) 347.1256 found 347.1240; **TLC**: R_f = 0.35 (MeOH:DCM = 1:10).

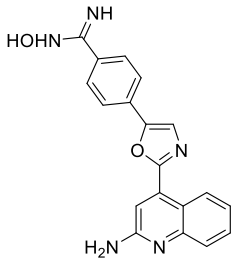

2-46

4-(2-(2-aminoquinolin-4-yl)oxazol-5-yl)-N-hydroxybenzimidamide 2-46.

1 mmol 2-aminoquinoline-4-carboxylic acid and 1 mmol 4-(2-bromoacetyl) benzo nitrile were dissolved in 10 mL anhydrous DMF, and 2 mmol of potassium carbonate was added. The reaction mixture was stirred at room temperature for 2 hours before solvents were removed under reduced pressure. 2 mL acetic acid and 680 mg urea were added and the mixture was heated to 140 ^{o}C for 6 hours. After the reaction mixture cooled to room temperature, water was added to quench the reaction. Saturated sodium carbonate was added to neutralize the reaction mixture, and ethyl acetate was used to extract the reaction mixture three times. Purification on silica gel column (90% DCM in methanol) provided the cyano intermediate. Re-dissolved the cyano intermediate in 1 mL absolutely ethanol and 1 mL hydroxylamine solution was added. The reaction mixture was further refluxed for 6 hours. Purification on silica gel column (10% methanol in DCM) provided the final product in 13% overall yield.

^{1}**H-NMR** (500 MHz, DMSO) δ 9.83 (s, 1H), 8.24 (s, 1H), 7.93 (d, *J* = 8.1 *Hz*, 1H), 7.63 (d, *J* = 8.1 *Hz*, 2H), 7.52 (s, 2H), 7.47 – 7.30 (m, 3H), 7.21 (d, *J* = 5.0 *Hz*, 1H), 6.61 (d, *J* = 54.4 *Hz*, 3H), 5.79 (s, 1H); ^{13}**C-NMR** (126 MHz, DMSO) δ 166.72, 160.26, 158.05, 155.36, 151.12, 148.88, 142.66, 138.44, 131.09, 129.72, 125.92, 123.44, 122.00, 119.95, 112.69, 112.34; **HR-MS(ESI)** m/z calcd for

$C_{19}H_{16}N_5O_2$ ($[M+H]^+$) 346.1304 found 346.1295; **TLC**: R_f = 0.40 (MeOH:DCM = 1:10).

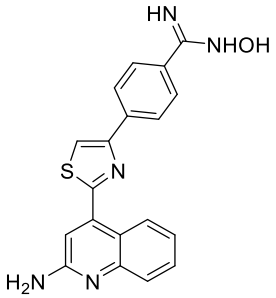

2-47

4-(2-(2-aminoquinolin-4-yl)thiazol-4-yl)-N-hydroxybenzimidamide 2-47.

1.5 mmol 2-aminoquinoline-4-carbonitrile was dissolved in 3 mL anhydrous DMF. To this slurry, 240 mg 68% NaSH and 306 mg $MgCl_2$ were added. The reaction mixture was stirred at room temperature for 1.5 hours. 50 mL water was added to the reaction mixture. After filtered the reaction mixture, the solid was re-suspended in 1 N HCl with stirring for 30 minutes. The reaction mixture was filtered again and the obtained solid was washed with water. The intermediate was dissolved in 10 mL anhydrous DMF, 1.5 mmol 4-(2-bromoacetyl)benzonitrile and 2 equiv. potassium carbonate were added to the reaction mixture at room temperature. After 12 hours stirring, the reaction was quenched with water. Saturated ammonium chloride was added to neutralize the reaction mixture, and ethyl acetate was used to extract the reaction mixture three times. Purification on silica gel column (90% DCM in methanol) provided the cyano intermediate. Re-dissolved the cyano intermediate in 1 mL absolutely ethanol and 1 mL hydroxylamine solution was added. The reaction mixture was refluxed for 6 hours. Purification on silica gel column (10% methanol in DCM) provided the final product in 20% overall yield.

^{1}H-NMR (500 MHz, DMSO) δ 10.46 (s, 1H), 9.73 (s, 1H), 8.02 (d, J = 8.2 Hz, 1H), 7.81 (s, 1H), 7.48 (d, J = 3.6 *Hz*, 2H), 7.27 – 7.05 (m, 1H), 6.82 (s, 1H), 6.58 (s, 2H), 6.00 (s, 2H); **^{13}C-NMR** (126 MHz, DMSO) δ 165.39, 163.75, 158.09, 157.56, 152.49, 150.73, 148.51, 141.47, 129.55, 126.27, 125.65, 121.65, 121.21, 112.53; **HR-MS(ESI)** m/z calcd for $C_{19}H_{16}N_5OS$ ($[M+H]^+$) 362.1076 found 362.1065; **TLC**: R_f = 0.45 (MeOH:DCM = 1:10).

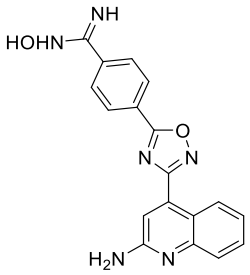

2-48

4-(3-(2-aminoquinolin-4-yl)-1,2,4-oxadiazol-5-yl)-N-hydroxybenzimidamide 2-48.

1 mmol 2-aminoquinoline-4-carbonitrile and 2 mL hydroxylamine solution were dissolved in absolutely ethanol and the reaction mixture was refluxed for 2 hours before solvents were removed under reduced pressure. Re-dissolved the intermediate in 1:1 pyridine/acetonitrile and 1.1 mmol 4-cyanobenzoyl chloride was added. The reaction mixture was refluxed for 12 hours before ice was added carefully at 0 ^{o}C. Extracted with ethyl acetate three times and removed solvents under vacuum gave the cyano intermediate. Re-dissolved the cyano intermediate in 1 mL absolutely ethanol and 1 mL hydroxylamine solution was also added to the reaction mixture. The reaction mixture was further refluxed for 6 hours. Purification on silica gel column (10% methanol in DCM) provided the final product in 38% overall yield.

^{1}H-NMR (500 MHz, DMSO) δ 8.47 (s, 1H), 7.89 (s, 1H), 7.69 (d, *J* = 8.2 *Hz*, 4H), 7.57 (d, *J* = 8.2 *Hz*, 2H), 7.32 (d, *J* = 8.1 *Hz*, 1H); **^{13}C-NMR** (126 MHz, DMSO) δ 153.20, 152.53, 151.09, 150.93, 148.26, 141.11, 134.85, 134.12, 133.78, 131.85, 129.26, 128.66, 125.33, 125.08; **HR-MS(ESI)** m/z calcd for $C_{18}H_{15}N_6O_2$ ($[M+H]^+$) 347.1256 found 347.1243; **TLC**: R_f = 0.40 (MeOH:DCM = 1:10).

6.3.2 General synthesis of 4-ethynyl-N-substituted-benzamide.

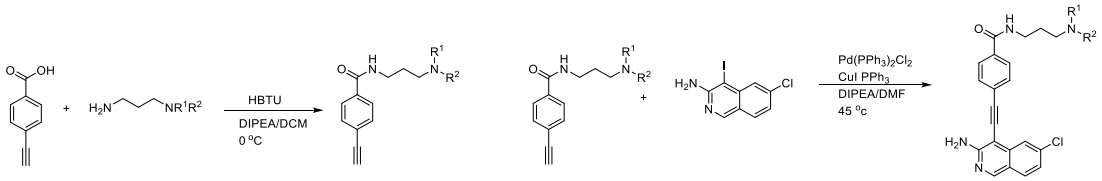

A 50 mL round bottom flask was charged with 4-ethynylbenzoic acid (1 equiv.) in dichloromethane. HBTU (1.5 equiv.) was added all at once at 0 ℃ and the solution was further stirred for 5 minutes at the same temperature before amine (1.1 equiv.) was added all at once followed by DIPEA (5 equiv.). The solution was allowed to reach room temperature and further stirred at room temperature overnight. Work up: After TLC showed the reaction was complete, the reaction mixture was poured into water and back extracted with dichloromethane three times. Combined solution was dried over sodium sulfate and then solvent was removed under reduced pressure, a viscous orange oil was obtained which was directly subjected to silica column chromatography (dichloromethane: methanol = 100:0 to 90:10, v/v) to afford pure 4-ethynyl-N-substituted-benzamide as white foam.

6.3.3 General synthesis of isoquinoline-3-amine amide kinase inhibitors.

To a 10 mL glass vial was charged **2-1** (1 equiv.), $Pd(PPh_3)_2Cl_2$ (5 mol%), PPh_3 (5 mol%), CuI (10 mol%) and degassed with an argon balloon three times. Anhydrous DMF was added to the vial and the reaction mixture was stired at 50 ^oC, then a solution of 4-ethynyl-N-substituted-benzamide was introduced slowly during 10 minutes. DIPEA was added all at once and the solution was stirred overnight at 50 ^oC. Work up: After TLC indicated complete consumption of starting material, the mixture was poured into water and back extracted with dichloromethane three times. The combined solution was dried over sodium sulfate and solvent was removed under reduced pressure, a dark yellow oil was obtained which was subjected to silica column chromatography (dichloromethane: methanol = 80:20, v/v) to afford pure compound as light-yellow solid.

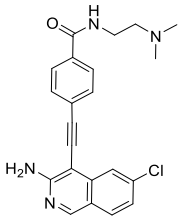

3-12

4-((3-amino-6-chloroisoquinolin-4-yl)ethynyl)-N-(2-(dimethylamino)ethyl)benzamide 3-12.

This compound was synthesized using the general protocol described in **6.3.2** and **6.3.3**.

Yield = 22%.**^{1}H-NMR** (500 MHz, MeOD) δ 7.90 (d, *J* = 8.6 *Hz*, 1H), 7.88 – 7.84 (m, 1H), 7.81 (d, *J* = 8.6 *Hz*, 1H), 7.76 (d, *J* = 8.6 *Hz*, 1H), 7.64 (s, 2H), 7.54 (d, *J* = 8.5 *Hz*, 1H), 7.36 (d, *J* = 7.8 *Hz*, 1H), 7.30 (d, *J* = 7.7 *Hz*, 1H), 3.57 – 3.51 (m,

3H), 2.62 (d, *J* = 6.8 *Hz*, 2H), 2.34 (s, 6H); **HR-MS(ESI)** m/z calcd for $C_{22}H_{22}ClN_4O$ ($[M+H]^+$) 393.1482 found 393.1466; **TLC**: R_f = 0.20 (MeOH:DCM = 1:5).

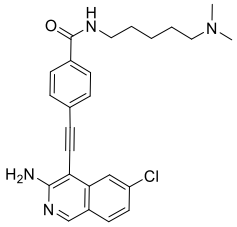

3-13

4-((3-amino-6-chloroisoquinolin-4-yl)ethynyl)-N-(5-(dimethylamino)pentyl)benzamide 3-13.

This compound was synthesized using the general protocol described in **6.3.2** and **6.3.3**.

Yield = 22%.**^{1}H-NMR** (500 MHz, MeOD) δ 7.92 (s, 1H), 7.90 (s, 1H), 7.86 (d, *J* = 8.7 *Hz*, 1H), 7.76 (d, *J* = 8.3 *Hz*, 1H), 7.43 (s, 2H), 7.26 (dd, *J* = 8.6, 1.9 *Hz*, 1H), 3.45 (t, *J* = 6.9 *Hz*, 2H), 3.21-3.12 (m, 2H), 2.91 (s, 6H), 1.82 (dt, *J* = 12.0, 8.0 *Hz*, 2H), 1.77-1.68 (m, 2H), 1.49 (dt, *J* = 15.0, 7.7 *Hz*, 2H); **^{13}C-NMR** (125 MHz, MeOD) δ 167.99, 157.58, 151.86, 138.75, 138.05, 133.79, 131.02, 130.40, 127.16, 126.31, 125.93, 124.96, 123.70, 121.29, 99.25, 84.50, 57.52, 44.62, 42.04, 39.07, 28.53, 23.85, 23.35; **HR-MS(ESI)** m/z calcd for $C_{25}H_{28}ClN_4O$ ($[M+H]^+$) 435.1952, found 435.1950; **TLC**: R_f = 0.15 (MeOH:DCM = 1:5).

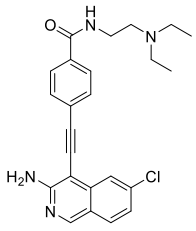

3-15

4-((3-amino-6-chloroisoquinolin-4-yl)ethynyl)-N-(2-(diethylamino)ethyl)benzamide 3-15.

This compound was synthesized using the general protocol described in **6.3.2** and **6.3.3**.

Yield = 52%.**^{1}H-NMR** (500 MHz, DMSO) δ 8.93 (s, 1H), 8.77 (s, 1H), 7.96 (d, *J* = 8.6 *Hz*, 1H), 7.91 (d, *J* = 9.7 *Hz*, 3H), 7.89 (d, *J* = 1.4 *Hz*, 1H), 7.29 (dd, *J* = 8.6, 1.9 *Hz*, 1H), 6.88 (s, 2H), 3.62 (d, *J* = 5.9 Hz, 2H), 3.30 – 3.08 (m, 6H), 1.22 (t, *J* = 7.2 *Hz*, 7H); **^{13}C-NMR** (126 MHz, DMSO) δ 166.68, 158.78, 153.45, 138.74, 137.46, 133.39, 131.68, 131.60, 127.87, 126.53, 123.56, 121.30, 120.63, 99.49, 88.30, 86.32, 50.27, 47.15, 35.06, 9.11. **HR-MS (ESI)** m/z calcd for $C_{26}H_{24}ClN_4O$ ($[M+H]^+$) 421.1795 found 421.1792; **TLC**: R_f = 0.20 (MeOH:DCM = 1:5).

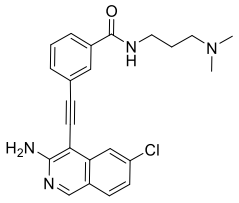

3-16

3-((3-amino-6-chloroisoquinolin-4-yl)ethynyl)-N-(3-(dimethylamino)propyl)benzamide 3-16.

This compound was synthesized using the general protocol described in **6.3.2** and **6.3.3**.

Yield = 22%.**^{1}H-NMR** (500 MHz, DMSO) δ 8.90 (s, 1H), 8.64 (t, *J* = 5.4 *Hz*, 1H), 8.16 (s, 1H), 7.92 (dd, *J* = 18.9, 8.2 *Hz*, 2H), 7.86 (d, *J* = 1.3 *Hz*, 1H), 7.82 (d, *J* = 7.9 *Hz*, 1H), 7.52 (t, *J* = 7.7 Hz, 1H), 7.26 (dd, *J* = 8.6, 1.9 *Hz*, 1H), 6.82 (s, 2H), 3.30 (dd, *J* = 12.8, 6.7 *Hz*, 2H), 2.35 (t, *J* = 7.1 *Hz*, 2H), 2.19 (s, 6H), 1.73-1.60 (m, 2H); **^{13}C-NMR** (125 MHz, DMSO) δ 165.99, 158.69, 153.15, 138.77, 137.37,

135.51, 134.23, 131.58, 130.35, 129.09, 127.53, 123.49, 123.45, 121.30, 120.63, 99.47, 88.53, 84.37, 57.13, 45.32, 38.16, 27.21; **HR-MS(ESI)** m/z calcd for $C_{23}H_{24}ClN_4O$ ($[M+H]^+$) 407.1639, found 407.1618; **TLC**: R_f = 0.20 (MeOH:DCM = 1:5).

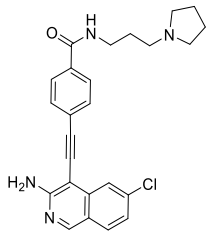

3-17

4-((3-amino-6-chloroisoquinolin-4-yl)ethynyl)-N-(3-(pyrrolidin-1-yl)propyl)benzamide 3-17.

This compound was synthesized using the general protocol described in **6.3.2** and **6.3.3**.

Yield = 53%.**^{1}H-NMR** (500 MHz, MeOD) δ 8.80 (s, 1H), 7.97-7.84 (m, 4H), 7.77 (dd, *J* = 5.8, 4.1 *Hz*, 2H), 7.26 (dd, *J* = 8.7, 2.0 *Hz*, 1H), 3.50 (t, *J* = 6.8 *Hz*, 2H), 3.33 (dt, *J* = 3.3, 1.6 *H*z, 4H), 2.86-2.80 (m, 2H), 1.94 (d, *J* = 3.6 *Hz*, 6H); **^{13}C-NMR** (125 MHz, MeOD) δ 168.08, 157.58, 151.92, 138.76, 138.05, 133.59, 131.02, 130.36, 127.13, 126.43, 123.68, 121.30, 120.79, 99.19, 90.18, 84.55, 53.68, 53.37, 37.58, 27.33, 22.74; **HR-MS(ESI)** m/z calcd for $C_{25}H_{26}ClN_4O$ ($[M+H]^+$) 433.1795, found 433.1799; **TLC**: R_f = 0.25 (MeOH:DCM = 1:5).

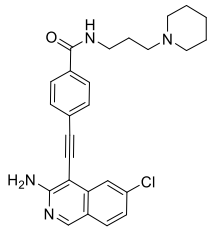

3-18

4-((3-amino-6-chloroisoquinolin-4-yl)ethynyl)-N-(3-(piperidin-1-yl)propyl)benzamide 3-18.

This compound was synthesized using the general protocol described in **6.3.2** and **6.3.3**.

Yield = 42%.**^{1}H-NMR** (500 MHz, MeOD) δ 8.81 (s, 1H), 7.95 (s, 1H), 7.93 (d, *J* = 1.9 *Hz*, 2H), 7.87 (d, *J* = 8.8 *Hz*, 1H), 7.78 (d, *J* = 8.5 *Hz*, 2H), 7.27 (dd, *J* = 8.6, 2.0 *Hz*, 1H), 3.54 (t, *J* = 6.6 *Hz*, 2H), 3.33 (dt, *J* = 3.3, 1.6 *Hz*, 6H), 3.22-3.17 (m, 2H), 1.91 (s, 6H); **^{13}C-NMR** (125 MHz, MeOD) δ 168.53, 157.63, 152.01, 137.98, 133.10, 131.06, 130.41, 127.33, 125.30, 123.70, 121.29, 117.28, 110.55, 99.15, 90.11, 86.23, 84.74, 54.45, 52.95,36.48, 24.18, 22.99, 21.36; **HR-MS(ESI)** m/z calcd for $C_{26}H_{28}ClN_4O$ ($[M+H]^+$) 447.2, found 447.3; **TLC**: R_f = 0.25 (MeOH:DCM = 1:5).

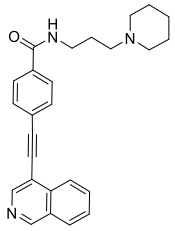

3-19

4-(isoquinolin-4-ylethynyl)-N-(3-(piperidin-1-yl)propyl)benzamide 3-19.

This compound was synthesized using the general protocol described in **6.3.2** and **6.3.3**.

^{1}H-NMR (500 MHz, MeOD) δ 9.26 (s, 1H), 8.70 (s, 1H), 8.38 (d, J = 8.3 Hz, 1H), 8.19 (d, J = 8.2 Hz, 1H), 8.03 – 7.93 (m, 3H), 7.82 (d, J = 9.6 Hz, 3H), 3.20 (d, J = 6.1 Hz, 2H), 2.27 – 1.45 (m, 10H), 1.42 – 1.29 (m, 4H); **^{13}C-NMR** (126 MHz, CDCl3) δ 167.99, 151.85, 145.84, 135.58, 132.83, 131.89, 131.76, 128.08,

126.34, 125.90, 125.08, 117.65, 96.25, 81.05, 54.72, 42.88, 36.52, 19.33, 18.61, 17.34; **HR-MS(ESI)** m/z calcd for $C_{26}H_{28}N_3$ ($[M+H]^+$) 398.2232 found 398.2230; **TLC**: R_f = 0.35 (MeOH:DCM = 1:50).

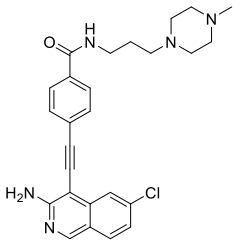

3-20

4-((3-amino-6-chloroisoquinolin-4-yl)ethynyl)-N-(3-(4-methylpiperazin-1-yl)propyl)benzamide 3-20.

This compound was synthesized using the general protocol described in **6.3.2** and **6.3.3**.

Yield = 49%.**^{1}H-NMR** (500 MHz, MeOD) δ 8.76 (s, 1H), 7.90-7.87 (m, 1H), 7.87-7.84 (m, 2H), 7.82 (d, *J* = 8.6 *Hz*, 1H), 7.75-7.71 (m, 2H), 7.22 (dd, *J* = 8.6, 2.0 *Hz*, 1H), 3.44 (t, *J* = 6.9 *Hz*, 2H), 2.77-2.37 (m, 10H), 2.28 (s, 3H), 1.83 (dd, *J* = 14.5, 7.2 *Hz*, 2H); **^{13}C-NMR** (125 MHz, MeOD) δ 167.90, 157.57, 151.90, 138.77, 138.05, 133.85, 131.03, 130.36, 127.13, 126.34, 123.68, 121.32, 120.79, 99.23, 90.21, 84.51, 55.88, 54.24, 52.27, 44.56, 38.25, 25.80; **HR-MS(ESI)** m/z calcd for $C_{26}H_{29}ClN_5O$ ($[M+H]^+$) 462.2061, found 462.2055; **TLC**: R_f = 0.15 (MeOH:DCM = 1:5).

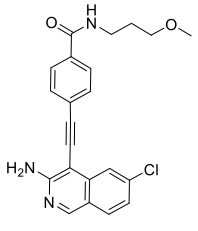

3-21

4-((3-amino-6-chloroisoquinolin-4-yl)ethynyl)-N-(3-methoxypropyl)benzamide 3-21.

This compound was synthesized using the general protocol described in **6.3.2** and **6.3.3**.

Yield = 32%.**^{1}H-NMR** (500 MHz, MeOD) δ 8.75 (s, 1H), 7.86 (dd, *J* = 10.5, 5.2 *Hz*, 3H), 7.81 (d, *J* = 8.7 *Hz*, 1H), 7.73 (d, *J* = 8.5 *Hz*, 2H), 7.22 (dd, *J* = 8.6, 2.0 *Hz*, 1H), 3.46 (s, 7H), 3.31 (s, 2H), 1.93 – 1.80 (m, 3H); **^{13}C-NMR** (126 MHz, MeOD) δ 168.02, 157.56, 154.87, 151.91, 138.74, 138.04, 133.73, 131.04, 130.36, 127.13, 126.38, 123.69, 121.32, 120.78, 99.24, 90.22, 84.55, 80.06, 54.44, 52.46, 27.23, 25.62; **HR-MS(ESI)** m/z calcd for $C_{22}H_{21}ClN_3O_2$ ($[M+H]^+$) 393.1322 found 393.1848; **TLC**: R_f = 0.35 (MeOH:DCM = 1:5).

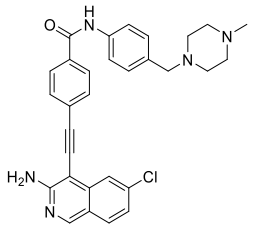

3-22

4-((3-amino-6-chloroisoquinolin-4-yl)ethynyl)-N-(4-((4-methylpiperazin-1-yl)methyl)phenyl)benzamide 3-22.

This compound was synthesized using the general protocol described in **6.3.2** and **6.3.3**.

Yield = 42%.**^{1}H-NMR** (500 MHz, DMSO) δ 10.34 (s, 1H), 8.91 (s, 1H), 8.03 (d, *J* = 8.3 *Hz*, 2H), 7.96-7.85 (m, 3H), 7.74 (d, *J* = 8.4 *Hz*, 2H), 7.32-7.20 (m, 3H), 6.88 (s, 2H), 3.43 (s, 2H), 2.63-2.31 (m, 8H), 2.24 (s, 3H);**^{13}C-NMR** (125 MHz, DMSO) δ 165.16, 158.79, 153.44, 138.78, 138.45, 137.47, 134.50, 131.64, 129.62, 128.32, 126.51, 123.54, 121.35, 120.76, 120.63, 99.58, 88.35, 86.33,

61.88, 54.71, 52.25, 45.47; **HR-MS(ESI)** m/z calcd for $C_{30}H_{29}ClN_5O$ ($[M+H]^+$) 510.2061, found 510.2048; **TLC**: R_f = 0.10 (MeOH:DCM = 1:5).

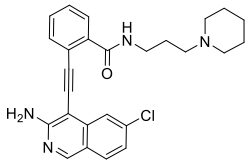

3-23

2-((3-amino-6-chloroisoquinolin-4-yl)ethynyl)-N-(3-(piperidin-1-yl)propyl)benzamide 3-23.

This compound was synthesized using the general protocol described in **6.3.2** and **6.3.3**.

Yield = 16%.**^{1}H-NMR** (500 MHz, DMSO) δ 8.90 (d, *J* = 0.4 *Hz*, 1H), 8.61 (s, 1H), 7.98 (d, *J* = 2.0 *Hz*, 1H), 7.93 (d, *J* = 8.6 *Hz*, 1H), 7.88 (dd, *J* = 7.7, 0.9 *Hz*, 1H), 7.58 – 7.50 (m, 2H), 7.46 (td, *J* = 7.5, 1.3 *Hz*, 1H), 7.26 (dd, *J* = 8.6, 2.0 *Hz*, 1H), 6.92 (s, 2H), 2.51 (dt, *J* = 3.6, 1.8 *Hz*, 3H), 2.30 – 2.21 (m, 2H), 2.16 (s, 4H), 1.71 – 1.59 (m, 2H), 1.42 – 1.30 (m, 4H), 1.27 (d, *J* = 4.7 *Hz*, 2H); **^{13}C-NMR** (126 MHz, DMSO) δ 168.30, 159.29, 153.12, 138.80, 138.68, 137.32, 132.81, 131.37, 130.23, 128.44, 127.80, 123.43, 121.69, 121.39, 120.54, 98.53, 88.83, 87.85, 56.93, 54.41, 39.65, 39.48, 38.55, 26.68, 26.00, 24.55; **HR-MS(ESI)** m/z calcd for $C_{26}H_{28}ClN_4O$ ($[M+H]^+$) 447.1952, found 447.1936; **TLC**: R_f = 0.20 (MeOH:DCM = 1:5).

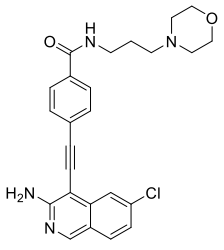

3-24

4-((3-amino-6-chloroisoquinolin-4-yl)ethynyl)-N-(3-morpholinopropyl)benzamide 3-24.

This compound was synthesized using the general protocol described in **6.3.2** and **6.3.3**.

Yield = 36%.**^{1}H-NMR** (500 MHz, MeOD) δ 8.79 (s, 1H), 7.93-7.82 (m, 4H), 7.76 (d, *J* = 8.4 *Hz*, 2H), 7.25 (dd, *J* = 8.6, 1.9 *Hz*, 1H), 3.72 (t, J = 4.6 *Hz*, 4H), 3.47 (t, J = 6.9 *Hz*, 2H), 2.58-2.49 (m, 6H), 1.93-1.81 (m, 2H); **^{13}C-NMR** (125 MHz, MeOD) δ 167.91, 157.55, 151.88, 138.75, 138.03, 133.81, 131.01, 130.33, 127.09, 126.33, 123.67, 121.30, 120.77, 99.21, 90.21, 84.49, 66.25, 56.38, 53.35, 38.16, 25.52; **HR-MS(ESI)** m/z calcd for $C_{25}H_{26}ClN_4O_2$ ($[M+H]^+$) 449.1744, found 449.1725; **TLC**: R_f = 0.25 (MeOH:DCM = 1:5).

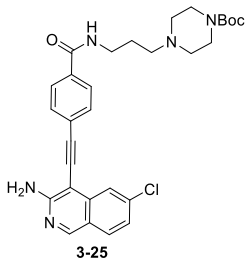

3-25

tert-butyl 4-(3-(4-((3-amino-6-chloroisoquinolin-4-yl)ethynyl)benzamido)propyl)piperazine-1-carboxylate 3-25.

This compound was synthesized using the general protocol described in **6.3.2** and **6.3.3**.

Yield = 29%.**^{1}H-NMR** (500 MHz, MeOD) δ 8.78 (s, 1H), 7.97 (s, 1H), 7.91 (d, *J* = 2.0 *Hz*, 1H), 7.88 (s, 1H), 7.86 (s, 2H), 7.75 (d, *J* = 8.6 *Hz*, 2H), 7.24 (dd, *J* = 8.7, 2.0 *Hz*, 1H), 3.76 – 3.68 (m, 2H), 3.48 (dd, *J* = 13.9, 7.0 *Hz*, 6H), 3.31 (dt, *J* = 3.3, 1.6 *Hz*, 4H), 3.22 (q, *J* = 7.4 *Hz*, 2H), 1.90 (dd, *J* = 14.3, 7.1 *Hz*, 2H), 1.45 (s, 9H); **^{13}C-NMR** (126 MHz, MeOD) δ 168.14, 163.60, 157.70, 154.95, 152.10,

137.83, 133.72, 131.05, 130.33, 127.15, 126.34, 123.70, 121.43, 120.69, 109.71, 99.21, 90.17, 84.55, 80.19, 55.53, 54.37, 52.18, 42.53, 27.03, 25.56; **HR-MS(ESI)** m/z calcd for $C_{20}H_{35}ClN_5O_3$ ($[M+H]^+$) 548.2328 found 548.2325; **TLC**: R_f = 0.25 (MeOH:DCM = 1:5).

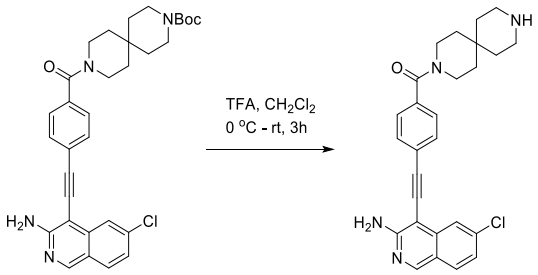

(4-((3-amino-6-chloroisoquinolin-4-yl)ethynyl)phenyl)(3,9-diazaspiro[5.5]undecan-3-yl)methanone 3-26.

To a solution of Boc protected benzamide **3-15** (30 mg, 0.06 mmol, 1 equiv.) in CH_2Cl_2 (3 mL) was added trifluoroacetic acid (90 µL, 1.2 mmol, 20 equiv.) at 0 ^oC slowly over a period of 5 minutes. The resulting solution was stirred at room temperature for 3 hours. After completion of the reaction, solvent was evaporated under reduced pressure and the remaining crude solid was purified by flash column chromatography. Yield = 42%.

^{1}H-NMR (500 MHz, MeOD) δ 8.77 (s, 1H), 7.89 (d, *J* = 1.2 *Hz*, 1H), 7.83 (d, *J* = 8.7 *Hz*, 1H), 7.73 (d, *J* = 8.1 *Hz*, 2H), 7.45 (d, *J* = 8.1 *Hz*, 2H), 7.23 (dd, *J* = 8.6, 1.8 *Hz*, 1H), 3.74 (s, 2H), 3.43 (s, 2H), 2.85 (s, 4H), 1.57 (t, *J* = 27.2 *Hz*, 8H); **^{13}C-NMR** (126 MHz, MeOD) δ 170.23, 157.55, 151.83, 138.77, 138.03, 135.51, 131.19, 130.37, 126.86, 124.75, 123.68, 121.31, 120.80, 99.20, 90.26, 83.76, 43.04, 40.59, 37.78, 34.76, 30.02; **HR-MS(ESI)** m/z calcd for $C_{27}H_{28}ClN_4O$ ($[M+H]^+$) 459.1952 found 459.1949; **TLC**: R_f = 0.20 (MeOH:DCM = 1:5).

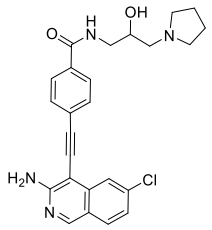

3-28

4-((3-amino-6-chloroisoquinolin-4-yl)ethynyl)-N-(2-hydroxy-3-(pyrrolidin-1-yl)propyl)benzamide 3-28.

This compound was synthesized using the general protocol described in **6.3.2** and **6.3.3**.

Yield = 28%.**^{1}H-NMR** (500 MHz, MeOD) δ 8.71 (s, 1H), 7.88 – 7.79 (m, 3H), 7.76 (d, *J* = 8.7 *Hz*, 1H), 7.69 (d, *J* = 8.1 *Hz*, 2H), 7.21 – 7.12 (m, 1H), 4.00 (dt, *J* = 11.9, 6.2 *Hz*, 1H), 3.53 (dd, *J* = 13.6, 5.0 *Hz*, 1H), 3.39 (dd, *J* = 13.6, 6.8 *Hz*, 1H), 2.69 (t, *J* = 6.0 *Hz*, 6H), 1.82 (s, 4H); **^{13}C-NMR** (126 MHz, MeOD) δ 168.19, 157.48, 151.83, 138.68, 137.99, 133.58, 130.98, 130.28, 127.17, 126.42, 123.66, 121.31, 120.73, 99.25, 90.27, 84.60, 68.17, 60, 54.23, 44.74, 22.85; **HR-MS(ESI)** m/z calcd for $C_{25}H_{24}ClN_4O_2$ ($[M+H]^+$) 449.1744, found 449.1748; **TLC**: R_f = 0.15 (MeOH:DCM = 1:5).

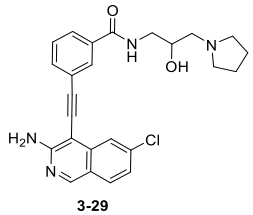

3-29

3-((3-amino-6-chloroisoquinolin-4-yl)ethynyl)-N-(2-hydroxy-3-(pyrrolidin-1-yl)propyl)benzamide 3-29.

This compound was synthesized using the general protocol described in **6.3.2** and **6.3.3**.

Yield = 33%. **^{1}H-NMR** (500 MHz, MeOD) δ 8.75 (s, 1H), 8.10 (s, 1H), 7.90 – 7.79 (m, 4H), 7.51 (t, *J* = 7.8 *Hz*, 1H), 7.21 (dd, *J* = 8.7, 1.9 *Hz*, 1H), 4.00 (ddd, *J* = 12.1, 7.2, 5.1 *Hz*, 1H), 3.54 (dd, *J* = 13.6, 5.1 *Hz*, 1H), 3.41 (dd, *J* = 13.6, 6.8 *Hz*, 1H), 2.69 (s, 6H), 1.82 (s, 4); **^{13}C-NMR** (126 MHz, MeOD) δ 168.10, 157.53, 151.72, 138.72, 137.99, 134.68, 133.90, 130.33, 129.67, 128.59, 126.95, 123.67, 123.51, 121.33, 120.78, 99.07, 90.37, 83.03, 68.12, 60.08, 54.24, 44.80, 22.86; **HR-MS(ESI)** m/z calcd for $C_{25}H_{24}ClN_4O_2$ ($[M+H]^+$) 449.1744, found 449.1736; **TLC**: R_f = 0.15 (MeOH:DCM = 1:5).

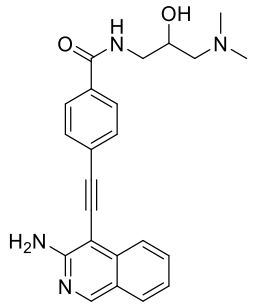

3-30

4-((3-aminoisoquinolin-4-yl)ethynyl)-N-(3-(dimethylamino)-2-hydroxypropyl)benzamide 3-30.

This compound was synthesized using the general protocol described in **6.3.2** and **6.3.3**.

^{1}H-NMR (500 MHz, MeOD) δ 8.79 (s, 1H), 8.00 (d, *J* = 8.4 Hz, 1H), 7.92 (t, *J* = 7.7 Hz, 2H), 7.85 (d, *J* = 8.1 Hz, 1H), 7.74 (d, *J* = 8.0 Hz, 2H), 7.67 – 7.62 (m, 1H), 7.30 (t, *J* = 7.5 Hz, 1H), 4.11 (s, 1H), 3.54 (dd, *J* = 13.6, 4.8 Hz, 1H), 3.42 (dd, *J* = 13.6, 6.4 Hz, 1H), 2.81 (s, 2H), 2.61 (s, 6H); **^{13}C-NMR** (126 MHz, MeOD) δ 168.39, 156.88, 151.86, 138.08, 133.33, 131.62, 130.96, 128.32, 127.27, 126.76, 123.11, 122.72, 122.59, 99.01, 91.39, 85.31, 66.07, 61.86, 44.19, 43.74;

HR-MS(ESI) m/z calcd for $C_{23}H_{25}N_4O_2$ ($[M+H]^+$) 389.1978, found 383.1982; **TLC**: R_f = 0.20 (MeOH:DCM = 1:5).

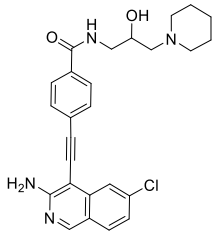

3-32

4-((3-amino-6-chloroisoquinolin-4-yl)ethynyl)-N-(2-hydroxy-3-(piperidin-1-yl)propyl)benzamide 2-32.

This compound was synthesized using the general protocol described in **6.3.2** and **6.3.3**.

^{1}H-NMR (500 MHz, DMSO) δ 8.92 (s, 1H), 7.96 (d, J = 8.6 Hz, 1H), 7.88 (d, J = 1.8 Hz, 1H), 7.83 (d, J = 8.3 Hz, 2H), 7.62 (d, J = 8.3 Hz, 2H), 7.29 (dd, J = 8.6, 2.0 Hz, 1H), 6.85 (s, 2H), 5.04 (d, J = 11.8 Hz, 1H), 3.76 (t, J = 9.9 Hz, 3H), 3.44 – 3.38 (m, 6H), 1.58 – 1.39 (m, 5H); **^{13}C-NMR** (126 MHz, DMSO) δ 166.58, 158.48, 153.46, 138.99, 137.45, 131.83, 131.62, 131.56, 128.58, 124.55, 123.48, 121.43, 120.79, 99.59, 88.79, 85.30, 72.75, 60.97, 54.89, 47.24, 26.07, 24.46; **HR-MS(ESI)** m/z calcd for $C_{26}H_{28}ClN_4O_2$ ($[M+H]^+$) 463.1901, found 463.1905; **TLC**: R_f = 0.18 (MeOH:DCM = 1:10).

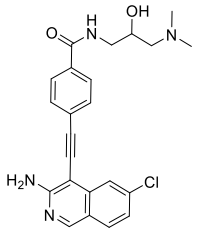

3-33

4-((3-amino-6-chloroisoquinolin-4-yl)ethynyl)-N-(3-(dimethylamino)-2-hydroxypropyl)benzamide 3-33.

This compound was synthesized using the general protocol described in **6.3.2** and **6.3.3**.

Yield = 69%.**^{1}H-NMR** (500 MHz, MeOD) δ 8.79 (s, 1H), 7.92 (s, 2H), 7.90 (s, 1H), 7.85 (d, *J* = 8.7 *Hz*, 1H), 7.76 (d, *J* = 8.4 *Hz*, 2H), 7.25 (dd, *J* = 8.6, 1.9 *Hz*, 1H), 4.05-3.94 (m, 1H), 3.55 (dd, *J* = 13.6, 4.8 *Hz*, 1H), 3.42-3.35 (m, 1H), 2.47-2.43 (m, 2H), 2.33 (s, 6H); **^{13}C-NMR** (125 MHz, MeOD) δ 168.24, 157.56, 151.88, 138.76, 138.05, 133.69, 131.00, 130.34, 127.18, 126.38, 123.67, 121.30, 120.78, 99.22, 90.21, 84.49, 67.43, 63.23, 44.75, 44.70; **HR-MS(ESI)** m/z calcd for $C_{23}H_{24}ClN_4O_2$ ($[M+H]^+$) 423.1588, found 423.1587; **TLC**: R_f = 0.20 (MeOH:DCM = 1:5).

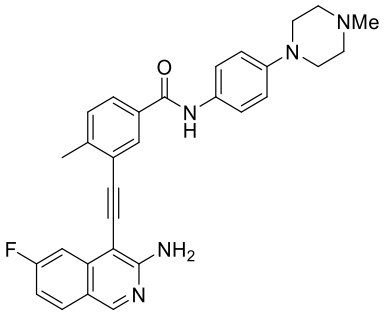

4-1

3-((3-amino-6-fluoroisoquinolin-4-yl)ethynyl)-4-methyl-N-(4-(4-methylpiperazin-1-yl)phenyl)benzamide 4-1.

This compound was synthesized using the general protocol described in **6.3.2** and **6.3.3**.

Yield = 23%. **^{1}H-NMR** (500 MHz, DMSO) δ 10.11 (s, 1H), 8.92 (s, 1H), 8.37 (s, 1H), 8.05 (dd, *J* = 8.8, 5.9 *Hz*, 1H), 7.87 (s, 1H), 7.56 (ddd, *J* = 35.7, 28.9, 8.4 *Hz*, 4H), 7.18 (td, *J* = 8.7, 2.2 *Hz*, 1H), 6.95 (d, *J* = 9.0 *Hz*, 2H), 6.73 (s, 2H), 3.14 (s, 3H), 2.64 (s, 2H), 2.53 (d, *J* = 22.3 *Hz*, 6H), 2.29 (s, 3H); **^{13}C-NMR** (126 MHz,

DMSO) δ 165.61, 164.68, 163.63, 158.41, 153.01, 147.81, 142.56, 139.70, 133.45, 133.04, 131.51, 131.29, 130.03, 127.87, 123.36, 121.97, 119.81, 115.99, 113.20, 113.00, 106.02, 98.31, 88.56, 54.86, 48.66, 45.84, 21.26; **HR-MS(ESI)** m/z calcd for $C_{30}H_{29}FN_5O$ ([M+H]+) 494.2456, found 494.2347; **TLC**: R_f = 0.20 (MeOH:DCM = 1:10).

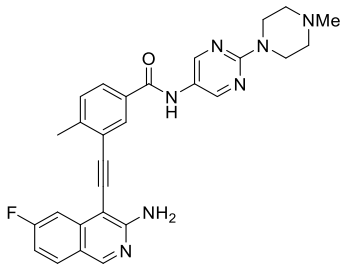

4-2

3-((3-amino-6-fluoroisoquinolin-4-yl)ethynyl)-4-methyl-N-(2-(4-methylpiperazin-1-yl)pyrimidin-5-yl)benzamide 4-2.

This compound was synthesized using the general protocol described in **6.3.2** and **6.3.3**.

Yield = 20%. **^{1}H-NMR** (500 MHz, DMSO) δ 8.92 (s, 1H), 8.70 (s, 2H), 8.40 (s, 1H), 8.09 – 8.00 (m, 2H), 7.89 (d, *J* = 7.8 *Hz*, 1H), 7.53 (s, 2H), 7.19 (t, *J* = 8.6 *Hz*, 1H), 6.75 (s, 2H), 3.00 (s, 3H), 2.38 (s, 8H), 2.23 (s, 3H); **^{13}C-NMR** (126 MHz, DMSO) δ 165.15, 158.94, 158.44, 153.01, 151.61, 143.01, 139.77, 132.38, 131.28, 130.09, 127.87, 124.56, 123.53, 119.73, 106.19, 105.97, 98.07, 89.54, 88.71, 54.80, 46.27, 44.07, 42.57, 21.31; **HR-MS(ESI)** m/z calcd for $C_{28}H_{27}FN_7O$ ([M+H]+) 496.2261, found 496.2308; **TLC**: R_f = 0.20 (MeOH:DCM = 1:10).

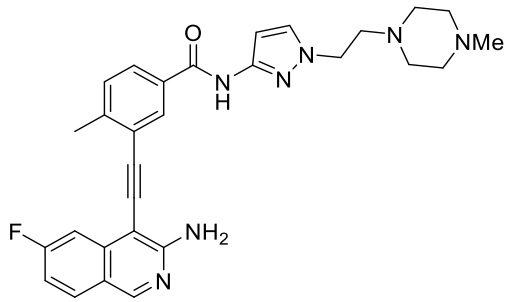

4-3

3-((3-amino-6-fluoroisoquinolin-4-yl)ethynyl)-4-methyl-N-(1-(2-morpholinoethyl)-1H-pyrazol-3-yl)benzamide 4-3.

This compound was synthesized using the general protocol described in **6.3.2** and **6.3.3**.

Yield = 15%. **^{1}H-NMR** (500 MHz, DMSO) δ 9.37 (s, 1H), 8.92 (s, 1H), 8.35 (s, 1H), 8.05 (dd, *J* = 8.8, 5.9 *Hz*, 1H), 7.86 (t, *J* = 9.1 *Hz*, 2H), 7.54 (t, *J* = 9.1 *Hz*, 2H), 7.18 (dd, *J* = 9.9, 7.6 *Hz*, 1H), 6.72 (dd, *J* = 31.2, 14.4 *Hz*, 4H), 2.55 – 2.40 (m, 16H), 2.23 (s, 3H), 0.83 (d, *J* = 6.3 *Hz*, 3H); **^{13}C-NMR** (126 MHz, DMSO) δ 165.56, 163.63, 158.34, 153.06, 148.83, 145.99, 142.69, 133.10, 130.84, 130.37, 127.31, 124.83, 123.73, 123.09, 119.72, 113.09, 112.93, 110.76, 108.55, 106.25, 106.02, 97.99, 89.40, 88.41, 70.10, 55.14, 52.57, 49.03, 46.09, 35.24, 29.38, 22.56, 22.24; **HR-MS(ESI)** m/z calcd for $C_{29}H_{29}FN_7O_2$ ([M+H]+) 526.2367, found 526.2372; **TLC**: R_f = 0.20 (MeOH:DCM = 1:10).

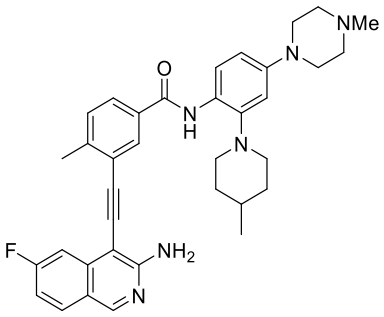

4-4

3-((3-amino-6-fluoroisoquinolin-4-yl)ethynyl)-4-methyl-N-(1-(2-morpholinoethyl)-1H-pyrazol-3-yl)benzamide 4-4.

This compound was synthesized using the general protocol described in **6.3.2** and **6.3.3**.

Yield = 22%. **^{1}H-NMR** (500 MHz, DMSO) δ 9.37 (s, 1H), 8.92 (s, 1H), 8.35 (s, 1H), 8.05 (dd, *J* = 8.8, 5.9 *Hz*, 1H), 7.86 (t, *J* = 9.1 *Hz*, 2H), 7.54 (t, *J* = 9.1 *Hz*, 2H), 7.18 (dd, *J* = 9.9, 7.6 *Hz*, 1H), 6.72 (dd, *J* = 31.2, 14.4 *Hz*, 4H), 2.55 – 2.40 (m, 16H), 2.23 (s, 3H), 0.83 (d, *J* = 6.3 *Hz*, 3H); **^{13}C-NMR** (126 MHz, DMSO) δ 165.56, 163.63, 158.34, 153.06, 148.83, 145.99, 142.69, 133.10, 130.84, 130.37, 127.31, 124.83, 123.73, 123.09, 119.72, 113.09, 112.93, 110.76, 108.55, 106.25, 106.02, 97.99, 89.40, 88.41, 70.10, 55.14, 52.57, 49.03, 46.09, 35.24, 29.38, 22.56, 22.24; **HR-MS(ESI)** m/z calcd for $C_{36}H_{40}FN_6O$ ([M+H]+) 591.3248, found 591.322; **TLC**: R_f = 0.25 (MeOH:DCM = 1:10).

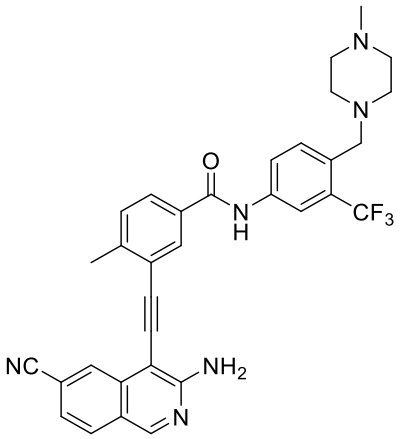

4-5

3-((3-amino-6-cyanoisoquinolin-4-yl)ethynyl)-4-methyl-N-(4-((4-methylpiperazin-1-yl)methyl)-3-(trifluoromethyl)phenyl)benzamide 4-5.

This compound was synthesized using the general protocol described in **6.3.2** and **6.3.3**.

Yield = 63%. **^{1}H-NMR** (500 MHz, DMSO) δ 10.57 (s, 1H), 9.07 (s, 1H), 8.43 (d, *J* = 1.9 *Hz*, 1H), 8.37 – 8.33 (m, 1H), 8.23 (d, *J* = 2.1 *Hz*, 1H), 8.13 (d, *J* = 8.2 *Hz*, 1H), 8.08 (dd, *J* = 8.5, 1.9 *Hz*, 1H), 7.91 (dd, *J* = 8.0, 1.9 *Hz*, 1H), 7.72 (d, *J* = 8.5 *Hz*, 1H), 7.61 – 7.50 (m, 2H), 6.97 (s, 2H), 3.58 (s, 2H), 2.67 (s, 3H), 2.41 (s, 8H), 2.21 (s, 3H); **^{13}C-NMR** (126 MHz, MeOD) δ 166.36, 159.65, 154.34, 149.12, 144.32, 139.53, 137.70, 133.60, 133.11, 132.52, 131.66, 131.01, 129.48, 129.03, 124.74, 124.21, 124.13, 123.84, 123.61, 120.06, 118.12, 115.18, 111.60, 99.57, 90.34, 88.85, 58.64, 55.78, 53.43, 46.63, 22.09; **HR-MS(ESI)** m/z calcd for $C_{33}H_{30}F_3N_6O$ ([M+H]+) 583.2433, found 583.2431; **TLC**: R_f = 0.30 (MeOH:DCM = 1:10).

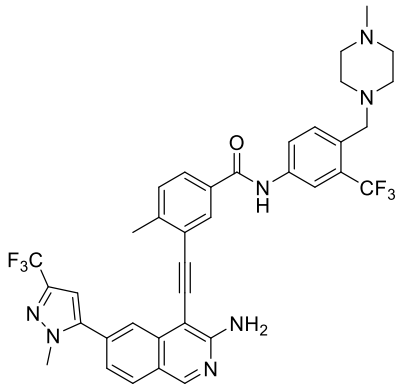

4-6

3-((3-amino-6-(1-methyl-3-(trifluoromethyl)-1H-pyrazol-5-yl)isoquinolin-4-yl)ethynyl)-4-methyl-N-(4-((4-methylpiperazin-1-yl)methyl)-3-(trifluoromethyl)phenyl)benzamide 4-6.

This compound was synthesized using the general protocol described in **6.3.2** and **6.3.3**.

Yield = 8%. **^{1}H-NMR** (500 MHz, MeOD) δ 11.36 (s, 1H), 9.82 (s, 1H), 9.22 (d, *J* = 1.8 Hz, 1H), 9.05 (s, 1H), 8.93 – 8.90 (m, 1H), 8.69 (dd, *J* = 8.0, 1.8 *Hz*, 1H), 8.53 (d, *J* = 8.5 *Hz*, 1H), 8.34 (d, *J* = 8.4 *Hz*, 2H), 8.10 (s, 1H), 7.92 (s, 1H), 7.67 (d, *J* = 2.3 *Hz*, 1H), 7.57 (s, 2H), 6.25 (s, 3H), 4.85 (s, 3H), 3.45 (s, 3H), 3.18 (d, *J* = 1.9 *Hz*, 8H), 2.99 (s, 3H); **^{13}C-NMR** (126 MHz, MeOD) δ 207.76, 166.38, 163.57, 159.34, 153.92, 149.09, 145.87, 144.03, 139.51, 138.49, 133.60, 133.09, 132.72, 132.49, 132.34, 130.99, 130.83, 124.69, 124.37, 123.91, 122.66, 118.12, 111.54, 106.32, 99.28, 90.67, 89.77, 58.80, 55.92, 53.82, 53.66, 46.77, 31.97, 22.09; **HR-MS(ESI)** m/z calcd for $C_{37}H_{34}F_6N_7O$ ([M+H]+) 706.2729, found 706.2803; **TLC**: R_f = 0.10 (MeOH:DCM = 1:10).

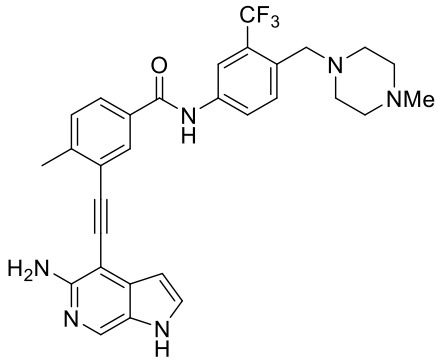

4-7

3-((3-amino-6-fluoroisoquinolin-4-yl)ethynyl)-4-methyl-N-(1-(2-morpholinoethyl)-1H-pyrazol-3-yl)benzamide 4-7.

This compound was synthesized using the general protocol described in **6.3.2** and **6.3.3**.

Yield = 11%. **^{1}H-NMR** (500 MHz, DMSO) δ 8.27 (s, 1H), 8.23 (d, *J* = 1.8 *Hz*, 1H), 8.07 (d, *J* = 7.0 *Hz*, 1H), 7.86 (dd, *J* = 8.0, 1.6 *Hz*, 1H), 7.72 (d, *J* = 8.5 *Hz*, 1H), 7.59 – 7.46 (m, 1H), 6.37 (s, 1H), 5.60 (s, 1H), 3.58 (s, 2H), 3.51 (s, 3H), 3.33 (s, 8H), 2.17 (s, 3H); **HR-MS(ESI)** m/z calcd for $C_{30}H_{29}F_3N_6O$ ([M+H]+) 547.2428, found 547.2434; **TLC**: R_f = 0.25 (MeOH:DCM = 1:10).

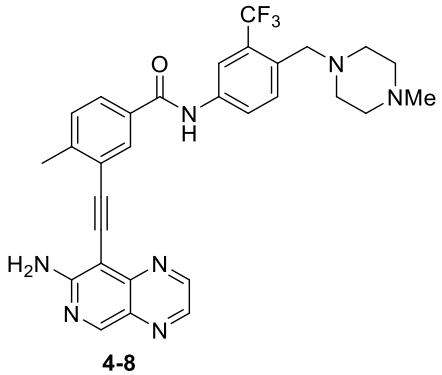

4-8

3-((3-amino-6-fluoroisoquinolin-4-yl)ethynyl)-4-methyl-N-(1-(2-morpholinoethyl)-1H-pyrazol-3-yl)benzamide 4-8.

This compound was synthesized using the general protocol described in **6.3.2** and **6.3.3**. The starting material was prepared as below.

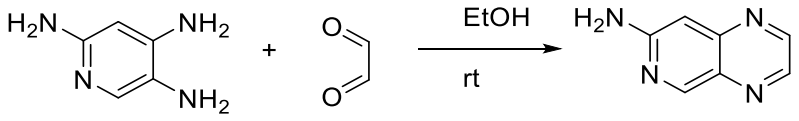

To a 50 mL round bottom flask, 1 equiv. of pyridine-2,4,5-triamine was dissolved in anhydrous ethanol at room temperature. The mixture was stirred for 5 minutes before oxalaldehyde was added all at once, and the mixture was stirred overnight. After TLC showed the reaction was complete, 100 mL cooled water was added. The reaction mixture was extracted with DCM three times (50 mL *3), washed with brine and dried over anhydrous sodium sulfate. Solvent was removed under reduced pressure to give crude product. Pure product was obtained by purification on Combi-flash using 100% DCM to 35% MeOH.

Yield = 14%. **^{1}H-NMR** (500 MHz, DMSO) δ 10.58 (s, 1H), 9.05 (s, 1H), 8.95 (d, *J* = 1.7 *Hz*, 1H), 8.65 (d, *J* = 1.7 *Hz*, 1H), 8.35 (d, *J* = 1.7 *Hz*, 1H), 8.23 (d, *J* = 1.9 *Hz*, 1H), 8.15 – 8.04 (m, 1H), 7.90 (dd, *J* = 8.0, 1.7 *Hz*, 1H), 7.72 (d, *J* = 8.5 *Hz*, 1H), 7.52 (d, *J* = 8.1 *Hz*, 1H), 7.15 (s, 2H), 2.66 (s, 3H), 2.38 (d, *J* = 15.6 *Hz*, 8H), 2.17 (s, 3H); **^{13}C-NMR** (126 MHz, DMSO) δ 175.08, 165.52, 160.51, 154.45, 150.77, 147.66, 143.97, 142.74, 138.70, 132.62, 132.48, 132.22, 131.69, 131.31, 130.14, 128.08, 123.94, 123.64, 117.70, 97.84, 91.40, 88.21, 57.92, 55.18, 53.14, 46.16, 29.49; **HR-MS(ESI)** m/z calcd for $C_{30}H_{29}F_3N_7O$ ([M+H]+) 560.2381, found 560.2377. **TLC**: R_f = 0.20 (MeOH:DCM = 1:10).

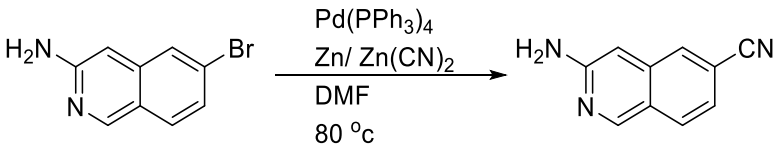

In a 50 mL round bottom flask, 50 mg 6-bromo-isoquinolin-3-amine, 10 mol% tetrakis(triphenylphosphine)palladium(0), 1 mol% zinc, 1.5 equiv. zinc cyanide were added. The system was sealed and purged with nitrogen three times before 5 mL anhydrous DMF was added. The reaction mixture was stirred at 80 ^{o}C overnight. After TLC showed the reaction was complete, equal volume of distilled water was added. The reaction mixture was extracted with DCM three times (50 mL *3), washed with brine and dried over anhydrous sodium sulfate. Solvent was removed under reduced pressure to give crude product. Pure product was obtained by further purifications on Combi-flash using 100% DCM to 35% MeOH. ^{1}**H-NMR** (500 MHz, DMSO) δ 8.95 (s, 1H), 8.18 (s, 1H), 7.67 – 7.50 (m, 2H), 7.35 (dd, J = 8.4, 1.3 Hz, 1H), 6.69 (s, 1H), 6.32 (s, 2H); **HR-MS(ESI)** m/z calcd for C10H7N3 ([M+H]+) 170.1 found 170.6.

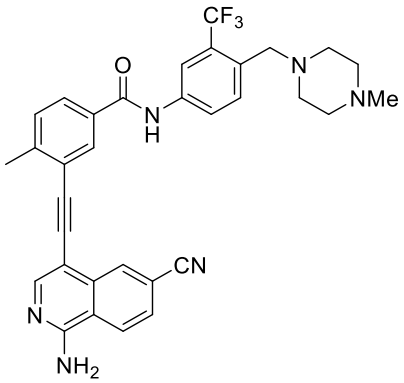

4-9

3-((1-amino-6-cyanoisoquinolin-4-yl)ethynyl)-4-methyl-N-(4-((4-methylpiperazin-1-yl)methyl)-3-(trifluoromethyl)phenyl)benzamide 4-9.

This compound was synthesized using the general protocol described in **6.3.2** and **6.3.3**.

Yield = 43%. **^{1}H-NMR** (500 MHz, DMSO) δ 10.55 (s, 1H), 8.92 (s, 1H), 8.36 (s, 1H), 8.21 (d, J = 7.8 Hz, 3H), 8.09 (t, J = 8.0 Hz, 2H), 7.90 (d, J = 7.9 Hz, 1H), 7.79 (s, 2H), 7.71 (d, J = 8.5 Hz, 1H), 7.52 (d, J = 8.0 Hz, 1H), 3.57 (s, 2H), 2.61 (s, 3H), 2.40 (s, 7H), 2.18 (s, 3H); **^{13}C-NMR** (126 MHz, DMSO) δ 165.27, 158.06, 150.92, 143.44, 138.66, 138.59, 132.66, 132.46, 131.66, 131.46, 130.80, 130.33, 128.10, 126.17, 123.97, 123.31, 119.28, 117.69, 115.90, 108.70, 102.91, 92.25, 90.64, 57.88, 55.11, 53.04, 46.05, 21.17; **HR-MS(ESI)** m/z calcd for $C_{33}H_{30}F_3N_6O$ ([M+H]+) 583.2433, found 583/2435. **TLC**: R_f = 0.18 (MeOH:DCM = 1:10).

Appendix NMR spectra

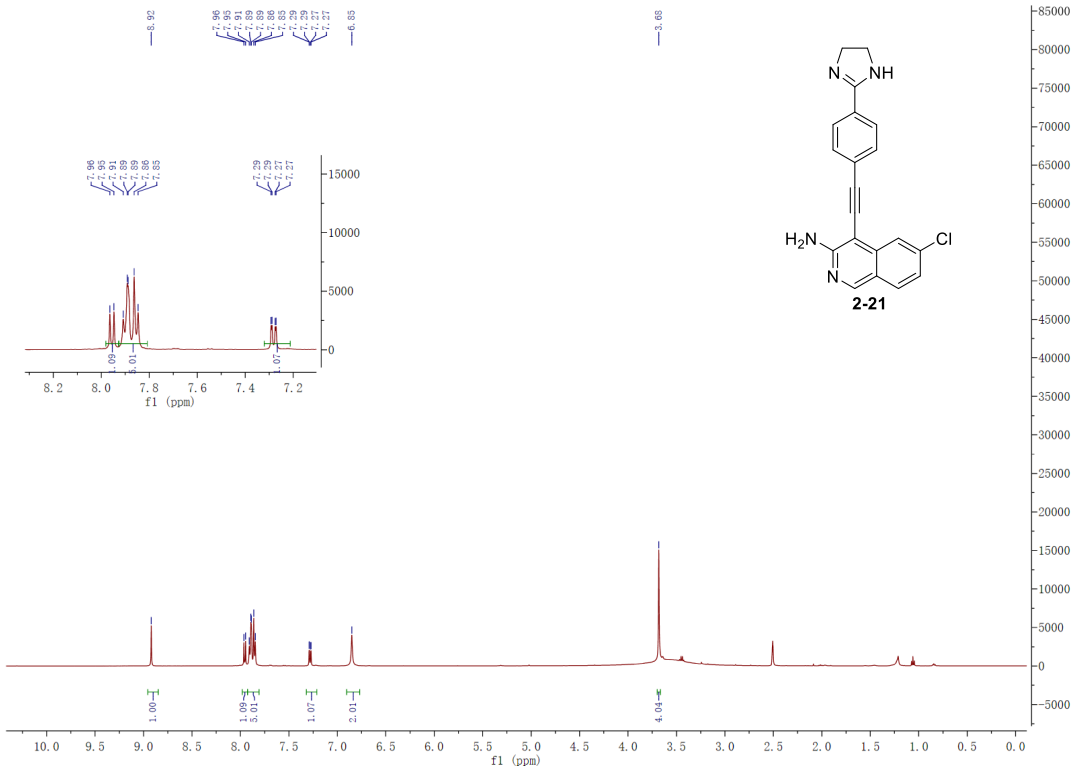

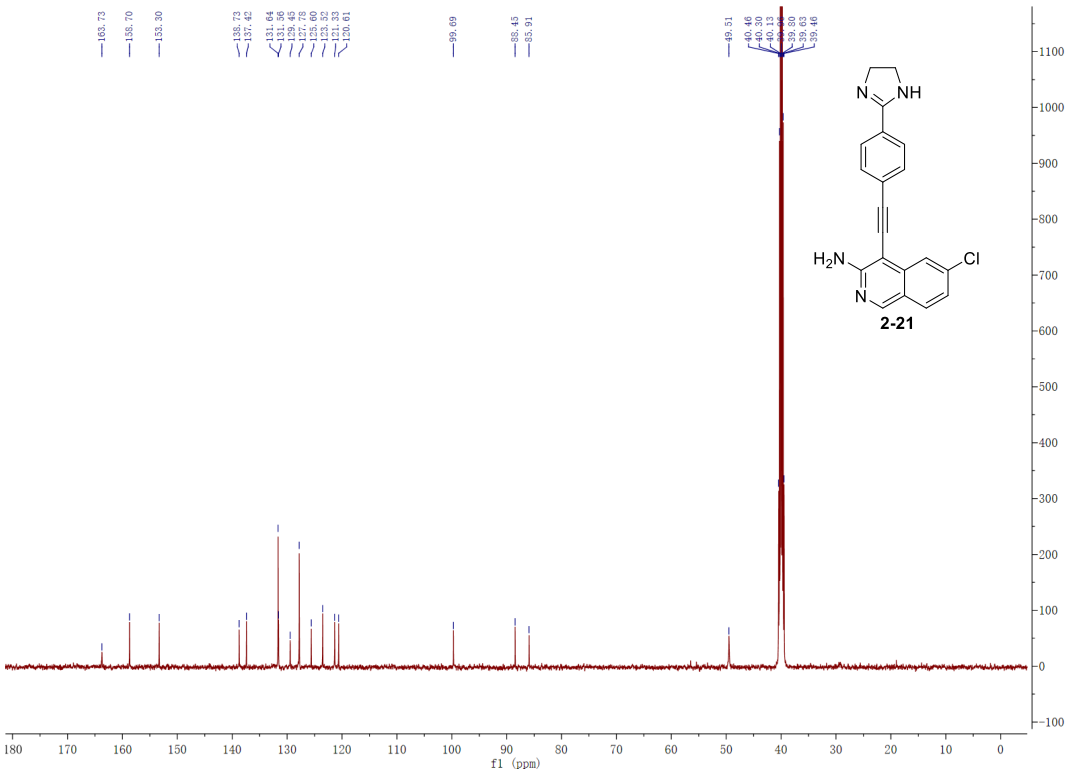

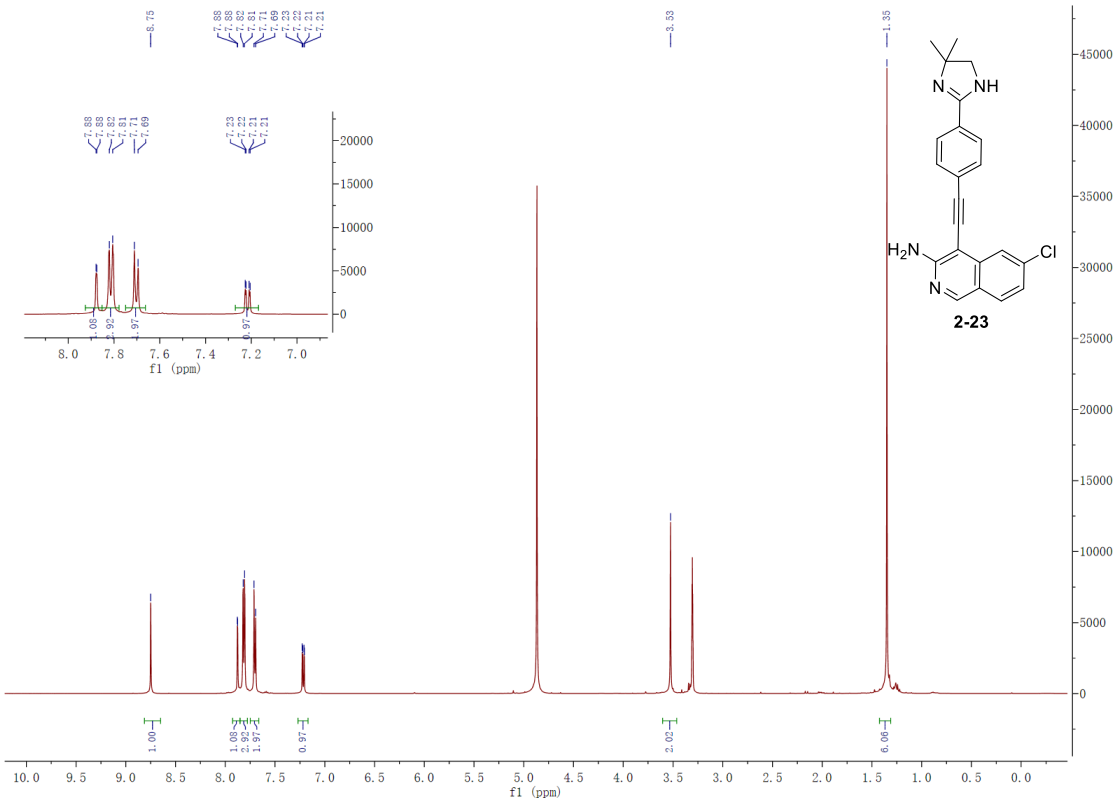
8.75
7.88
7.88
7.82
7.81
7.71
7.69
7.23
7.22
7.21
7.21
3.53
1.35
1.00
1.08
2.92
1.97
0.97
2.02
6.06
f1 (ppm)
NH
N
H2N
Cl
2-23

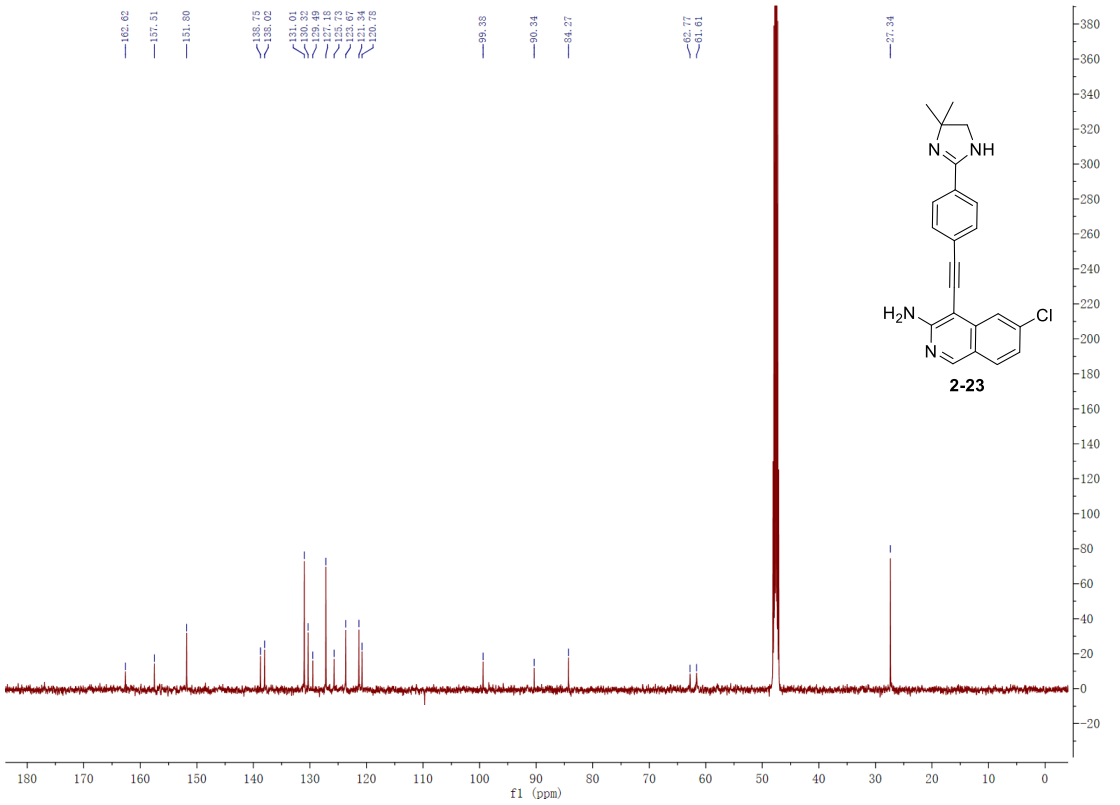
162.62
157.51
151.80
138.75
138.02
131.01
130.23
129.49
127.18
125.73
123.67
121.34
120.76
99.38
90.34
84.27
62.77
61.61
27.34
f1 (ppm)
NH
N
H2N
Cl
2-23

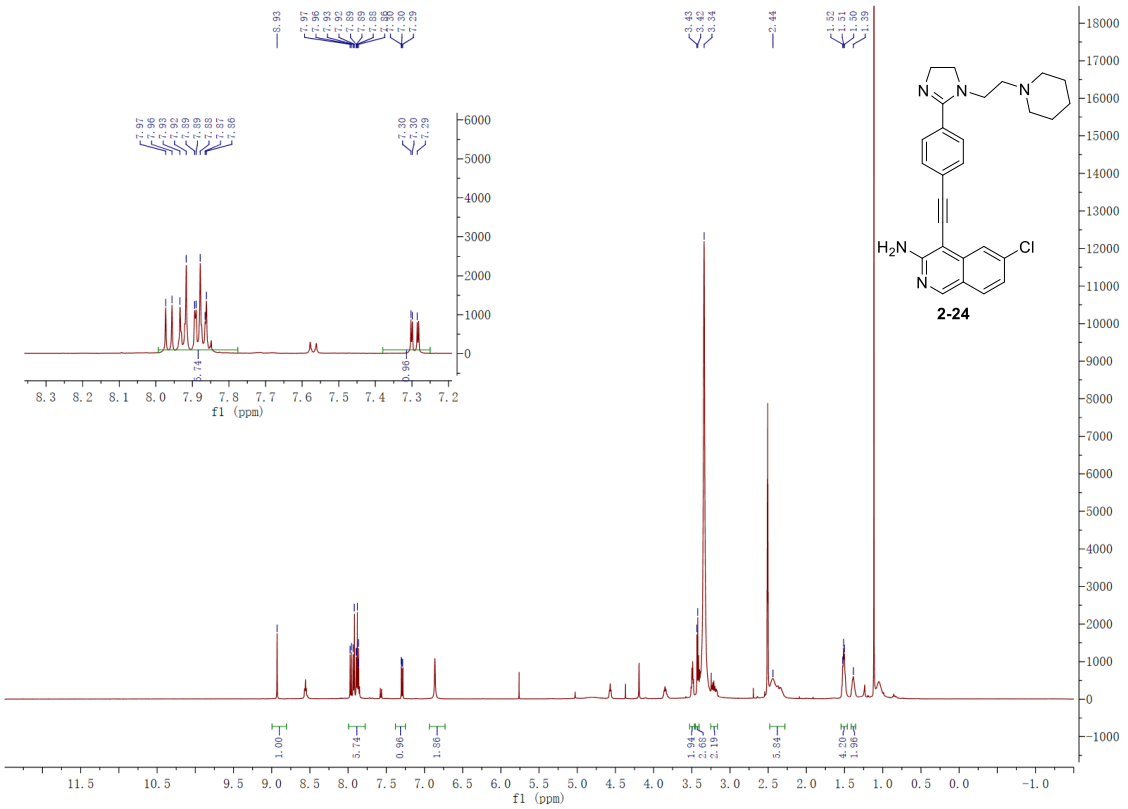
8.93
7.97
7.96
7.93
7.92
7.89
7.88
7.30
7.29
3.43
3.42
3.34
2.44
1.32
1.31
1.30
1.29
1.00
5.74
0.96
1.86
1.94
2.68
2.19
3.84
4.20
1.96
f1 (ppm)
2-24

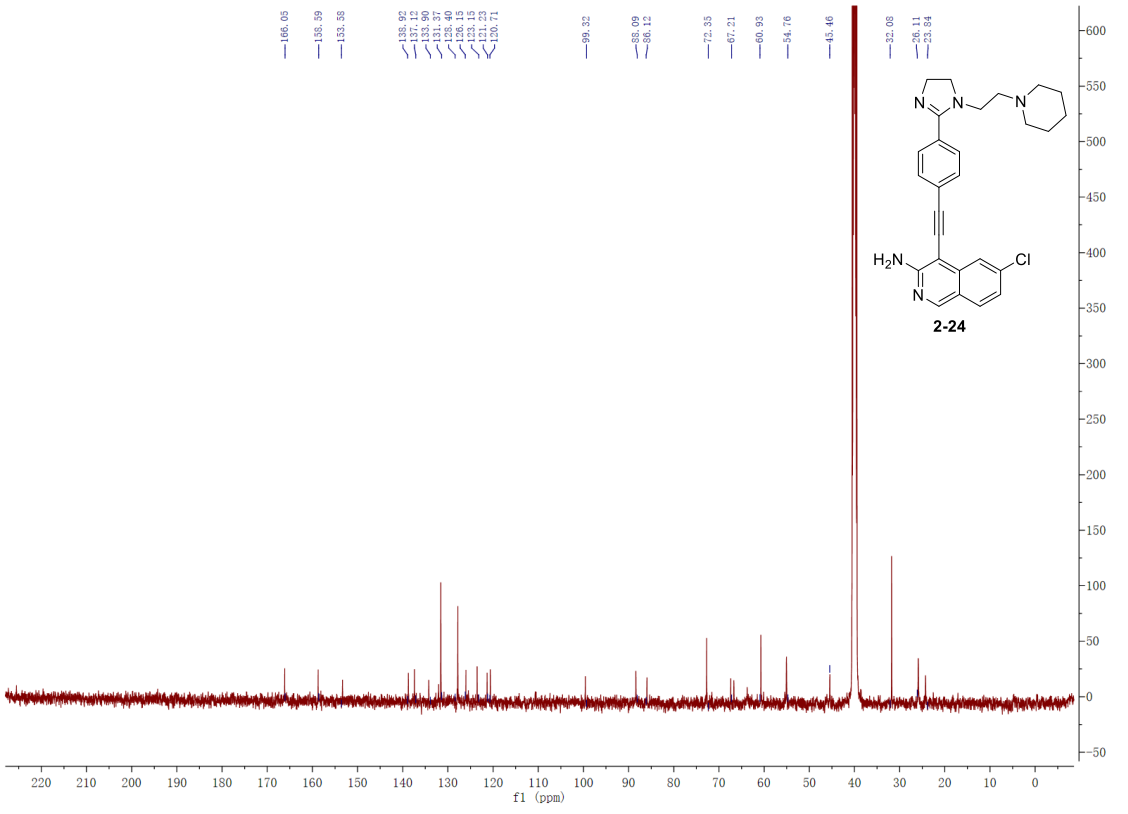
166.05
158.59
153.58
138.92
137.12
133.90
131.37
128.40
123.15
121.23
120.71
99.32
88.09
86.12
72.35
67.21
60.93
54.76
45.46
32.08
26.11
23.84
f1 (ppm)
2-24

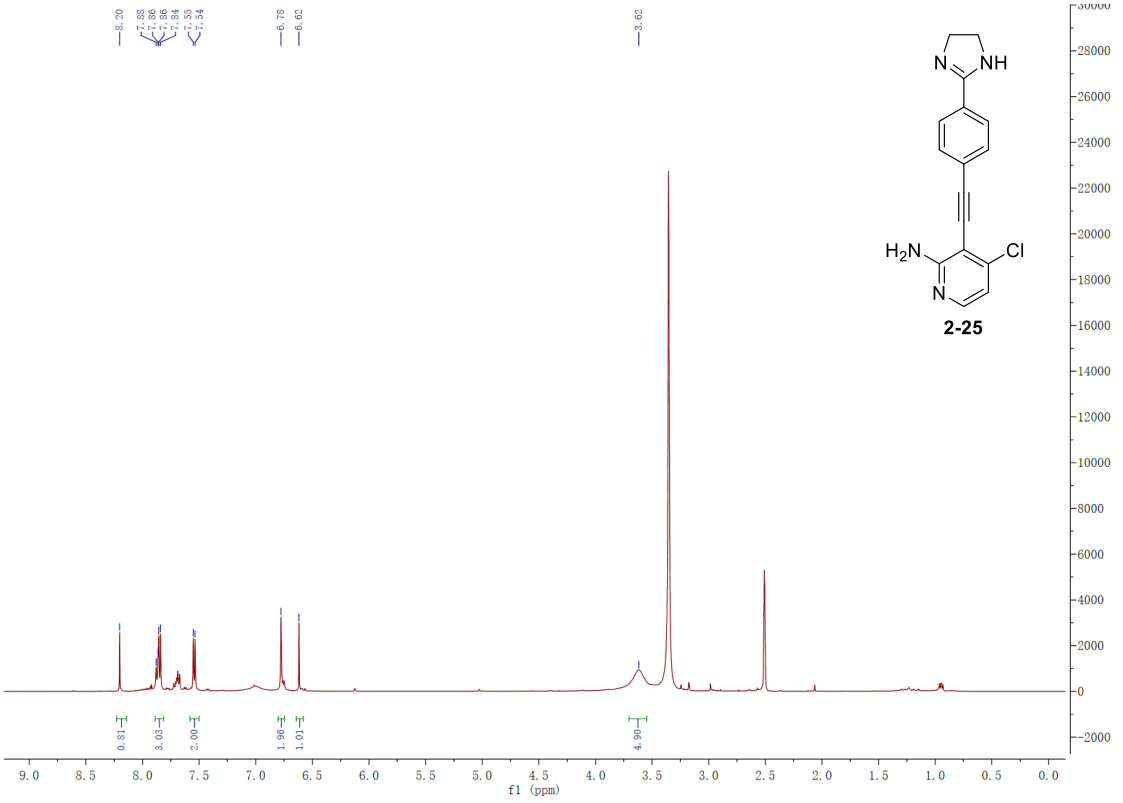
8.20
7.88
7.86
7.86
7.84
7.55
7.54
6.78
6.62
3.62
0.81
3.03
2.00
1.96
1.01
4.90
f1 (ppm)
2-25

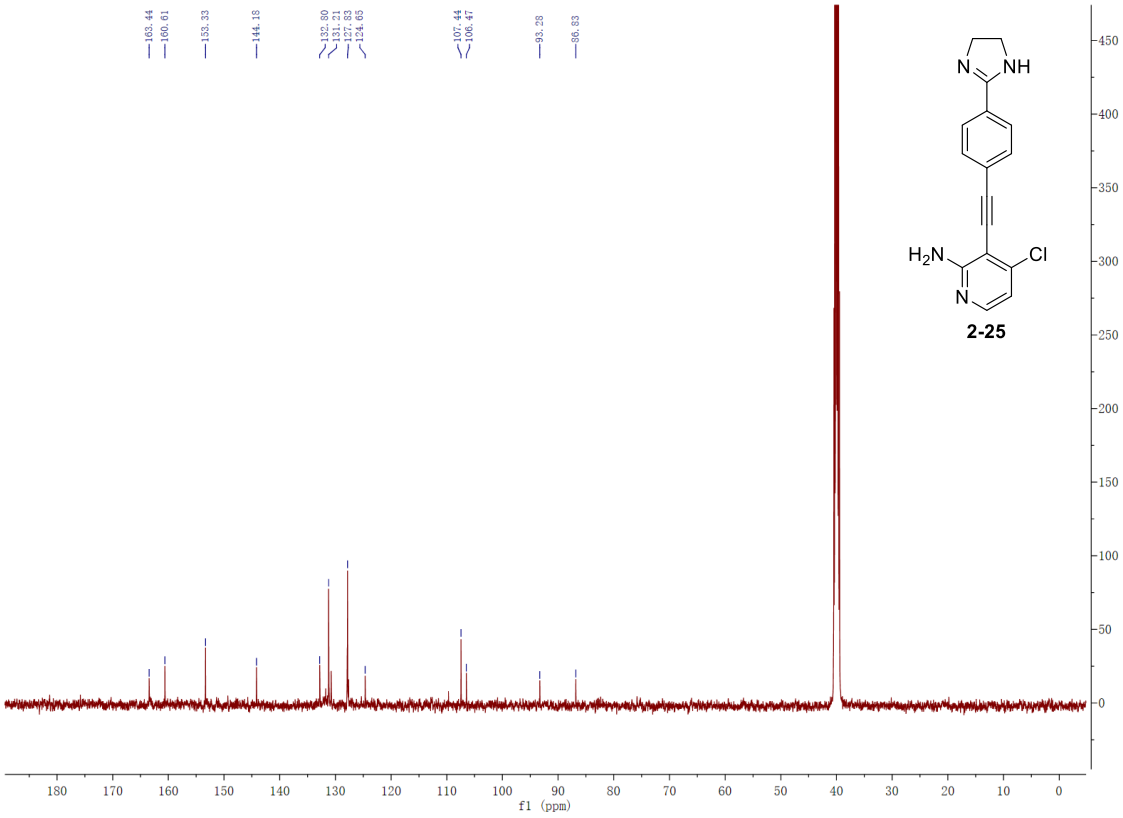
163.44
160.61
153.33
144.18
132.80
131.21
127.83
124.65
107.44
106.47
93.28
86.83
f1 (ppm)
2-25

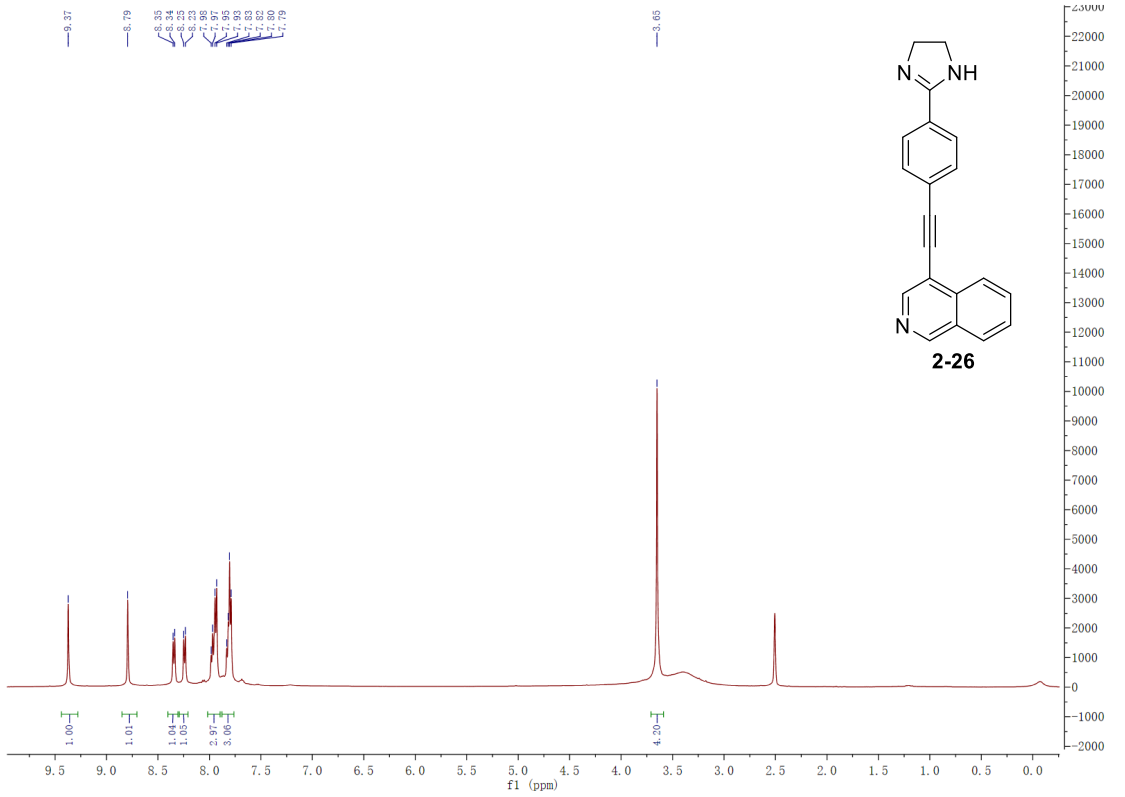
9.37
8.79
8.35
8.34
8.25
8.23
7.98
7.97
7.95
7.93
7.83
7.82
7.80
7.79
3.65
1.00
1.01
1.04
1.05
2.97
3.06
4.20
f1 (ppm)
2-26

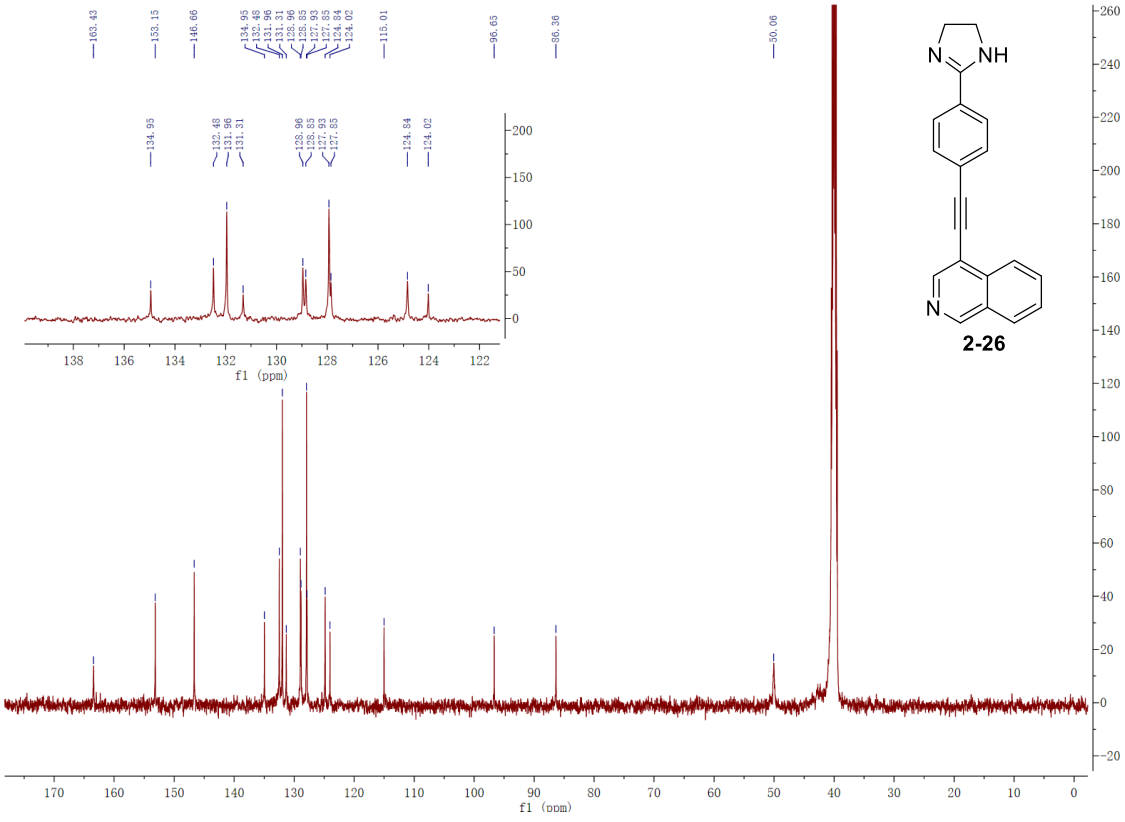
163.43
153.15
146.66
134.95
132.48
131.96
131.31
128.96
128.85
127.93
127.85
124.84
124.02
115.01
96.65
86.36
80.06
f1 (ppm)
2-26

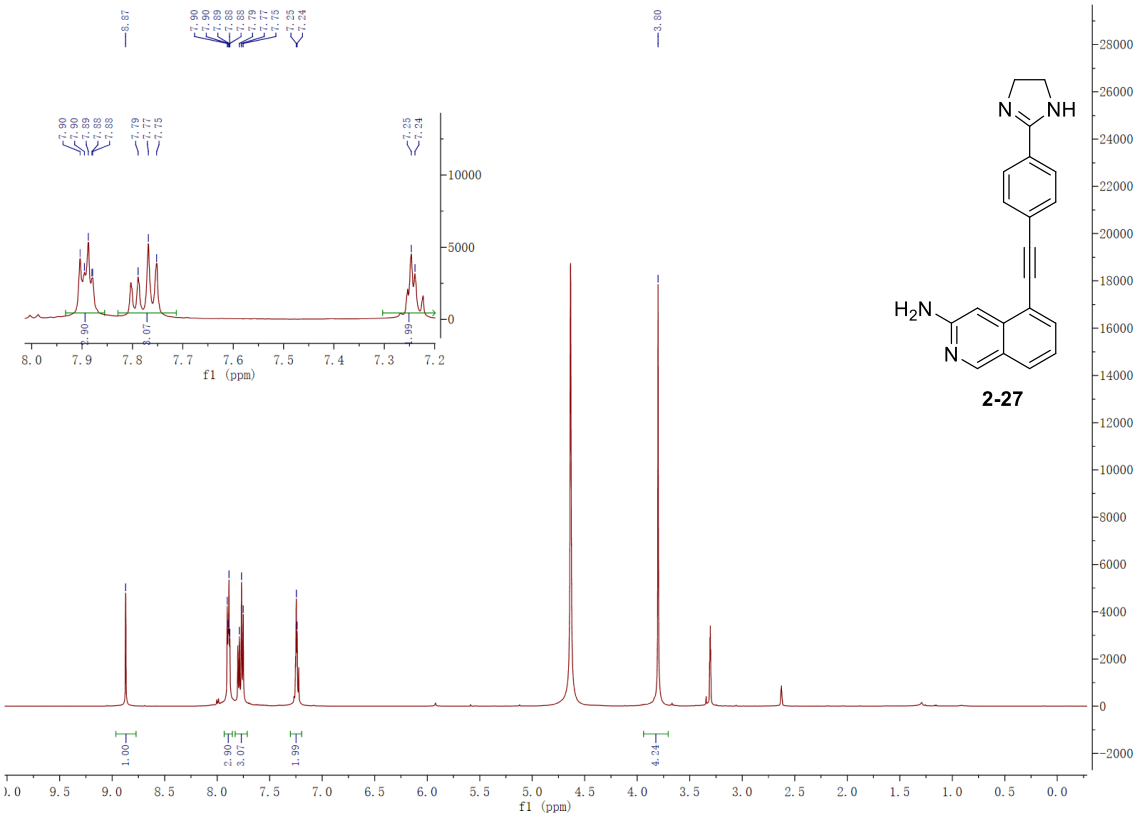
8.67
7.90
7.89
7.88
7.79
7.77
7.75
7.25
7.24
3.80
1.00
2.90
3.07
1.99
4.24
f1 (ppm)
N
NH
H2N
N
2-27

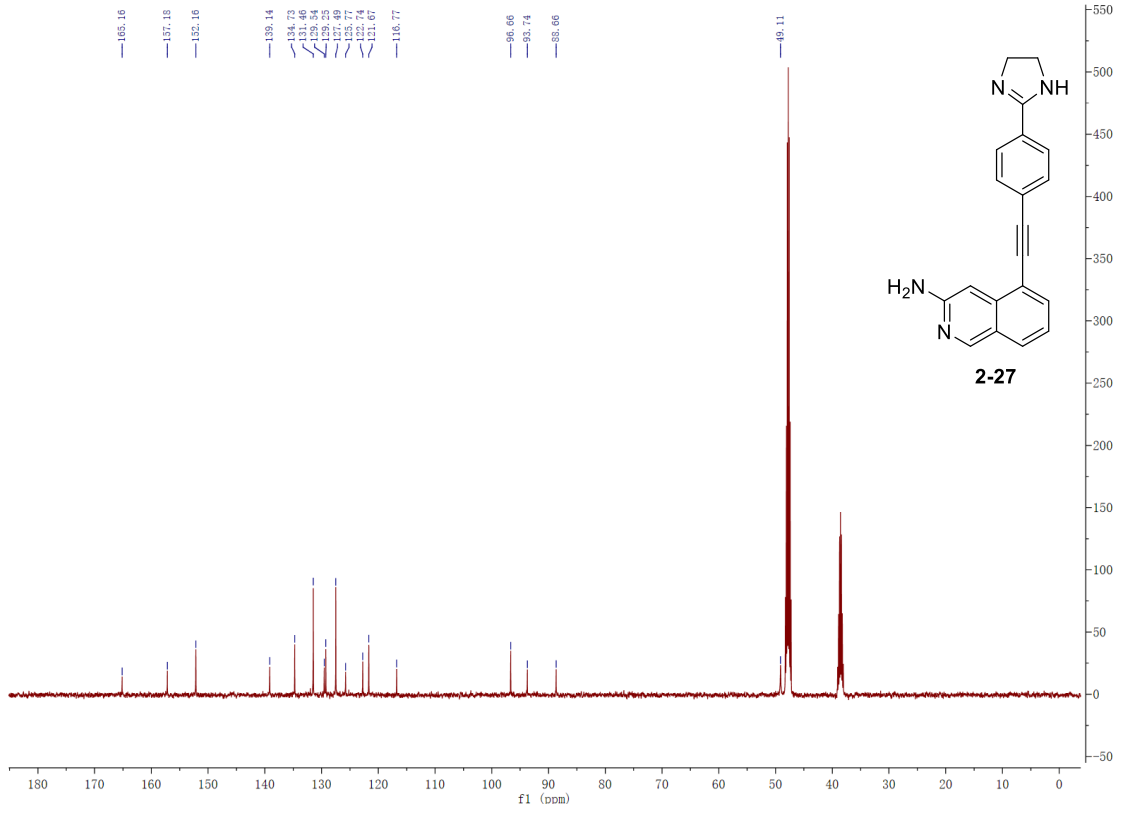
165.16
157.18
152.16
139.14
134.73
131.46
129.54
129.25
127.49
125.77
122.74
121.67
116.77
96.66
93.74
88.66
49.11
f1 (ppm)
N
NH
H2N
N
2-27

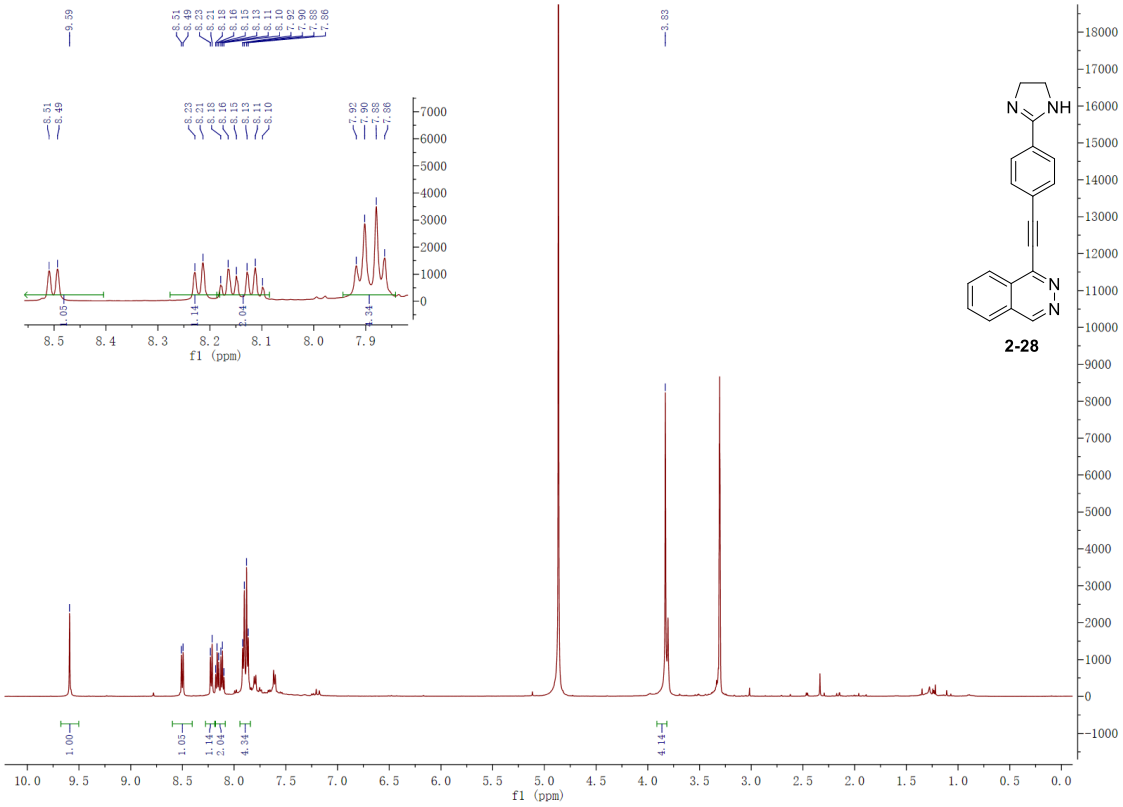
9.59
8.51
8.49
8.23
8.21
8.18
8.16
8.15
8.13
8.11
8.10
7.92
7.90
7.88
7.86
3.83
1.00
1.05
1.14
2.04
4.34
4.14
f1 (ppm)
2-28

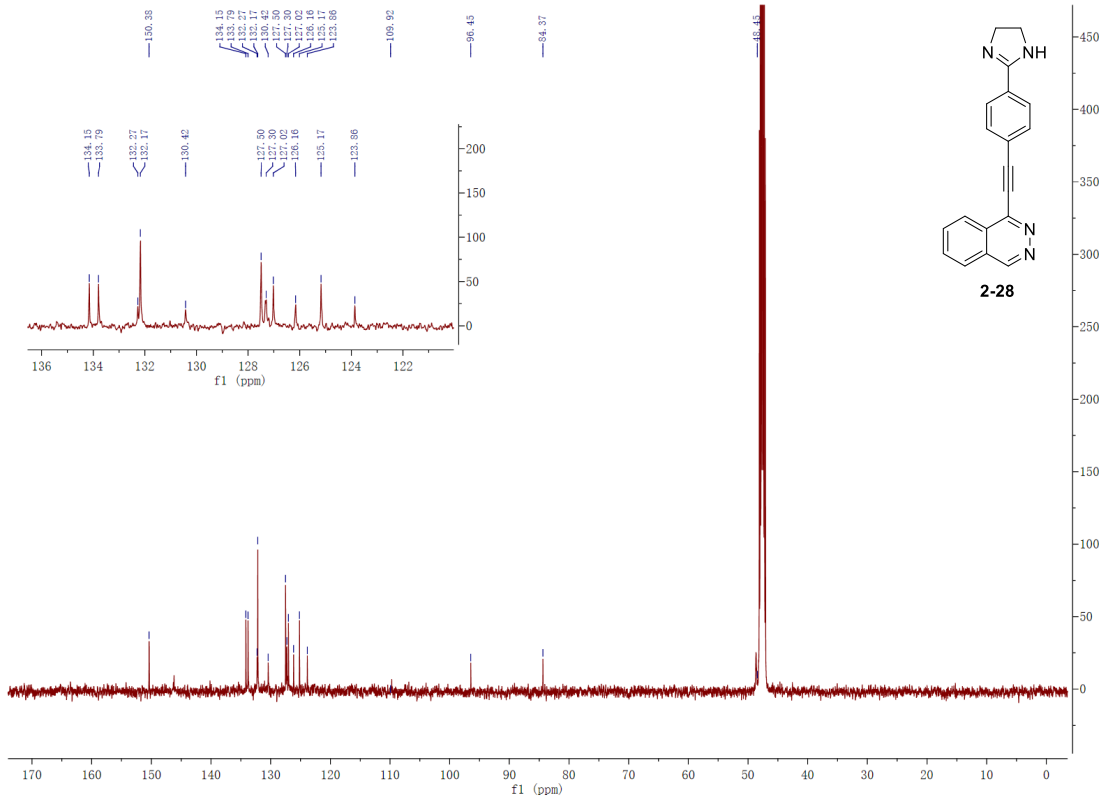
130.38
134.15
133.79
132.27
132.17
130.42
127.50
127.30
127.02
126.16
125.17
123.86
109.92
96.45
84.37
48.45
f1 (ppm)
2-28

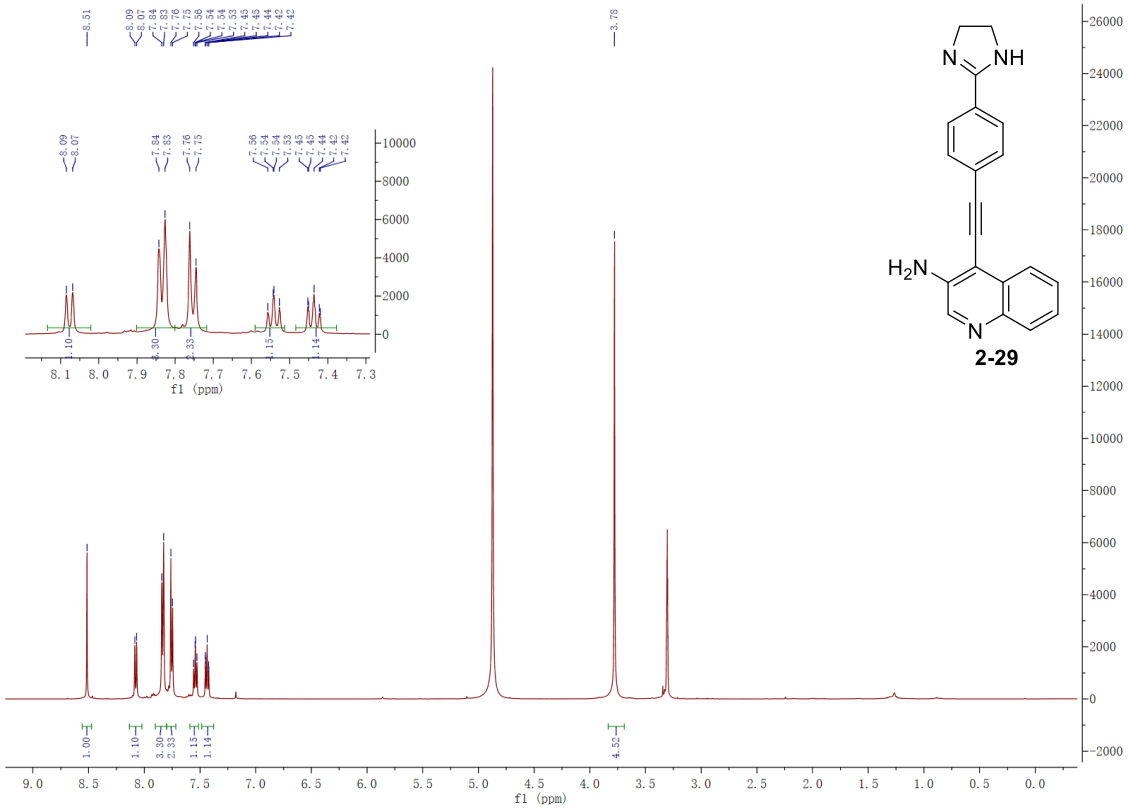
8.51
8.09
8.07
7.84
7.83
7.76
7.75
7.56
7.54
7.53
7.45
7.44
7.42
7.42
3.78
1.00
1.10
3.30
2.33
1.15
1.14
4.52
f1 (ppm)
N
NH
H2N
N
2-29

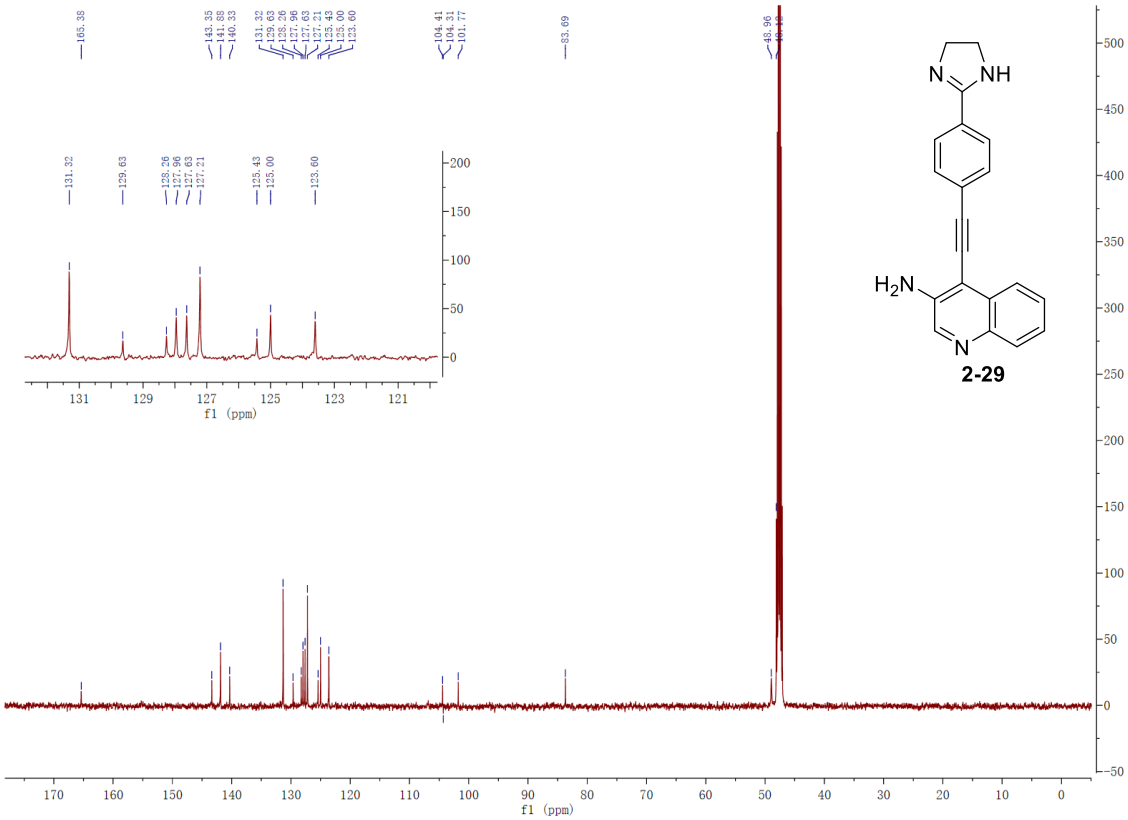
165.38
143.35
141.88
140.33
131.32
129.63
128.26
127.96
127.63
127.21
125.43
125.00
123.60
104.41
104.31
101.77
83.69
48.96
48.42
f1 (ppm)
N
NH
H2N
N
2-29

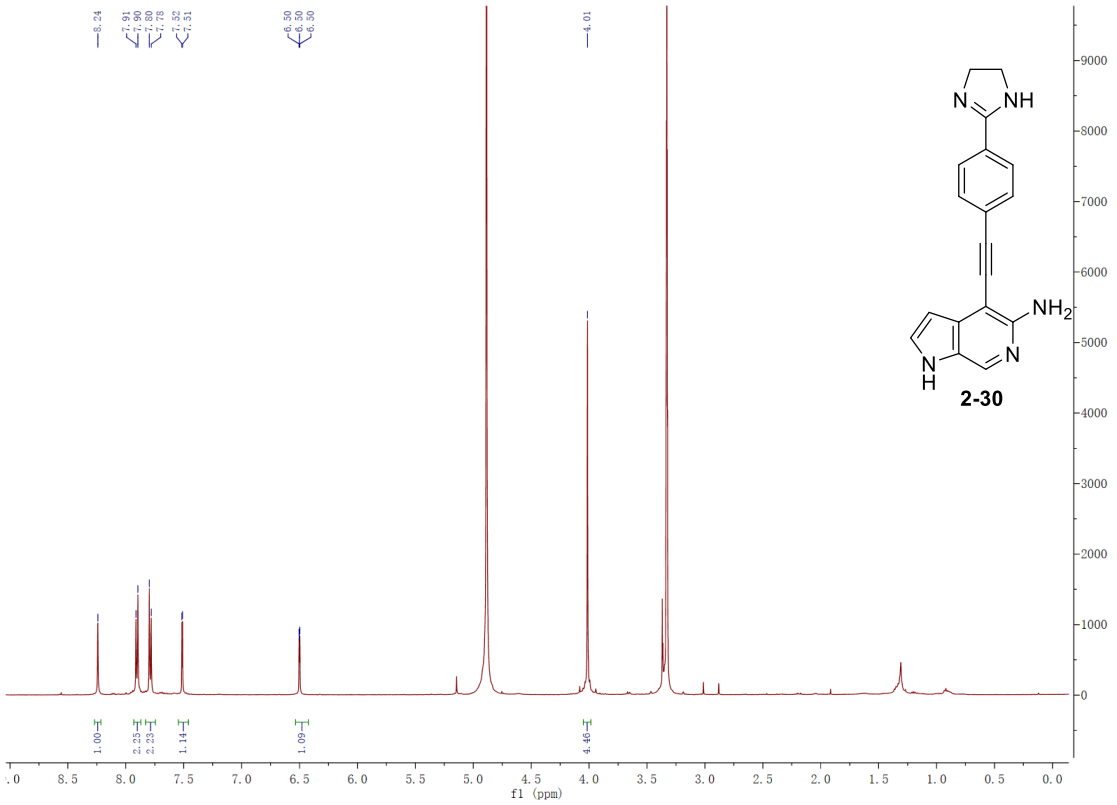
8.24
7.91
7.90
7.80
7.78
7.52
7.51
6.50
6.50
6.50
4.01
1.00
2.25
2.23
1.14
1.09
4.46
f1 (ppm)
NH
NH2
N
H
2-30

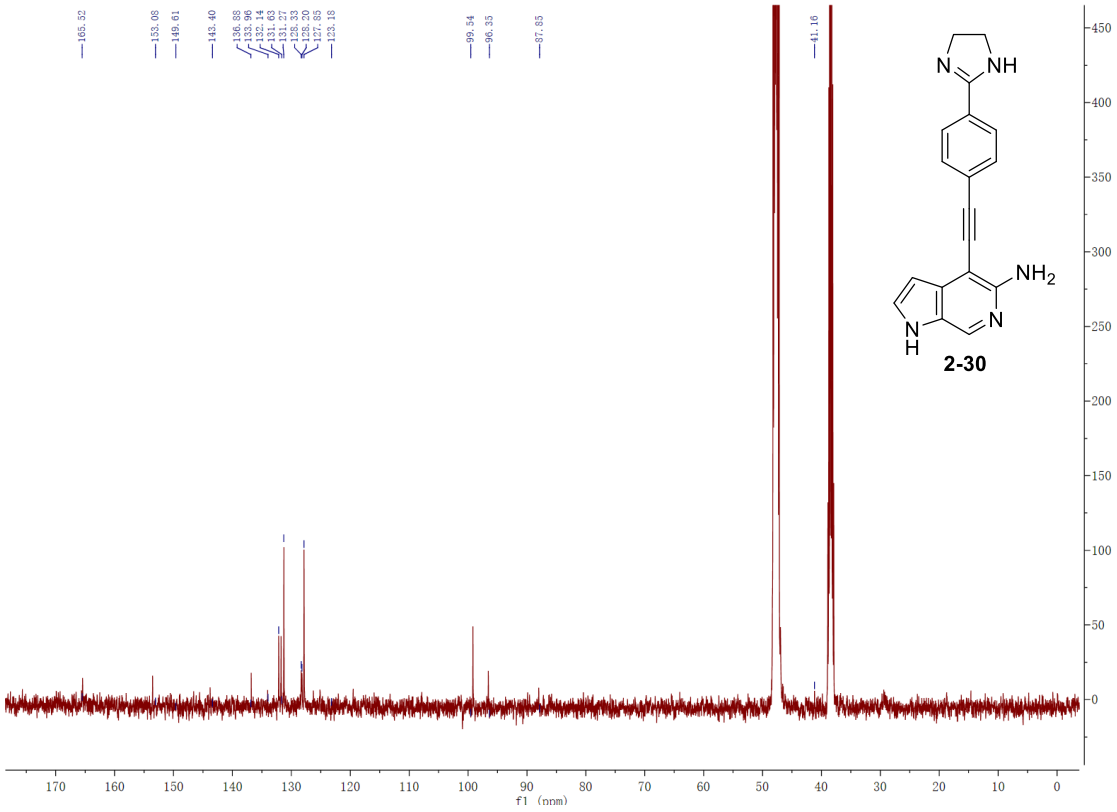
165.52
153.08
149.61
143.40
136.88
133.96
132.14
131.63
131.27
128.33
128.30
127.85
123.18
99.54
96.35
87.85
41.16
f1 (ppm)
NH
NH2
N
H
2-30

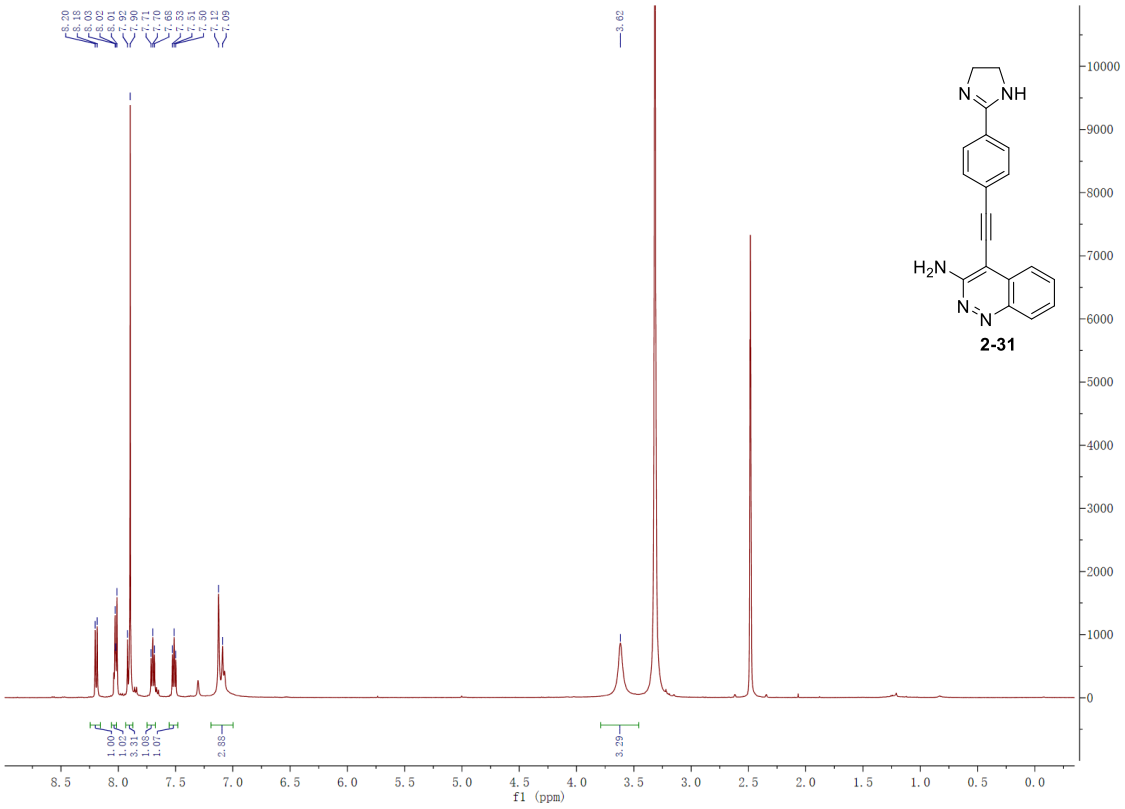
8.20
8.18
8.03
8.02
8.01
7.92
7.90
7.71
7.70
7.68
7.53
7.51
7.50
7.12
7.09
3.62
1.00
1.02
3.31
1.08
1.07
2.88
3.39
f1 (ppm)
NH
H_2N
N
N
2-31

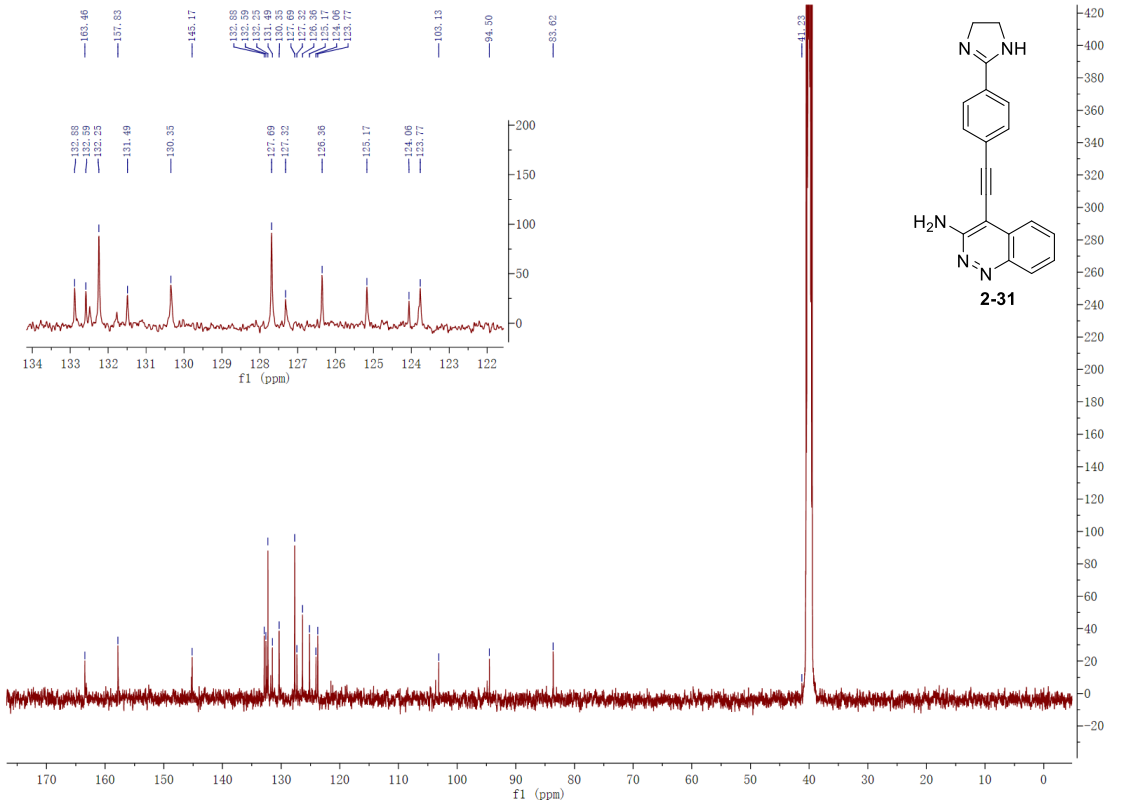
163.46
157.83
145.17
132.88
132.59
132.25
131.49
130.35
127.69
127.32
126.36
125.17
124.06
123.77
103.13
94.50
83.62
41.23
f1 (ppm)
NH
H_2N
N
N
2-31

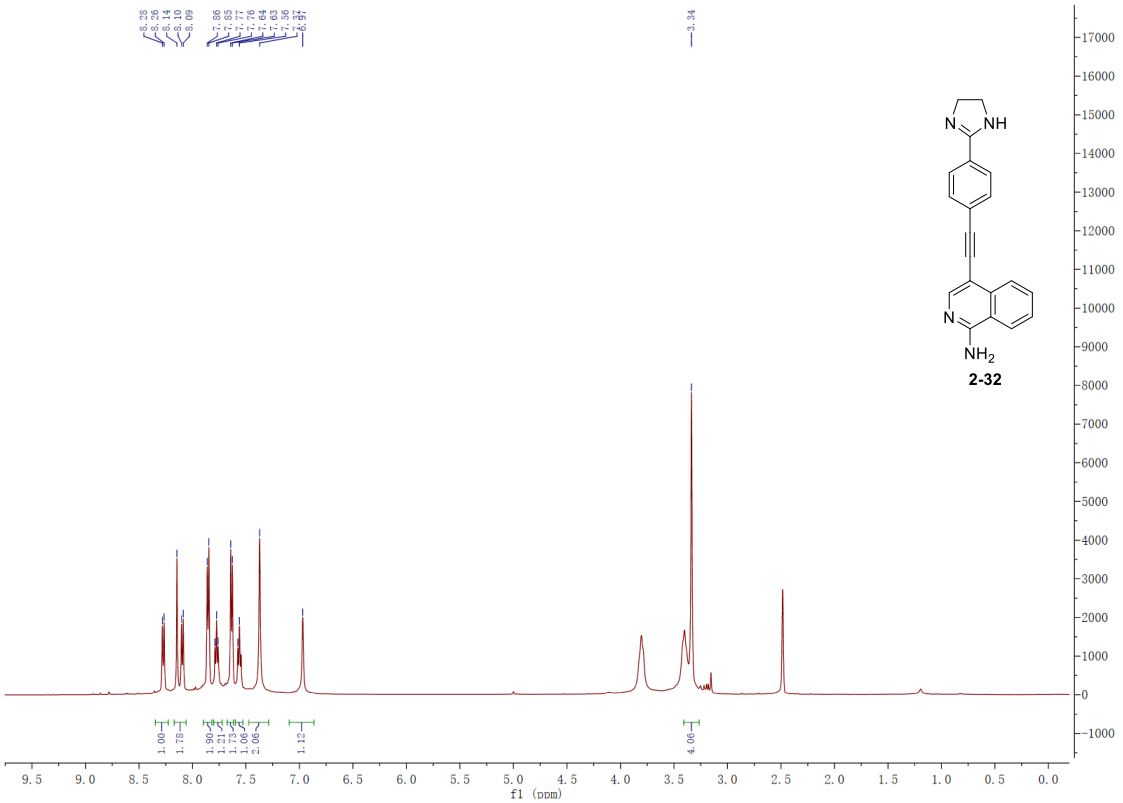
8.28
8.26
8.14
8.10
8.09
7.86
7.85
7.77
7.76
7.64
7.63
7.56
7.47
7.47
3.34
1.00
1.78
1.90
1.72
1.06
2.06
1.12
4.06
f1 (ppm)
2-32

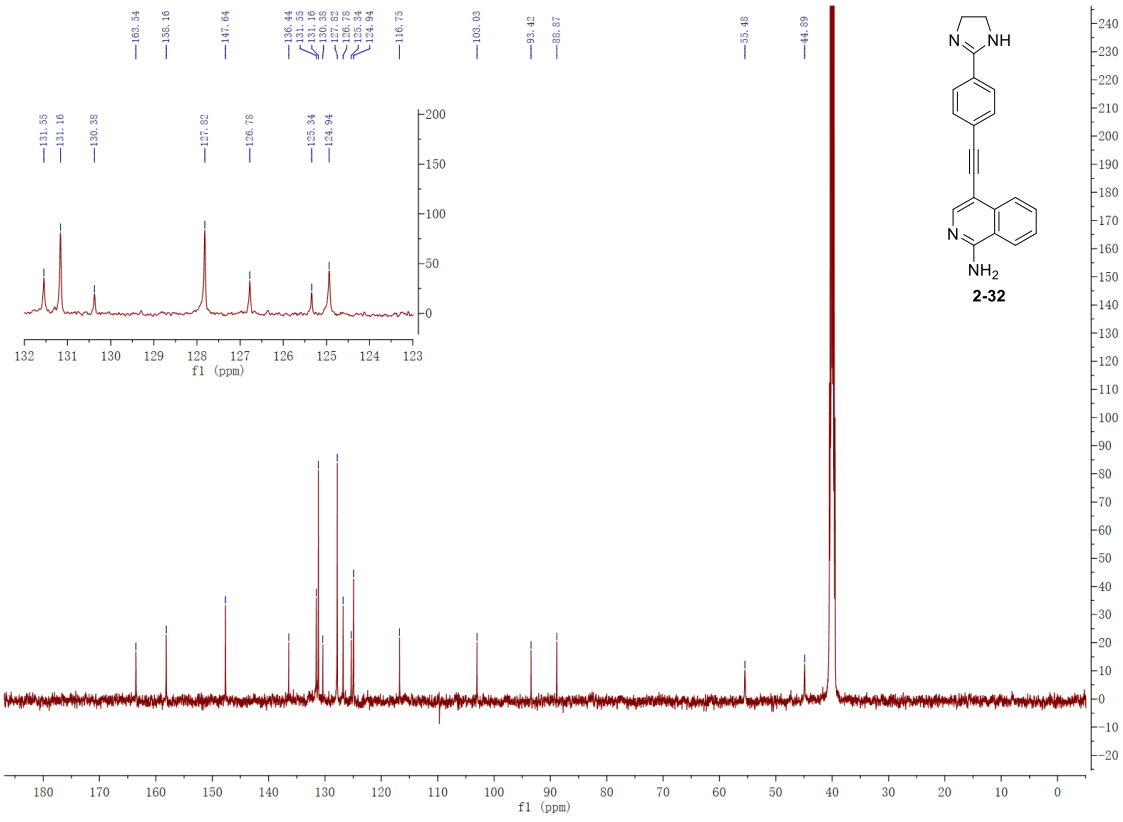
163.54
158.16
147.64
136.44
131.55
131.16
130.38
127.82
126.78
125.34
124.94
116.75
103.03
93.42
88.87
55.48
44.89
f1 (ppm)
2-32

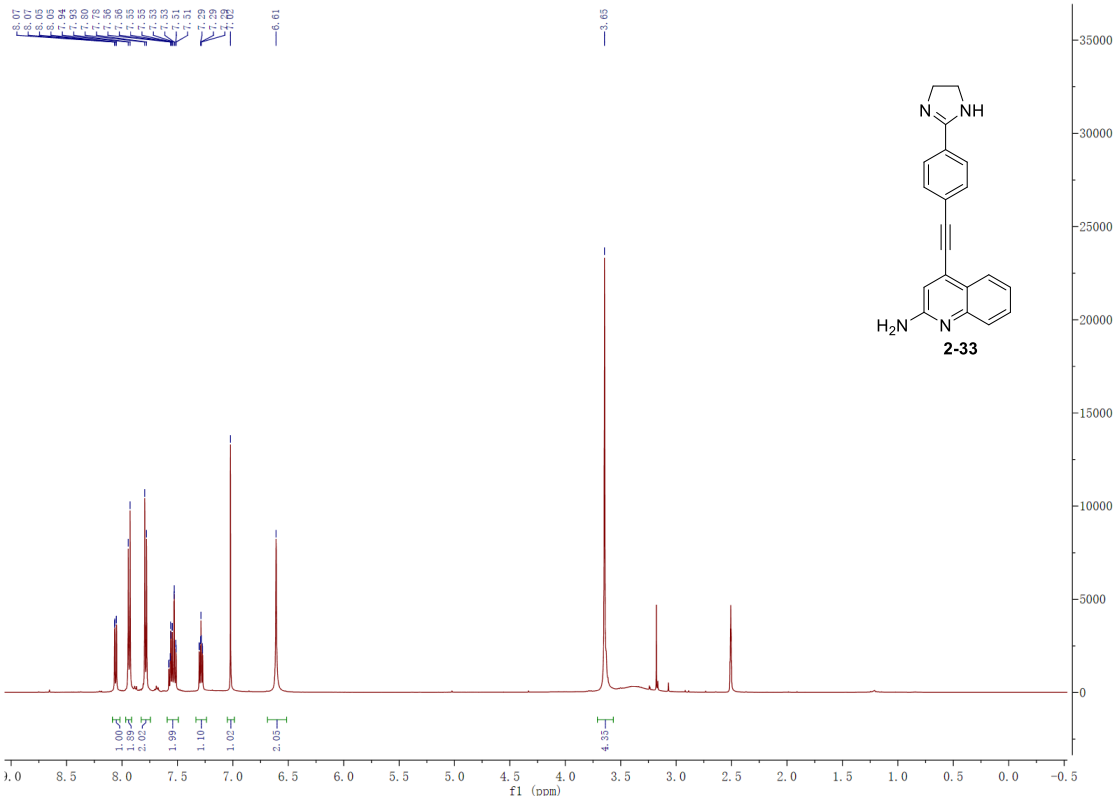
8.07
8.07
8.06
8.05
7.94
7.93
7.80
7.78
7.56
7.56
7.55
7.55
7.33
7.33
7.51
7.51
7.29
7.29
7.02
6.61
3.65
1.00
1.89
2.02
1.99
1.10
1.02
2.03
4.35
f1 (ppm)
N
NH
H2N
N
2-33

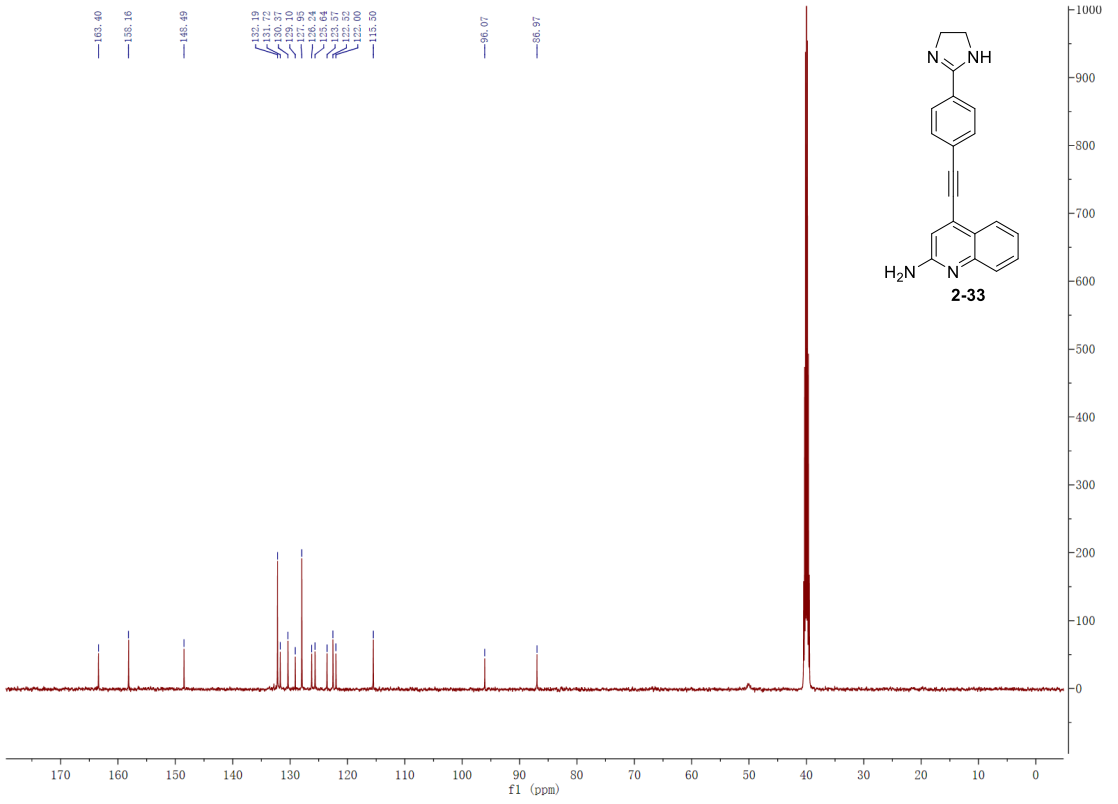
163.40
138.16
148.49
132.19
131.72
130.37
129.10
127.95
126.24
125.64
123.57
123.32
122.00
115.50
96.07
86.97
f1 (ppm)
N
NH
H2N
N
2-33

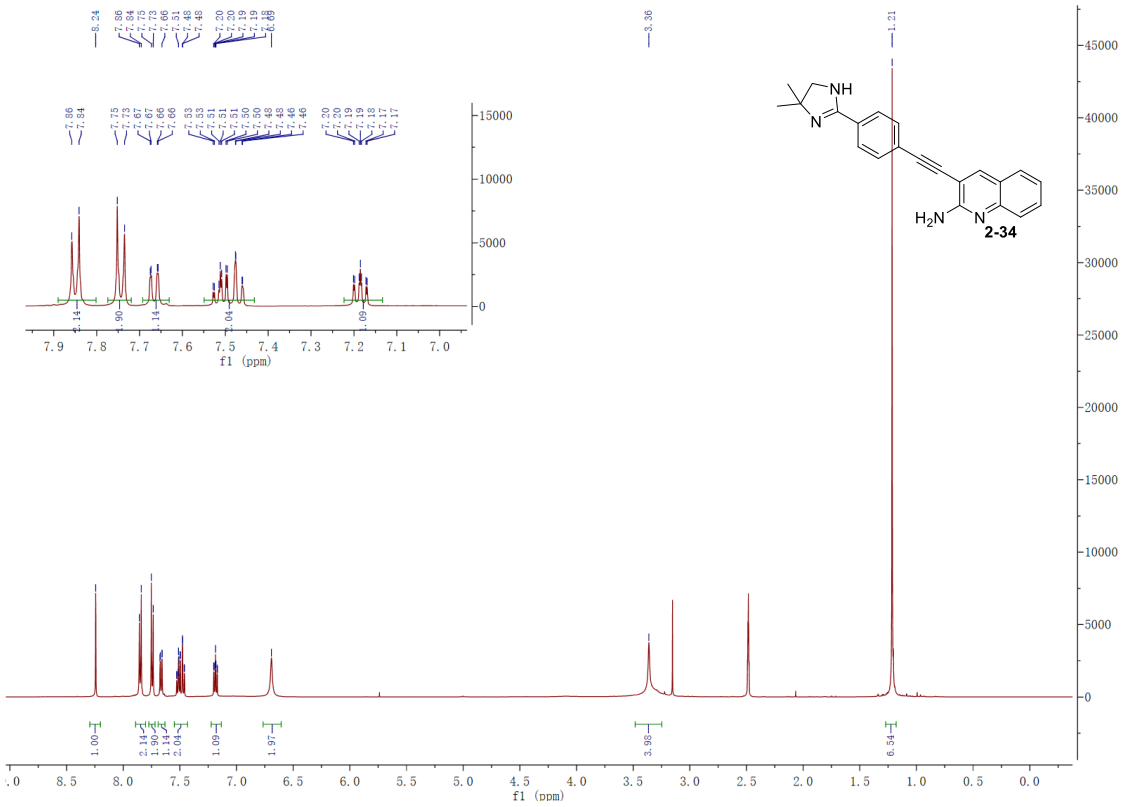
NH
N
H_2N
N
2-34
f1 (ppm)

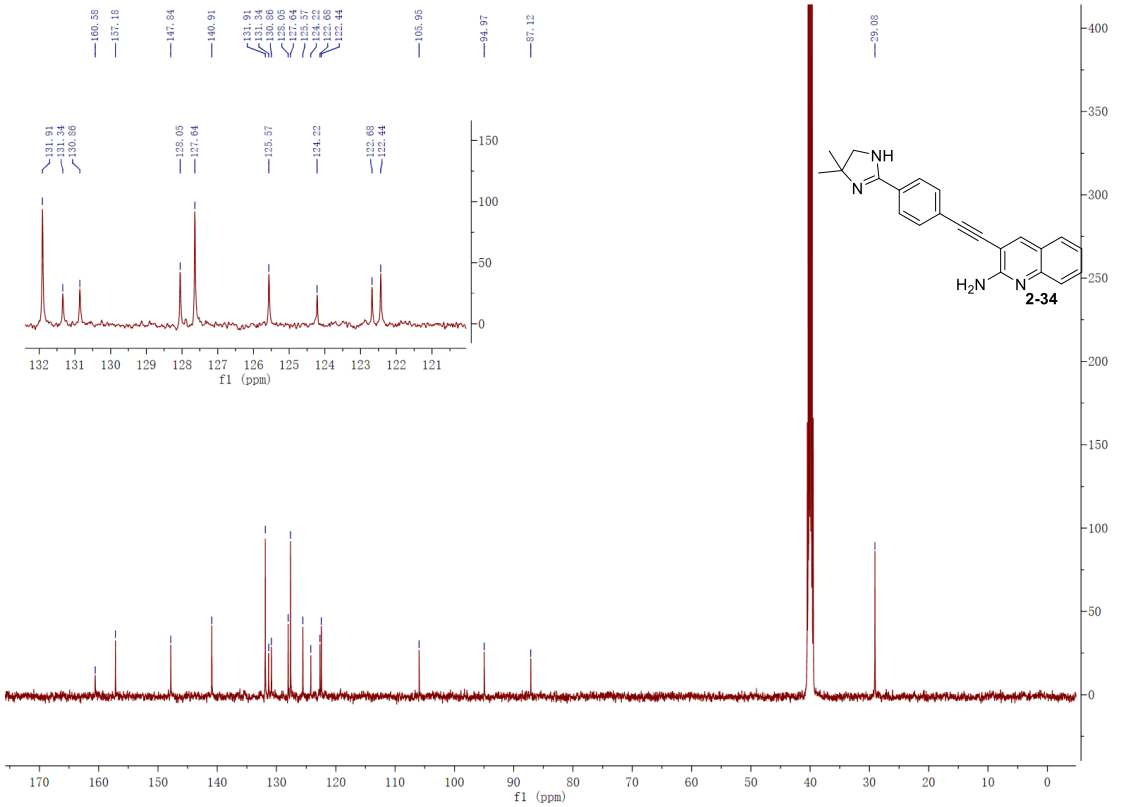
NH
N
H_2N
N
2-34
f1 (ppm)

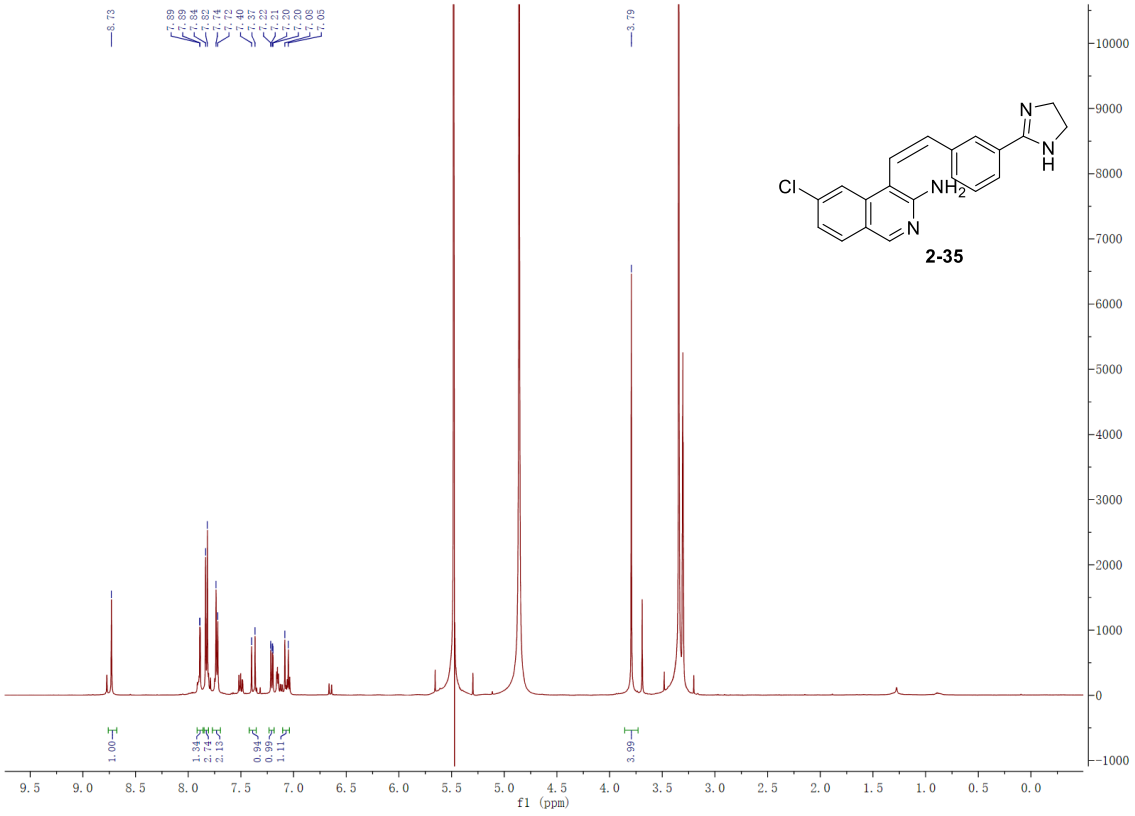
8.73
7.89
7.89
7.84
7.82
7.74
7.72
7.40
7.37
7.22
7.21
7.20
7.09
7.09
7.05
3.79
1.00
1.34
2.74
2.13
0.94
0.99
1.11
3.99
Cl
NH2
N
N
H
2-35
f1 (ppm)

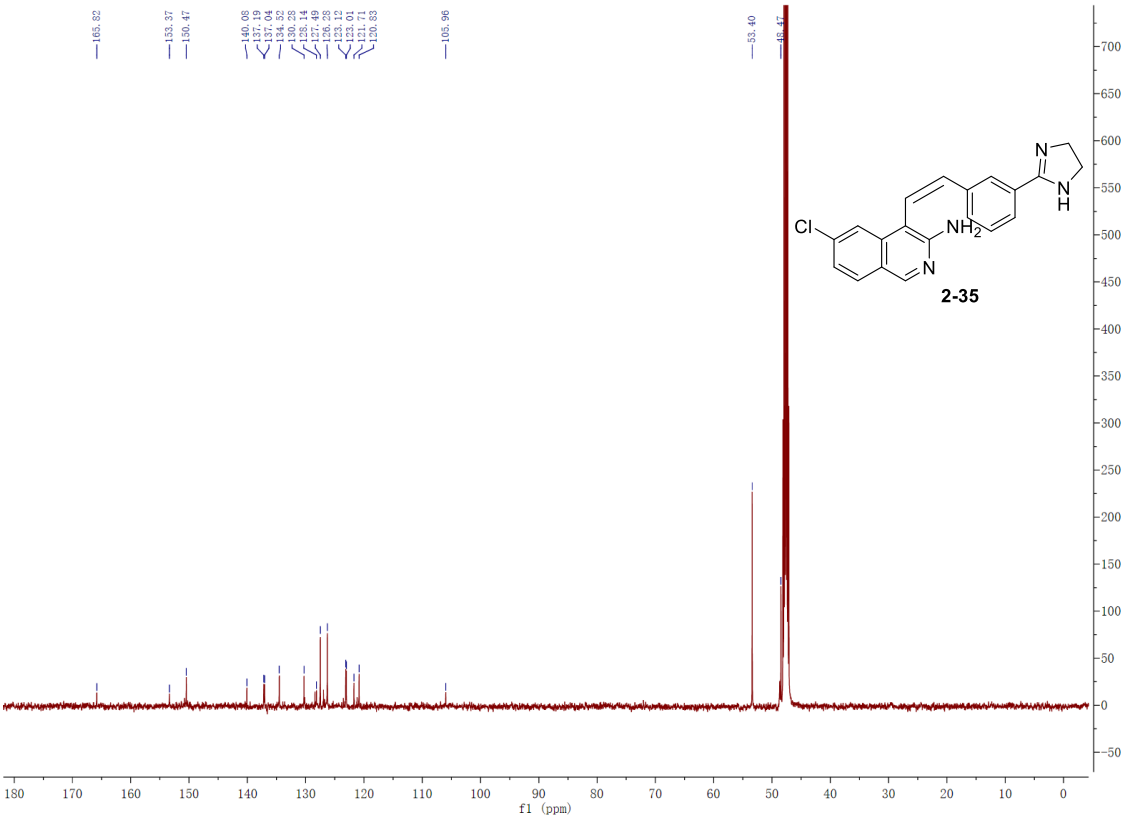
165.82
153.37
150.47
140.08
137.19
135.04
134.52
130.28
128.14
127.49
126.23
123.23
123.01
121.71
120.83
105.96
53.40
48.47
Cl
NH2
N
N
H
2-35
f1 (ppm)

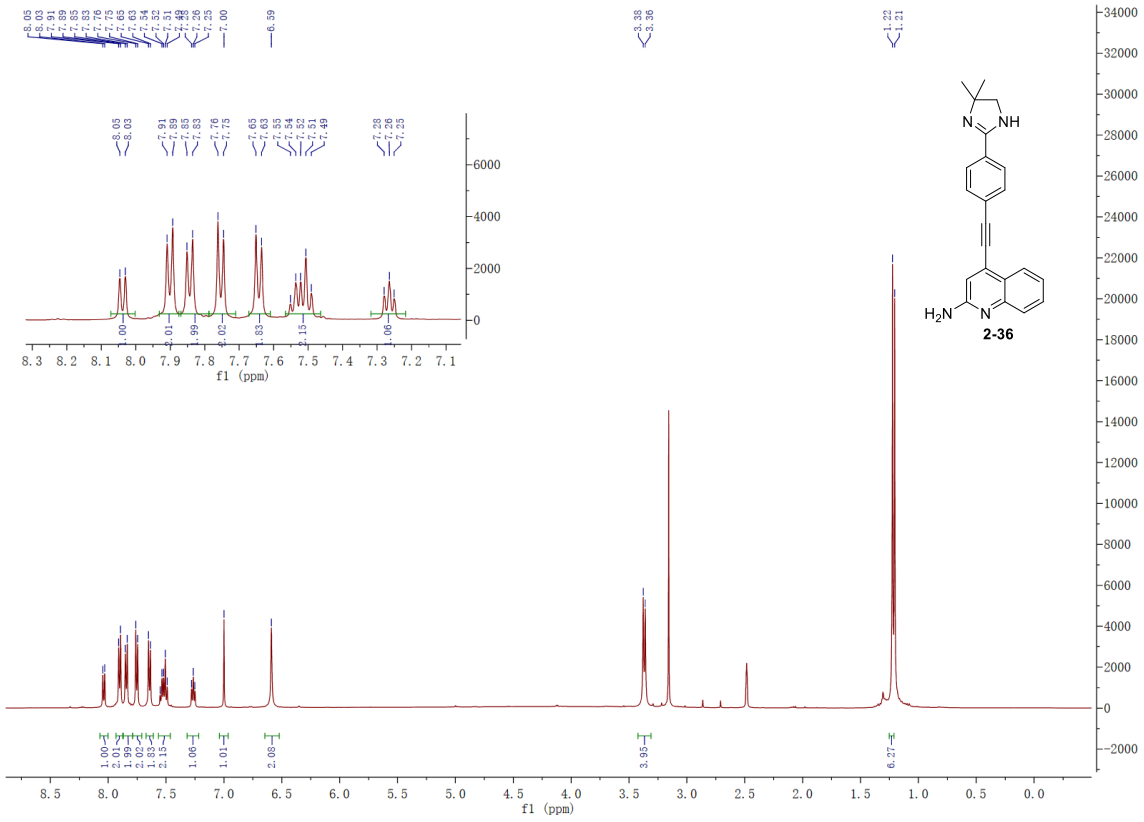
8.05
8.03
7.91
7.89
7.85
7.83
7.76
7.75
7.65
7.63
7.54
7.52
7.51
7.49
7.26
7.25
7.00
6.59
3.38
3.36
1.22
1.21
1.00
2.01
1.99
2.02
1.83
2.15
1.06
1.01
2.08
3.95
6.27
f1 (ppm)
2-36

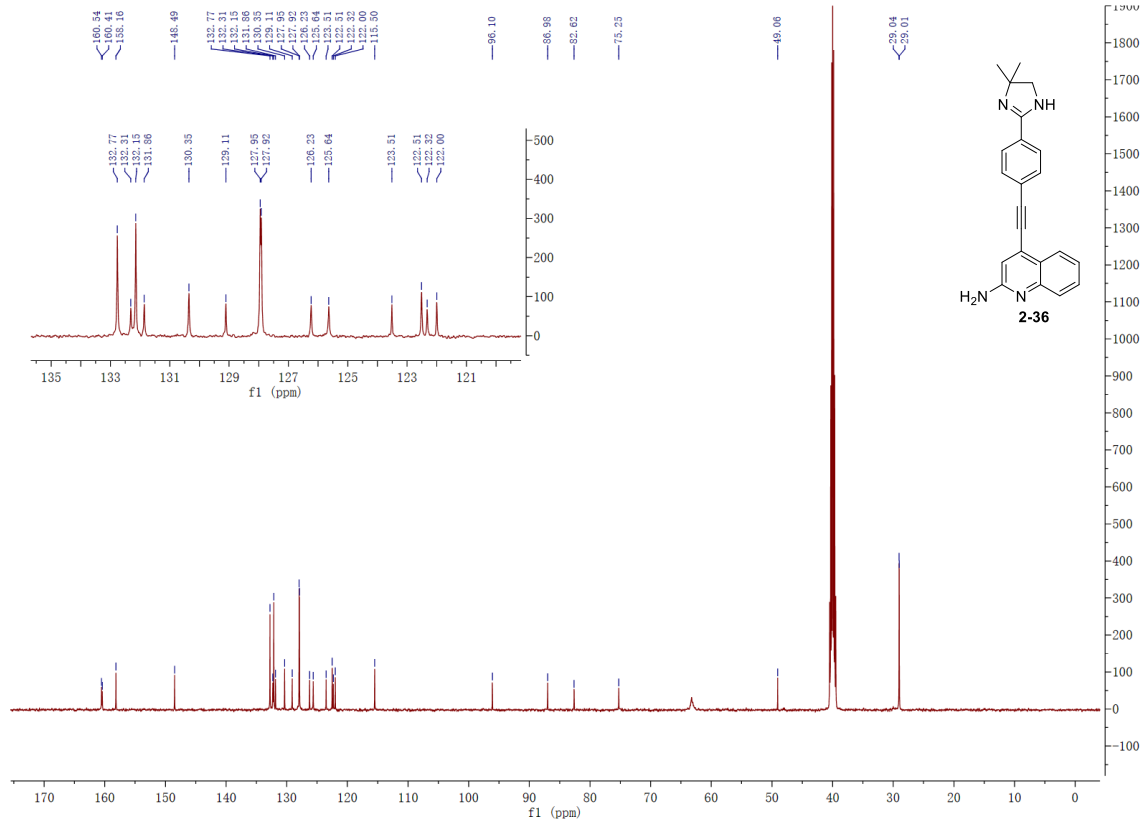
160.54
160.41
158.16
148.49
132.77
132.31
132.15
131.86
130.35
129.11
127.95
127.92
126.23
125.64
123.51
122.51
122.32
122.00
115.50
96.10
86.98
82.62
75.25
49.06
29.04
29.01
f1 (ppm)
2-36

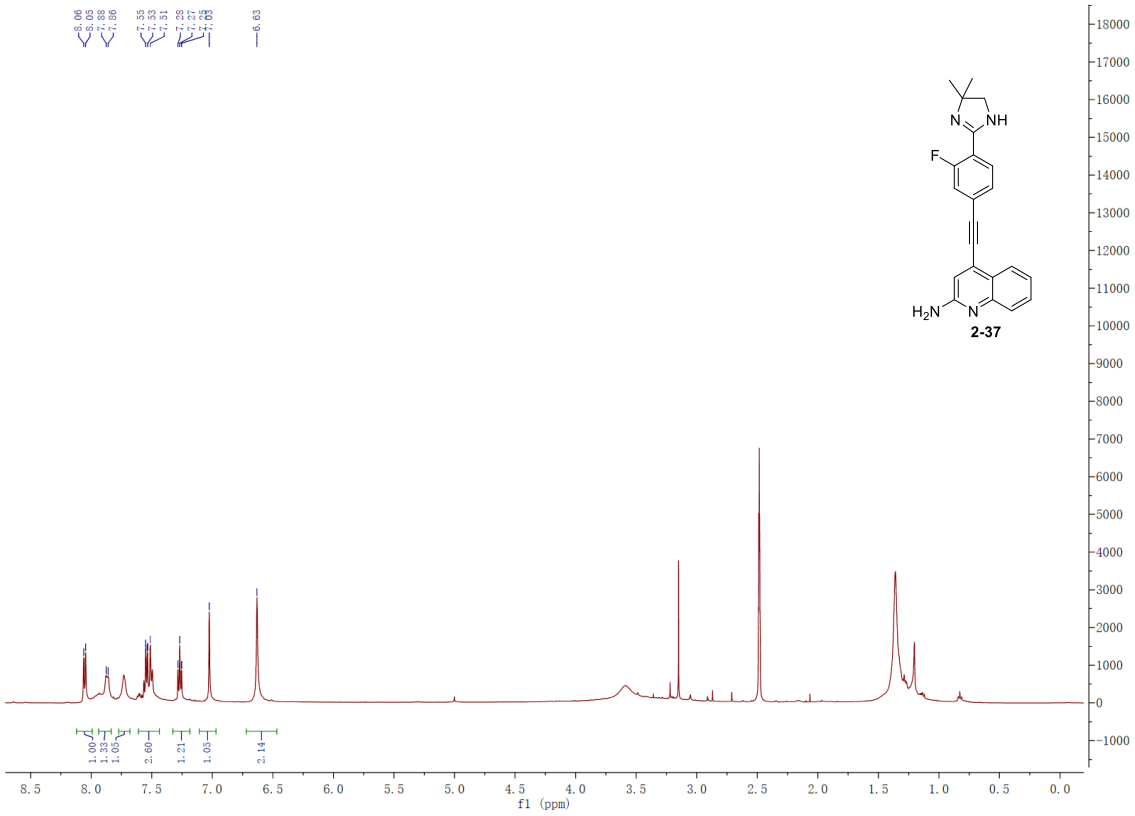
8.06
8.05
7.88
7.86
7.55
7.53
7.51
7.28
7.27
7.25
7.03
6.63
1.00
1.33
1.05
2.60
1.21
1.05
2.14
F
NH
N
H2N
N
2-37
f1 (ppm)

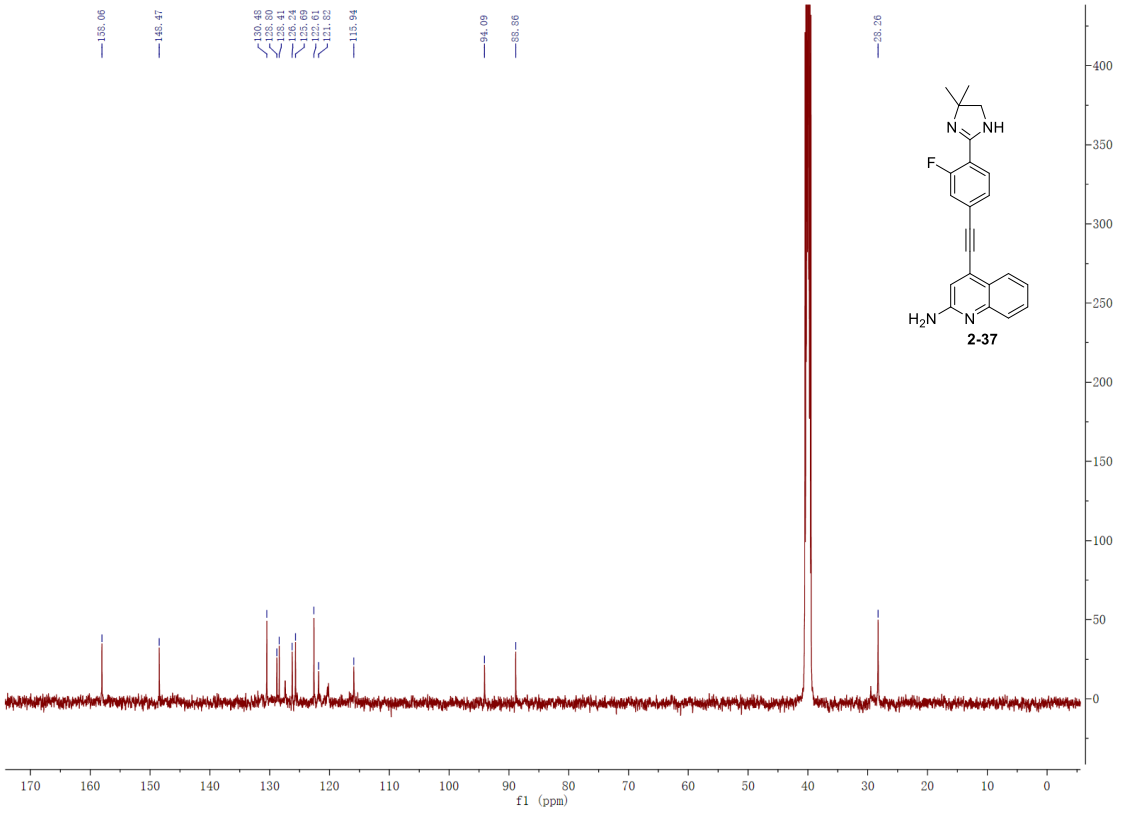
158.06
148.47
130.48
128.80
128.41
126.24
125.69
122.61
121.82
115.94
94.09
88.86
28.26
F
NH
N
H2N
N
2-37
f1 (ppm)

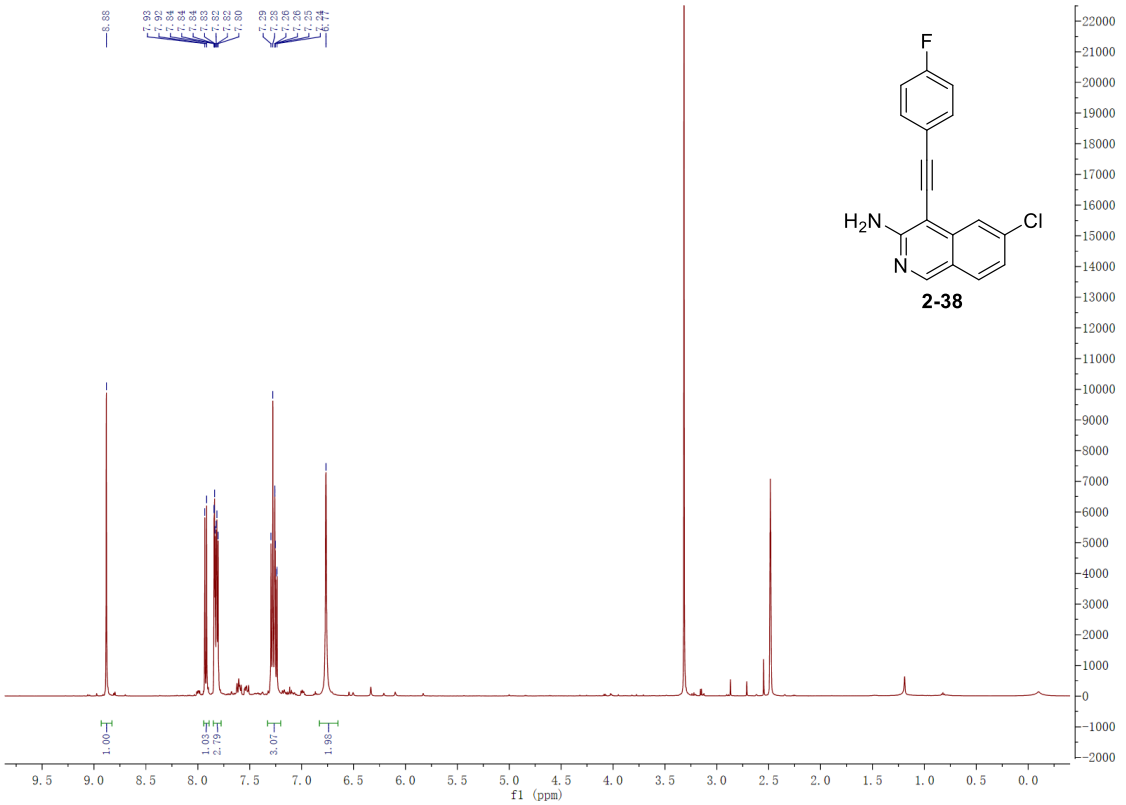
8.88
7.93
7.92
7.84
7.84
7.83
7.82
7.82
7.80
7.29
7.28
7.26
7.25
7.24
6.74
1.00
1.03
2.79
3.07
1.98
f1 (ppm)
F
H2N
Cl
N
2-38

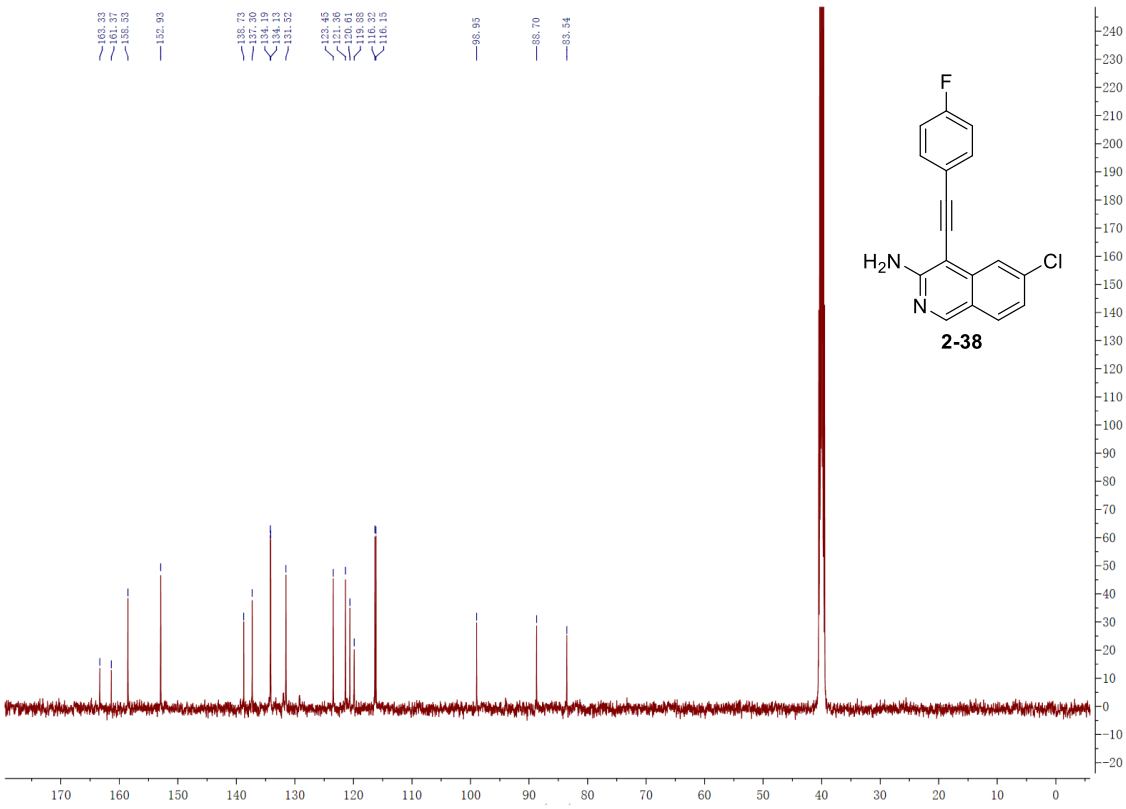
163.33
161.37
158.53
132.93
138.73
137.30
134.19
134.13
131.52
123.45
121.36
120.61
119.88
116.32
116.15
98.95
88.70
83.54
F
H2N
Cl
N
2-38

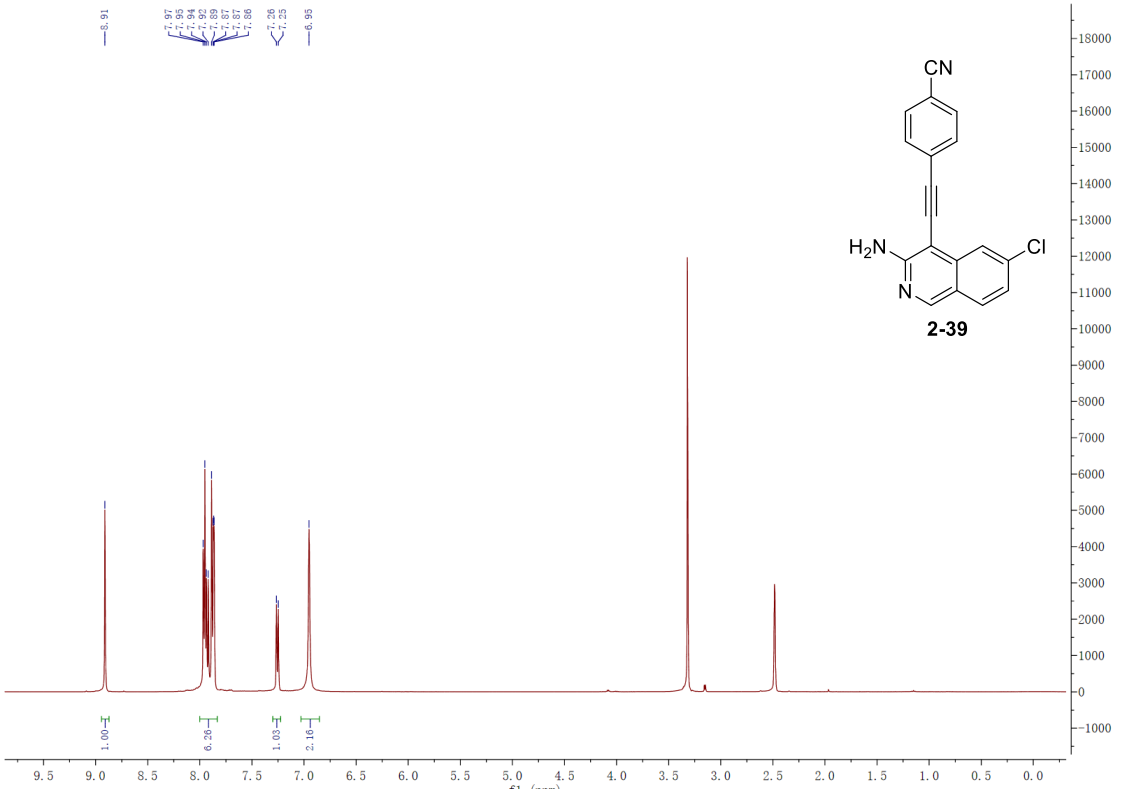
8.91
7.97
7.95
7.94
7.92
7.89
7.87
7.87
7.86
7.26
7.25
6.95
1.00
6.26
1.03
2.16
CN
H2N
Cl
N
2-39

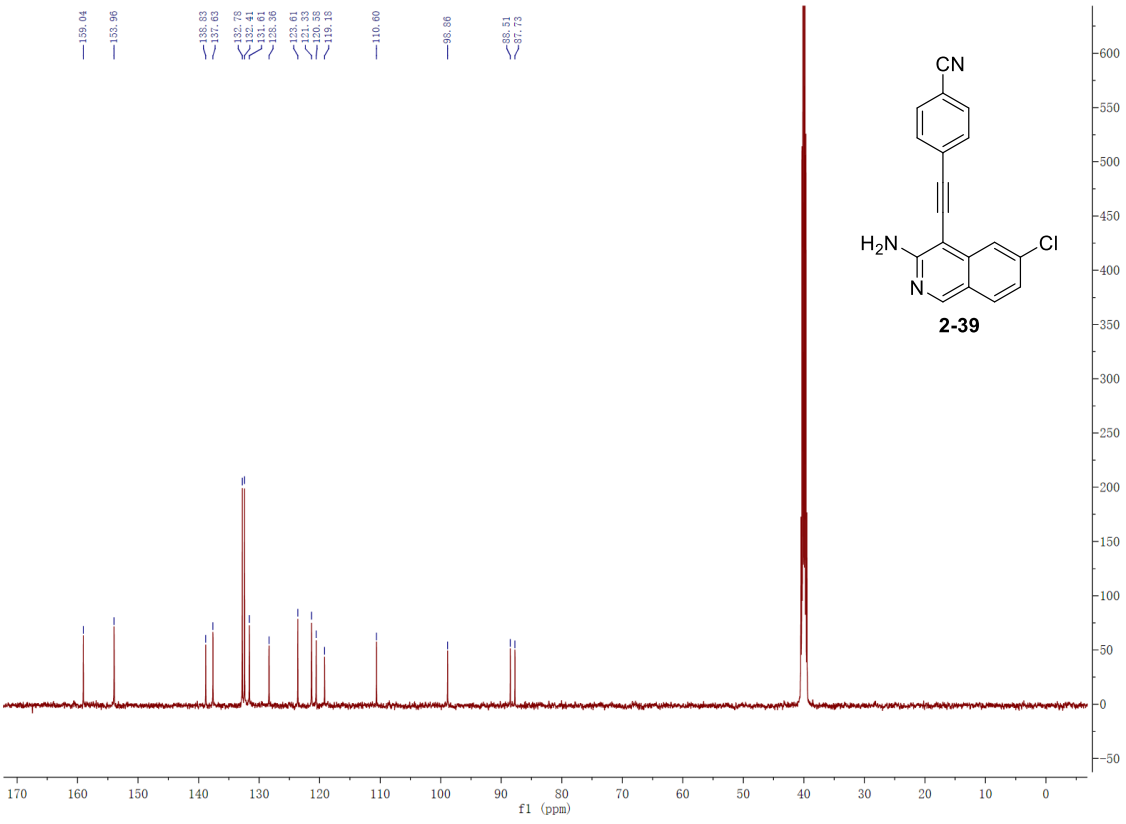
159.04
153.96
138.83
137.63
132.78
132.41
131.41
128.36
123.61
121.33
120.36
119.18
110.60
98.86
88.51
87.73
CN
H2N
Cl
N
2-39
f1 (ppm)

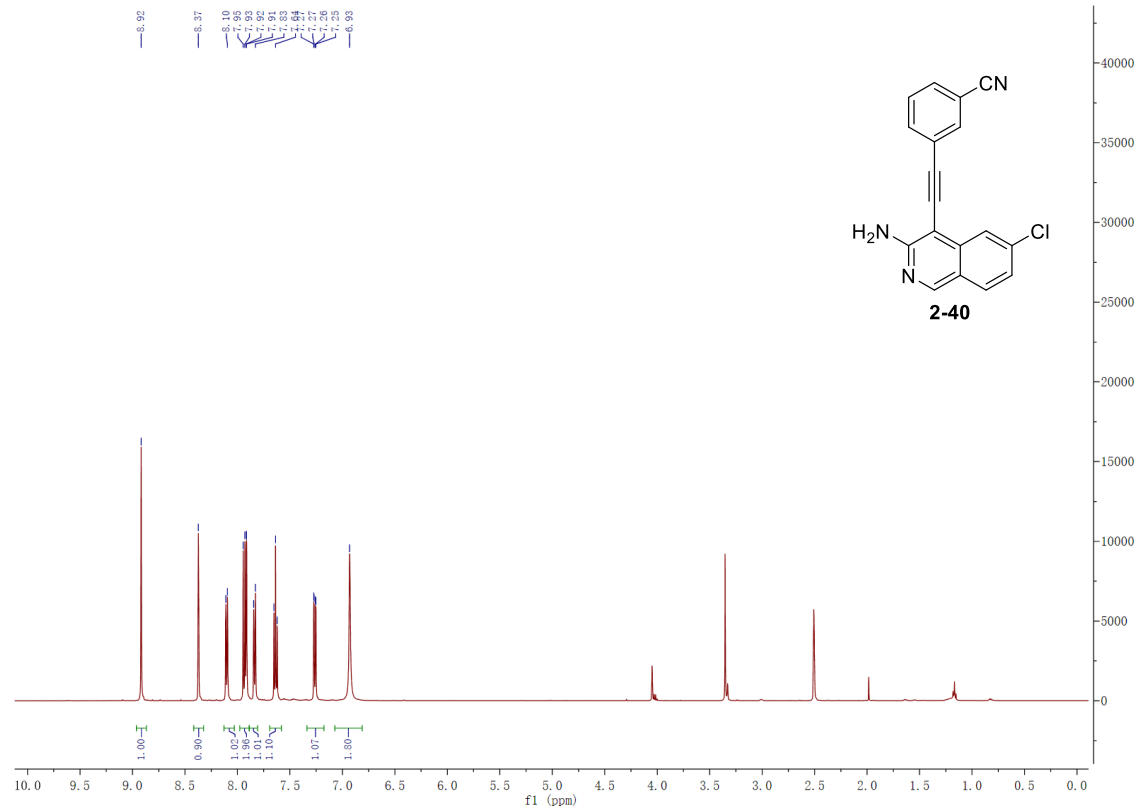
8.92
8.37
8.10
7.95
7.93
7.92
7.91
7.83
7.64
7.61
7.27
7.26
7.25
6.93
CN
H2N
Cl
N
2-40
1.00
0.90
1.02
1.96
1.01
1.10
1.07
1.80
f1 (ppm)

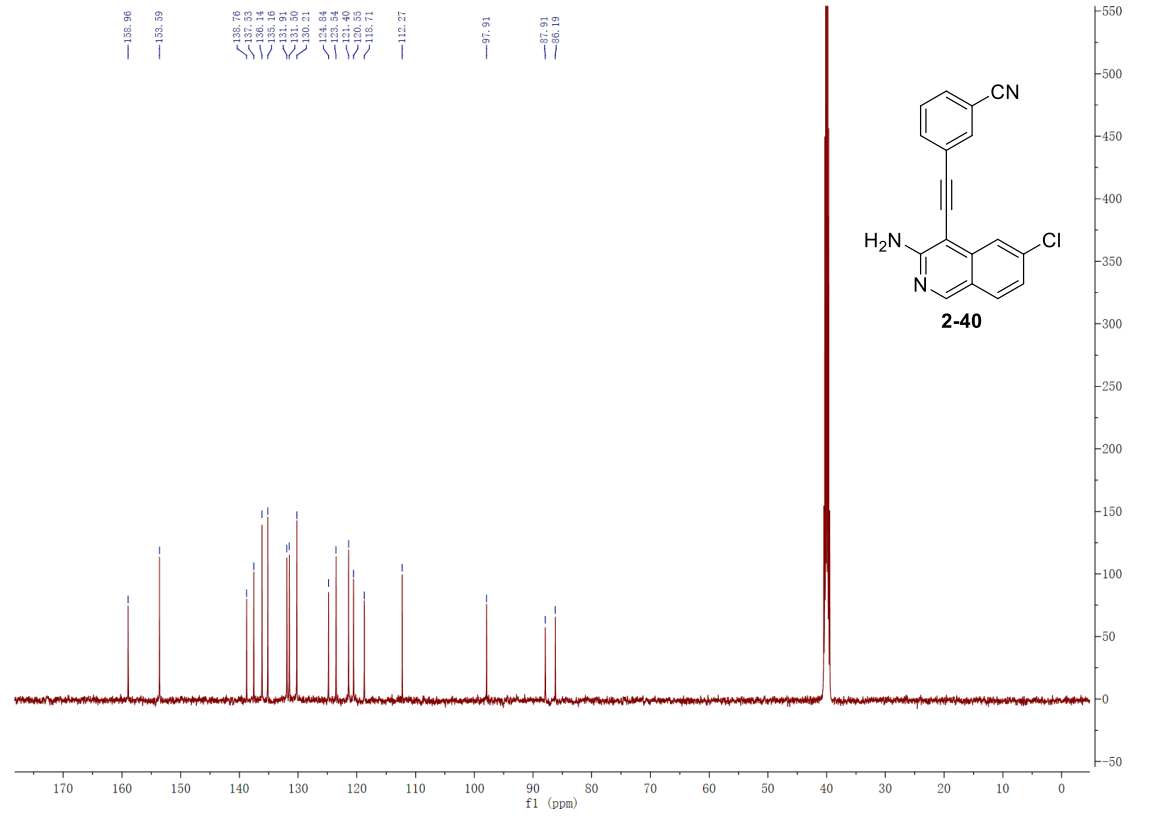
158.96
153.39
135.76
135.53
134.14
133.16
131.91
131.50
130.21
124.84
123.54
123.40
120.55
118.71
112.27
97.91
87.91
86.19
CN
H2N
Cl
N
2-40
f1 (ppm)

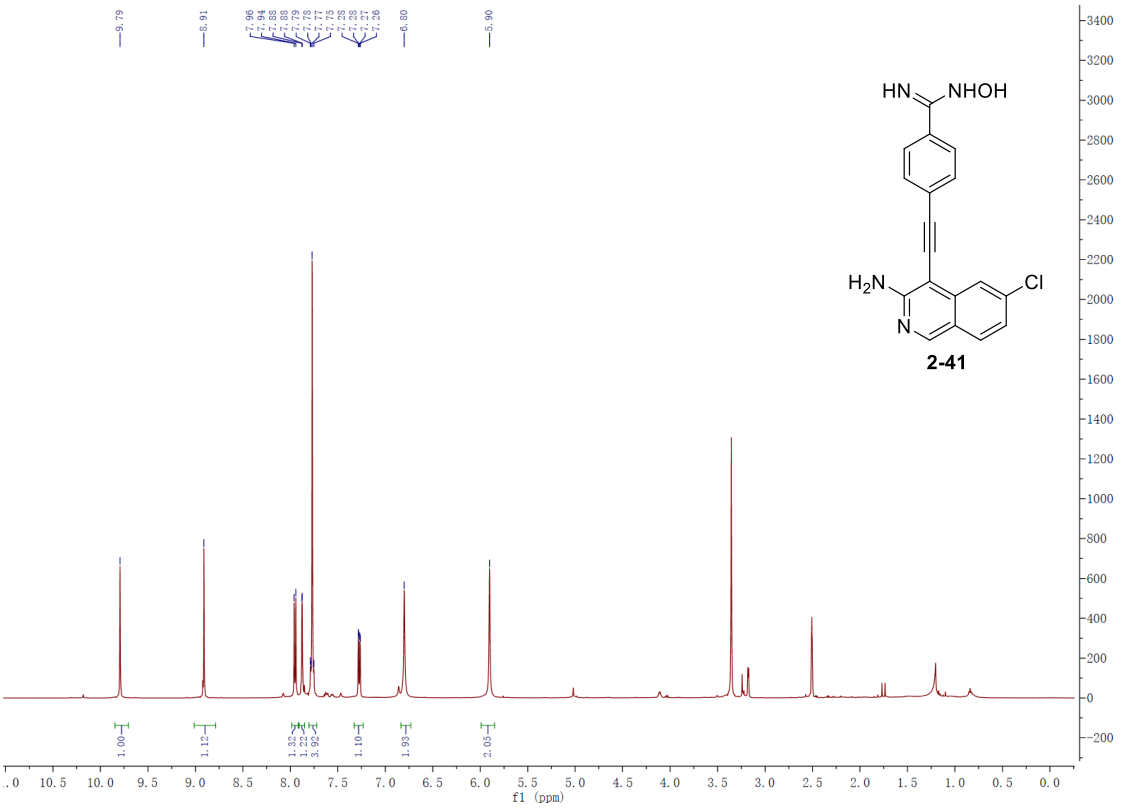
HN
NHOH
H2N
N
Cl
2-41
f1 (ppm)

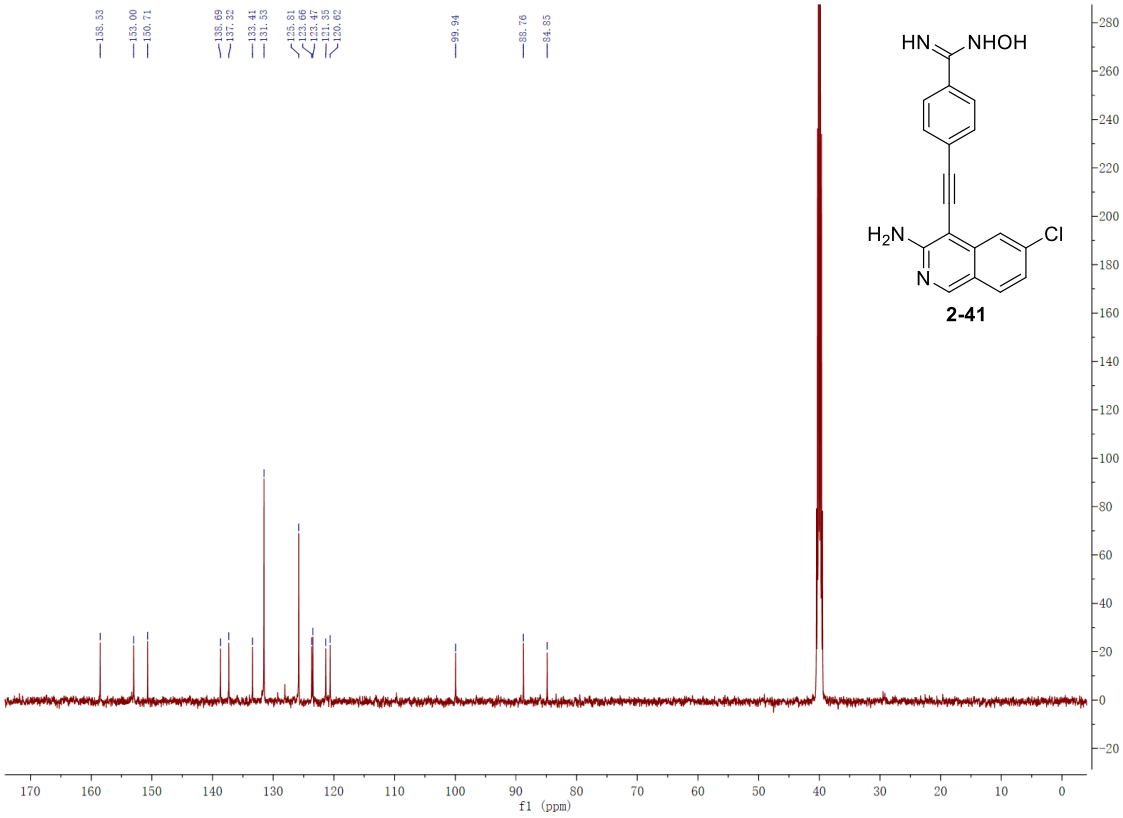
HN
NHOH
H2N
N
Cl
2-41
f1 (ppm)

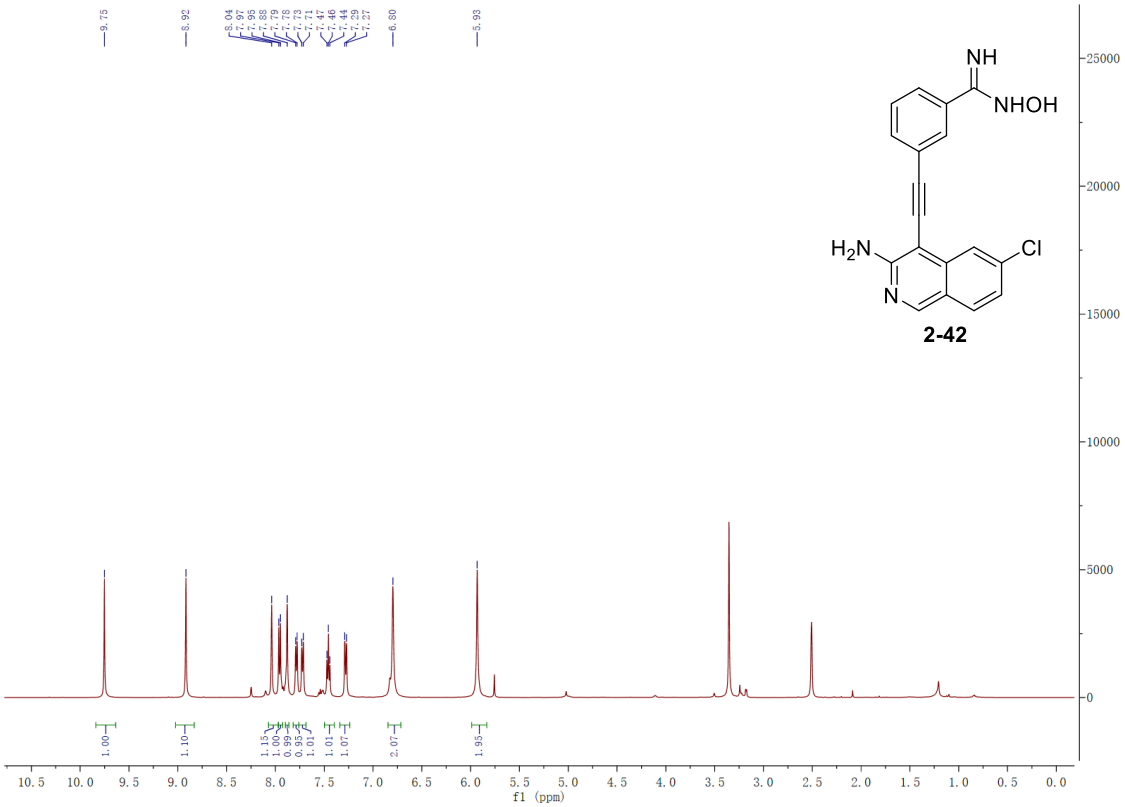
9.75
8.92
8.04
7.97
7.96
7.88
7.79
7.78
7.73
7.71
7.47
7.46
7.44
7.29
7.27
6.80
5.93
NH
NHOH
H2N
Cl
N
2-42
1.00
1.10
1.15
1.04
0.99
0.95
1.01
1.01
1.07
2.07
1.95
f1 (ppm)

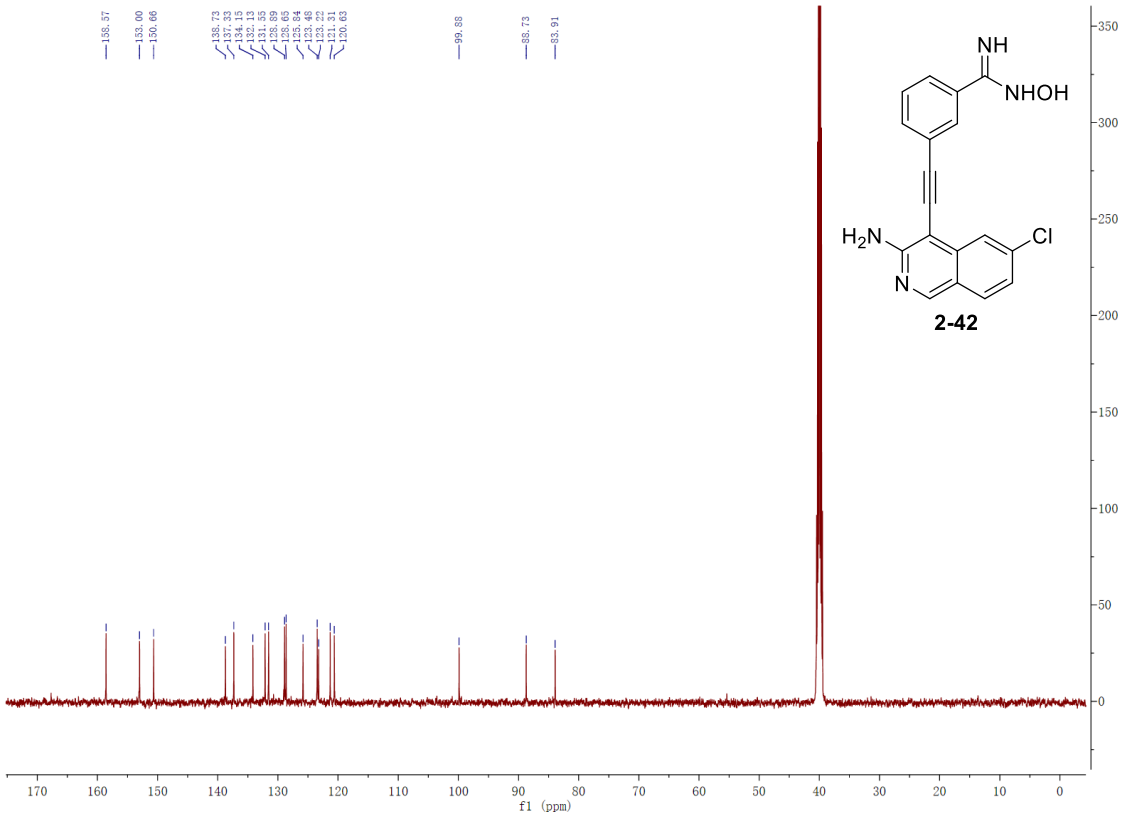
158.57
153.00
150.66
138.73
137.33
134.15
132.13
131.55
131.89
128.65
125.84
123.48
123.22
121.31
120.63
99.88
88.73
83.91
NH
NHOH
H2N
Cl
N
2-42
f1 (ppm)

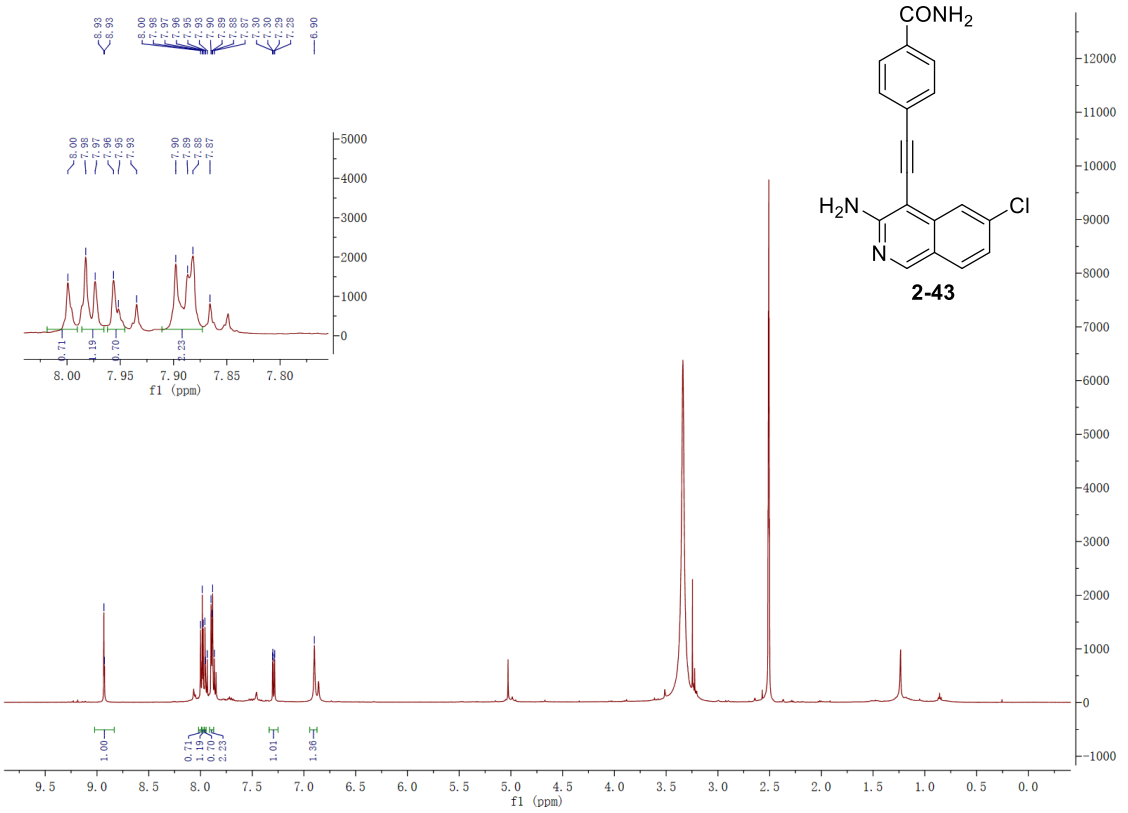
CONH2
H2N
Cl
N
2-43
f1 (ppm)

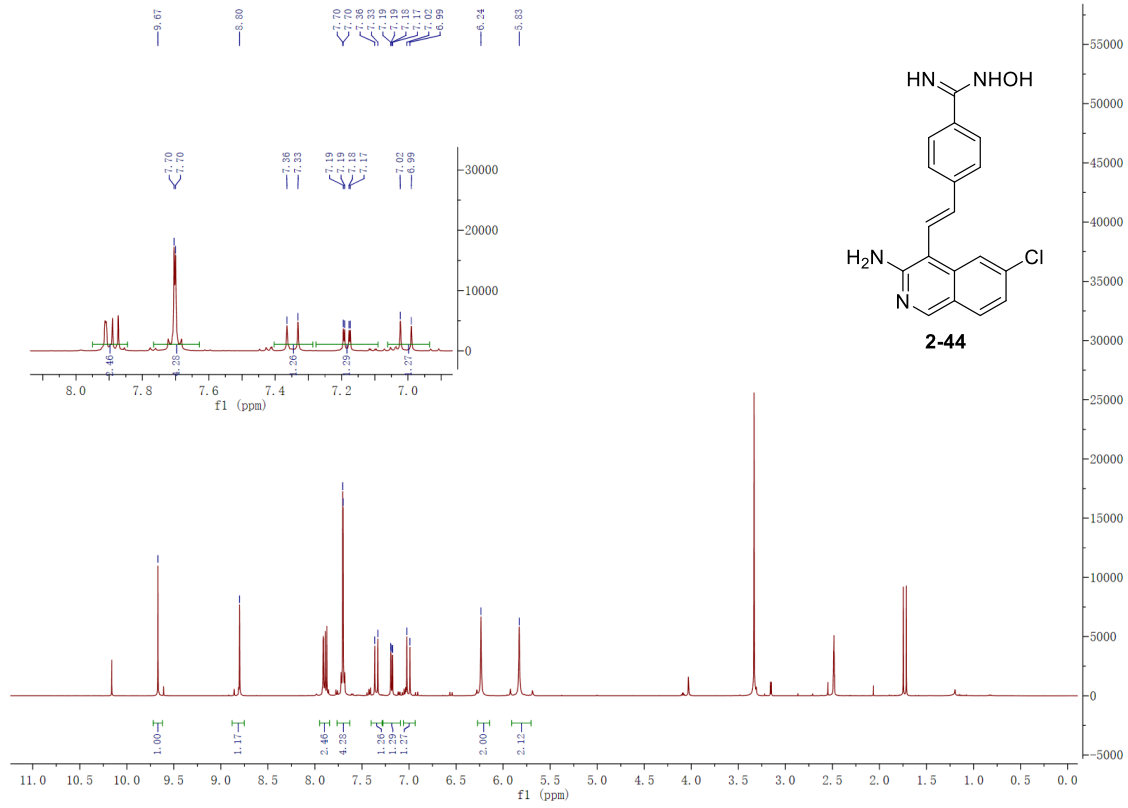
HN
NHOH
H2N
Cl
N
2-44
f1 (ppm)

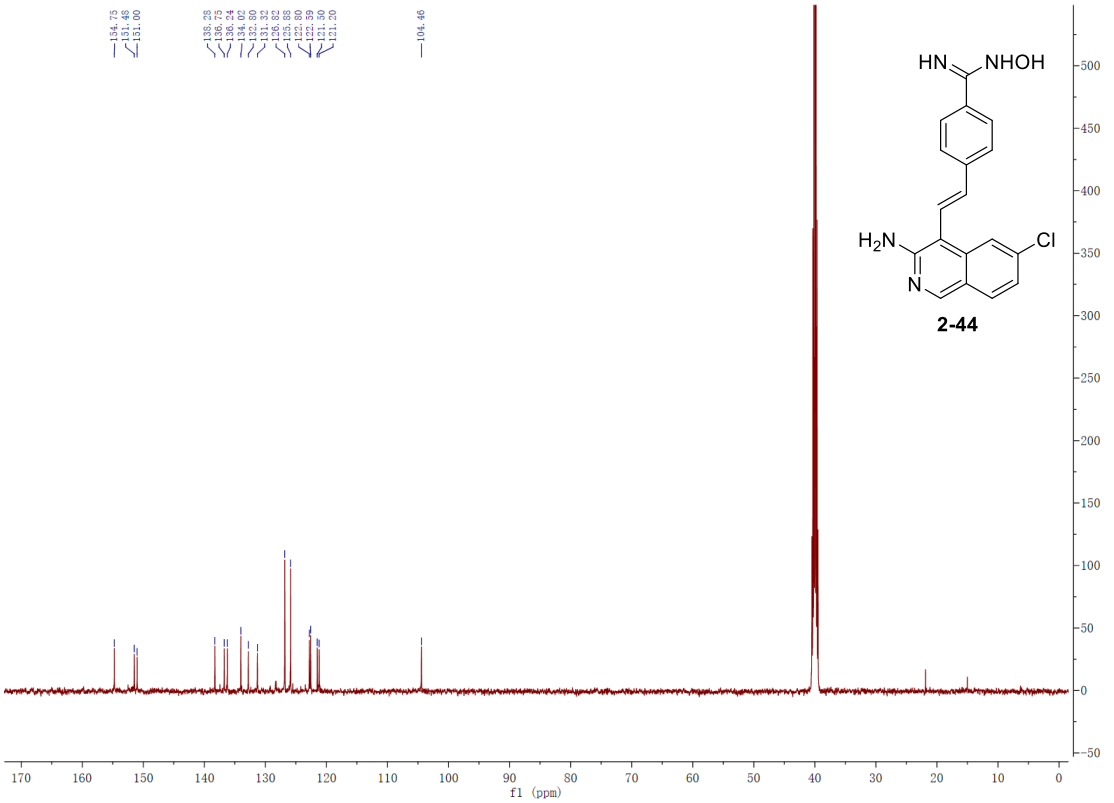
134.75
131.48
131.00
138.28
136.75
136.24
134.02
132.80
131.32
125.82
125.88
122.80
122.59
121.30
121.20
104.46
HN
NHOH
H2N
Cl
N
2-44
f1 (ppm)

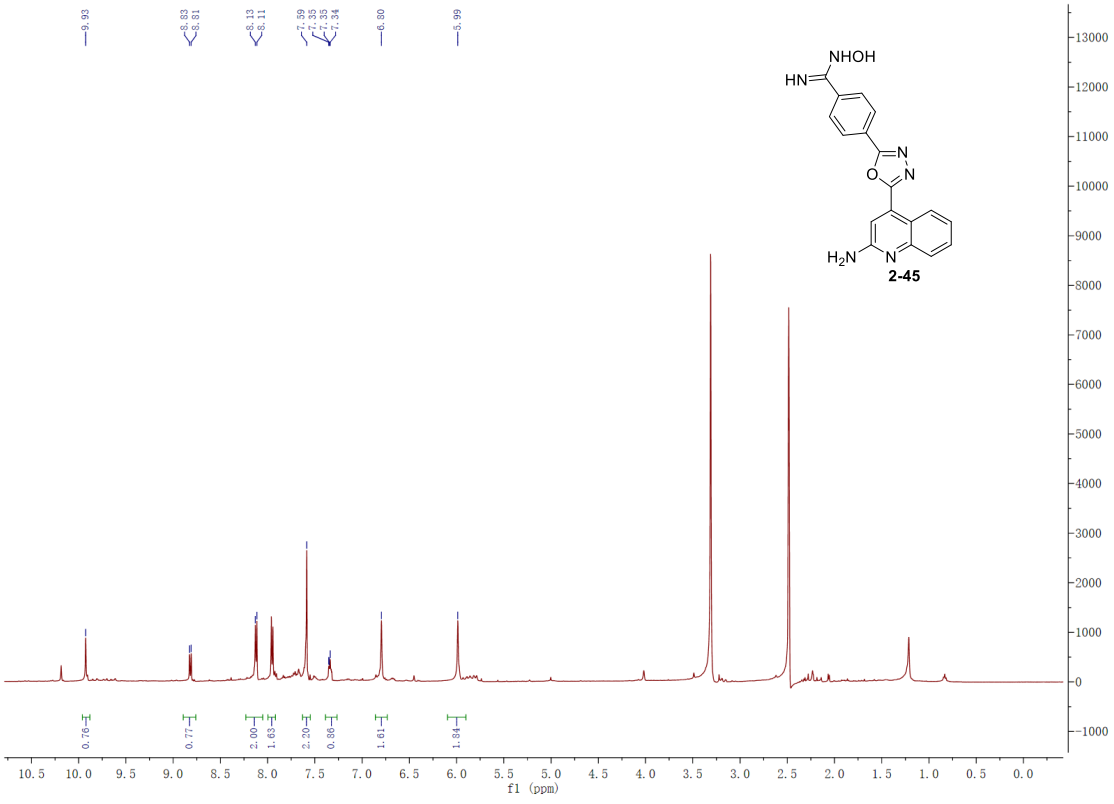
9.93
8.83
8.81
8.13
8.11
7.99
7.35
7.35
7.34
6.80
5.99
NHOH
HN
N
O
N
H2N
N
2-45
0.76
0.77
2.00
1.63
2.20
0.86
1.61
1.84
f1 (ppm)

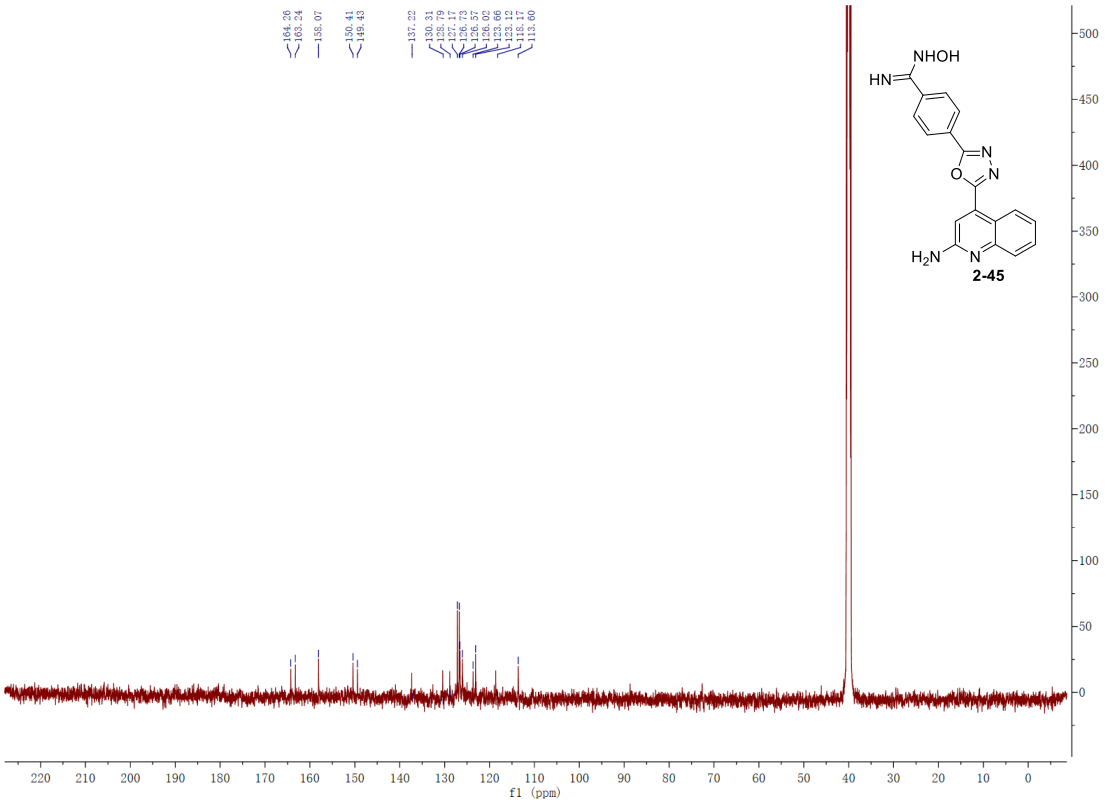
NHOH
HN
N
O
N
H_2N
N
2-45
f1 (ppm)

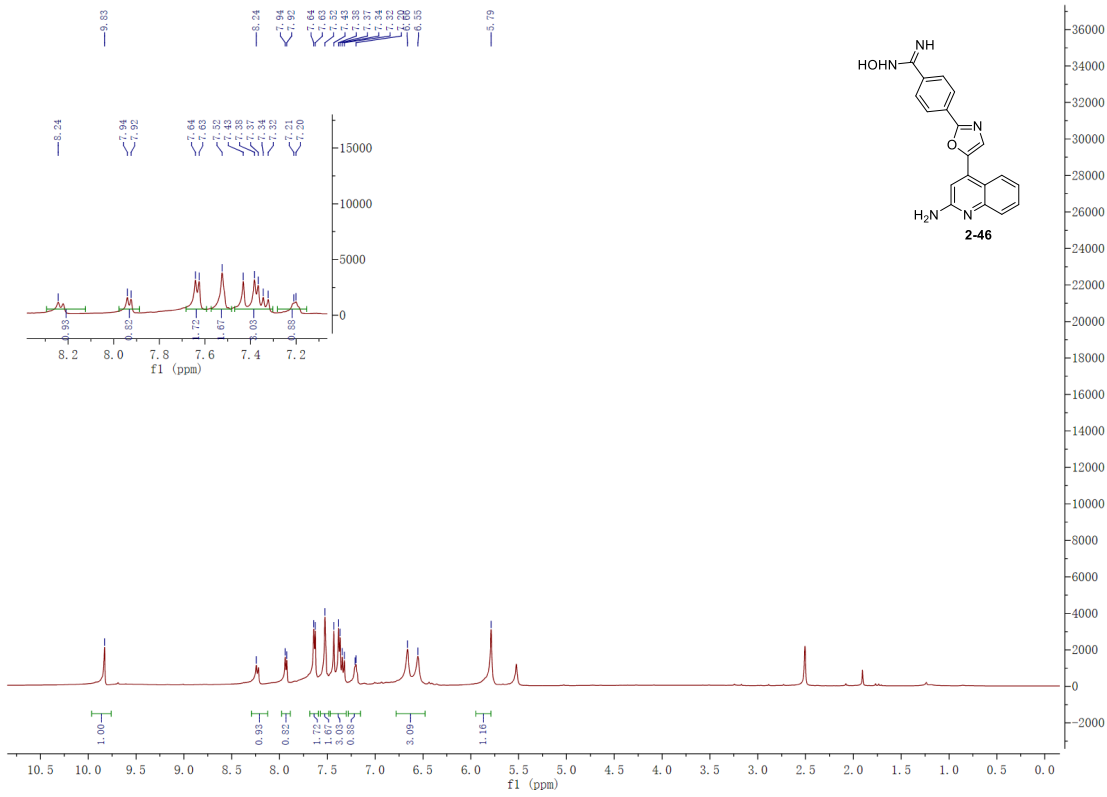
NH
HOHN
N
O
H_2N
N
2-46
f1 (ppm)

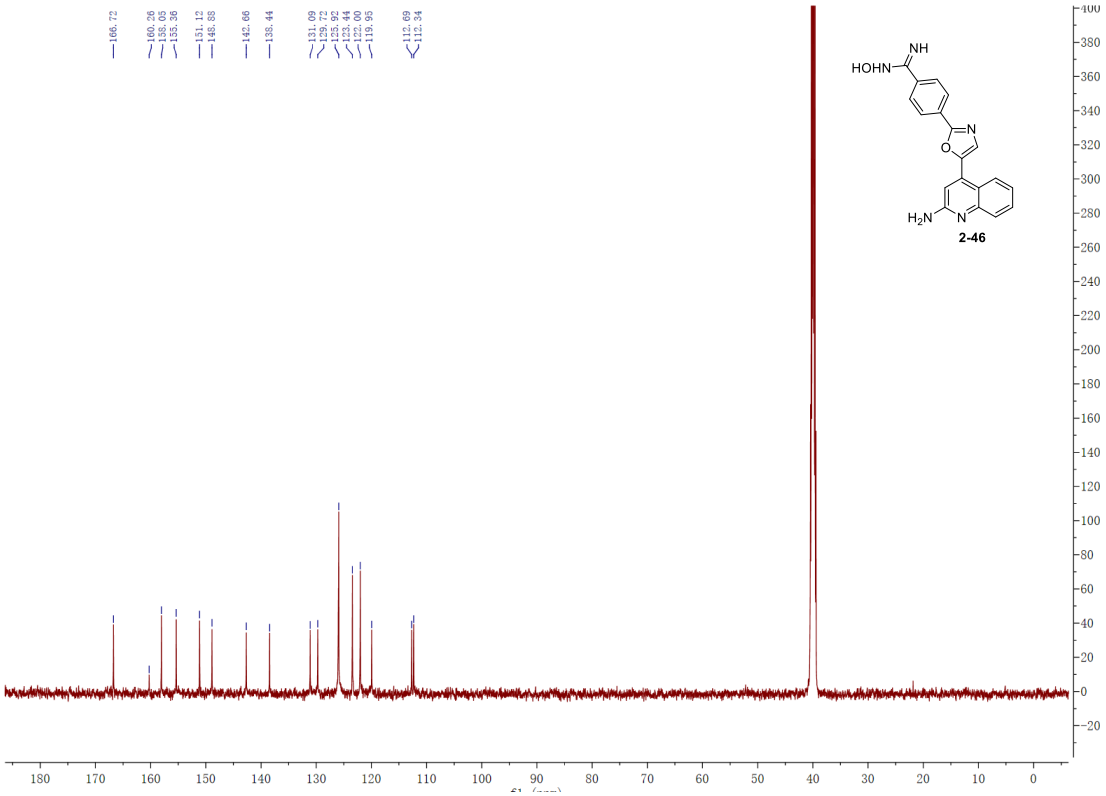
166.72
160.26
158.05
155.36
151.12
148.88
142.66
138.44
131.09
129.72
125.92
123.44
122.00
119.95
112.69
112.34
NH
HOHN
N
O
H_2N
N
2-46

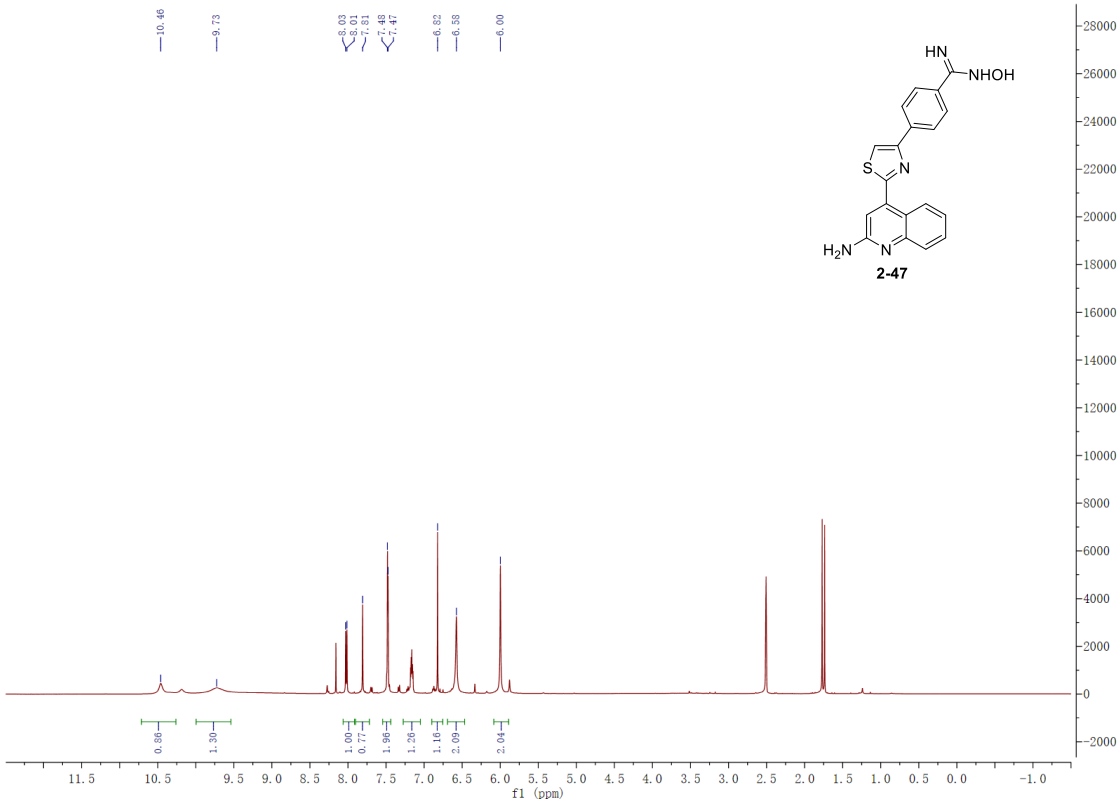
10.46
9.73
8.03
8.01
7.81
7.48
7.47
6.82
6.58
6.00
HN
NHOH
S
N
H_2N
N
2-47
0.86
1.30
1.00
0.77
1.96
1.26
1.16
2.09
2.04
f1 (ppm)

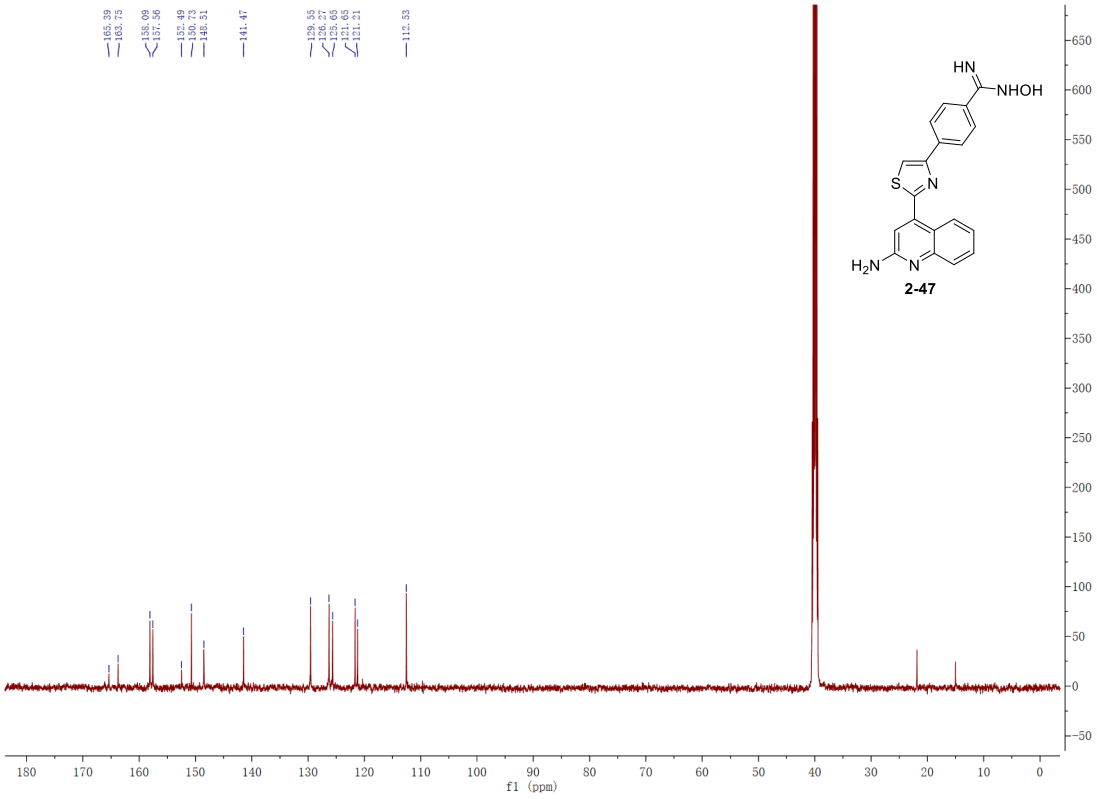
165.39
163.75
158.09
157.56
152.49
150.73
148.51
141.47
139.55
136.27
125.66
121.65
121.21
112.53
HN
NHOH
S
N
H2N
N
2-47
f1 (ppm)

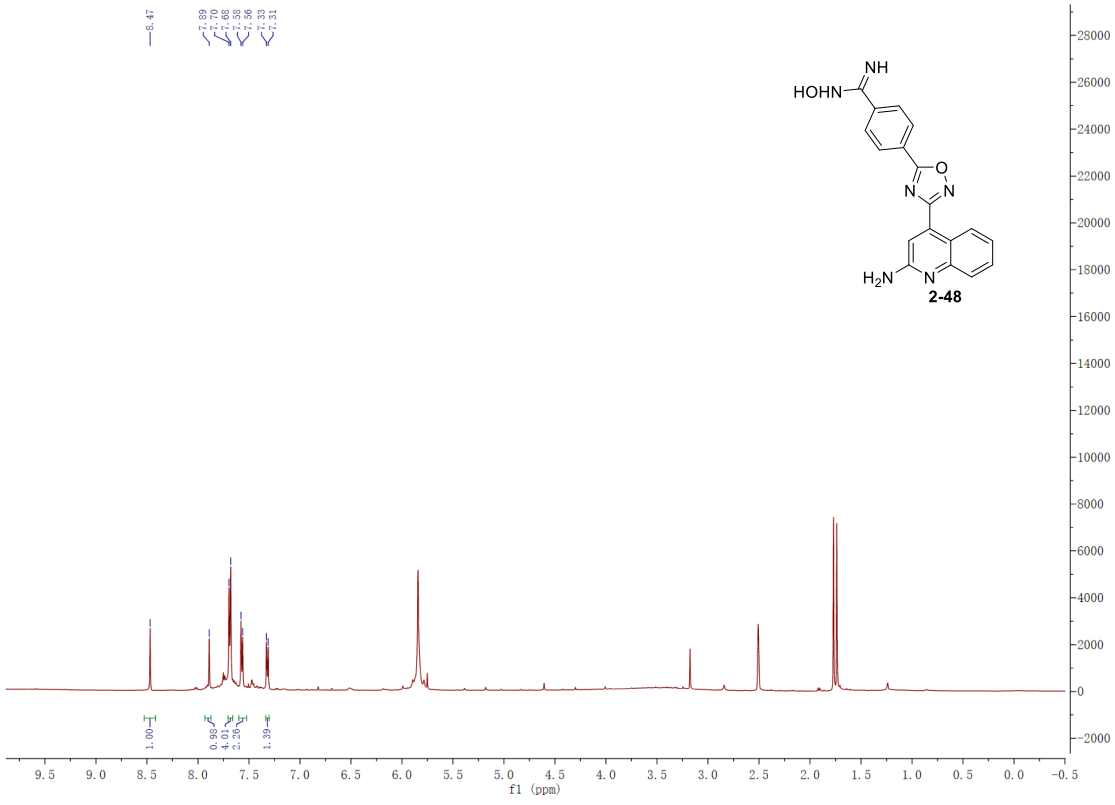
8.47
7.89
7.70
7.68
7.38
7.36
7.33
7.31
NH
HOHN
O
N
N
H2N
N
2-48
1.00
0.98
4.01
2.26
1.39
f1 (ppm)

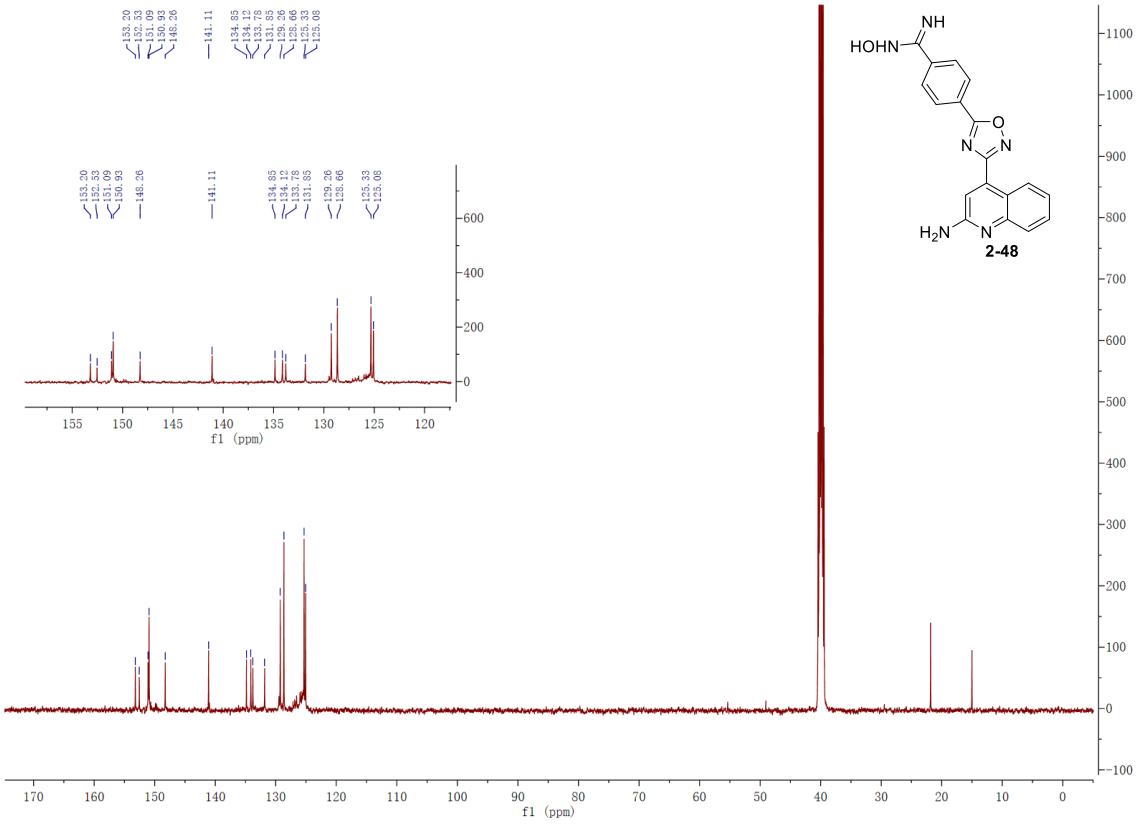
153.20
152.53
151.09
150.93
148.26
141.11
134.85
134.12
133.78
131.65
129.26
128.66
125.33
125.08
NH
HOHN
O
N
N
H_2N
N
2-48
f1 (ppm)

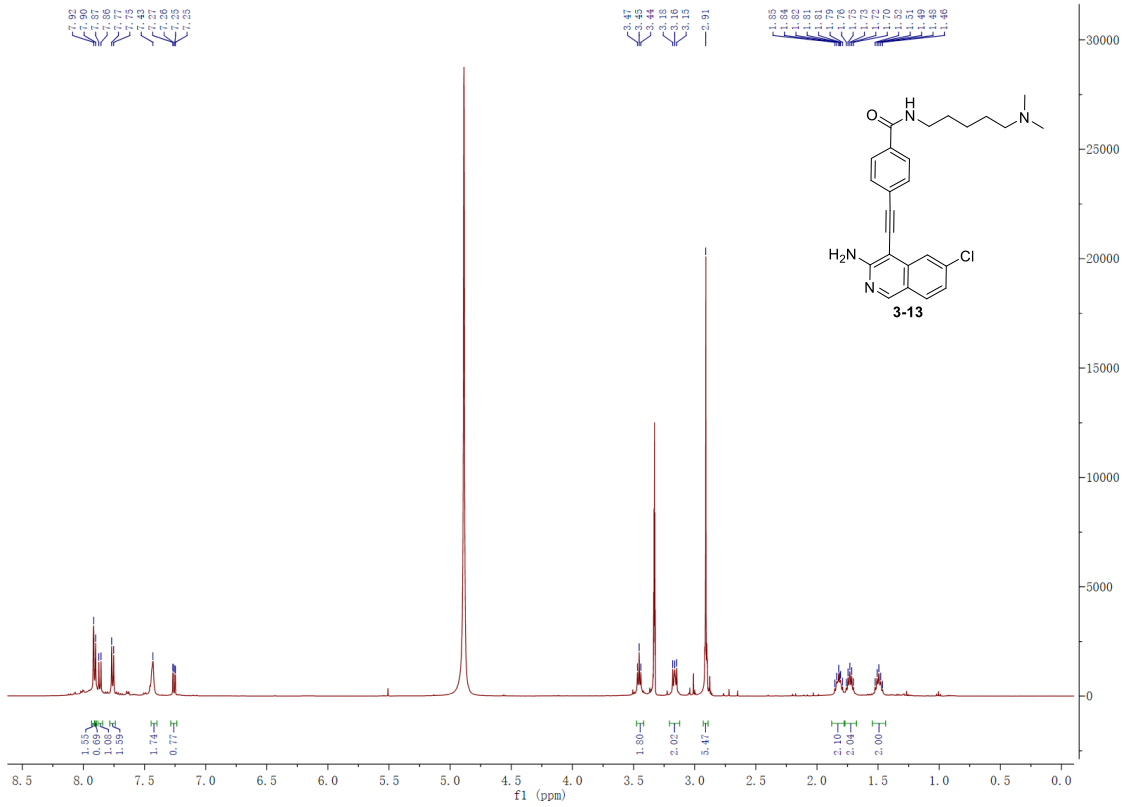
7.92
7.90
7.87
7.86
7.77
7.75
7.43
7.37
7.26
7.25
7.25
3.47
3.45
3.44
3.18
3.16
3.15
2.91
1.85
1.84
1.82
1.81
1.81
1.79
1.76
1.75
1.73
1.72
1.70
1.32
1.31
1.49
1.48
1.46
H
N
O
N
H_2N
Cl
N
3-13
f1 (ppm)

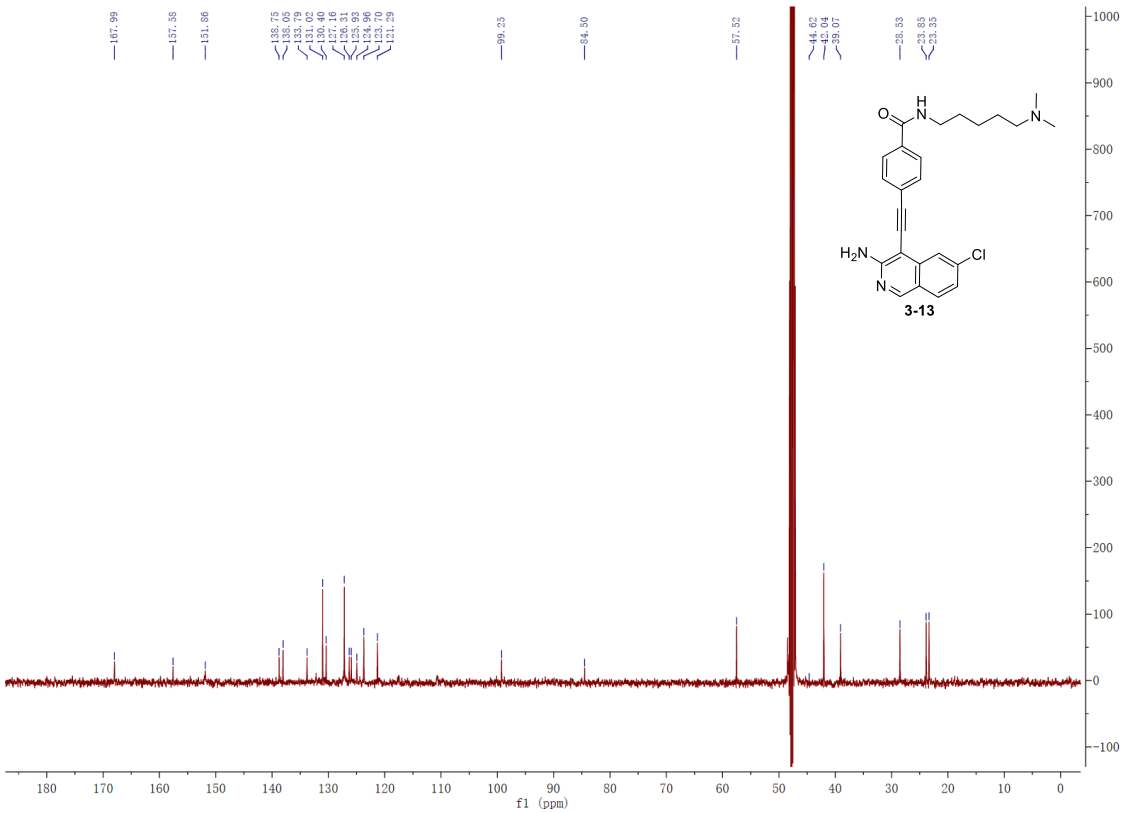
167.99
157.58
151.86
138.75
138.05
133.79
131.02
130.46
127.16
126.31
125.93
124.96
123.70
121.29
99.25
84.50
57.52
44.62
43.84
39.07
28.53
23.85
23.35
3-13
f1 (ppm)

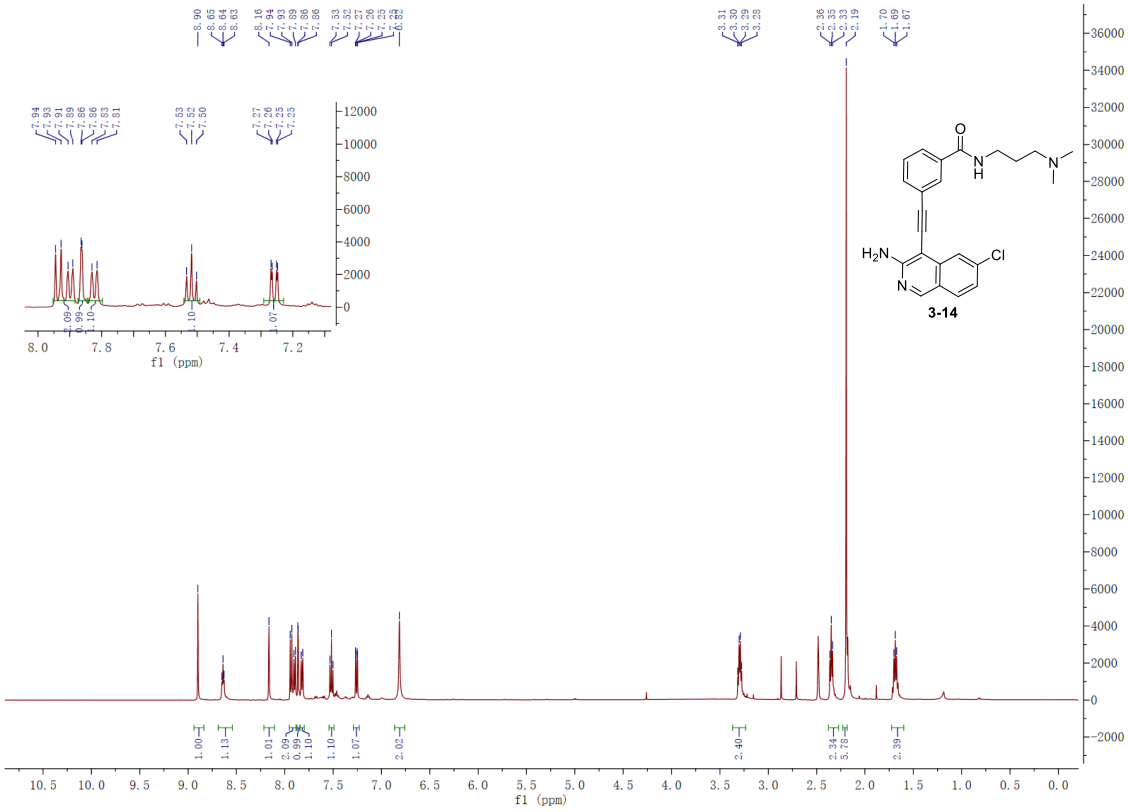
8.90
8.65
8.64
8.63
8.16
7.94
7.93
7.91
7.89
7.88
7.86
7.53
7.52
7.50
7.27
7.26
7.25
7.23
3.31
3.30
3.29
3.28
2.36
2.35
2.33
2.19
1.70
1.69
1.67
3-14
f1 (ppm)

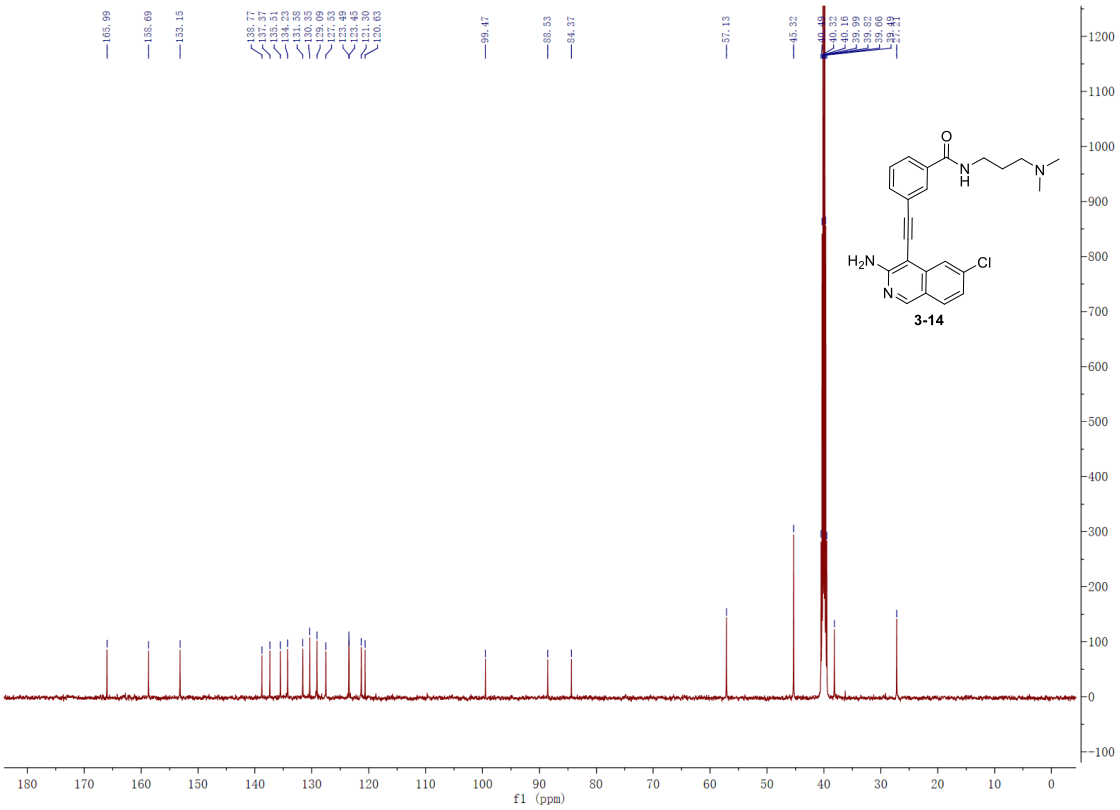
165.99
158.69
153.15
138.77
137.37
135.31
134.23
131.58
130.35
129.09
127.53
123.49
123.45
121.30
120.63
99.47
86.53
84.37
57.13
45.32
40.49
40.32
40.16
39.99
39.82
39.66
39.49
27.21
O
N
H
N
H2N
Cl
N
3-14
f1 (ppm)

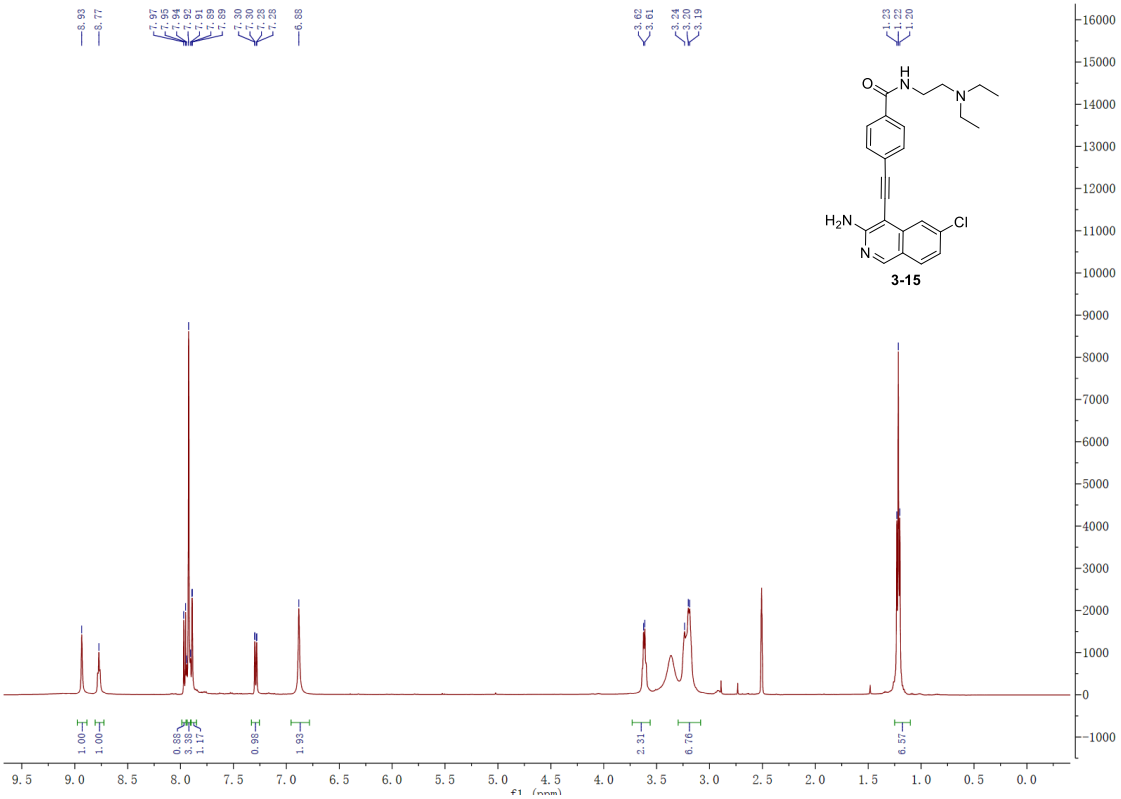
8.93
8.77
7.97
7.95
7.94
7.92
7.91
7.89
7.89
7.30
7.30
7.28
7.28
6.88
3.62
3.61
3.24
3.20
3.19
1.23
1.22
1.20
O
H
N
N
H2N
Cl
N
3-15
1.00
1.00
0.88
3.38
1.17
0.98
1.93
2.31
6.76
6.57
f1 (ppm)

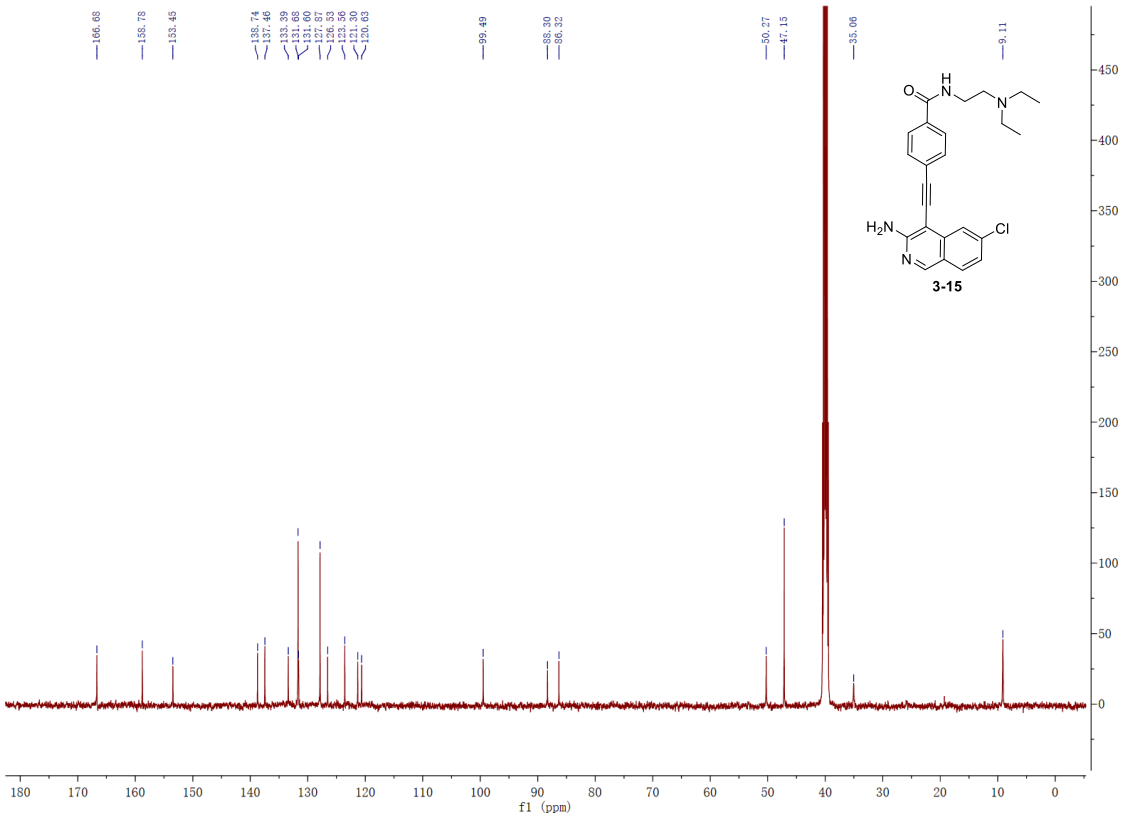
166.68
158.78
153.45
138.74
137.46
133.39
131.68
131.60
127.87
126.53
123.56
121.30
120.63
99.49
88.30
86.32
50.27
47.15
35.06
9.11
3-15
f1 (ppm)

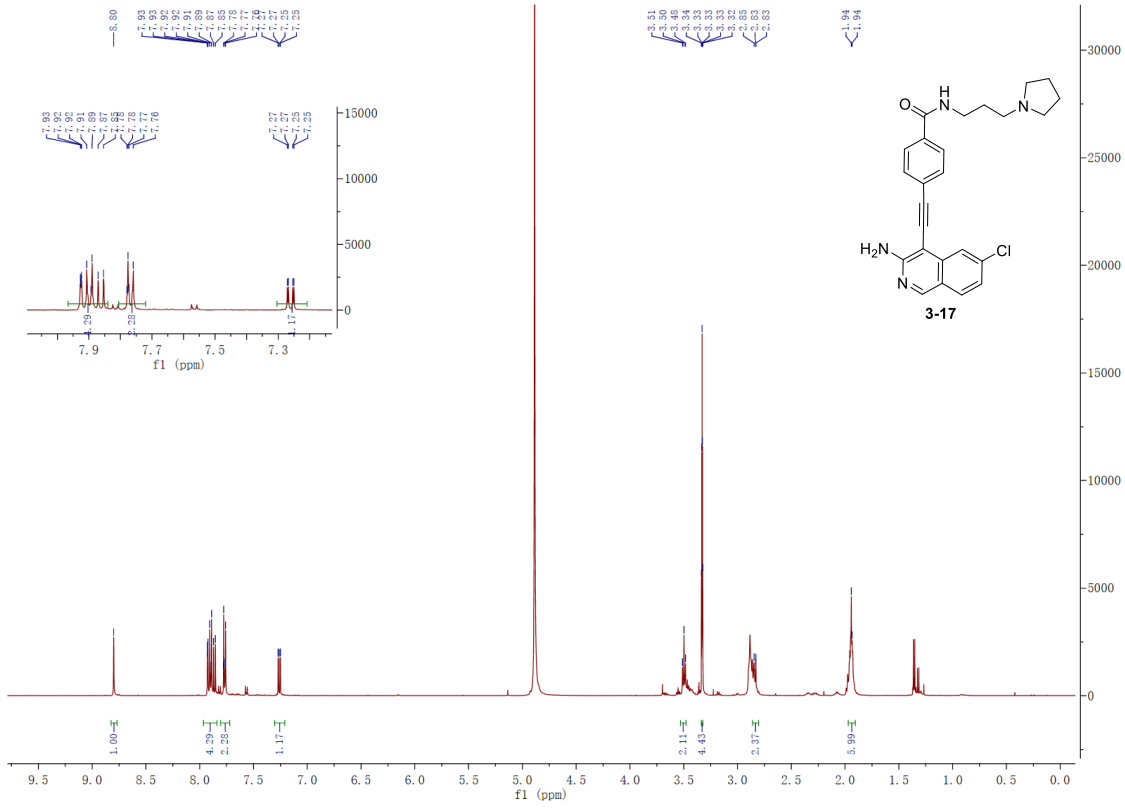
8.80
7.93
7.92
7.92
7.91
7.89
7.87
7.86
7.78
7.77
7.76
7.27
7.25
7.25
3.51
3.50
3.48
3.34
3.33
3.33
3.32
2.85
2.83
2.83
1.94
1.94
3-17
1.00
4.29
2.28
1.17
2.11
4.43
2.37
5.99
f1 (ppm)

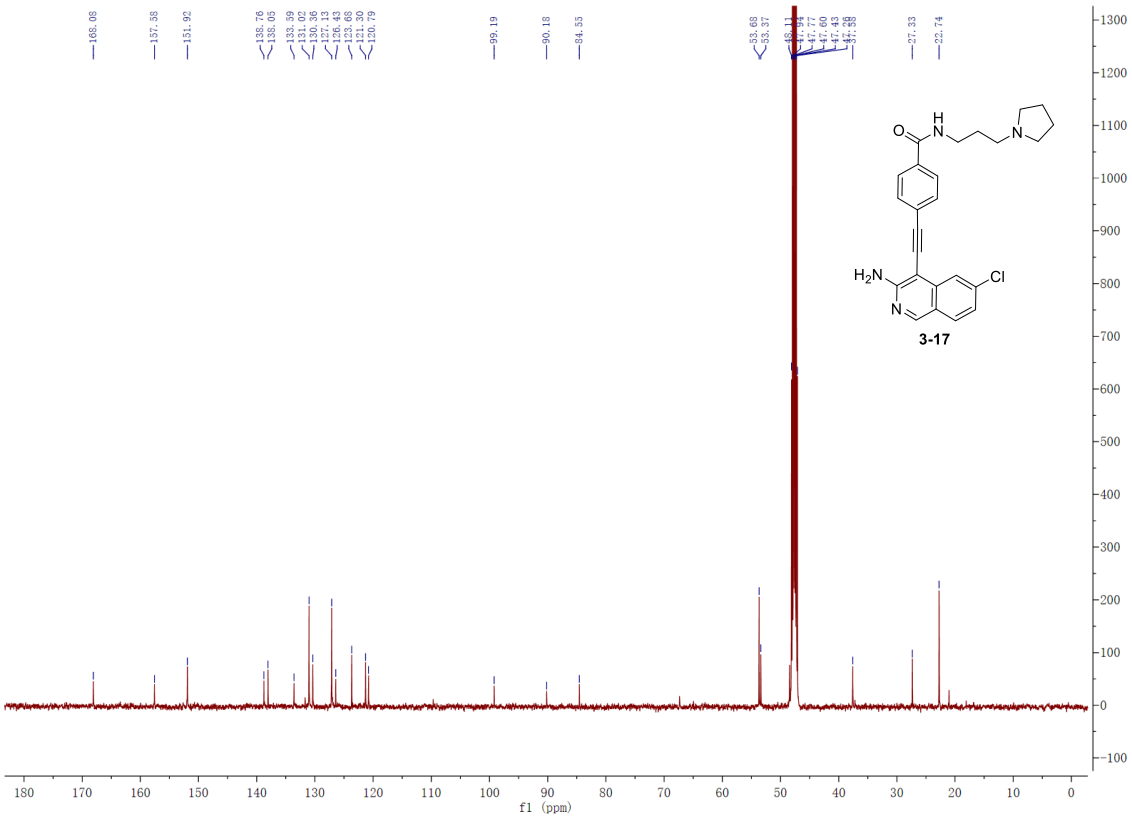
168.08
157.38
151.92
138.76
138.05
133.59
131.02
130.36
127.13
126.43
123.66
121.80
120.79
99.19
90.18
84.55
53.68
53.37
48.11
47.94
47.77
47.60
47.43
47.26
37.88
27.33
22.74
H
O
N
N
H2N
Cl
N
3-17
f1 (ppm)

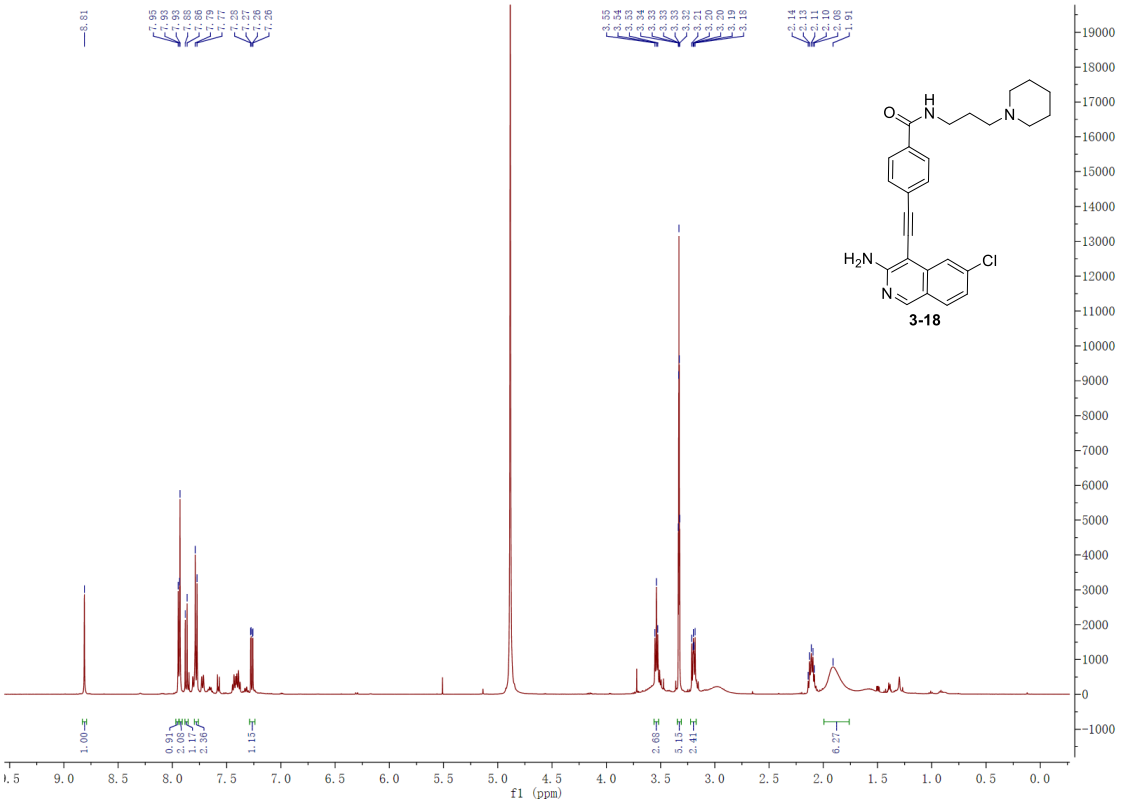
8.81
7.95
7.93
7.88
7.86
7.79
7.77
7.27
7.26
7.26
3.55
3.54
3.53
3.34
3.33
3.33
3.32
3.21
3.20
3.20
3.19
3.18
2.14
2.13
2.11
2.10
2.08
1.91
1.00
0.91
2.08
1.17
2.36
1.15
2.68
5.15
2.41
6.27
H
O
N
N
H2N
Cl
N
3-18
f1 (ppm)

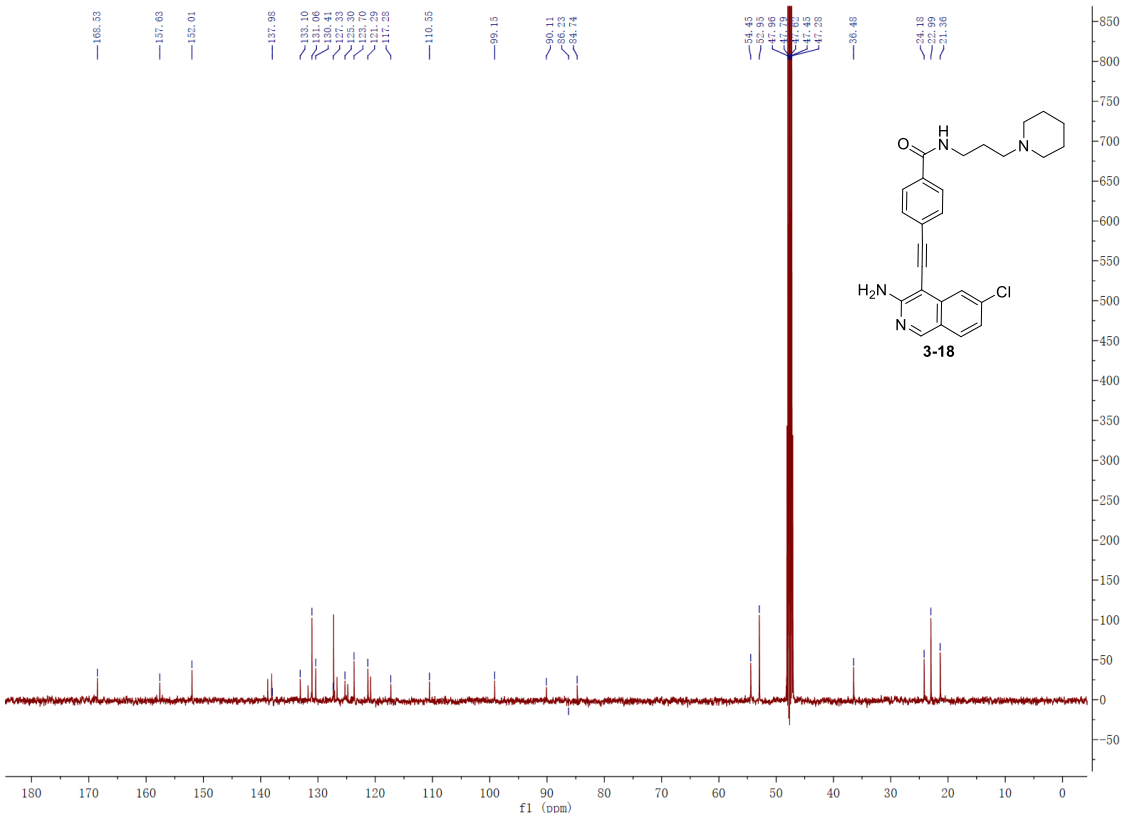
168.53
157.63
152.01
137.98
133.10
131.06
130.41
127.33
125.30
123.70
121.29
117.28
110.55
99.13
90.11
86.23
84.74
54.45
53.95
47.96
47.82
47.45
47.28
36.48
24.18
22.99
21.36
3-18

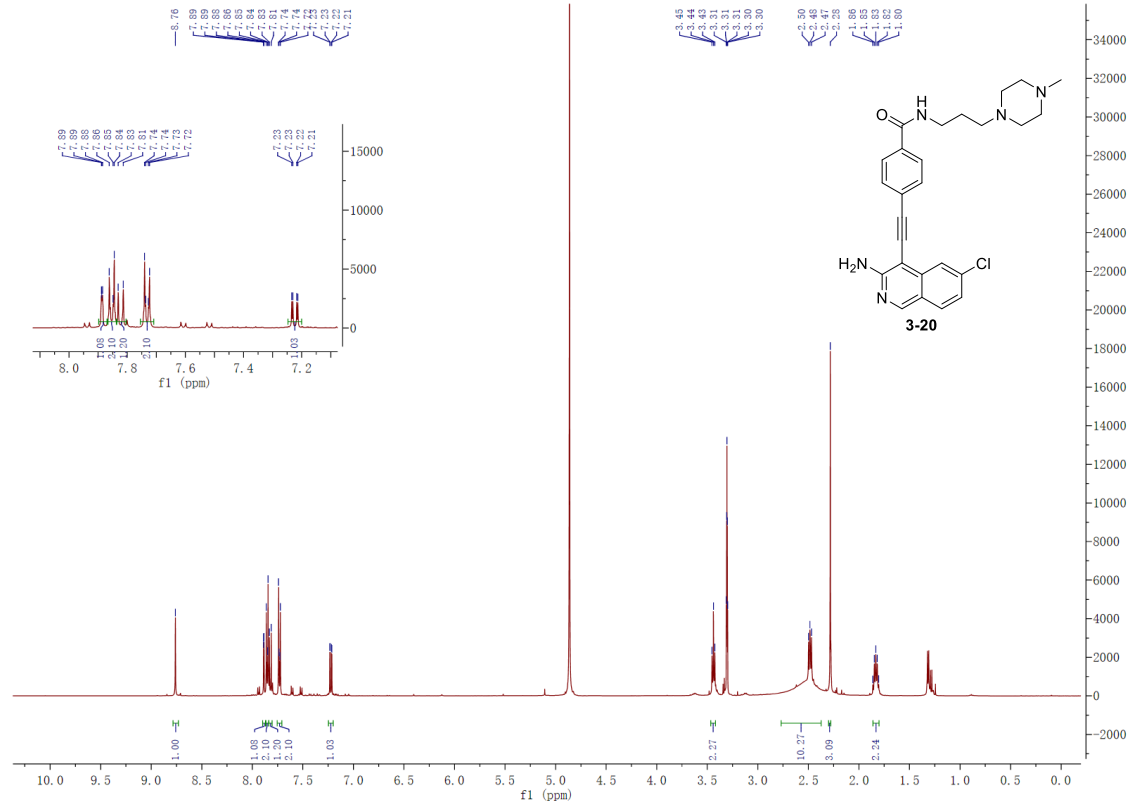
8.76
7.89
7.88
7.86
7.85
7.84
7.83
7.81
7.74
7.73
7.23
7.22
7.21
3.45
3.44
3.43
3.33
3.31
3.30
2.50
2.46
2.47
2.28
1.86
1.85
1.83
1.82
1.80
3-20
f1 (ppm)

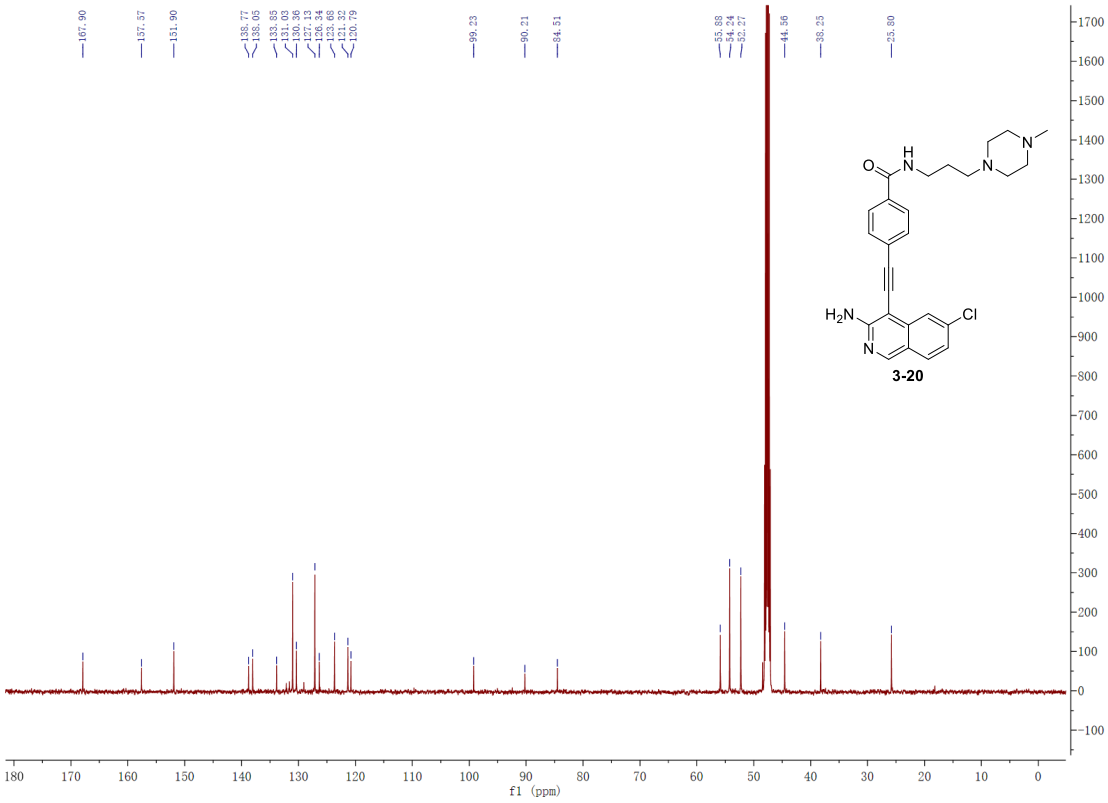
167.90
157.57
151.90
138.77
138.05
133.85
131.03
130.36
127.13
126.34
123.66
121.32
120.79
99.23
90.21
84.51
55.88
54.24
52.27
44.56
38.25
25.80
3-20
f1 (ppm)

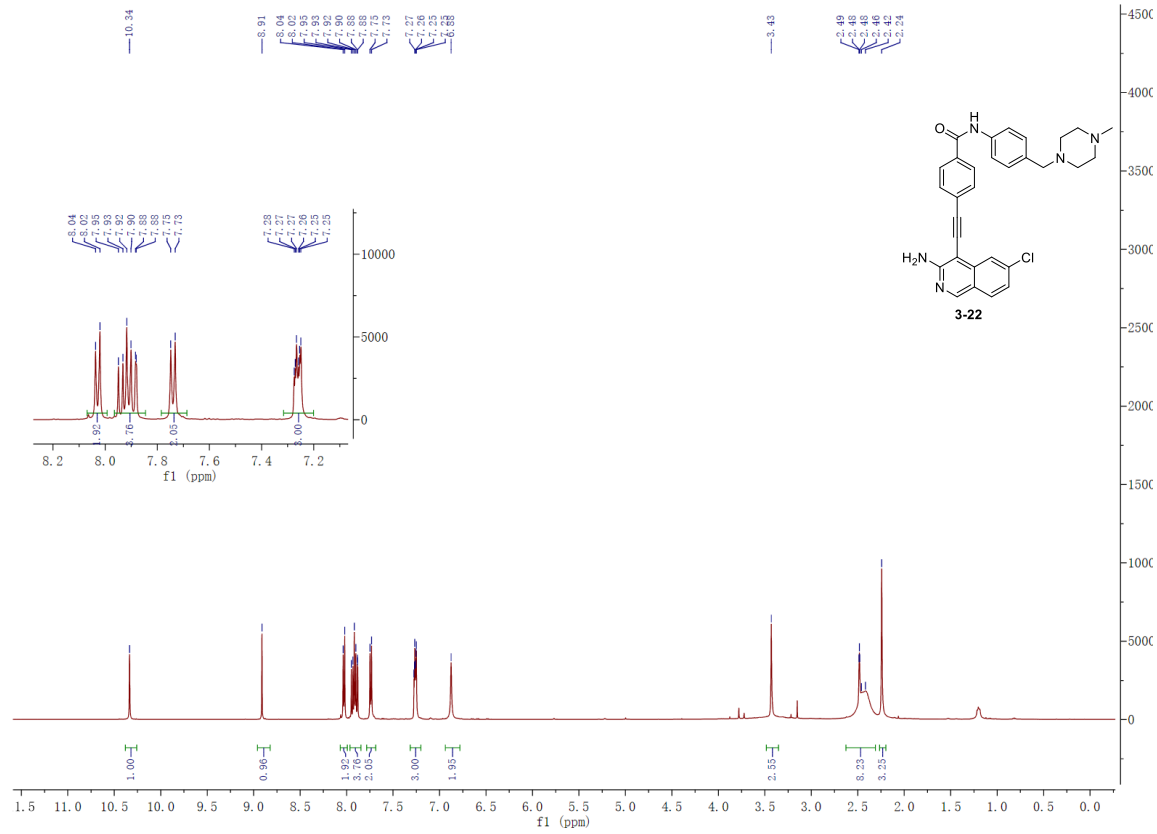
10.34
8.91
8.04
8.02
7.95
7.93
7.92
7.90
7.88
7.75
7.73
7.27
7.26
7.25
3.43
2.49
2.48
2.46
2.42
2.24
3-22
f1 (ppm)

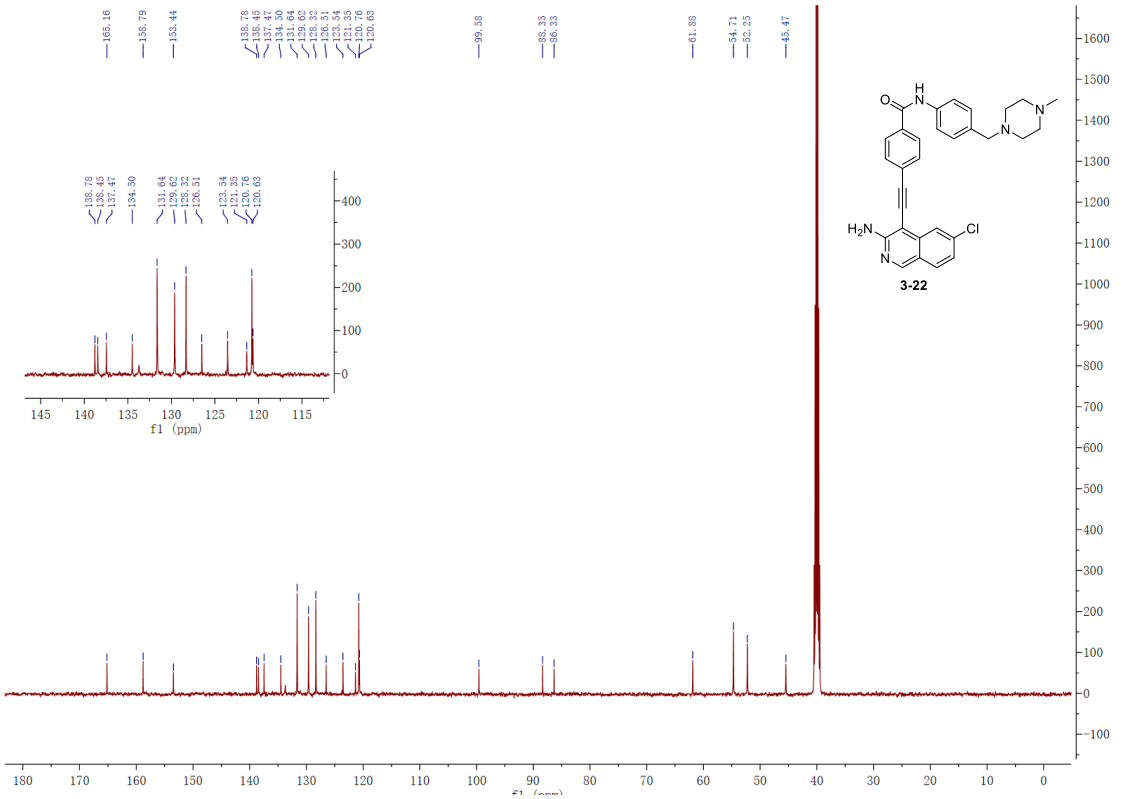
165.16
158.79
153.44
138.78
138.45
137.47
134.50
131.64
129.62
128.32
126.51
123.54
121.35
120.76
120.63
99.58
88.35
86.33
61.88
54.71
52.25
45.47
f1 (ppm)
3-22

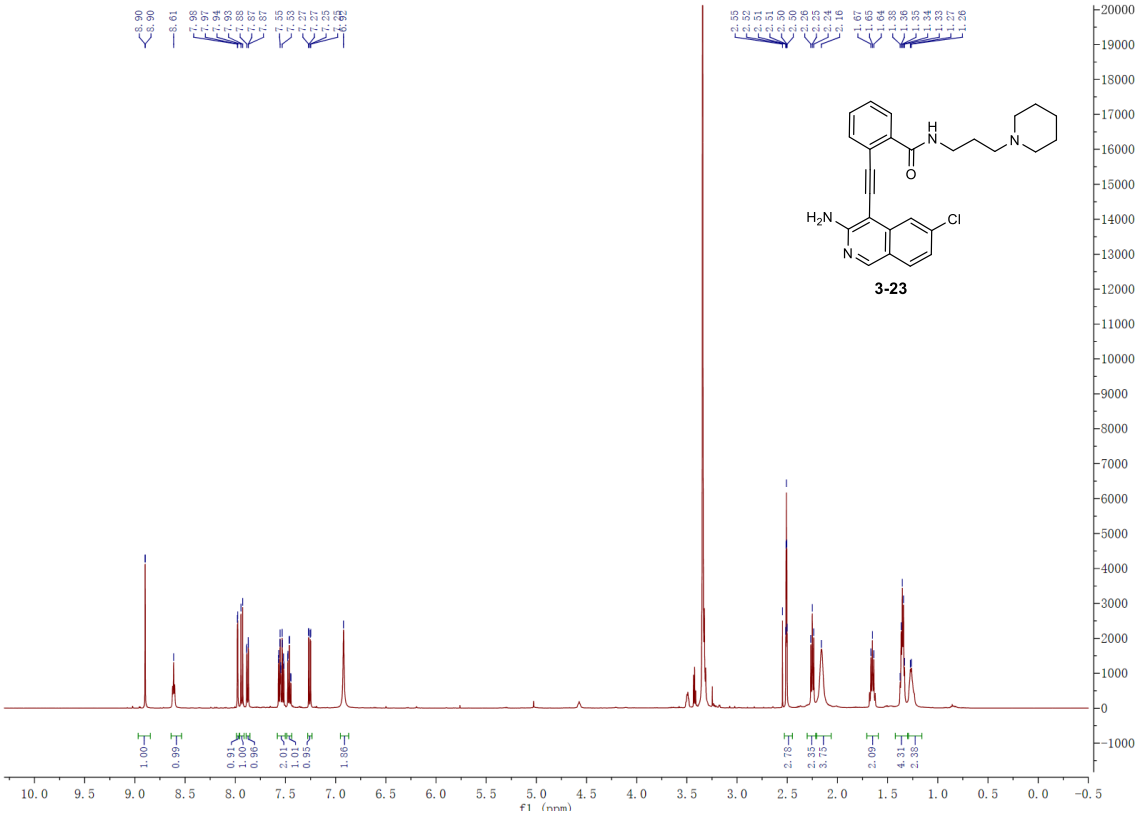
8.90
8.90
8.61
7.98
7.97
7.94
7.93
7.88
7.87
7.87
7.55
7.53
7.27
7.27
7.25
6.94
6.92
2.55
2.52
2.51
2.51
2.50
2.50
2.26
2.25
2.24
2.16
1.67
1.65
1.64
1.38
1.36
1.35
1.34
1.33
1.27
1.26
1.00
0.99
0.91
1.00
0.96
2.01
1.01
0.95
1.86
2.78
2.35
2.15
2.09
4.31
2.38
f1 (ppm)
3-23

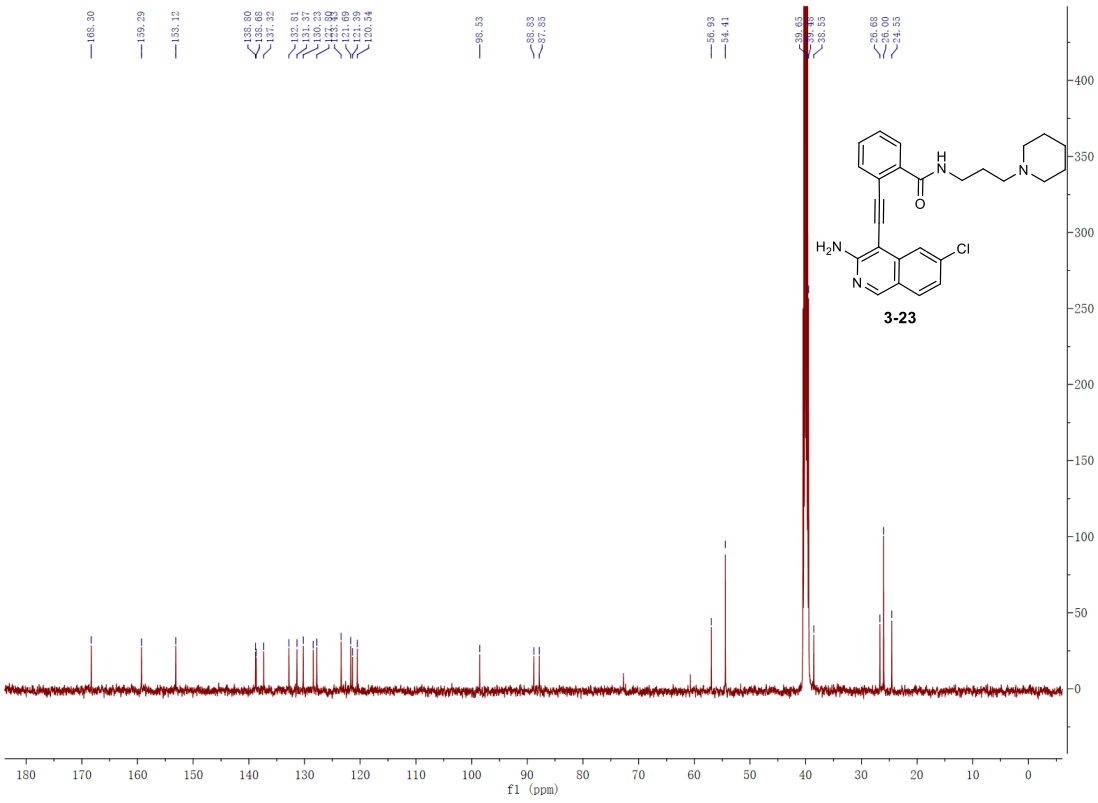
168.30
159.29
133.12
138.80
138.68
137.32
132.81
131.37
130.23
121.69
121.39
120.94
98.53
88.83
87.55
56.93
54.41
39.65
39.44
38.55
26.68
26.00
24.55
H2N
Cl
N
H
O
3-23
f1 (ppm)

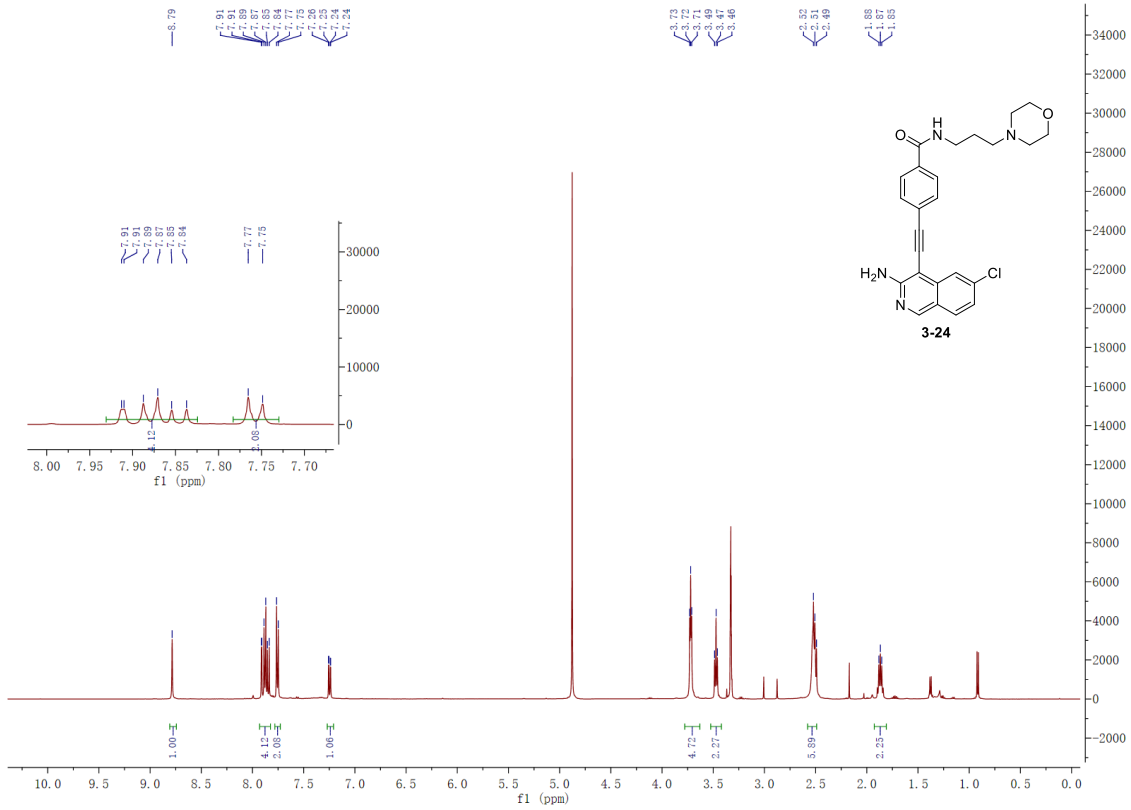
8.79
7.91
7.91
7.89
7.87
7.85
7.84
7.77
7.75
7.26
7.25
7.24
7.24
3.73
3.72
3.71
3.49
3.47
3.46
2.52
2.51
2.49
1.88
1.87
1.85
H2N
Cl
N
H
O
3-24
1.00
4.12
2.08
1.06
4.72
2.27
5.89
2.25
f1 (ppm)

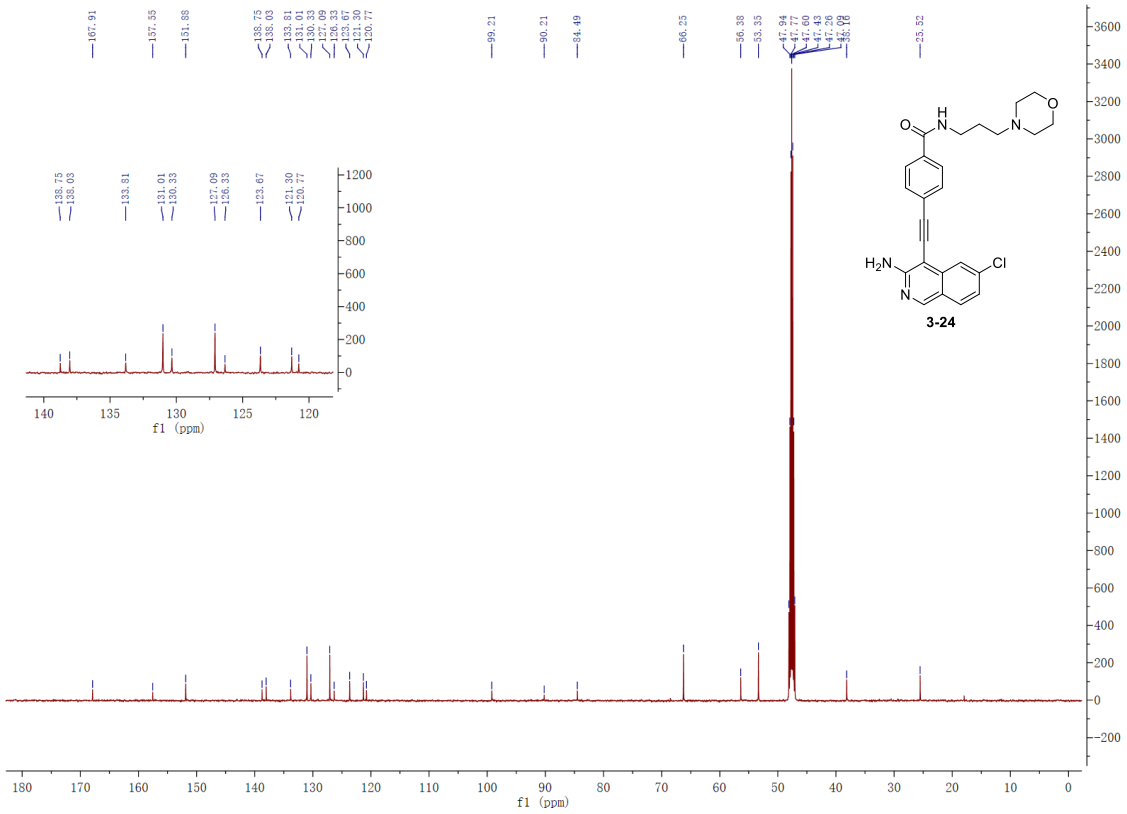
167.91
157.55
151.88
138.75
138.03
133.81
131.01
130.33
127.09
126.33
123.67
121.30
120.77
99.21
90.21
84.49
66.25
56.38
53.35
47.94
47.77
47.60
47.43
47.26
47.09
45.10
25.52
f1 (ppm)
3-24

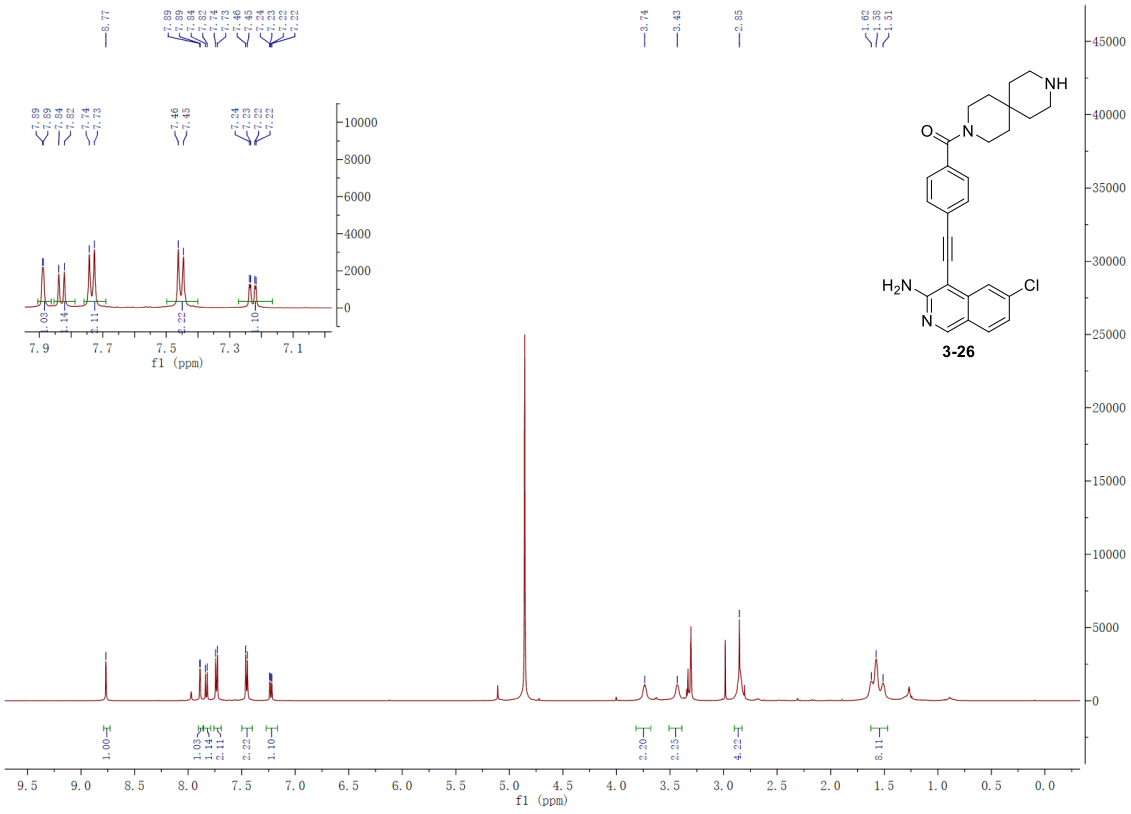
3-26
f1 (ppm)

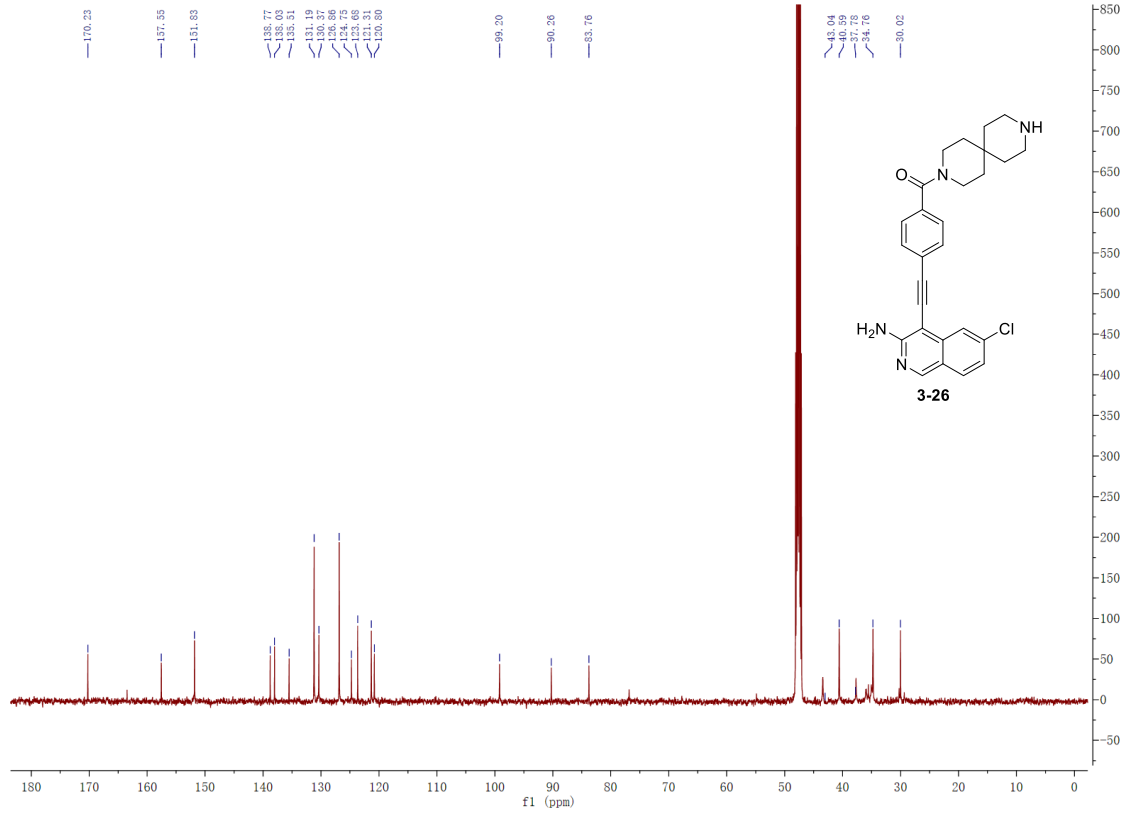
3-26
f1 (ppm)

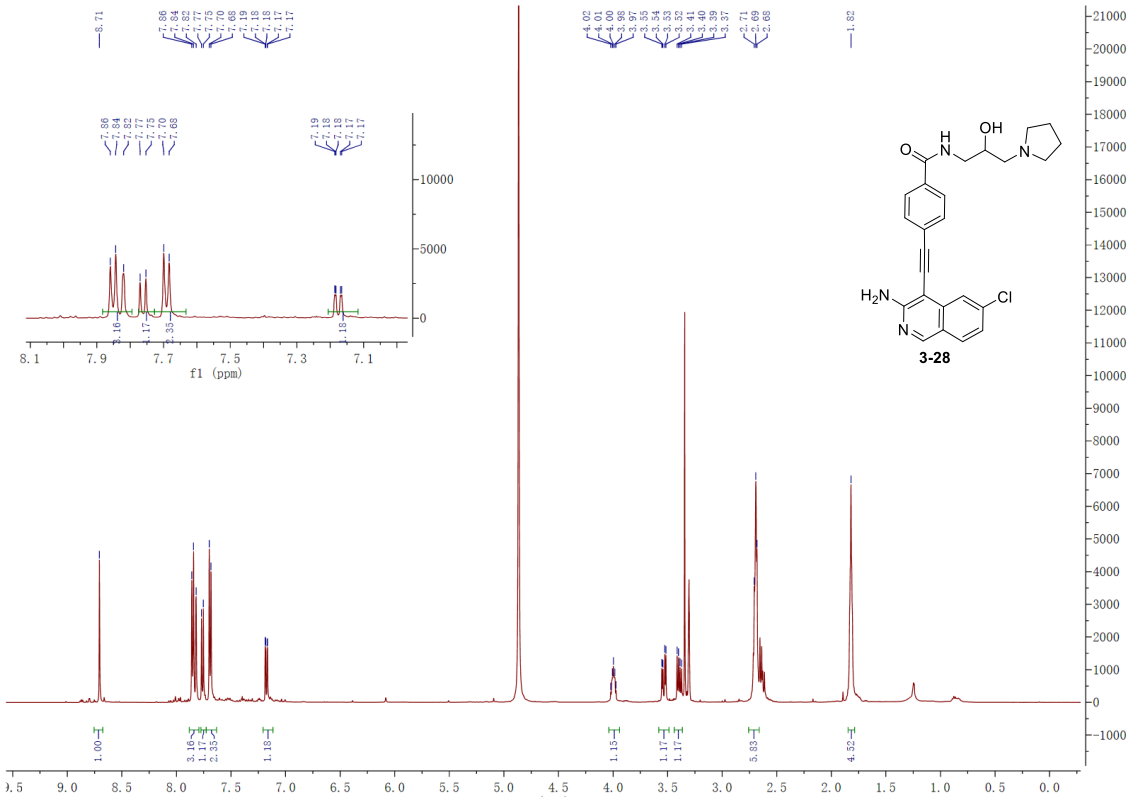
3-28

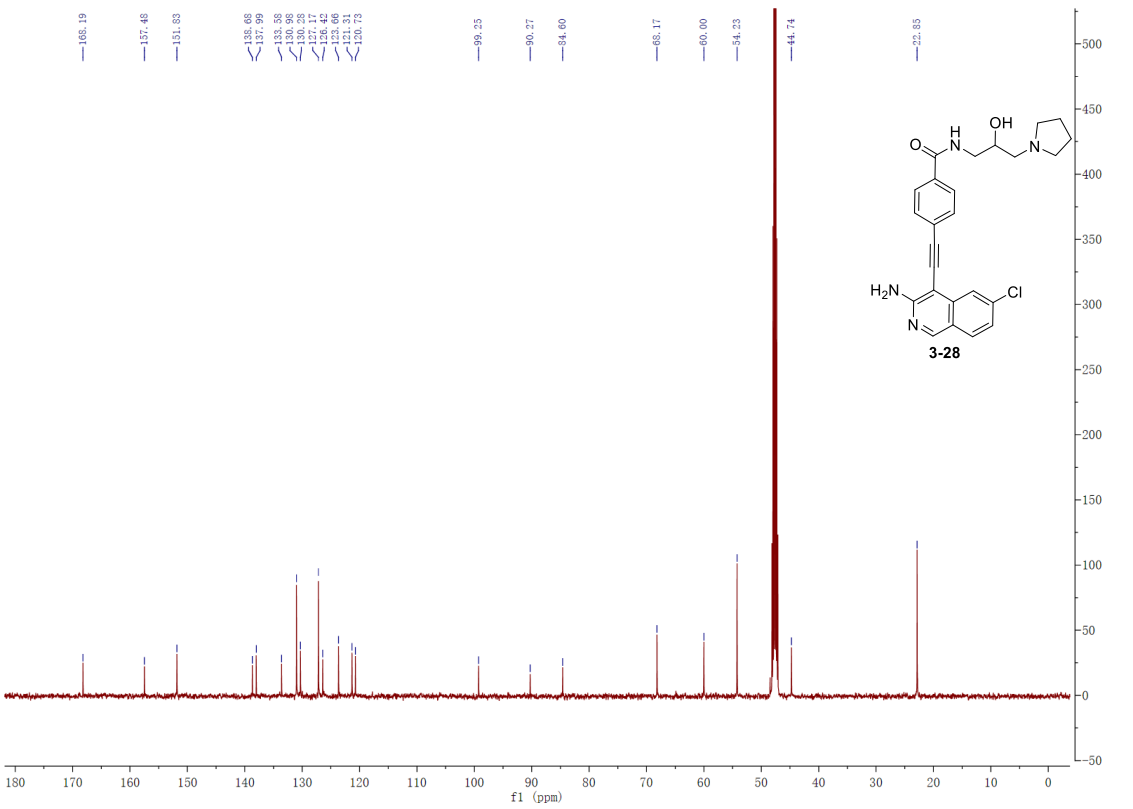
3-28

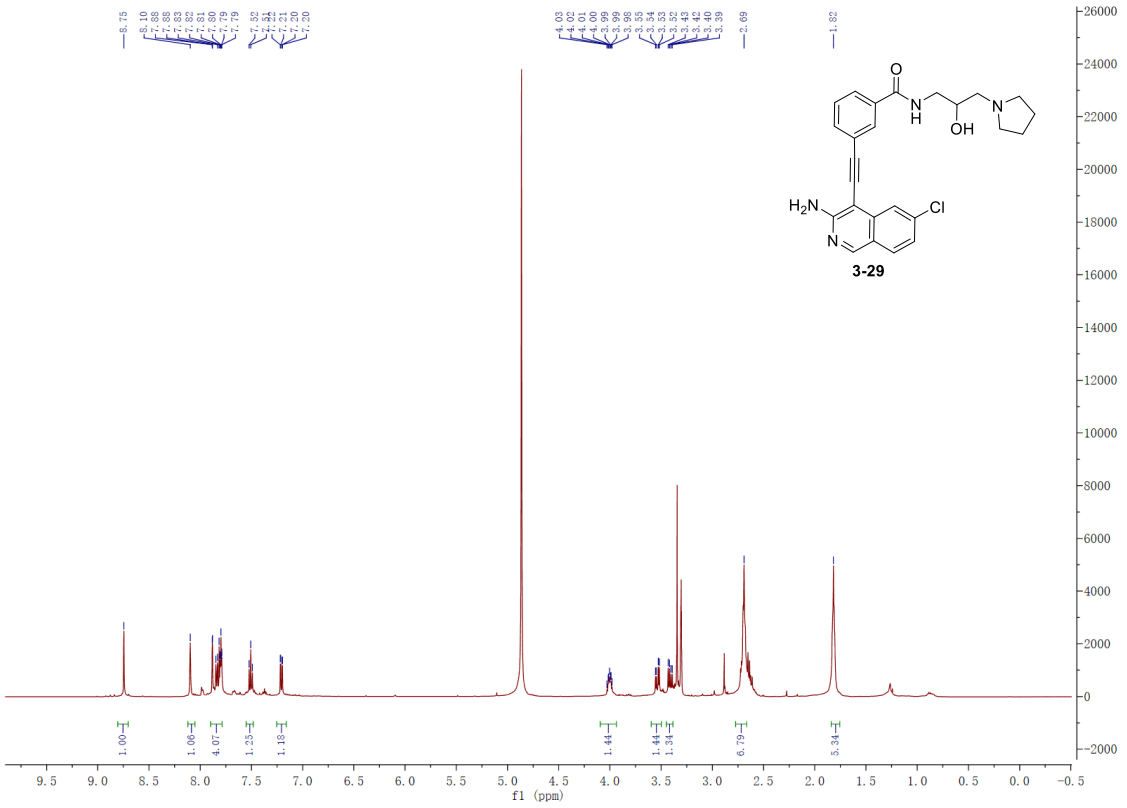
8.75
8.10
7.88
7.83
7.82
7.81
7.80
7.79
7.79
7.52
7.21
7.20
7.20
4.03
4.02
4.01
4.00
3.99
3.99
3.96
3.55
3.54
3.53
3.52
3.43
3.42
3.40
3.39
2.69
1.82
1.00
1.06
4.07
1.25
1.18
1.44
1.44
1.34
6.79
5.34
f1 (ppm)
O
N
H
OH
N
H_2N
Cl
N
3-29

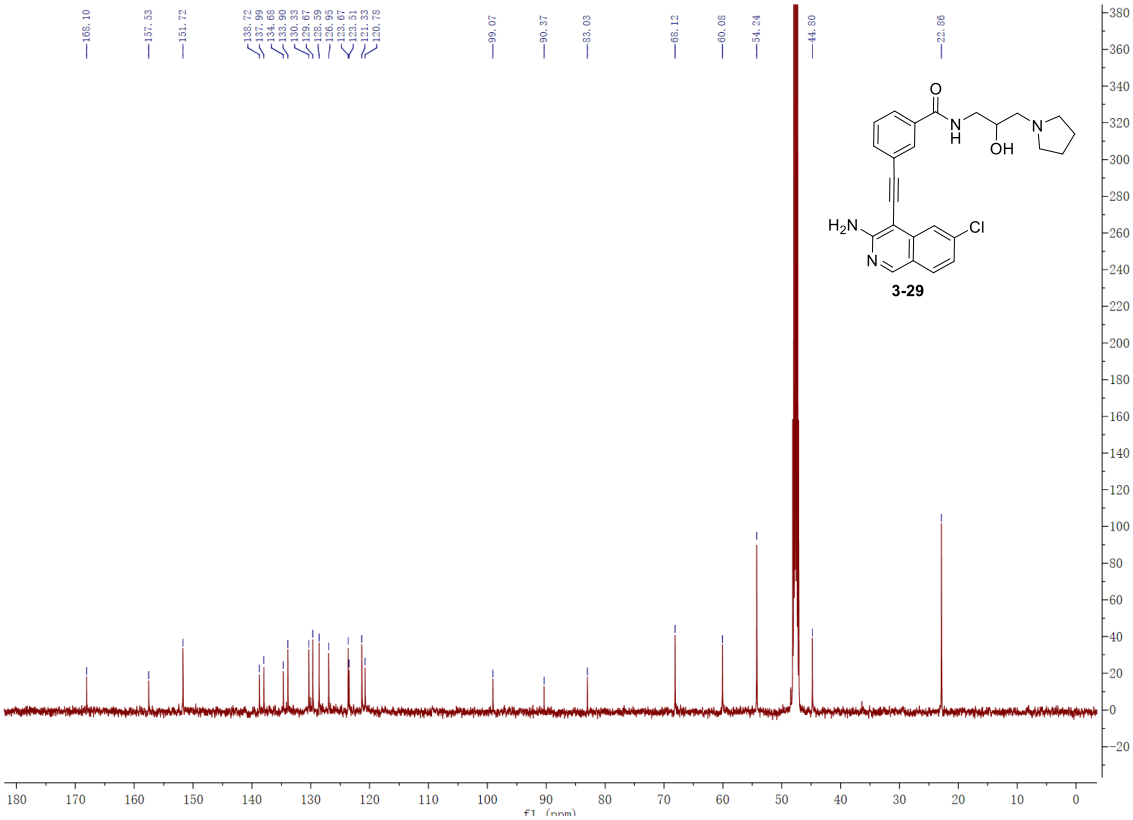
166.10
157.53
151.72
138.72
137.99
134.68
133.90
130.33
129.67
128.59
126.95
123.67
123.51
121.33
120.78
99.07
90.37
83.03
68.12
60.08
54.24
44.80
22.86
f1 (ppm)
O
N
H
OH
N
H_2N
Cl
N
3-29

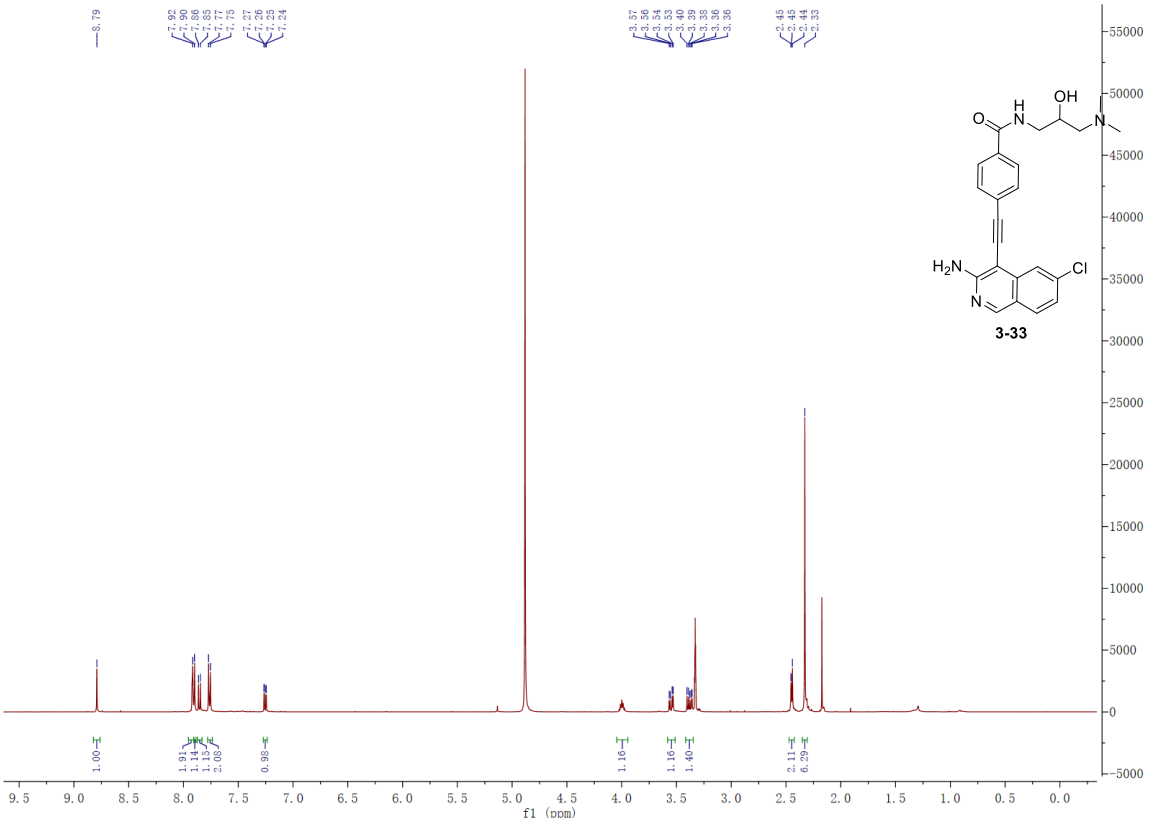
8.79
7.92
7.90
7.86
7.85
7.77
7.75
7.27
7.26
7.25
7.24
3.57
3.56
3.54
3.53
3.40
3.39
3.38
3.36
2.45
2.44
2.33
1.00
1.91
1.14
1.15
2.08
0.98
1.16
1.16
1.40
2.11
6.29
f1 (ppm)
3-33

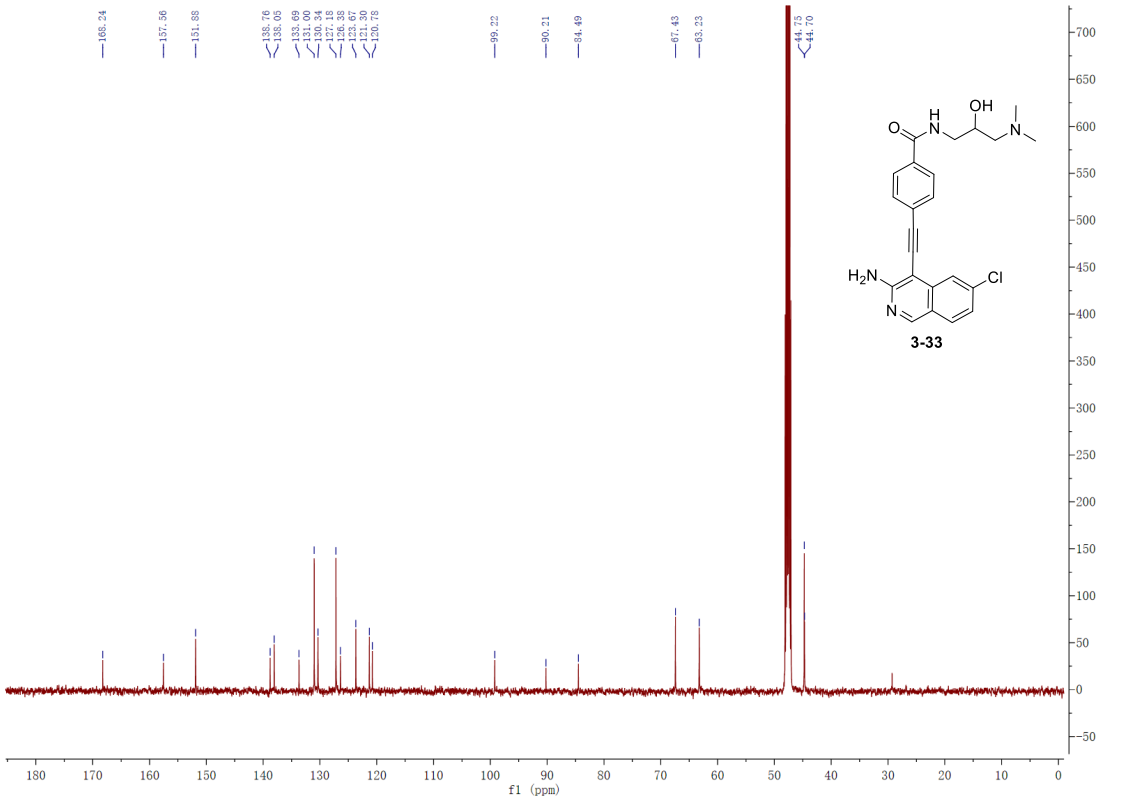
168.24
157.56
151.88
138.76
138.05
133.69
131.00
130.34
127.15
126.38
123.67
121.30
120.78
99.22
90.21
84.49
67.43
63.23
44.75
44.70
f1 (ppm)
3-33

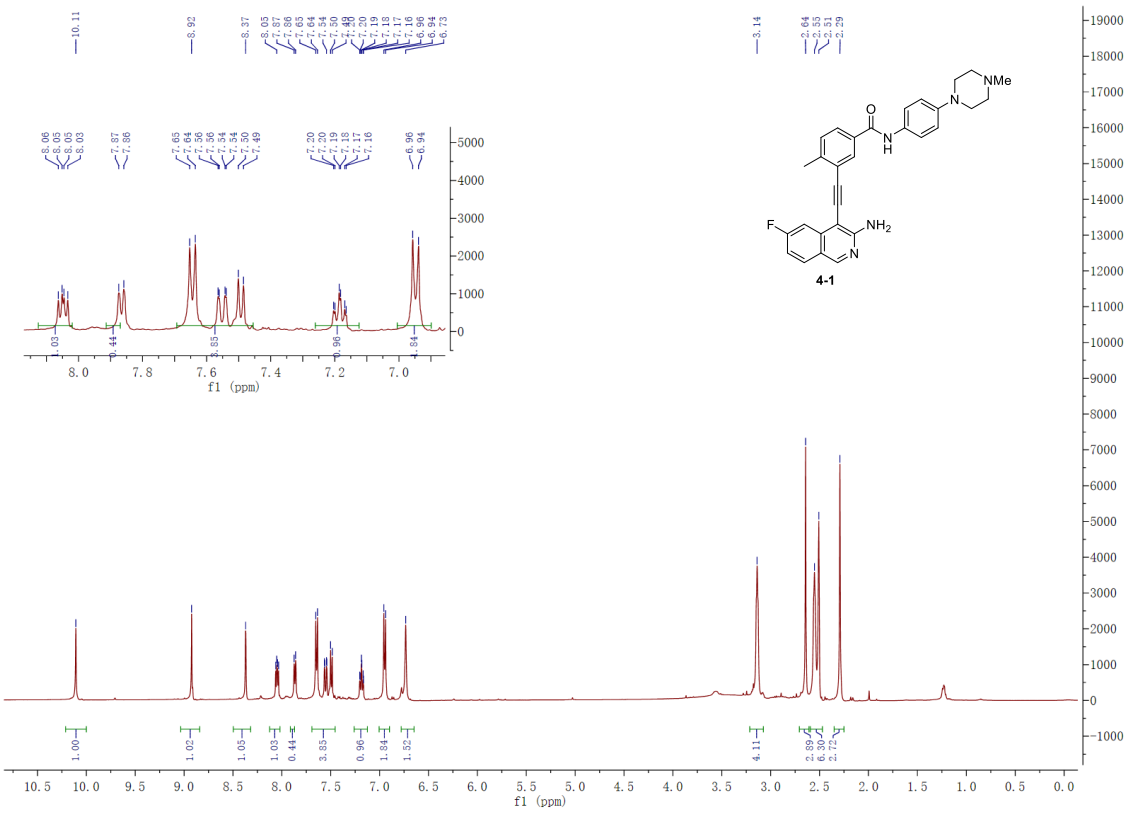
4-1

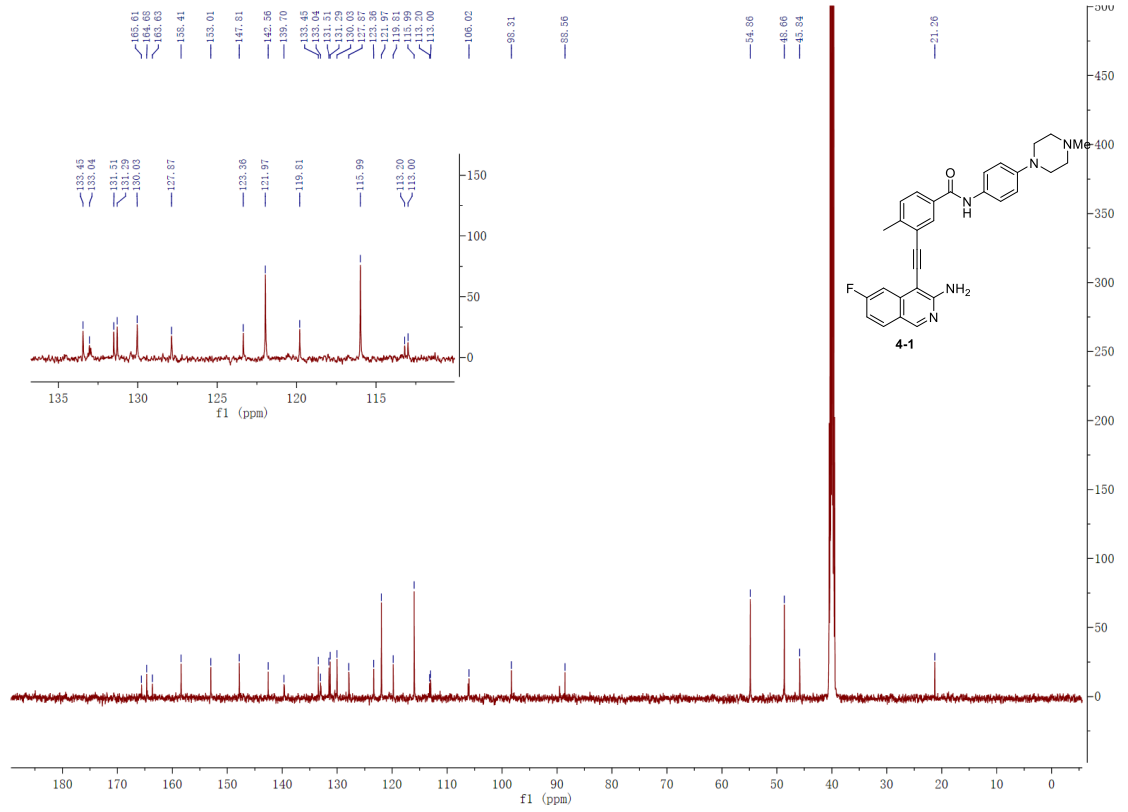
4-1

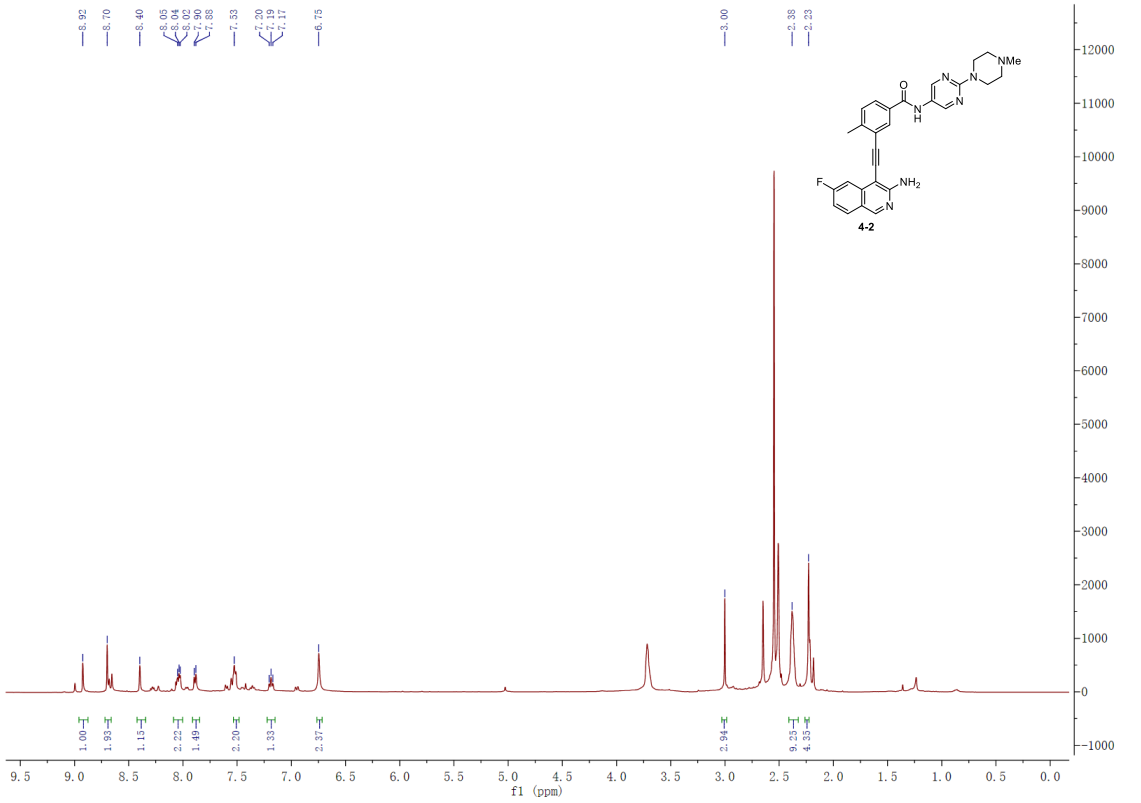
8.92
8.70
8.40
8.05
8.04
8.02
7.90
7.88
7.53
7.20
7.19
7.17
6.75
3.00
2.38
2.23
1.00
1.93
1.15
2.22
1.49
2.20
1.33
2.37
2.94
9.25
4.35
f1 (ppm)
NMe
NH2
F
4-2

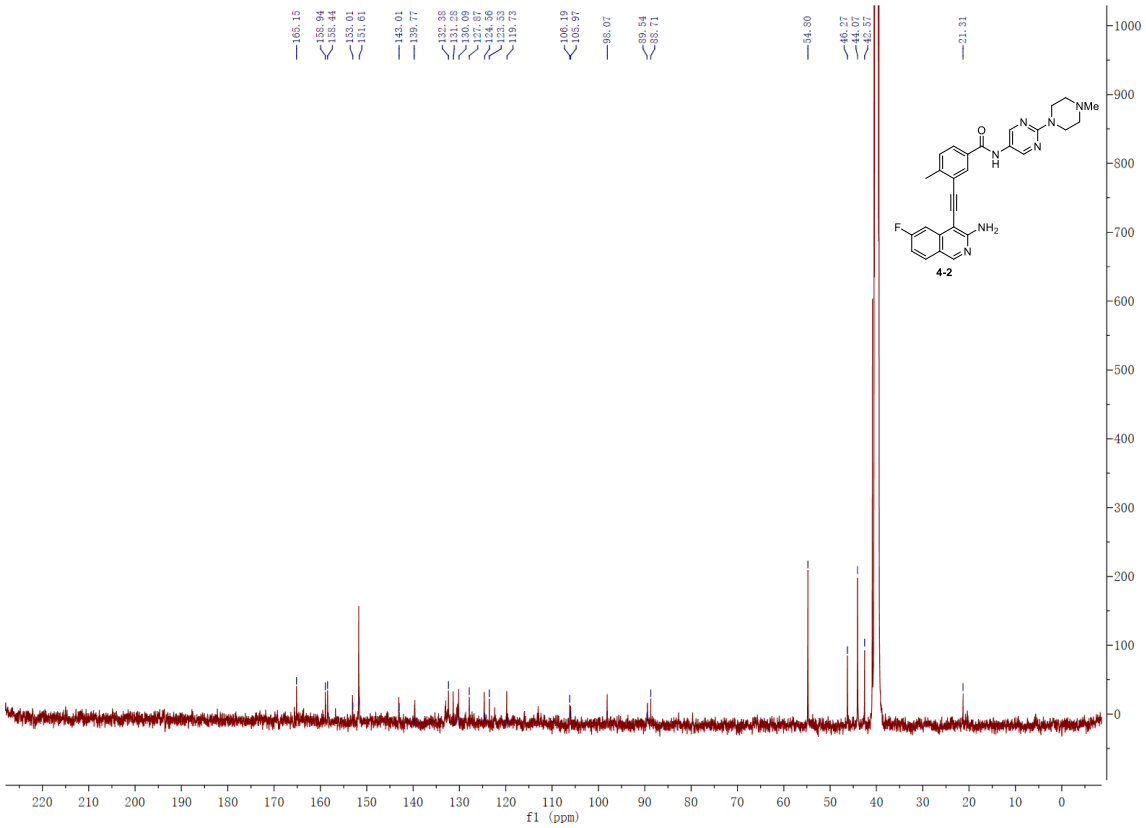
165.15
158.94
158.44
153.01
151.61
143.01
139.77
132.38
131.28
130.09
127.67
124.96
123.33
119.73
106.19
105.97
98.07
89.54
88.71
54.80
46.27
44.07
42.23
21.31
f1 (ppm)
NMe
NH2
F
4-2

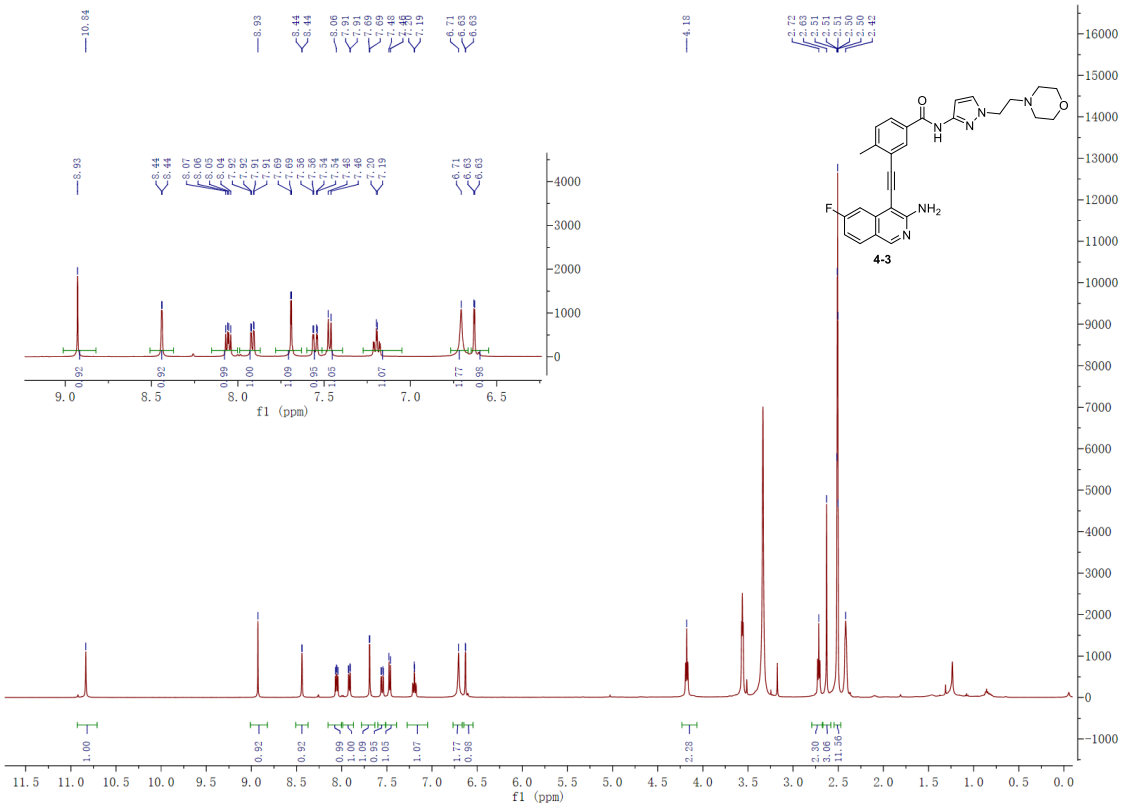
10.84
8.93
8.44
8.44
8.06
8.05
8.04
7.92
7.91
7.69
7.56
7.54
7.48
7.46
7.20
7.19
6.71
6.63
6.63
4.18
2.72
2.63
2.51
2.51
2.50
2.50
2.42
f1 (ppm)
4-3

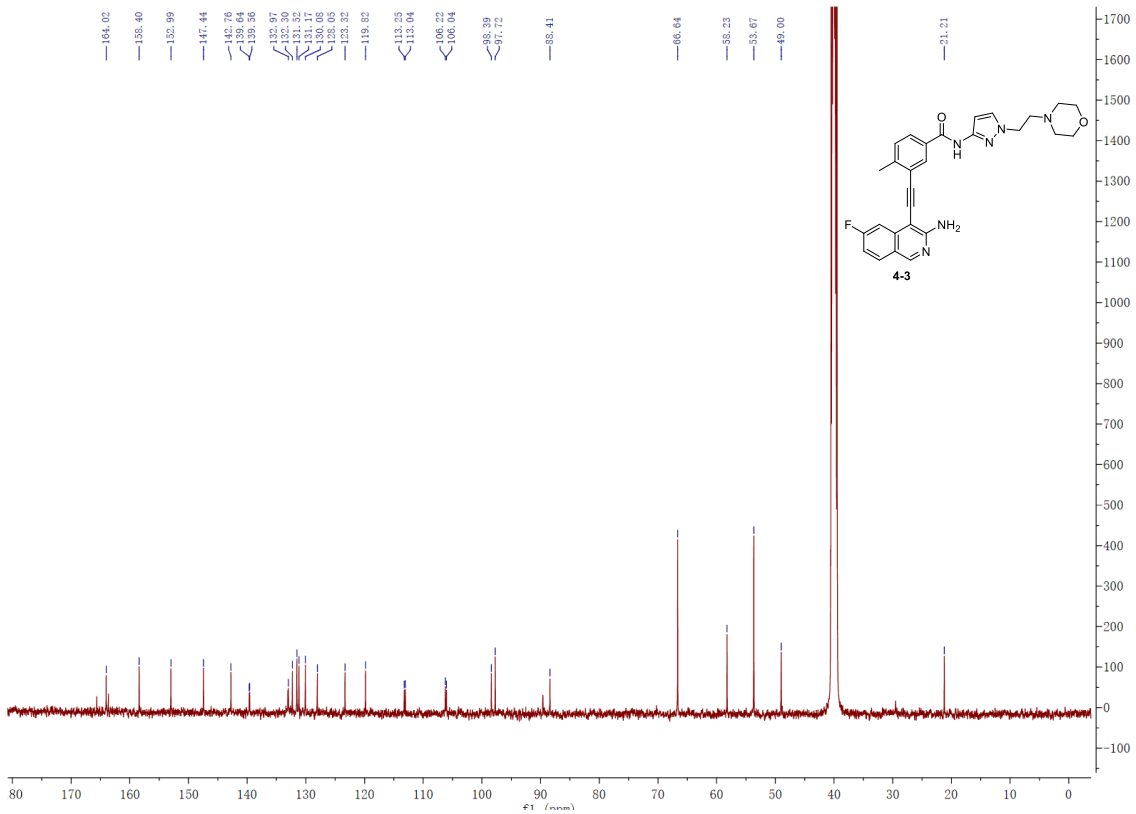
164.02
158.40
152.99
147.44
142.76
139.64
139.36
132.97
132.30
131.52
131.17
130.08
130.05
123.32
119.82
113.25
113.04
106.22
106.04
98.39
97.72
88.41
66.64
58.23
53.67
49.00
21.21
f1 (ppm)
4-3

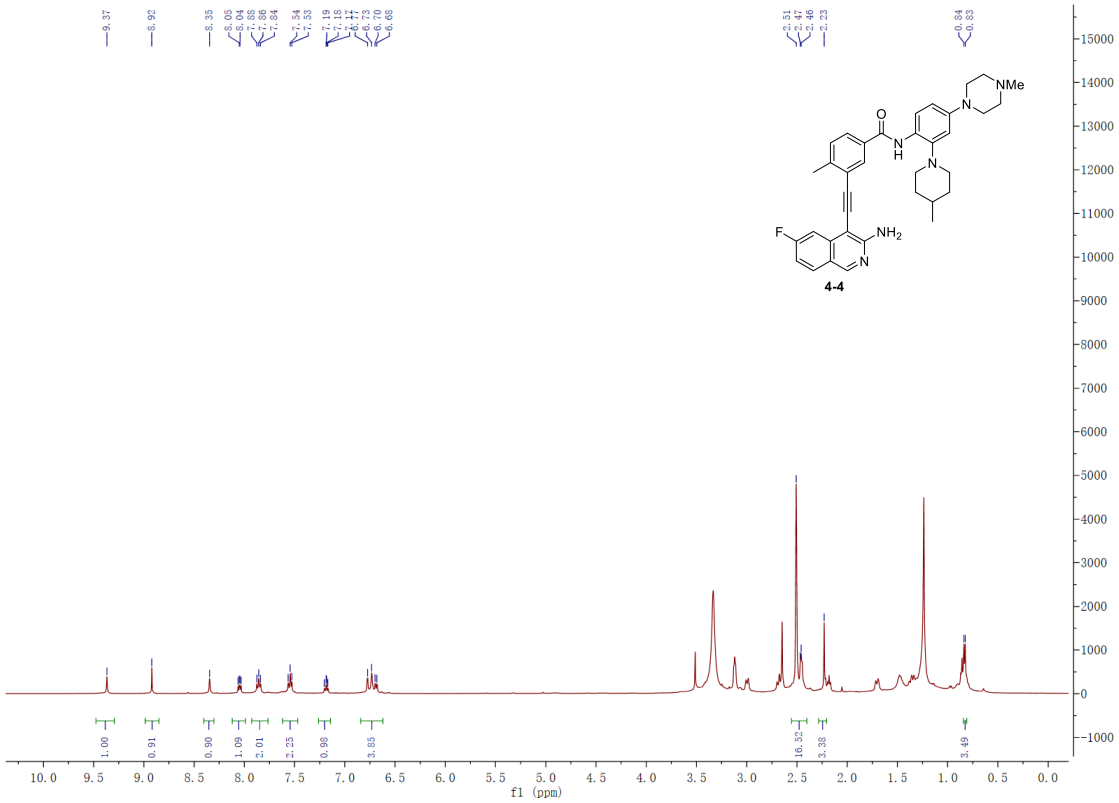
9.37
8.92
8.35
8.05
8.04
7.88
7.86
7.84
7.54
7.53
7.19
7.18
6.73
6.70
6.68
2.51
2.47
2.46
2.23
0.84
0.83
NMe
O
N
H
F
NH2
N
4-4
1.00
0.91
0.90
1.09
2.01
2.25
0.98
3.85
16.52
3.38
3.49
f1 (ppm)

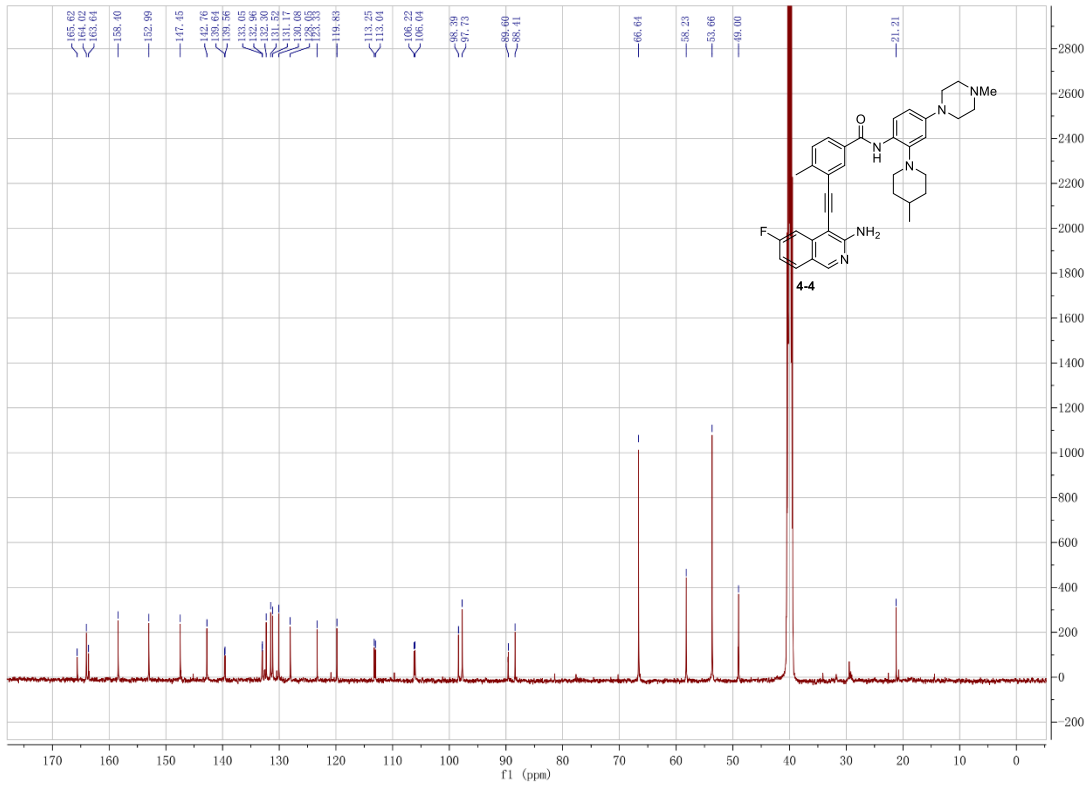
165.62
164.02
163.64
158.40
152.99
147.45
142.76
139.64
139.56
133.05
132.96
132.30
132.22
131.17
130.08
119.83
113.25
113.04
106.22
106.04
98.39
97.73
89.60
88.41
66.64
58.23
53.86
49.00
21.21
NMe
O
N
H
F
NH2
N
4-4
f1 (ppm)

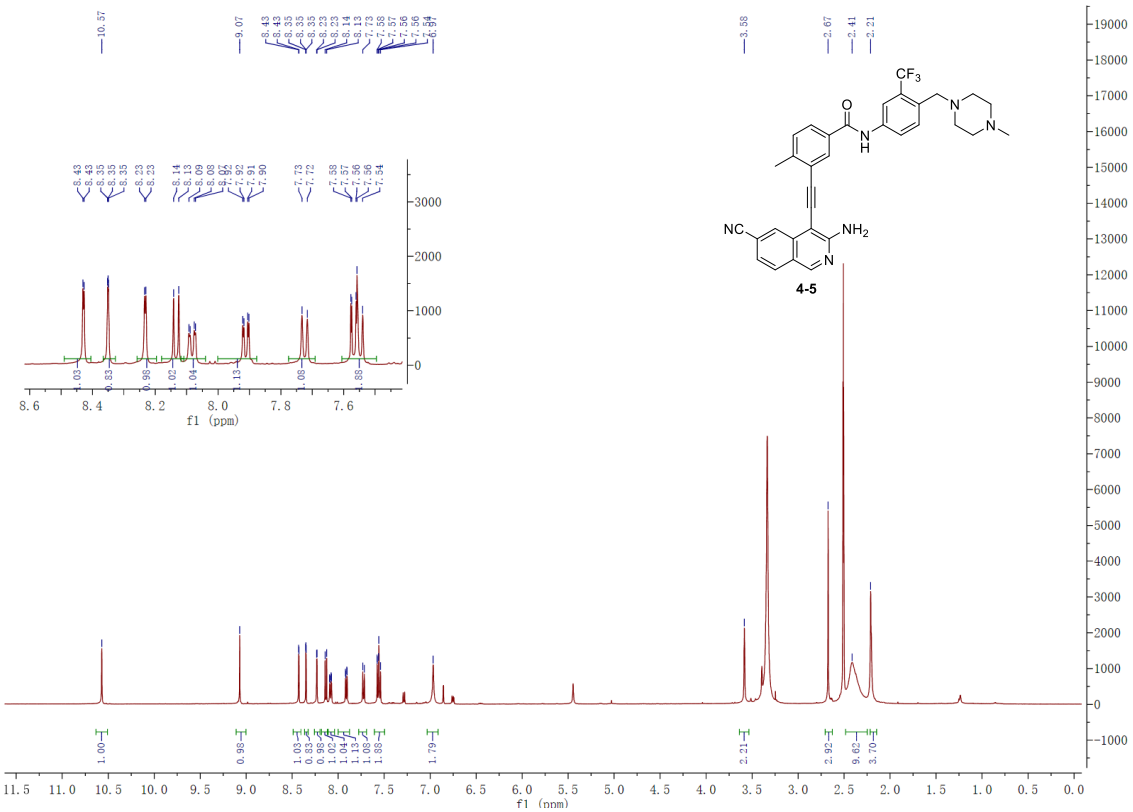
4-5
f1 (ppm)

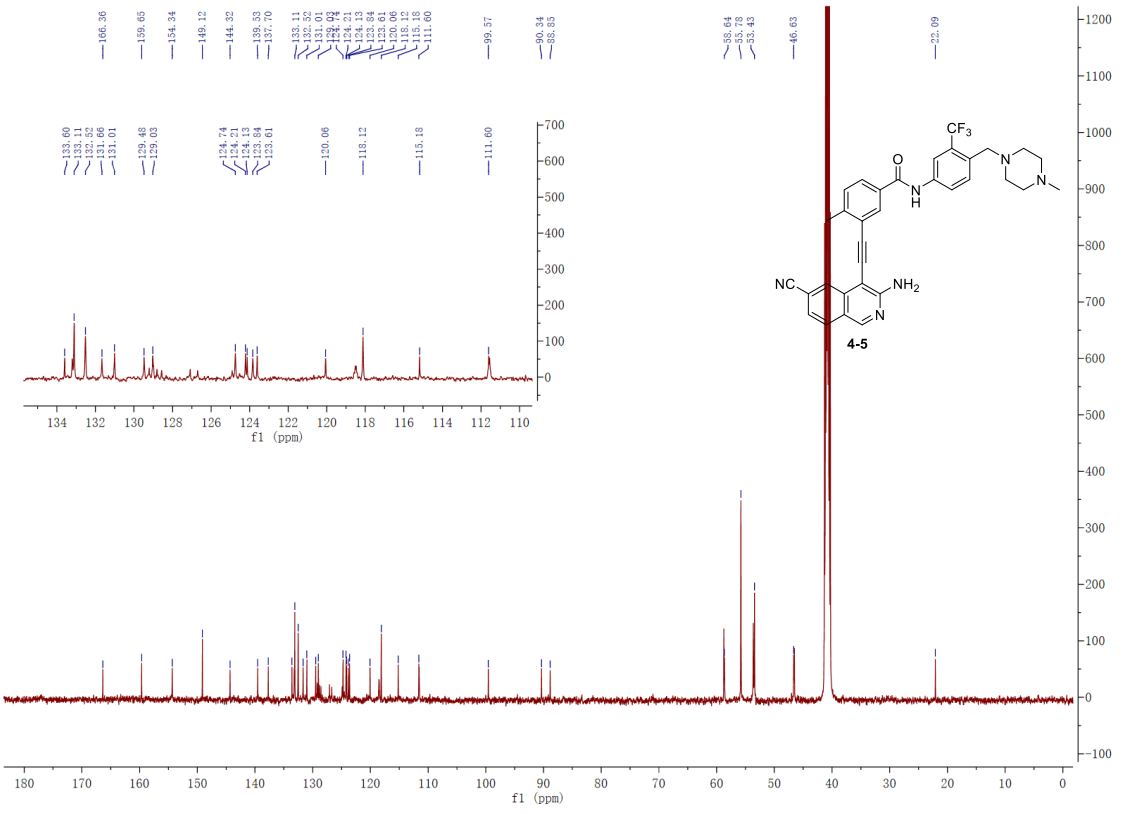
4-5
f1 (ppm)

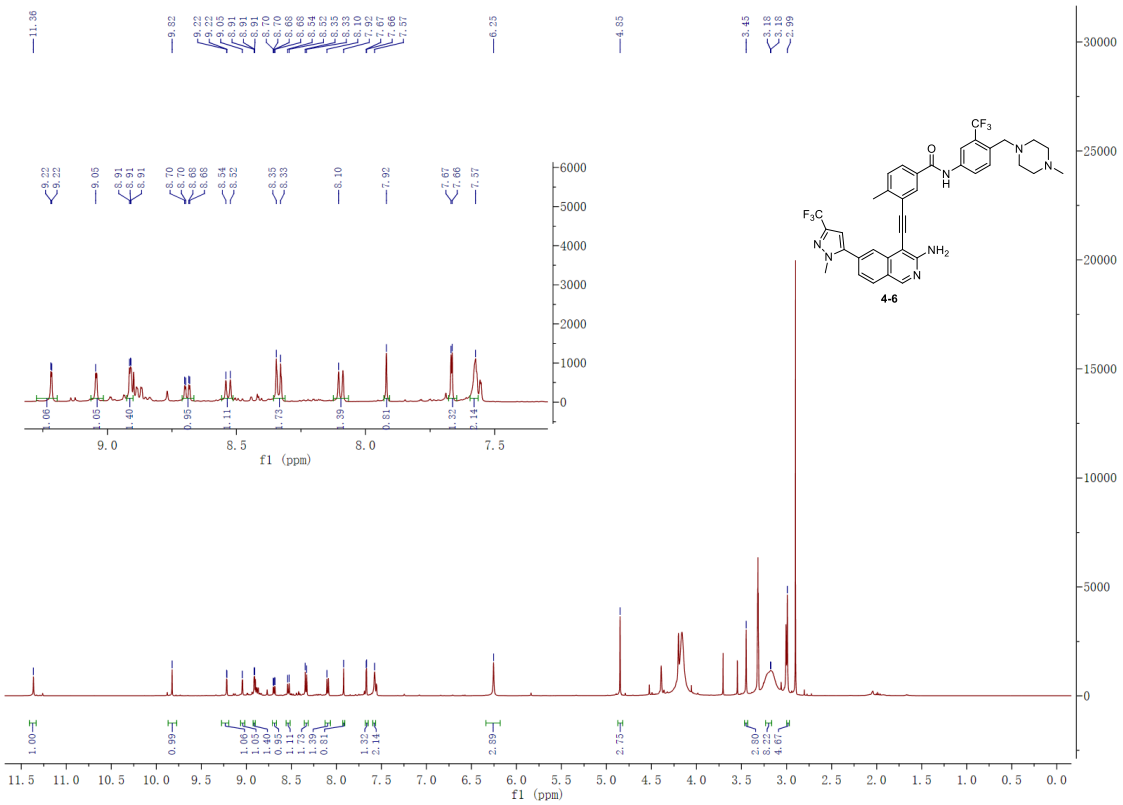
4-6
f1 (ppm)

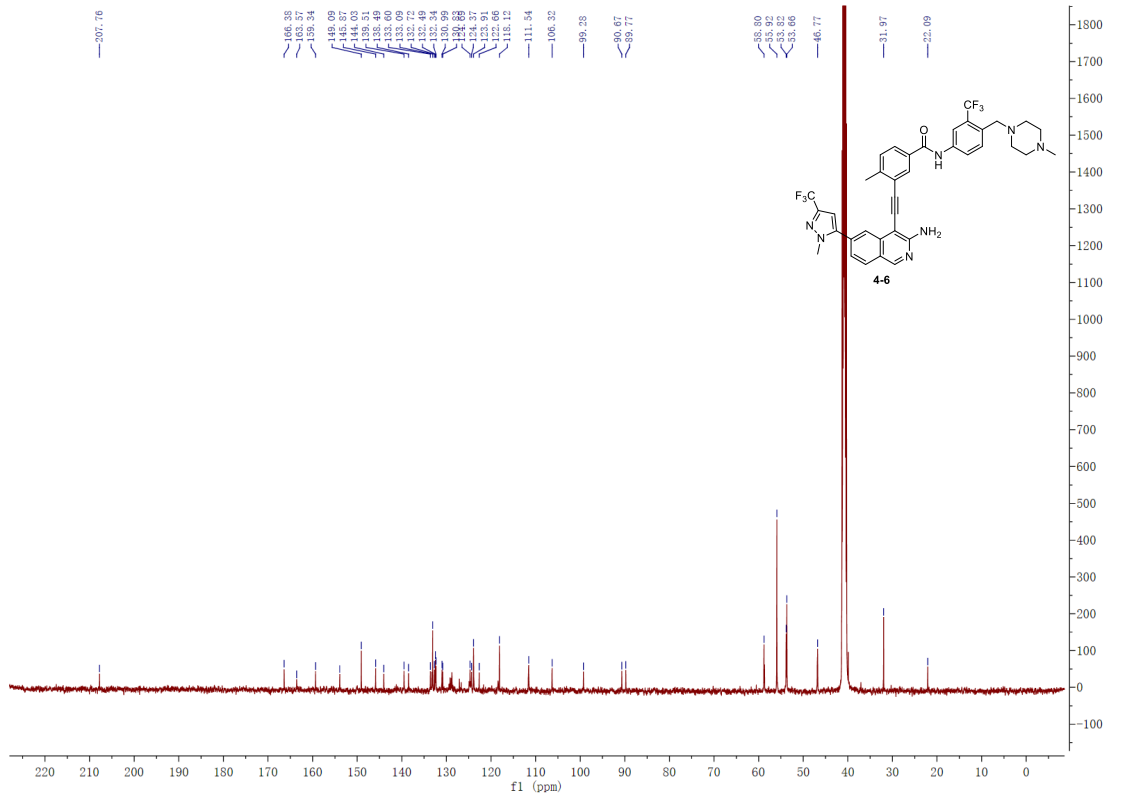
4-6
f1 (ppm)

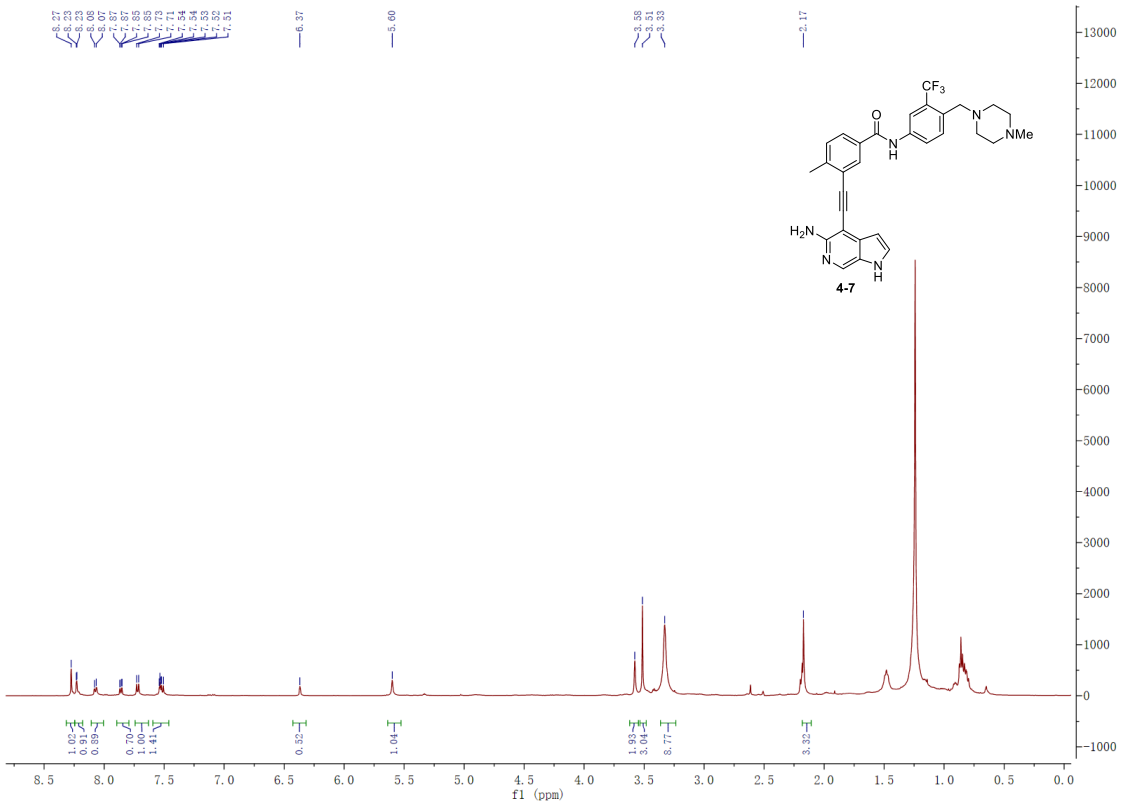
8.27
8.23
8.23
8.06
8.07
7.87
7.87
7.85
7.85
7.73
7.71
7.54
7.54
7.53
7.52
7.51
6.37
5.60
3.58
3.51
3.33
2.17
CF3
O
N
H
N
NMe
H2N
N
N
H
4-7
1.02
0.91
0.89
0.70
1.00
1.41
0.32
1.04
1.93
3.04
8.77
3.32
f1 (ppm)

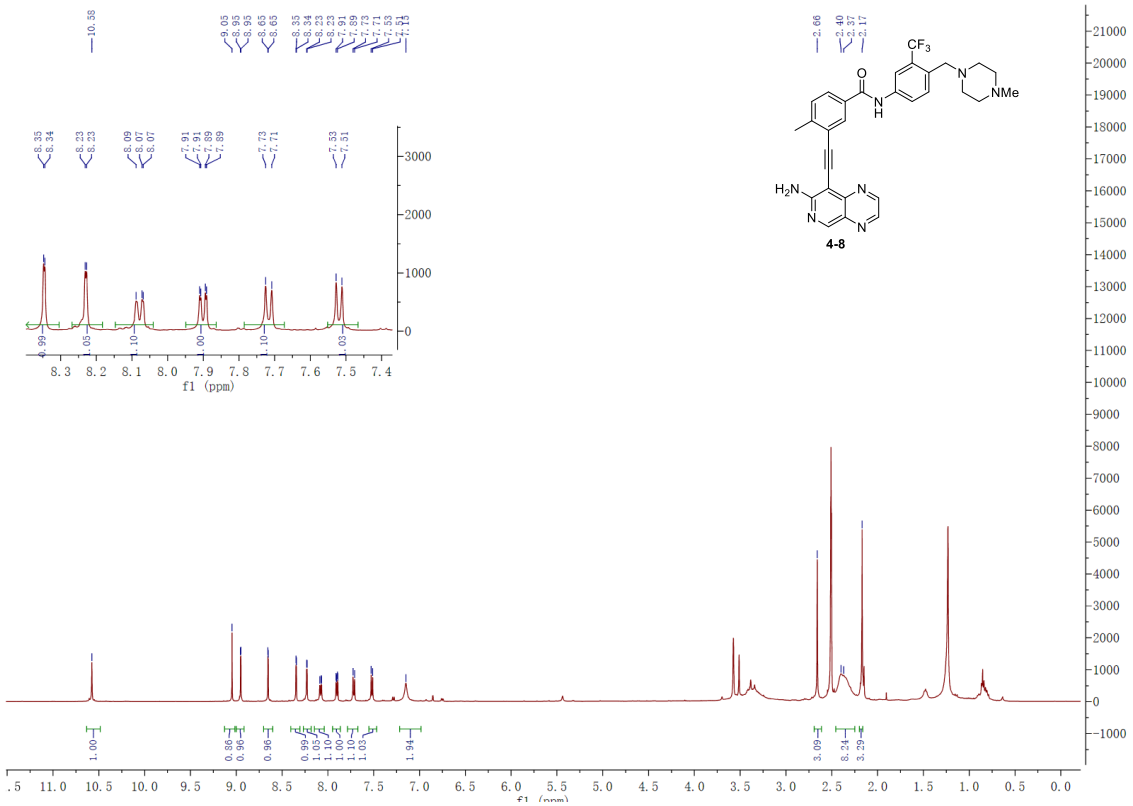
4-8

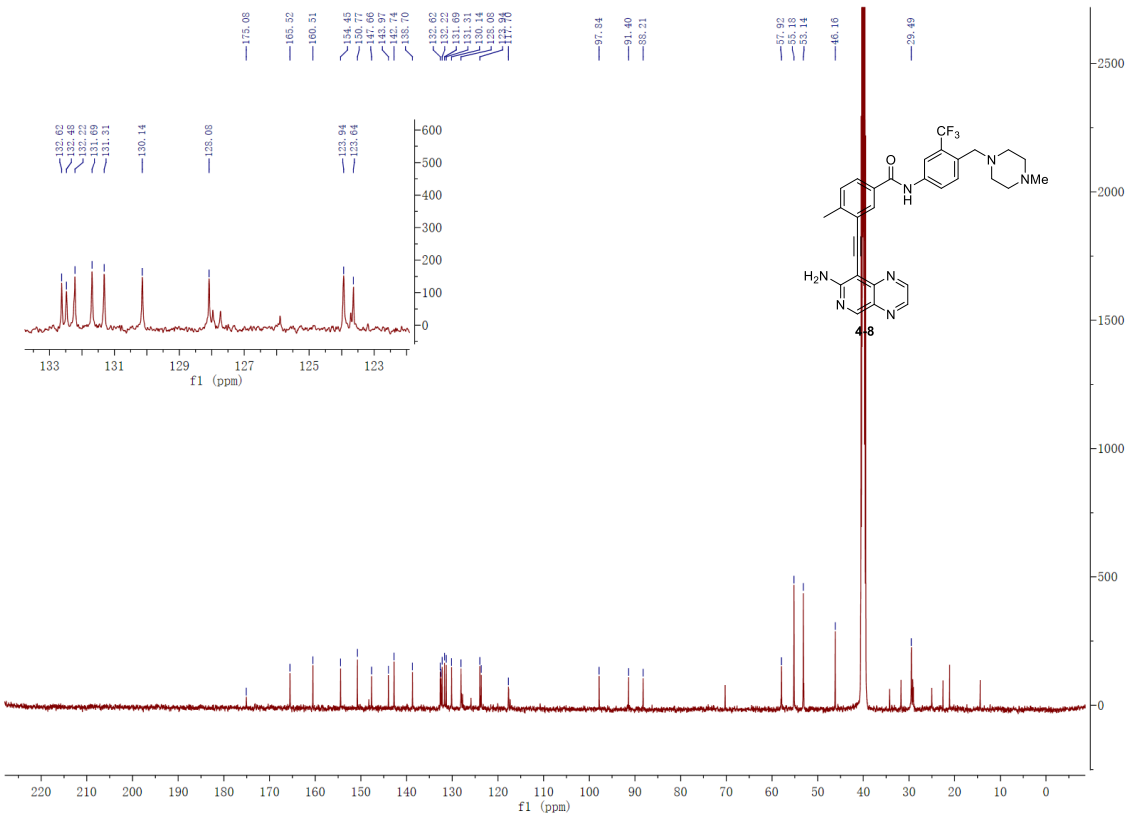
4-8

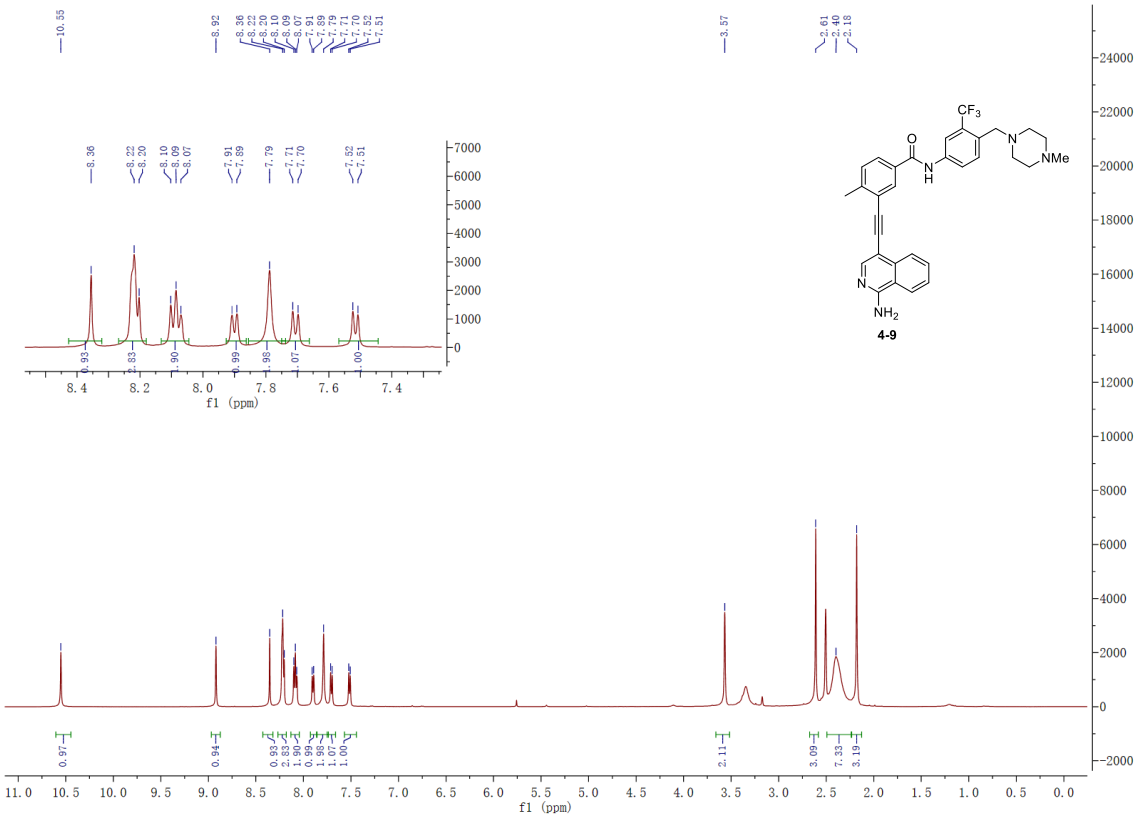
4-9
f1 (ppm)

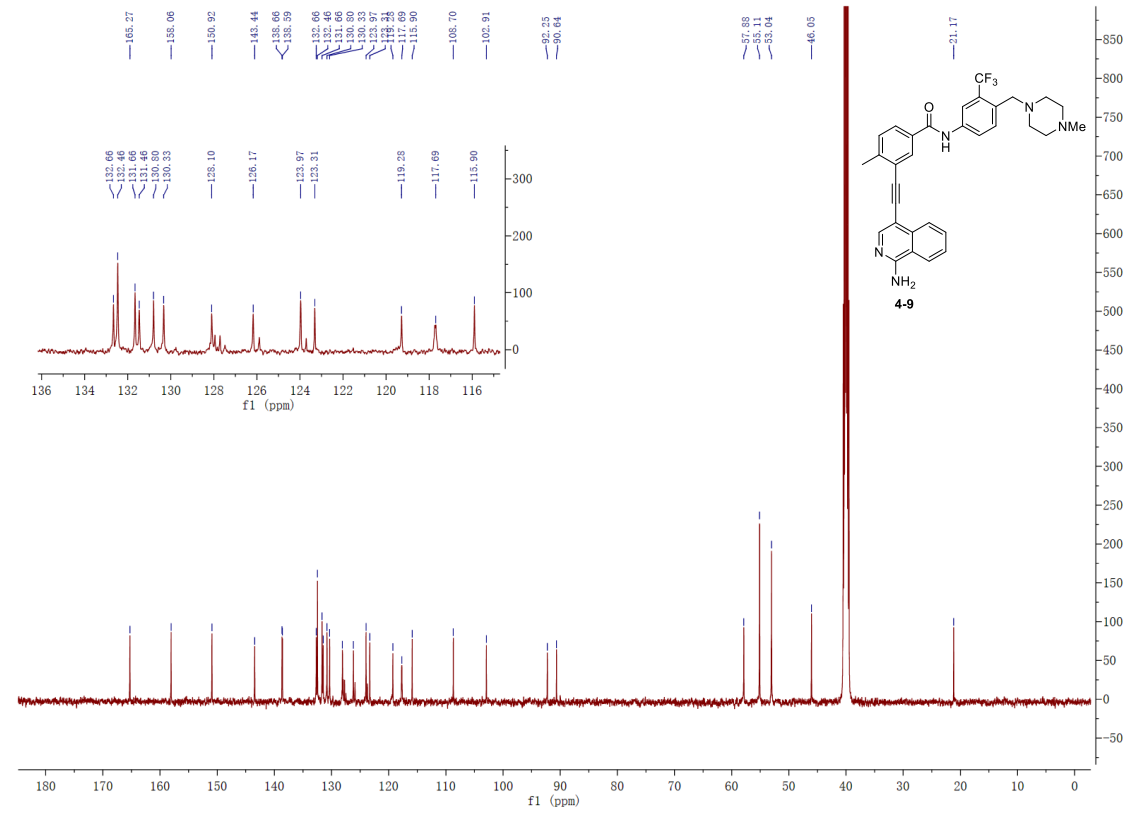
4-9
f1 (ppm)

References

1. Papavramidou, N., T. Papavramidis, and T. Demetriou, Ancient Greek and Greco–Roman methods in modern surgical treatment of cancer. *Ann Surg Oncol*, **2010**, 17 (3), 665-667.
2. Santoro, E., The history of gastric cancer: legends and chronicles. *Gastric Cancer*, **2005**, 8 (2), 71-74.
3. Rahib, L., Smith, B.D., Aizenberg, R., Rosenzweig, A.B., Fleshman, J.M. and Matrisian, L.M., Projecting cancer incidence and deaths to 2030: the unexpected burden of thyroid, liver, and pancreas cancers in the United States, *Cancer Res*, **2014**, 74 (11), 2913-2921.
4. Siegel, R.L., K.D. Miller, and A. Jemal, Cancer statistics*, CA: Cancer J Clin*, **2016**, 66 (1), 7-30.
5. Burstein, H.J., Krilov, L., Aragon-Ching, J.B., Baxter, N.N., Chiorean, E.G., Chow, W.A., De Groot, J.F., Devine, S.M., DuBois, S.G., El-Deiry, W.S. and Epstein, A.S., Clinical Cancer Advances 2017: Annual Report on Progress Against Cancer From the American Society of Clinical Oncology, *J Clin Oncol*, **2017**, 35(12), 1341-1367.
6. Marshall, E., Cancer research and the $90 billion metaphor, *American Association for the Advancement of Science*, **2011**.
7. Wang, X., Cancer Moonshot 2020: a new march of clinical and translational medicine, *Clin Transl Med*, **2016**, 5 (1) 11.
8. Weinberg, R., The biology of cancer, *Garland science*, **2013**.
9. Siegel, R.L., K.D. Miller, and A. Jemal, Cancer statistics*,* 2017*, CA: Cancer J Clin*, **2017**, 67 (1), 7-30.
10. Kapur, B., The fruits of long endeavors–200 years of oncology, *Med J Armed Forces India*, **2014**. 70 (2), 95.
11. Kampen, K.R., The discovery and early understanding of leukemia, *Leuk Res*, **2012**, 36 (1), 6-13.
12. Freireich, E.J., P.H. Wiernik, and D.P. Steensma, The leukemias: a half-century of discovery, *J Clin Oncol*, **2014**, 32 (31), 3463-3469.
13. Mehranfar, S., Zeinali, S., Hosseini, R., Mohammadian, M., Akbarzadeh, A. and Feizi, A.H.P., History of Leukemia: Diagnosis and Treatment from Beginning to Now, *Galen Medical Journal*, **2017**, 6 (1), 12-22.
14. Walter, E. and M. Scott, The life and work of Rudolf Virchow 1821–1902:"Cell theory, thrombosis and the sausage duel", *J Intensive Care Soc*, **2017**, *18* (3), 234-235.
15. Lagunas-Rangel, F.A., Chávez-Valencia, V., Gómez-Guijosa, M.Á. and Cortes-Penagos, C., Acute Myeloid Leukemia—Genetic Alterations and Their Clinical Prognosis, *Int J Hematol Oncol Stem Cell Res*, **2017**, 11 (4), 328.
16. Wolpe, S.D. and L. Koh, Hematopoietic Stem Cells*,* Stem Cells in Regenerative Medicine: Science, regulation and business strategies, **2015**, 397-414.
17. Doulatov, S., Notta, F., Laurenti, E. and Dick, J.E., Hematopoiesis: a human perspective, *Cell stem cell*, **2012**, 10 (2), 120-136.

18. Estey, E. and H. Döhner, Acute myeloid leukaemia, *Lancet*, **2006**, 368 (9550), 1894-1907.
19. Wakeford, R., Childhood leukaemia following medical diagnostic exposure to ionizing radiation in utero or after birth, *Radiat Prot Dosim*, **2008**, 132 (2), 166-174.
20. Sigurdson, A.J. and E. Ron, Cosmic radiation exposure and cancer risk among flight crew, *Cancer Investig*, **2004**, 22 (5), 743-761.
21. Khalade, A., Jaakkola, M.S., Pukkala, E. and Jaakkola, J.J., Exposure to benzene at work and the risk of leukemia: a systematic review and meta-analysis, *Environ Health*, **2010**, 9 (1), 31.
22. Musselman, J.R., Blair, C.K., Cerhan, J.R., Nguyen, P., Hirsch, B. and Ross, J.A., Risk of adult acute and chronic myeloid leukemia with cigarette smoking and cessation, *Cancer Epidemiol*, **2013**, 37 (4), 410-416.
23. Dabaja, B.S., Faderl, S., Thomas, D., Cortes, J., O'Brien, S., Nasr, F., Pierce, S., Hayes, K., Glassman, A., Keating, M. and Kantarjian, H.M., Deletions and losses in chromosomes 5 or 7 in adult acute lymphocytic leukemia: incidence, associations and implications, *Leukemia*, **1999**, 3 (6), 869-872.
24. Pendleton, M., Lindsey, R.H., Felix, C.A., Grimwade, D. and Osheroff, N., Topoisomerase II and leukemia, *Ann N Y Acad Sci*, **2014**, 1310 (1), 98-110.
25. Inaba, H., M. Greaves, and C.G. Mullighan, Acute lymphoblastic leukaemia, *Lancet*, **2013**, 381 (9881),1943-1955.
26. Kipps, T.J., Stevenson, F.K., Wu, C.J., Croce, C.M., Packham, G., Wierda, W.G., O'brien, S., Gribben, J. and Rai, K., Chronic lymphocytic leukaemia, *Nat Rev Dis Primers*, **2017**, 3, 16096.
27. Döhner, H., D.J. Weisdorf, and C.D. Bloomfield, Acute myeloid leukemia, *N Engl J Med*, **2015**, 373 (12),1136-1152.
28. O'Brien, S., Radich, J.P., Abboud, C.N., Akhtari, M., Altman, J.K., Berman, E., Curtin, P., DeAngelo, D.J., Deininger, M., Devine, S. and Fathi, A.T., Chronic myelogenous leukemia, version 1.2015, *J Natl Compr Cancer Netw*, **2014**, 12 (11), 1590-1610.
29. Sud, A. and C. Dearden, T-cell Prolymphocytic Leukemia, *Hematol Oncol Clin*, **2017**, 31 (2), 273-283.
30. Matutes, E., Large granular lymphocytic leukemia. Current diagnostic and therapeutic approaches and novel treatment options, *Expert Rev Hematol*, **2017**, 10 (3), 251-258.
31. Kataoka, K., Nagata, Y., Kitanaka, A., Shiraishi, Y., Shimamura, T., Yasunaga, J.I., Totoki, Y., Chiba, K., Sato-Otsubo, A., Nagae, G. and Ishii, R.,Integrated molecular analysis of adult T cell leukemia/lymphoma, *Nat Genet*, **2015**, 47 (11), 1304.
32. Watts, J.M. and M.S. Tallman, Hairy cell leukemia, Cancer Consult: Expertise for Clinical Practice, **2014**, 220-225.
33. Gotlib, J., World Health Organization-defined eosinophilic disorders: 2014 update on diagnosis, risk stratification, and management, *Am J Hematol*, **2014**, 89 (3), 325-337.
34. Sachdeva, M.U., Ahluwalia, J., Das, R., Varma, N. and Garewal, G., Role of FAB classification of acute leukemias in era of immunophenotyping, *Indian J Pathol Microbiol*, **2006**, 49 (4), 524-527.

35. Bain, B., Bone marrow aspiration, *J Clin Pathol*, **2001**, 54 (9), 657-663.
36. Arber, D.A., Orazi, A., Hasserjian, R., Thiele, J., Borowitz, M.J., Le Beau, M.M., Bloomfield, C.D., Cazzola, M. and Vardiman, J.W., The 2016 revision to the World Health Organization (WHO) classification of myeloid neoplasms and acute leukemia, *Blood*, **2016**, 127 (20), 2391-2405.
37. Falini, B., Martelli, M.P., Bolli, N., Bonasso, R., Ghia, E., Pallotta, M.T., Diverio, D., Nicoletti, I., Pacini, R., Tabarrini, A. and Galletti, B.V., Immunohistochemistry predicts nucleophosmin (NPM) mutations in acute myeloid leukemia, *Blood*, **2006**, 108 (6), 1999-2005.
38. Cohen, P., The origins of protein phosphorylation, *Nat Cell Biol*, **2002**, 4 (5), 127-130.
39. Manning, G., Whyte, D.B., Martinez, R., Hunter, T. and Sudarsanam, S., The protein kinase complement of the human genome, *Science*, **2002**, 298 (5600),1912-1934.
40. Hubbard, S.R. and J.H. Till, Protein tyrosine kinase structure and function, *Annu Rev Biochem*, **2000**, 69 (1), 373-398.
41. McClendon, C.L., Kornev, A.P., Gilson, M.K. and Taylor, S.S., Dynamic architecture of a protein kinase, *Proc Natl Acad Sci*, **2014**, 111 (43), 4623-4631.
42. Peng, Y.H., Shiao, H.Y., Tu, C.H., Liu, P.M., Hsu, J.T.A., Amancha, P.K., Wu, J.S., Coumar, M.S., Chen, C.H., Wang, S.Y. and Lin, W.H., Protein kinase inhibitor design by targeting the Asp-Phe-Gly (DFG) motif: the role of the DFG motif in the design of epidermal growth factor receptor inhibitors, *J Med Chem*, **2013**, 56 (10), 3889-3903.
43. Treiber, D.K. and N.P. Shah, Ins and outs of kinase DFG motifs, *Chemistry & biology*, **2013**, 20 (6), 745-746.
44. Brautigan, D.L., Protein phosphatases. in Recent Progress in Hormone Research-Volume 49, *Proceedings of the 1992 Laurentian Hormone Conference*, **2013**, Academic Press.
45. Rosnet, O., Marchetto, S. and Birnbaum, D., Murine Flt3, a gene encoding a novel tyrosine kinase receptor of the PDGFR/CSF1R family, *Oncogene*, **1991**, 6 (9), 1641-1650.
46. De Vries, C., Escobedo, J.A., Ueno, H., Houck, K., Ferrara, N. and Williams, L.T., The fms-like tyrosine kinase, a receptor for vascular endothelial growth factor, *Science*, **1992**, 989-991.
47. Rappold, I., Ziegler, B.L., Köhler, I., Marchetto, S., Rosnet, O., Birnbaum, D., Simmons, P.J., Zannettino, A.C., Hill, B., Neu, S. and Knapp, W., Functional and phenotypic characterization of cord blood and bone marrow subsets expressing FLT3 (CD135) receptor tyrosine kinase, *Blood*, **1997**, 90 (1), 111-125.
48. Choudhary, C., Müller-Tidow, C., Berdel, W.E. and Serve, H., Signal transduction of oncogenic Flt3, *Int J Hematol*, **2005**, 82 (2), 93-99.
49. Deeb, K.K., Smonskey, M.T., DeFedericis, H., Deeb, G., Sait, S.N., Wetzler, M., Wang, E.S. and Starostik, P., Deletion and deletion/insertion mutations in the juxtamembrane domain of the FLT3 gene in adult acute myeloid leukemia, *Leukemia research reports*, **2014**, 3(2), 86-89.

50. Meshinchi, S. and D.L. Stirewalt, FMS-related tyrosine kinase 3, in Molecular Oncology: Causes of Cancer and Targets for Treatment, **2015**, Cambridge University Press.
51. Behera, P.M. and A. Dixit, The Story of Kinase Inhibitors Development with Special Reference to Allosteric Site, in Drug Design: Principles and Applications, **2017**, Springer, 57-68.
52. DeZern, A.E., Sung, A., Kim, S., Smith, B.D., Karp, J.E., Gore, S.D., Jones, R.J., Fuchs, E., Luznik, L., McDevitt, M. and Levis, M., Role of allogeneic transplantation for FLT3/ITD acute myeloid leukemia: outcomes from 133 consecutive newly diagnosed patients from a single institution, *Biol Blood Marrow Transplant*, **2011**, 17 (9), 1404-1409.
53. Stirewalt, D.L., Kopecky, K.J., Meshinchi, S., Engel, J.H., Pogosova-Agadjanyan, E.L., Linsley, J., Slovak, M.L., Willman, C.L. and Radich, J.P.,Size of FLT3 internal tandem duplication has prognostic significance in patients with acute myeloid leukemia, *Blood*, **2006**, 107 (9), 3724-3726.
54. Grimwade, D. and R.K. Hills, Independent prognostic factors for AML outcome, ASH Education Program Book, **2009** (1), 385-395.
55. Choudhary, C., Schwäble, J., Brandts, C., Tickenbrock, L., Sargin, B., Kindler, T., Fischer, T., Berdel, W.E., Müller-Tidow, C. and Serve, H., AML-associated Flt3 kinase domain mutations show signal transduction differences compared with Flt3 ITD mutations, *Blood*, **2005**, 106 (1), 265-273.
56. Hayakawa, F., Towatari, M., Kiyoi, H., Tanimoto, M., Kitamura, T., Saito, H. and Naoe, T.,Tandem-duplicated Flt3 constitutively activates STAT5 and MAP kinase and introduces autonomous cell growth in IL-3-dependent cell lines, *Oncogene*, **2000**, 19 (5), 624.
57. Choudhary, C., Brandts, C., Schwable, J., Tickenbrock, L., Sargin, B., Ueker, A., Böhmer, F.D., Berdel, W.E., Müller-Tidow, C. and Serve, H., Activation mechanisms of STAT5 by oncogenic Flt3-ITD, *Blood*, **2007**, 110 (1), 370-374.
58. Kolch, W., Coordinating ERK/MAPK signalling through scaffolds and inhibitors, *Nat Rev Mol Cell Biol*, **2005**, 6 (11), 827.
59. Huang, T., Karsy, M., Zhuge, J., Zhong, M. and Liu, D., B-Raf and the inhibitors: from bench to bedside, *J Hematol Oncol*, **2013**, 6 (1), 30.
60. Fritsche-Guenther, R., Witzel, F., Kempa, S., Brummer, T., Sers, C. and Blüthgen, N., Effects of RAF inhibitors on PI3K/AKT signalling depend on mutational status of the RAS/RAF signalling axis, *Oncotarget*, **2016**, 7 (7), 7960.
61. Larkin, J., Ascierto, P.A., Dréno, B., Atkinson, V., Liszkay, G., Maio, M., Mandalà, M., Demidov, L., Stroyakovskiy, D., Thomas, L. and De La Cruz-Merino, L., Combined vemurafenib and cobimetinib in BRAF-mutated melanoma, *N Engl J Med*, **2014**, 371 (20), 1867-1876.
62. Menzies, A.M. and G.V. Long, Dabrafenib and trametinib, alone and in combination for BRAF-mutant metastatic melanoma, *Clin Cancer Res*, **2014**, 20 (8), 2035-2043.
63. Antony, R., Emery, C.M., Sawyer, A.M. and Garraway, L.A.,C-RAF mutations confer resistance to RAF inhibitors, *Cancer research*, **2013**, 73 (15), 4840-4851.

64. Ruvinsky, I. and O. Meyuhas, Ribosomal protein S6 phosphorylation: from protein synthesis to cell size, *Trends Biochem Sci*, **2006**, 31 (6), 342-348.
65. Chakraborty, A.A., Scuoppo, C., Dey, S., Thomas, L.R., Lorey, S.L., Lowe, S.W. and Tansey, W.P., A common functional consequence of tumor-derived mutations within c-MYC, *Oncogene*, **2015**, 34 (18), 2406.
66. Arabi, A., R. Berkson, and A.P. Wright, Regulation of the nucleolar structure by the oncoprotein c-Myc and proteasomes, **2017**.
67. LoPiccolo, J., Blumenthal, G.M., Bernstein, W.B. and Dennis, P.A., Targeting the PI3K/Akt/mTOR pathway: effective combinations and clinical considerations, *Drug Resist Update*, **2008**, 11 (1), 32-50.
68. Cantley, L.C., The phosphoinositide 3-kinase pathway, *Science*, **2002**, 296 (5573), 1655-1657.
69. Lemmon, M. and K. Ferguson, Pleckstrin homology domains, in Protein modules in signal transduction, **1998**, Springer, 39-74.
70. COFFER, P.J., J. Jing, and J.R. WOODGETT, Protein kinase B (c-Akt): a multifunctional mediator of phosphatidylinositol 3-kinase activation, *Biochem J,* **1998**, 335 (1), 1-13.
71. Osaki, M., M.a. Oshimura, and H. Ito, PI3K-Akt pathway: its functions and alterations in human cancer, *Apoptosis*, **2004**, 9 (6), 667-676.
72. Altomare, D.A., Wang, H.Q., Skele, K.L., De Rienzo, A., Klein-Szanto, A.J., Godwin, A.K. and Testa, J.R., AKT and mTOR phosphorylation is frequently detected in ovarian cancer and can be targeted to disrupt ovarian tumor cell growth, *Oncogene*, **2004**, 23 (34), 5853.
73. Missiaglia, E., Dalai, I., Barbi, S., Beghelli, S., Falconi, M., della Peruta, M., Piemonti, L., Capurso, G., Di Florio, A., delle Fave, G. and Pederzoli, P., Pancreatic endocrine tumors: expression profiling evidences a role for AKT-mTOR pathway, *J Clin Oncol*, **2009**, 28 (2), 245-255.
74. Friedrichs, W.E., Russell, D.H., Donzis, E.J., Middleton, A.K., Silva, J.M., Roth, R.A. and Hidalgo, M., Inhibition of mTOR activity restores tamoxifen response in breast cancer cells with aberrant Akt Activity, *Clin Cancer Res*, **2004**, 10 (23), 8059-8067.
75. Soliman, G.A., The role of mechanistic target of rapamycin (mTOR) complexes signaling in the immune responses, *Nutrients*, **2013**, 5 (6), 2231-2257.
76. Sabatini, D.M., mTOR and cancer: insights into a complex relationship, *Nat Rev Cancer*, **2006**, 6 (9), 729.
77. Bolinger, A.M., Zangwill, A.B., Slattery, J.T., Glidden, D., DeSantes, K., Heyn, L., Risler, L.J., Bostrom, B. and Cowan, M.J., An evaluation of engraftment, toxicity and busulfan concentration in children receiving bone marrow transplantation for leukemia or genetic disease, *Bone Marrow Transplant*, **2000**, 25 (9), 925.
78. Hirsch, J., An anniversary for cancer chemotherapy, *Jama*, **2006**, 296 (12), 1518-1520.
79. Graef, I., Karnofsky, D.A., Jager, V.B., Krichesky, B. and Smith, H.W., The clinical and pathologic effects of the nitrogen and sulfur mustards in laboratory animals, *Am J Pathol*, **1948**, 24 (1), 1.

80. Santos, G.W., Tutschka, P.J., Brookmeyer, R., Saral, R., Beschorner, W.E., Bias, W.B., Braine, H.G., Burns, W.H., Elfenbein, G.J., Kaizer, H. and Mellits, D., Marrow transplantation for acute nonlymphocytic leukemia after treatment with busulfan and cyclophosphamide, *Engl J Med*, **1983**, 309 (22),1347-1353.
81. Griffin, J.D., Blood's 70th anniversary: arsenic—from poison pill to magic bullet, **2016**, Am Soc Hematology.
82. Shen, Z.X., Chen, G.Q., Ni, J.H., Li, X.S., Xiong, S.M., Qiu, Q.Y., Zhu, J., Tang, W., Sun, G.L., Yang, K.Q. and Chen, Y., Use of arsenic trioxide (As2O3) in the treatment of acute promyelocytic leukemia (APL): II. Clinical efficacy and pharmacokinetics in relapsed patients, *Blood*, **1997**, 89 (9), 3354-3360.
83. Rao, Y., R. Li, and D. Zhang, A drug from poison: how the therapeutic effect of arsenic trioxide on acute promyelocytic leukemia was discovered, *Sci China Life Sci*, **2013**, 56 (6), 495.
84. O'Donnell, M.R., Tallman, M.S., Abboud, C.N., Altman, J.K., Appelbaum, F.R., Arber, D.A., Attar, E., Borate, U., Coutre, S.E., Damon, L.E. and Lancet, J., Acute myeloid leukemia, version 2.2013, *J Natl Compr Cancer Netw*, **2013**, 11 (9), 1047-1055.
85. Damery, E., D.A. Solimando Jr, and J.A. Waddell, Arsenic Trioxide and Tretinoin (AsO/ATRA) for Acute Promyelocytic Leukemia (APL), *Hospital pharmacy*, **2016**, 51 (8), 628-632.
86. Capizzi, R.L., Poole, M., Cooper, M.R., Stuart, J.J., Jackson, D.J., White, D.R., Spurr, C.L., Hopkins, J.O. and Muss, H.B., 1Treatment of poor risk acute leukemia with sequential high-dose ARA-C and asparaginase, *Blood*, **1984**, 63 (3), 694-700.
87. Gewirtz, D., A critical evaluation of the mechanisms of action proposed for the antitumor effects of the anthracycline antibiotics adriamycin and daunorubicin, *Biochem Pharmacol*, **1999**, 57 (7), 727-741.
88. Boiron, M., Jacquillat, C., Weil, M., Tanzer, J., Levy, D., Sultan, C. and Bernard, J., Daunorubicin in the treatment of acute myelocytic leukaemia, *Lancet*, **1969**, 293 (7590), 330-333.
89. Bodley, A., Liu, L.F., Israel, M., Seshadri, R., Koseki, Y., Giuliani, F.C., Kirschenbaum, S., Silber, R. and Potmesil, M., DNA topoisomerase II-mediated interaction of doxorubicin and daunorubicin congeners with DNA, *Cancer Res*, **1989**, 49 (21), 5969-5978.
90. Iqbal, N. and N. Iqbal, Imatinib: a breakthrough of targeted therapy in cancer, *Chemother Res Pract*, **2014**.
91. Wu, P., T.E. Nielsen, and M.H. Clausen, FDA-approved small-molecule kinase inhibitors, *Trends Pharmacol Sci*, **2015**, 36 (7), 422-439.
92. Schlessinger, J., Receptor tyrosine kinases: legacy of the first two decades, *Cold Spring Harb Perspect Biol*, **2014**, 6 (3), a008912.
93. Jeon, J.Y., A. Sparreboom, and S.D. Baker, Kinase Inhibitors: The Reality Behind the Success, *Clin Pharmacol Ther*, **2017**, 102 (5), 726-730.
94. Khan, H., PHILADELPHIA CHROMOSOME, *GJMS*, **2017**, 15 (1).
95. Huang, W.S., Metcalf, C.A., Sundaramoorthi, R., Wang, Y., Zou, D., Thomas, R.M., Zhu, X., Cai, L., Wen, D., Liu, S. and Romero, J., Discovery of 3-[2-(imidazo [1, 2-b] pyridazin-3-yl) ethynyl]-4-methyl-N-{4-[(4-methylpiperazin-1-yl) methyl]-3-

(trifluoromethyl) phenyl} benzamide (AP24534), a potent, orally active pan-inhibitor of breakpoint cluster region-abelson (BCR-ABL) kinase including the T315I gatekeeper mutant, *J Med Chem*, **2010**, 53 (12), 4701-4719.
96. Kantarjian, H., Giles, F., Wunderle, L., Bhalla, K., O'brien, S., Wassmann, B., Tanaka, C., Manley, P., Rae, P., Mietlowski, W. and Bochinski, K., Nilotinib in imatinib-resistant CML and Philadelphia chromosome–positive ALL, *N Engl J Med*, **2006**, 354 (24), 2542-2551.
97. Zhang, J., Adrián, F.J., Jahnke, W., Cowan-Jacob, S.W., Li, A.G., Iacob, R.E., Sim, T., Powers, J., Dierks, C., Sun, F. and Guo, G.R., Targeting wild-type and T315I Bcr-Abl by combining allosteric with ATP-site inhibitors, *Nature*, **2010**, 463 (7280), 501.
98. Schaffhausen, J., Advances in structure-based drug design, *Trends Pharmacol Sci,* **2012**, 33 (5), 223.
99. Prasad, V. and S. Mailankody, The accelerated approval of oncologic drugs: lessons from ponatinib, *Jama*, **2014**, 311 (4), 353-354.
100. Gainor, J.F. and B.A. Chabner, Ponatinib: accelerated disapproval, **2015**, AlphaMed Press.
101. Gani, O.A. and R.A. Engh, Protein kinase inhibition of clinically important staurosporine analogues, *Nat Prod Rep*, **2010**, 27 (4), 489-498.
102. Mackay, H.J. and C.J. Twelves, Targeting the protein kinase C family: are we there yet?, *Nat Rev Cancer*, **2007**, 7 (7), 554.
103. Barry, E.V., Clark, J.J., Cools, J., Roesel, J. and Gilliland, D.G.,Uniform sensitivity of FLT3 activation loop mutants to the tyrosine kinase inhibitor midostaurin, *Blood*, **2007**, 110 (13), 4476-4479.
104. Levis, M., Midostaurin approved for FLT3-mutated AML, *Blood*, **2017**, 129 (26), 3403-3406.
105. Kim, E.S., Midostaurin: First Global Approval, *Drugs*, **2017**, 1-9.
106. Knapper, S., Russell, N., Gilkes, A., Hills, R.K., Gale, R.E., Cavenagh, J.D., Jones, G., Kjeldsen, L., Grunwald, M.R., Thomas, I. and Konig, H., A randomized assessment of adding the kinase inhibitor lestaurtinib to first-line chemotherapy for FLT3-mutated AML, *Blood*, **2017**, 129 (9), 1143-1154.
107. Cortes, J., Perl, A.E., Döhner, H., Kantarjian, H., Martinelli, G., Kovacsovics, T., Rousselot, P., Steffen, B., Dombret, H., Estey, E. and Strickland, S., Quizartinib, an FLT3 inhibitor, as monotherapy in patients with relapsed or refractory acute myeloid leukaemia: an open-label, multicentre, single-arm, phase 2 trial, *Lancet Oncol*, **2018**.
108. Mathew, N.R., Baumgartner, F., Braun, L., O'Sullivan, D., Thomas, S., Waterhouse, M., Müller, T.A., Hanke, K., Taromi, S., Apostolova, P. and Illert, A.L., Sorafenib promotes graft-versus-leukemia activity in mice and humans through IL-15 production in FLT3-ITD-mutant leukemia cells, *Nat Med*, **2018**, 24 (3), 282.
109. Stein, E.M., FLT3 inhibitors for relapsed or refractory acute myeloid leukaemia, *Lancet Oncol*, **2018**, 19(7), 849-850.
110. Kampa-Schittenhelm, K.M., Frey, J., Haeusser, L.A., Illing, B., Pavlovsky, A.A., Blumenstock, G. and Schittenhelm, M.M., Crenolanib is a type I tyrosine kinase

inhibitor that inhibits mutant KIT D816 isoforms prevalent in systemic mastocytosis and core binding factor leukemia, *Oncotarget*, **2017**, 8 (47), 82897.
111. Koda, Y., Kikuzato, K., Mikuni, J., Tanaka, A., Yuki, H., Honma, T., Tomabechi, Y., Kukimoto-Niino, M., Shirouzu, M., Shirai, F. and Koyama, H., Identification of pyrrolo [2, 3-d] pyrimidines as potent HCK and FLT3-ITD dual inhibitorsm, *Bioorganic Med Chem Lett*, **2017**, 27 (22), 4994-4998.
112. Hsu, Y.C., Coumar, M.S., Wang, W.C., Shiao, H.Y., Ke, Y.Y., Lin, W.H., Kuo, C.C., Chang, C.W., Kuo, F.M., Chen, P.Y. and Wang, S.Y., Discovery of BPR1K871, a quinazoline based, multi-kinase inhibitor for the treatment of AML and solid tumors: Rational design, synthesis, in vitro and in vivo evaluation, *Oncotarget*, **2016**, 7 (52), 86239.
113. Weir, M.C., Hellwig, S., Tan, L., Liu, Y., Gray, N.S. and Smithgall, T.E., Dual inhibition of Fes and Flt3 tyrosine kinases potently inhibits Flt3-ITD+ AML cell growth, *PloS one*, **2017**, 12 (7), e0181178.
114. MacDonald, R.J., Bunaciu, R.P., Ip, V., Dai, D., Tran, D., Varner, J.D. and Yen, A., Src family kinase inhibitor bosutinib enhances retinoic acid-induced differentiation of HL-60 leukemia cells, *Leuk Lymphoma*, **2018**, 1-11.
115. Leischner, H., Albers, C., Grundler, R., Razumovskaya, E., Spiekermann, K., Bohlander, S., Rönnstrand, L., Götze, K., Peschel, C. and Duyster, J., SRC is a signaling mediator in FLT3-ITD but not in FLT3-TKD positive AML, *Blood*, **2012**, blood-2011-2007-365726.
116. Marhäll, A., J.U. Kazi, and L. Rönnstrand, The Src family kinase LCK cooperates with oncogenic FLT3/ITD in cellular transformation, *Sci Rep*, **2017**, 7 (1), 13734.
117. Staudt, D., Murray, H., McLachlan, T., Alvaro, F., Enjeti, A., Verrills, N. and Dun, M.,Targeting Oncogenic Signaling in Mutant FLT3 Acute Myeloid Leukemia: The Path to Least Resistance, *Int J Mol Sci*, **2018**, 19 (10), 3198.
118. Perl, A., FLT3 Inhibitors in AML, *Clin Lymphoma Myeloma Leuk*, **2018**, 18, S1-S2.
119. Smith, C.C., Lin, K., Stecula, A., Sali, A. and Shah, N.P., FLT3 D835 mutations confer differential resistance to type II FLT3 inhibitors, *Leukemia*, **2015**, 29 (12), 2390.
120. Müller, S., Chaikuad, A., Gray, N.S. and Knapp, S., The ins and outs of selective kinase inhibitor development, *Nat Chem Bio*, **2015**, 11 (11), 818.
121. Smith, C.C., Paguirigan, A., Jeschke, G.R., Lin, K.C., Massi, E., Tarver, T., Chin, C.S., Asthana, S., Olshen, A., Travers, K.J. and Wang, S.,Heterogeneous resistance to quizartinib in acute myeloid leukemia (AML) revealed by single cell analysis, *Blood*, **2017**, blood-2016-2004-711820.
122. Zhou, J., Le, V., Kalia, D., Nakayama, S., Mikek, C., Lewis, E.A. and Sintim, H.O., Diminazene or berenil, a classic duplex minor groove binder, binds to G-quadruplexes with low nanomolar dissociation constants and the amidine groups are also critical for G-quadruplex binding, *Mol BioSyst*, **2014**, 10 (10), 2724-2734.
123. Sintim, H.O., Nakayama, S., Kalia, D., Zhou, J., Guo, M., Jinbing, L.I.U., Wang, C. and Lapidus, R., University of Maryland, Baltimore, University of Maryland and College Park, **2017**, Linked diaryl compounds with anticancer properties and methods of using the same, U.S. Patent Application 15/327,485.

124. Sidwell, R.W., Bailey, K.W., Wong, M.H., Barnard, D.L. and Smee, D.F., In vitro and in vivo influenza virus-inhibitory effects of viramidine, *Antivir Res*, **2005**, 68 (1), 10-17.
125. Nakabayashi, T., Gotoh, Y., Kamada, N., Fujioka, M., Ishihara, T., Hirabayashi, A. and Sato, H., Pharmacokinetics of the amidine prodrug of a novel oral anticoagulant factor VIIa inhibitor (AS1924269-00) in rats, *Pharmazie*, **2013**, 68 (5), 349-354.
126. Thomas, X. and C. Le Jeune, The safety of treatment options for elderly people with acute myeloid leukemia, *Expert Opin Drug Saf*, **2016**, 15 (5), 635-645.
127. Lipinski, C.A., Rule of five in 2015 and beyond: Target and ligand structural limitations, ligand chemistry structure and drug discovery project decisions, *Adv Drug Deliv Rev*, **2016**, 101, 34-41.
128. Di, L. and E.H. Kerns, Drug-like properties: concepts, structure design and methods from ADME to toxicity optimization, **2015**, Academic press.
129. Yilancioglu, K., Weinstein, Z.B., Meydan, C., Akhmetov, A., Toprak, I., Durmaz, A., Iossifov, I., Kazan, H., Roth, F.P. and Cokol, M., Target-independent prediction of drug synergies using only drug lipophilicity, *J Chem Inf Model*, **2014**, 54 (8), 2286-2293.
130. Waring, M.J., Arrowsmith, J., Leach, A.R., Leeson, P.D., Mandrell, S., Owen, R.M., Pairaudeau, G., Pennie, W.D., Pickett, S.D., Wang, J. and Wallace, O., An analysis of the attrition of drug candidates from four major pharmaceutical companies, *Nat Rev Drug Discov*, **2015**, 14 (7), 475.
131. Jhoti, H., Williams, G., Rees, D.C. and Murray, C.W., The'rule of three'for fragment-based drug discovery: where are we now?, *Nat Rev Drug Discov*, **2013**, 12 (8),644-644.
132. Williams, H.D., Trevaskis, N.L., Charman, S.A., Shanker, R.M., Charman, W.N., Pouton, C.W. and Porter, C.J., Strategies to address low drug solubility in discovery and development, *Pharmacol Rev*, **2013**, 65 (1), 315-499.
133. Matsson, P., Fenu, L.A., Lundquist, P., Wiśniewski, J.R., Kansy, M. and Artursson, P., Quantifying the impact of transporters on cellular drug permeability, *Trends Pharmacol Sci*, **2015**, 36 (5), 255-262.
134. Ross, P.L. and J.L. Wolfe, Physical and chemical stability of antibody drug conjugates: current status, *J Pharm Sci*, **2016**, 105 (2), 391-397.
135. Kirchmair, J., Göller, A.H., Lang, D., Kunze, J., Testa, B., Wilson, I.D., Glen, R.C. and Schneider, G., Predicting drug metabolism: experiment and/or computation?, *Nat Rev Drug Discov*, **2015**, **14**(6), 387.
136. Nigam, S.K., What do drug transporters really do?, *Nat Rev Drug Discov*, **2015**, 14 (1), 29.
137. Abbott, N.J., Blood–brain barrier structure and function and the challenges for CNS drug delivery, *J Inherit Metab Dis*, **2013**, 36 (3), 437-449.
138. Piacentino, D., Grözinger, M., Saria, A., Scolati, F., Arcangeli, D., Girardi, P., Pompili, M. and Conca, A., Risperidone-treated children and adolescents with behavioral disorders: Do drug dose and patients' gender and age relate to drug and metabolite plasma levels?, *Euro Psychiatry*, **2017**, 41, S104.

139. König, J., F. Müller, and M.F. Fromm, Transporters and drug-drug interactions: important determinants of drug disposition and effects, *Pharmacol Rev*, **2013**, 65 (3), 944-966.
140. Mah, R., J.R. Thomas, and C.M. Shafer, Drug discovery considerations in the development of covalent inhibitors, *Bioorganic Med Chem Lett*, **2014**, 24 (1), 33-39.
141. Whitebread, S., Dumotier, B., Armstrong, D., Fekete, A., Chen, S., Hartmann, A., Muller, P.Y. and Urban, L., Secondary pharmacology: screening and interpretation of off-target activities–focus on translation, *Drug Discov Today*, **2016**, 21 (8), 1232-1242.
142. Vandenberg, J.I., E. Perozo, and T.W. Allen, Towards a Structural View of Drug Binding to hERG K+ Channels, *Trends Pharmacol Sci*, **2017**, 38 (10), 899-907..
143. Araújo, S.D.S., Fernandes, T.C., Marin-Morales, M.A., Brasileiro-Vidal, A.C. and Benko-Iseppon, A.M., Mutagenicity, genotoxicity and cytotoxicity assays of medicinal plants: first step for drug development, Therapeutic Medicinal Plants: From lab to the market, **2015**, 130-153.
144. Vajda, F.J.E., O'brien, T.J., Lander, C.M., Graham, J. and Eadie, M.J., The teratogenicity of the newer antiepileptic drugs–an update, *Acta Neurol Scand*, **2014**, 130 (4), 234-238.
145. Loftsson, T., Essential pharmacokinetics: A primer for pharmaceutical scientists, **2015**, Academic Press.
146. Zhang, W. and Zhang, Computer-Aided Drug Discovery, **2016**, Springer.
147. Moses, J.E. and A.D. Moorhouse, The growing applications of click chemistry, *Chem Soc Rev*, **2007**, 36 (8), 1249-1262.
148. Carey, J.S., Laffan, D., Thomson, C. and Williams, M.T., Analysis of the reactions used for the preparation of drug candidate molecules, *Org Biomol Chem*, **2006**, 4 (12), 2337-2347.
149. Trott, O. and A.J. Olson, AutoDock Vina: improving the speed and accuracy of docking with a new scoring function, efficient optimization, and multithreading, *J Comput Chem*, **2010**, 31 (2), 455-461.
150. Zorn, J.A., Wang, Q., Fujimura, E., Barros, T. and Kuriyan, J., Crystal structure of the FLT3 kinase domain bound to the inhibitor Quizartinib (AC220), *PloS one*, **2015**, 10 (4), e0121177.
151. Larocque, E., Naganna, N., Ma, X., Opoku-Temeng, C., Carter-Cooper, B., Chopra, G., Lapidus, R.G. and Sintim, H.O., Aminoisoquinoline benzamides, FLT3 and Src-family kinase inhibitors, potently inhibit proliferation of acute myeloid leukemia cell lines, *Future Med Chem*, **2017**, 9 (11), 1213-1225..
152. Heinrich, M.C., Corless, C.L., Duensing, A., McGreevey, L., Chen, C.J., Joseph, N., Singer, S., Griffith, D.J., Haley, A., Town, A. and Demetri, G.D., PDGFRA activating mutations in gastrointestinal stromal tumors, *Science*, **2003**, 299 (5607),708-710.
153. Appiah-Kubi, K., Lan, T., Wang, Y., Qian, H., Wu, M., Yao, X., Wu, Y. and Chen, Y., Platelet-derived growth factor receptors (PDGFRs) fusion genes involvement in hematological malignancies, *Crit Rev Oncol Hematol*, **2017**, 109, 20-34.

154. Oxnard, G.R., A. Binder, and P.A. Jänne, New targetable oncogenes in non–small-cell lung cancer, *J Clin Oncol*, **2013**, 31 (8), 1097-1104.
155. Holzer, T.R., Falcon, B.L., Fulford, A.D., McDonald, S.A., Ray, A.L., Finnegan, P., Uhlik, M.T., Benjamin, L.E., Schade, A.E. and Nasir, A., VEGFR2 expression and vascular phenotyping demonstrate different patterns of tumor angiogenesis in human gastric and breast cancers, *AACR*, **2014**.
156. Jänne, P.A., Yang, J.C.H., Kim, D.W., Planchard, D., Ohe, Y., Ramalingam, S.S., Ahn, M.J., Kim, S.W., Su, W.C., Horn, L. and Haggstrom, D., AZD9291 in EGFR inhibitor–resistant non–small-cell lung cancer, *N Engl J Med*, **2015**, 372 (18), 1689-1699.
157. Gil, M., Chidambaram, A., Khoury, T., Takabe, K., Puzanov, I., Gelman, I., D'Assoro, A. and Opyrchal, M., Inhibition of AURKA induces Raf1-independent activation of MAPK pathway in breast cancer cells, *AACR*, **2017**.
158. Divine, L., Grither, W., Gibson, A., Longmore, G. and Fuh, K., The receptor tyrosine kinase discoidin domain receptor 2 promotes invasion via epithelial mesenchymal transition in ovarian cancer, *Gynecol Oncol,* **2015**, 139 (1), 189.